

# **Molecular Design Strategies for Serological Breast Cancer Marker Analysis**

Ashkan Koushanpour



Department of experimental surgery

McGill University, Montreal, QC, Canada

November 7, 2022

A thesis submitted to McGill University in partial fulfillment of the requirements of the  
degree of Doctor of Philosophy (Ph.D.)

This page was left blank

## **Abstract:**

In this work, we propose a novel strategy for interfacial manipulations of electrochemical aptamer-based (E-AB) sensors to achieve a highly sensitive and reagentless sensing platform. We hope to see clinical relevance in the quantification of breast cancer biomarkers, particularly, MUC1 and VEGF<sub>165</sub> in human serum samples.

Chapter 1 consists of a comprehensive literature review of key parameters in the analytical performance and essential conditions in the optimization of the E-AB sensors, as well as a comprehensive account covering the significance of liquid biopsy and the biomarker's role in breast cancer. The following two chapters are devoted to a systematic assessment of the proposed molecular design and interfacial engineering, through which, we show the existence of a delicate synergistic interplay among lysine linker, twin-methylene blue (MB), and the finely tuned thickness of the backfilling agents within the inner Helmholtz layer (interfacial layer). Our findings imply that the spatial arrangement of the electrochemical tag doesn't necessarily enhance the analytical signal unless it is being assisted by a lysine linker and a 9-carbon chain in the SAM passivation layer. This strategy adaptation proved to be consistent with both signal-on and signal-off types of E-AB sensors when employed for the detection of MUC1 and VEGF<sub>165</sub> biomarkers, respectively.

In the fourth chapter, the effect of gold surface nano-dimensionality (including 1D, 2D, and 3D) on the E-AB sensor's analytical performance was examined. Our results suggest that the 1D gold surface provides the most efficient sensing platform, in terms of limit of detection (LOD), as well as linear dynamic range (LDR). We also conclude that a higher surface area can not always afford the best result unless spatial requirements in signal generation are met.

## **Resume:**

Dans ce travail, nous proposons une nouvelle stratégie pour les manipulations interfaciales de capteurs électrochimiques à base d'aptamères (E-AB) pour obtenir une plate-forme de détection très sensible et sans réactif. Nous espérons voir une pertinence clinique dans la quantification des biomarqueurs du cancer du sein, en particulier MUC1 et VEGF165 dans des échantillons de sérum humain.

Le chapitre 1 consiste en une revue complète de la littérature des paramètres clés de la performance analytique et des conditions essentielles à l'optimisation des capteurs E-AB. Les deux chapitres suivants sont consacrés à une évaluation systématique de la conception moléculaire proposée et de l'ingénierie interfaciale, à travers laquelle, nous avons montré l'existence d'une interaction synergique délicate entre le lieur lysine, le bleu de méthylène jumelé (MB) et l'épaisseur finement réglée de l'agent de remblai dans la couche interne de Helmholtz (couche interfaciale). Nos résultats impliquent que la disposition spatiale de l'étiquette électrochimique n'améliore pas nécessairement le signal analytique à moins qu'elle ne soit assistée par un lieur de lysine et une chaîne à 9 carbones dans la couche de passivation SAM. Cette adaptation de la stratégie s'est avérée cohérente avec les types de capteurs E-AB à signal activé et à signal désactivé lorsqu'ils sont utilisés pour la détection des biomarqueurs MUC1 et VEGF165, respectivement.

Dans le troisième chapitre, l'effet de la nanodimensionnalité de la surface d'or (y compris 1D, 2D et 3D) sur les performances analytiques du capteur E-AB a été examiné. Nos résultats suggèrent que la surface d'or 1D fournit la plate-forme de détection la plus efficace, en termes de limite de détection (LOD), ainsi que de plage dynamique linéaire (LDR). Nous concluons également qu'une surface plus élevée ne peut pas toujours offrir le meilleur résultat à moins que les exigences spatiales dans la génération du signal ne soient satisfaites.

## **Acknowledgment**

Pursuing research in a highly interdisciplinary branch of science, like the one that I have been involved in, would not be accomplished unless it receives a significant number of assistance. This thesis could not have gone so far, had I not benefitted from the sincere support and encouragement of my supervisor, and Co-supervisor. Here, I would like to express my heartfelt appreciation to my supervisor professor Dr. Edward J. Harvey for his thoughtful input, and his kind patience throughout the last three years. Also, I am very thankful to my Co-supervisor, Dr. Geraldine E. Merle, for the privilege of intellectual freedom, and the sense of scientific adventurousness that she nourished in me to dare to put my hypotheses to trial and be not afraid of the inevitable failures.

As my projects have been heavily dependent on advanced instrumental analysis and characterizations, I would like to especially thank Mr. Andrew Golsztajn, as if it weren't for him, initially I could hardly carry out the protein isolations and characterizations. Also, I would like to pay my respect to Mr. Rajan Roy for his incessant safety measure reminders. Furthermore, I would like to thank Dr. Alexander Wahba, who carried out one of the most important parts of instrumental characterizations. without which the foundation of many of my interpretations would have gone awry. Here, I also deem it necessary to express my gratitude to Mr. David Liu and Mr. Kelly Sears for their kind support and help with SEM, TEM, and metal sputtering experiments.

I would like to thank all my colleagues, Rachel Monk, Daniela Vieira, Yazan Honjol, Drew Schupbach, Matthew Zakaria, Justin Matta, and all the other folks I have met during my Ph.D.

Finally, I would like to have a big shoutout to my family whom I have long missed.

## **Contribution to the original knowledge**

**Chapter 1** – Ashkan Koushanpour, Dr. Harvey, Dr. Merle.

- Ashkan Koushanpour: gathered the literature and wrote the manuscript.
- Dr. Harvey and Dr. Merle supervised the study and revised the manuscripts.

Originality: we had a unique perspective in reviewing the parameters affecting the development of an E-AB sensor. it portrays a thorough perspective on the key parameters in the fabrication and optimization of the E-AB sensors which accounts for a distinct review paper.

**Chapter 2** – Ashkan Koushanpour, Dr. Harvey, Dr. Merle.

- Ashkan Koushanpour: designed the strategy, prepared the materials, carried out the experiments, and wrote the manuscripts.
- Dr Merle: suggested the use of lysine as the linker. Also, the one with protecting groups.
- Dr. Harvey and Dr. Merle supervised the study and revised the manuscripts.

Originality: for the first time we proposed the utilization of molecular assembly as a redox-reporter and their synergy with backfilling agents, as well as its application in the detection of breast cancer biomarker, MUC1, in human serum samples.

**Chapter 3** – Ashkan Koushanpour, Dr. Harvey, Dr. Merle.

- Ashkan Koushanpour: designed the strategy, prepared the materials, carried out the experiments, and wrote the manuscripts.
- Dr. Harvey and Dr. Merle supervised the study and revised the manuscripts.

Originality: we fabricated a novel signal-on type E-AB sensor and employed it for the detection of breast cancer biomarker, VEGF<sub>165</sub>, and evaluated the consistency of the molecular assembly of the redox-reporters with the corresponding signaling behavior of the probe aptamer.

**Chapter 4** – Ashkan Koushanpour, Dr. Harvey, Dr. Merle.

- Ashkan Koushanpour: designed the strategy, prepared the materials, carried out the experiments, and wrote the manuscripts.
- Dr. Merle: proposed the layout of the study.
- Dr. Harvey and Dr. Merle supervised the study and revised the manuscripts.

Originality: for the first time the role of surface nano-dimensionality, as an interfacial factor, was systematically addressed in E-AB sensors.

# Table of Contents

Abstract: .....	I
Resume:.....	II
Acknowledgment .....	III
Contribution to the original knowledge .....	IV
Chapter 1.....	1
Review .....	1
Molecular biointerfacing of electrochemical aptamer-based sensors for breast cancer biomarkers.....	1
Abstract.....	2
1.1 Introduction.....	3
1.2 E-AB sensors .....	10
1.2.1 Basic principles.....	10
1.2.2 E-AB signal and the gain .....	12
1.2.3 Probe packing density .....	12
1.2.4 Backfilling agents and surface homogeneity .....	15
1.2.5 The length and the chemistry of the backfilling agents .....	16
1.2.6 The length of the aptamer .....	19
1.2.7 The redox reporters and stability .....	20
1.3 Operational parameters .....	24
1.4 Breast cancer.....	26
1.5 Breast cancer biomarkers and clinical utility .....	28
1.6 Liquid biopsy: the general concept:.....	31
1.7 Liquid biopsy: package of tumor-derived materials .....	31
1.8 Liquid biopsy vs. tissue biopsy .....	33
1.9 The mucins : family of glycosylated proteins.....	35

1.10 The structure of MUC1 .....	38
1.11 Significance of MUC1 (CA15-3).....	39
1.12 Relationship between CA 15-3 and tumor and patient characteristics .....	42
1.12.1 Relationship between CA 15-3 and overall survival .....	44
1.13 Current use .....	45
1.14 Vascular Endothelial Growth Factor (VEGF) Protein.....	46
1.15 Significance of VEGF <sub>165</sub> .....	48
1.16 To determine the relationship between preoperative serum VEGF and to compare serum VEGF with two established tumor markers for breast cancer, namely, CEA and CA15.3 .....	49
1.17 Current technologies available in liquid biopsy.....	51
1.17.1 DNA.....	51
1.17.2 RNA.....	52
1.17.3 Proteins .....	52
1.17.4 Cells .....	52
1.18 E-AB sensor fabrication and interfacial engineering.....	53
1.18.1 Single-target electrochemical aptasensor.....	53
1.18.2 Dual target electrochemical aptasensor .....	54
1.18.3 Signal amplification strategy .....	61
Conclusion .....	66
References.....	68
Chapter 2.....	80
Engineering the interface of an electrochemical aptamer-based sensor to detect MUC 1 tumor marker in serum. ....	80
Abstract.....	81
2.1 Introduction.....	81
2.2 Experimental .....	84
2.2.1 Reagents.....	84

2.3 Chemical synthesis of lysine-MB and corresponding DNA aptamer conjugation .....	85
2.3.1 Synthesis of DNA aptamer-Fmoc-lysine(Fmoc)-OH .....	85
2.3.2 De-protection of aptamer-Fmoc-lysine (Fmoc)-OH .....	86
2.3.3 Methylene blue labeling of aptamer-lysine .....	86
2.4 Electron transfer kinetics .....	86
2.5 Preparation of E-AB sensor .....	87
2.6 Electrochemical characterization of E-AB sensors.....	88
2.7 Results and discussion .....	88
Conclusion .....	103
Supporting information.....	105
Engineering the interface of an electrochemical aptamer-based sensor to detect MUC 1 tumor marker in serum. ....	105
2.8 Methods and materials .....	106
2.9 DNA modification and purification: .....	108
2.9.1 Synthesis of DNA-Fmoc-lysine(Boc)-OH.....	108
2.10 Deprotection of Fmoc group .....	109
2.11 Synthesis of DNA-MB-lysine(Boc)-OH (referred to as remote MB) .....	109
2.12 Synthesis of DNA-Boc-lysine(MB)-OH (referred to as Vicinal MB).....	109
2.13 Synthesis of DNA-MB-lysine(MB)-OH (referred to as Twin-MB).....	110
2.14 Purification and isolation of the DNA products .....	110
2.15 The various spatial arrangement of MB on the lysine linker attached to the DNA-aptamer will influence the gain fluctuations .....	110
References.....	114
Amplifying VEGF signal-on multi-tagged probe aptamer .....	120
Abstract.....	121
3.1 Introduction.....	121
3.2 Experimental .....	126

3.2.1 Reagents.....	126
3.3 Chemical synthesis of lysine-MB and aptamer conjugation.....	126
3.3.1 Modification of aptamer-NHCO-lysine-(Fmoc) <sub>2</sub> .....	126
3.3.2 De-protection of aptamer-lysine (Fmoc) <sub>2</sub> .....	127
3.3.3 Labeling aptamer-lysine-(COOH) <sub>2</sub> with methylene blue (Modified aptamer).....	127
3.4 Preparation of E-AB sensor .....	128
3.5 Electrochemical characterization .....	129
3.6 Results and discussions.....	129
3.7 The E-AB sensor performance in diluted human serum.....	134
Conclusion .....	141
Supporting information.....	142
Amplifying VEGF signal-on multi-tagged probe aptamer .....	142
References.....	146
Chapter 4.....	150
Nano-dimensionality effect on the electrochemical aptamer-based sensor performance for serological MUC1 detection. ....	150
Abstract.....	151
4.1 Introduction.....	152
4.2 Experimental.....	155
4.2.1 Reagents.....	155
4.3 Preparation of E-AB sensor .....	156
4.4 Synthesis of gold nanostructures .....	157
4.4.1 Gold nanospike synthesis.....	157
4.4.2 Gold nanorods synthesis .....	157
4.5 Physico-chemical characterization and electrochemical measurements.....	158
4.6 Results and discussion .....	159

Conclusion .....	168
References.....	169
Chapter 5.....	173
Comprehensive scholarly discussion .....	173
References.....	185
Conclusion and summary.....	187
Reference list: .....	190
Chapter 1: References:.....	190
Chapter 2: References:.....	201
Chapter 3: References:.....	204
Chapter 4: References .....	206
Chapter 5: References:.....	209



# **Chapter 1.**

## **Review**

### **Molecular biointerfacing of electrochemical aptamer-based sensors for breast cancer biomarkers**

Ashkan Koushanpour, Edward J. Harvey, Geraldine E. Merle\*

A. Koushanpour,

Experimental Surgery, Faculty of Medicine, McGill University, Montreal, H3A 0C5, Canada

Dr. E. Harvey

Department of Surgery, Faculty of Medicine, McGill University, Montreal, H3A 0C5,  
Canada

Dr. G. E. Merle

Department of Chemical Engineering, Polytechnique, Montreal, H3T 1J4, Canada

To be submitted.

## **Abstract**

Analytical biosensing based on DNA and RNA aptamers has recently attracted attention. Electrochemical aptamer-based (E-AB) sensors have a specific ability to generate a real-time graded electrochemical signal in response to specific in Vivo binding. Previous technologies have been unable to match the sensing characteristics of E-AB sensing, in particular, for fast diagnosis during breast cancer resection. The characteristic that readily distinguishes the E-AB sensors from other classical alternatives (potentiometry, amperometry, and biocatalytic conversion), is that the signaling mechanism in E-AB sensors does not depend on the specific chemical reactivity of the targets. This means that the faradic signal is not induced by any chemical reaction with the target. This, in turn, will remove many of the complexities associated with variations in activity, pH, side reactions, and limitations linked to such reactions. Instead, the faradic signal is only induced by specific physical phenomena, which makes them uniquely suitable for diagnostics, pharmacological, and clinical applications even in complex physiological environments. Furthermore, due to the modularity offered by E-AB, there is theoretically no limitation over the target choice. Despite these strengths, widespread adoption as a diagnostic and therapeutic tool has been limited by a series of complex challenges. Many of these challenges are multi-disciplinary and depend on innovation in the fields of interfacial chemistry, biomedical engineering, material science, and data management. In this review, however, the main emphasis is held on a detailed examination of intrinsic challenges ahead of E-AB performance such as critical fabrication parameters and relative approaches for interfacial chemistry and constructional parameters. We discuss individual parameter case assessments for the innovations employed in the interfacial architecture and molecular design aiming to meet a new set of requirements in proof-of-the-

concept demonstrations of the latest E-AB sensors exclusively reported for breast cancer biomarkers.

## 1.1 Introduction

Cancer is a leading cause of mortality and a critical public health problem that will worsen with the aging of the population. According to statistics, the probability of being diagnosed with cancer is one in three, and the corresponding mortality rundown is one in four<sup>1</sup>. Globally, in 2018, 18.1 million people had cancer, and 9.6 million died from it. It has been estimated that by 2040, these numbers will double, with a higher preponderance in low-and middle-income countries<sup>1</sup>.

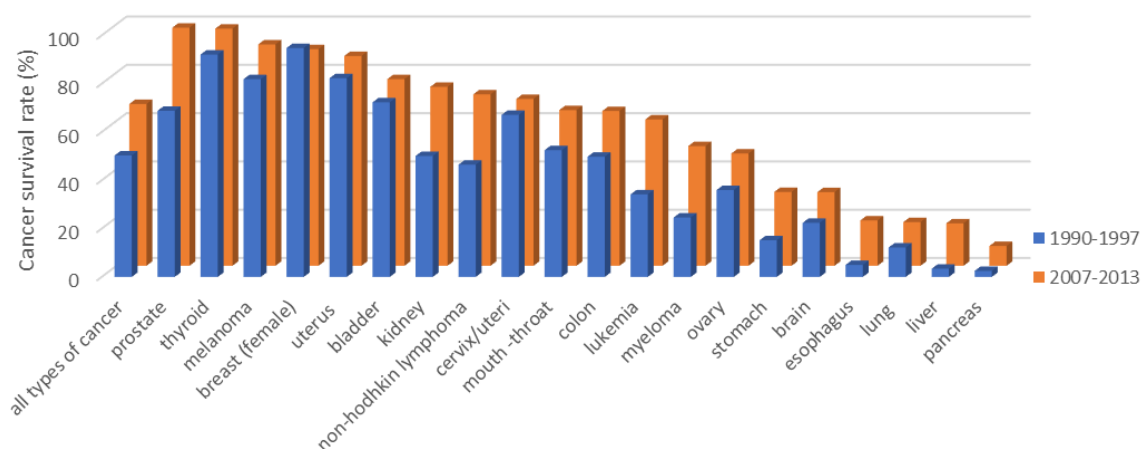


**Figure 1-1.** Profile of five-year cancer survival in the USA, shown as the rate over the period 1970-1977 (blue bars) and 2007-2013 (orange bars). This indicates the percentage of people who live beyond five years following the diagnosis. Data were reproduced from the WHO report<sup>1</sup>.

Recent decades have seen significant advancements in cancer diagnosis and treatment. As, in contrast to 50 years ago, the chances for 10-year survival with the most common types of cancer have doubled<sup>2,3</sup>. This achievement is chiefly due to recent advances in the early detection of tumors<sup>4-11</sup> and the far greater availability of screening tests<sup>12</sup> (**Figure 1-1**). Currently, in clinical practices, molecular identification of tumors is pivotal for better navigation toward a more

effective treatment. Tissue biopsies are the current gold-standard methods to achieve such molecular landscapes. However, they are invasive, as they require surgical extraction and are mostly non-ideal for long-term monitoring. As they are sometimes not feasible in the case of worsened clinical conditions and not practicable for tumors that lack accessibility which can further compromise the treatment, particularly concerning those cancers whose five-year survival index is very low such as pancreatic cancer (6%); oesophageal cancer (13%); and lung cancer (16%)<sup>13</sup>. Aggressive types of breast cancer, esophageal and liver cancers are also characterized by low five-year-survival rates - approximately less than 20%<sup>14</sup> (**Figure 1-1**) Alternatively, tremendous efforts have been put toward developing robust and non-invasive or minimally-invasive complementary methods referred to as liquid biopsy<sup>15-18</sup>. The latter, as opposed to solid biopsy, is a simple, fast, and informative technique that is based on the identification of specific species (biomarkers) in the blood (physiological fluids). During the apoptosis and necrosis of tumor cells, these biomarkers are released into the bloodstream, facilitating and promoting metastatic activity in nearby and/or distant organs<sup>19</sup>. Developing an efficient method for biomarker analysis is currently one of the most challenging problems in cancer diagnosis research<sup>20-23</sup>. Molecular biorecognition elements (antibodies, enzymes, and oligonucleotides) with a characteristic affinity towards such cancer biomarkers in physiological biofluids (blood, serum, plasma, urine, and saliva) account for the most crucial components in such developments.

Current analytical approaches are multistep, relying on preparation steps as well as chemical separation and isolation such as Western blots, ELISA, and other immunochemical methods<sup>24</sup>. Although these techniques have proven enormously useful; they are essentially laboratory-bound approaches, and therefore ill-suited for real-time or in Vivo applications. To overcome these limitations, a number of methods have been developed to detect real-time target binding based on

surface-bound biorecognition elements by monitoring changes in mass (quartz crystal microbalance, QCM)<sup>24</sup>, charge (field effect transistors, FET)<sup>25,26</sup>, refractive index (surface plasmon resonance, SPR)<sup>27-28</sup>, and /or steric hindrance (electrochemical impedance spectroscopy, EIS)<sup>29-30</sup>. Unfortunately, however, these techniques suffer from a serious disadvantage. As the core of these changes relies on target adsorption rather than specific binding, they cannot distinguish authentic targets from that of non-specific adsorption which limits their utilities in complex environments like blood or serum. Alternatively, electrochemical sensors may circumvent these limitations.

Electrochemical detection offers unprecedented sensitivity (can reach down to pM) and unique modularity (consistent/applicable with all ranges of biorecognition elements). These inherent attributes account for the fact that more than half of biosensors mentioned in the literature use electrochemical transducers. An electrochemical biosensor can be defined as a tool bearing two or more of the following parts: substrate for immobilization, linker, biorecognition elements, signal receptor, signal amplification component, and signal transducer. Among these, two parts are the most indispensable the biorecognition element and the signal transducer (**Figure 1-2**). The biorecognition element enables specific target detection with high selectivity, and the signal transducer translates the specific molecular interactions into a measurable physical quantity. In an electrochemical biosensor, the electrode functions as the transducer upon which, i.e., in the interfacial region, the electrical changes triggered by the protein binding to the biorecognition element are controlled and measured.

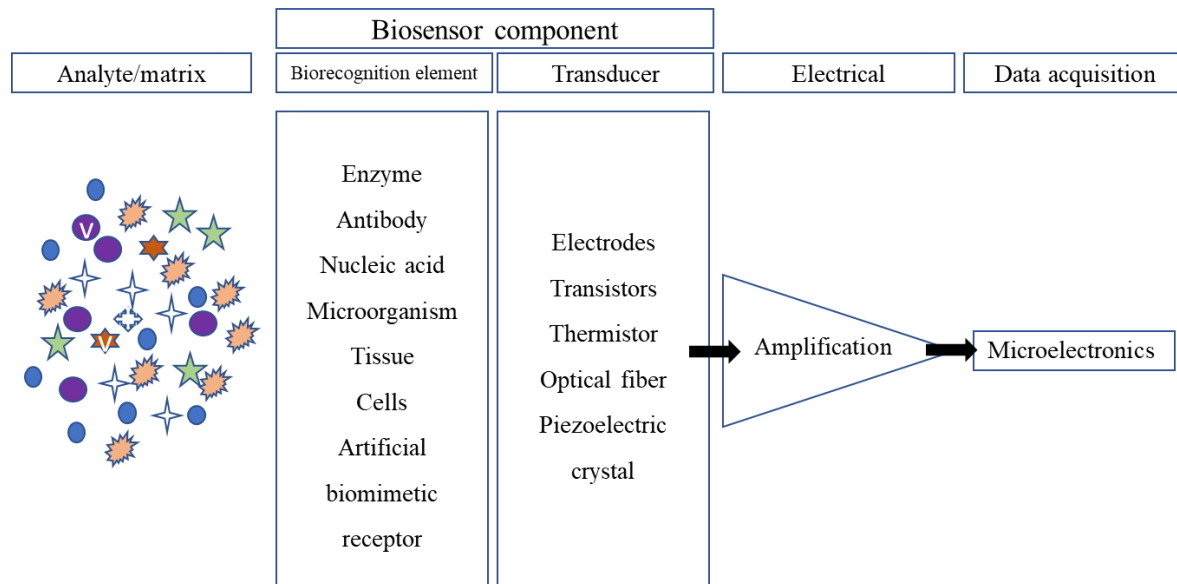


**Figure 1-2** Principle of biosensor operation.

Recently, a new class of biorecognition elements- short oligonucleotides termed aptamers- has emerged, and have been shown to be promising alternatives to the conventional recognition elements (enzymes and antibodies)<sup>31-33</sup>. Different attributes of antibodies and aptamers are summarized in **Table. 1-1**.

**Table. 1-1** Compilation of properties and comparison between aptamer and antibodies. Reproduced from<sup>34</sup>

<b>properties</b>	<b>Antibody</b>	<b>Aptamers</b>
Generation and synthesis	In Vivo selection Selection process cannot be tailored on demand.  Produced in animals or by recombinant technology. Difficult to raise antibodies against non-immunogenic entities.  High cost of production. Batch-to-batch variation.	In Vitro Selection Selection process can be tailored as per need  Chemically synthesized in Vitro conditions. Can be developed against non-immunogenic entities.  Economical cost of production. Negligible batch-to-batch variation.
Stability	Requires stringent storage conditions.  Low shelf life.  High susceptibility to change in pH, temperature, and ionic concentrations. Stability cannot be increased.	Can withstand a range of storage conditions.  Higher shelf life.  Relatively immune to changes in pH, temperature and ionic concentrations. Stability can be improved.
Modification, specificity and affinity	Comparable specificity and affinity with aptamers.  Affinity and specificity can be tailored.  Modification is challenging. Or not possible.  Difficulties in immobilization.	Comparable specificity and affinity with antibodies.  Affinity and specificity can be tailored on demand.  Amenable to modifications.  Immobilization is comparatively easier.
Structural switching	On binding to its target, the antibody does not undergo target-induced structural change.	Aptamers can easily undergo a target-induced structural change.

Aptamers are attractive biorecognition elements in biosensor technology. Their utilization for electrochemical detection has revealed characteristics that have made them not only indispensable tools in laboratory-based investigations but also turned them into market-viable techniques.

Attributes such as very simple instrumentation and miniaturization (suitable for implantable biosensors), cost-effectiveness (highly cost-competitive), and portability (suitable for field monitoring applications) are notable as desirable elements. In the DNA/RNA-based sensors, the interaction between the target and the aptamer (biorecognition element) is not based on the specific chemical reactivity but rather on a unique three-dimensional (3D) conformational change that is induced by specific atomic/molecular interactions. This recognition approach puts an onerous design challenge in the importance of interfacial design and molecular architecture. The relative spatial arrangement in the target-aptamer complex determines the class of targets which are broadly fallen into two categories - embedded group and outside-binding group. Most often targets are found buried in a specific pocket, formed by special oligonucleotides sequence of aptamers, belonging to the embedded group, such as ATP <sup>35</sup>, cocaine <sup>36</sup>, K<sup>+</sup> and, theophylline <sup>37</sup>. Here the design strategies are mostly based on the concept of target-induced conformational changes of the surface-bound aptamers, which lacks complexity. In the case of larger and more complex molecules, like proteins and oligonucleotides, because of the higher number of binding sites, there are more diverse design strategies. Proteins such as thrombin <sup>38</sup>, and platelet-derived growth factor-BB (PDGF-BB) <sup>39</sup>, are most often categorized under the second class (outside-binding group) for which the interfacial design is even more challenging. So far, these strategies can be divided into four major groups/modes including (a) target-induced structure switching mode; (b) target-induced dissociation or displacement mode; (c) sandwich structure mode; and (d) competitive replacement mode (**Figure 1-3**). E-AB sensors based on structural switching mode achieve their detection by relying on changes in electron transfer efficiency between surface-bound electrochemical tags and

the electrode. This mode forms the most important, yet basic strategy in the fabrication of E-AB sensors which in turn largely suffers from signal amplification and signal-to-noise ratio (**Figure 1-3 A**). Inspired by this, other interfacial strategies have been reported to address such frailties. For example, the target-induced dissociation strategy (**Figure 1-3 B**) affords higher signaling capability as it manages to hinder random stand fluctuations<sup>35</sup>. In sandwich structure mode (**Figure 1-3 C**), as inspired by ELISA, one can observe a more pronounced precision in the detection of the target, particularly, when complex biological fluids are analyzed<sup>36</sup>. Lastly, in the competitive replacement interfacial design (**Figure 1-3 D**), a readily electrochemical signal transducer can afford a very simple and sensitive readout<sup>38</sup>.

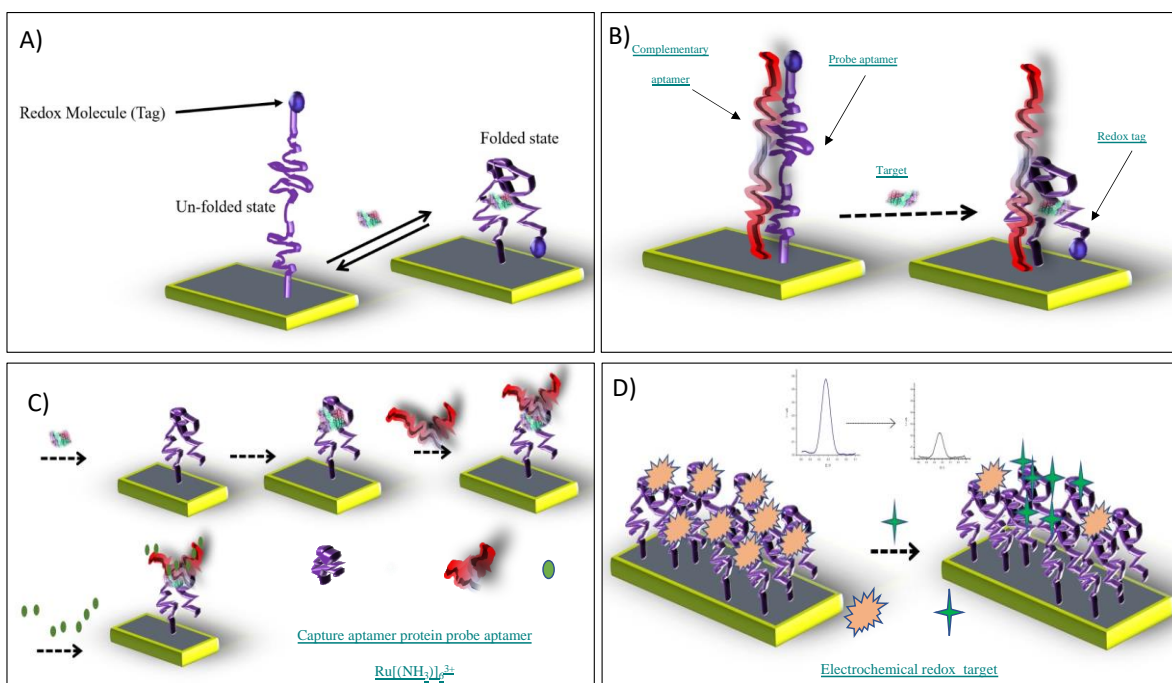


**Figure 1-3.** Various interfacial modes in signal generation in DNA/RNA-based sensors. (A) target-induced structure switching mode; (B) target-induced dissociation or displacement mode; (C) sandwich structure mode; (D) competitive replacement mode.

Fundamentally, the source of all signal changes, and hence the sensitivity of the assays, lies in the attributes and quality of the interfacial region, where the surface of the electrode (transducer) and the biorecognition element (aptamers) meet. A successful biosensor design critically depends on the strategy adaptation in the engineering of interfacial molecular organizations. To develop a sensing platform to be qualified for utilization in liquid-biopsy routine monitoring, there is a need to master the art of interfacial engineering. The scope of this review is to provide an objective perspective of the functional parameters to fabricate DNA/RNA sensors- particularly E-AB sensors. Subsequently, we will focus on recently adopted interfacial design and engineering in breast cancer-oriented E-AB biosensors to demonstrate how their utilization can benefit the application.

## **1.2 E-AB sensors**

### **1.2.1 Basic principles**

The only reagentless, quantitative biosensor that has garnered vast commercial success, so far, has been the household, and portable glucose biosensors<sup>40</sup>. Given that the field of biosensors is still in its early stages most concepts have failed translational from in Vitro laboratory studies to in Vivo preclinical research and face important challenges before being ready for widespread adoption and clinical application. Therefore, it is encouraging to briefly examine the principles underlying the success of glucose biosensors. The most important key to their success is the production of a readily measurable by-product that is detected unambiguously against the background. In addition, the reaction is enzymatically catalyzed and thus naturally associated with signal amplification. Furthermore, that reaction relies on target-binding-induced chemical evolution instead of specific chemical reactivity, which accounts for a key element that makes them well-suited even in contaminated samples like blood, as the enzyme-target complex is less

likely to be disrupted. In nature, the chemosensing phenomena rely on biomolecular switches - biomolecular equilibrium between two structural conformations, a process in which a special biomolecular output (biological signal) is brought about by binding-induced changes in conformation or oligomerization (be it a protein or nucleic acid). These natural biosensors enable real-time, continuous target monitoring in highly complex environments. Motivated by such phenomena, significant efforts have been invested in adoption of such switches into the construction of artificial biosensors, for which DNA/RNA aptamers have shown the capability to partially fulfill this goal.

With the publication of the first E-AB sensor on thrombin detection by Xiao and Plaxco<sup>41</sup>, a new research concept was born. The reversible action of nucleic acid aptamer, which binds to target molecules with high affinity<sup>42-44</sup> was seen as an important leverage for both target detection and signal transduction. This came after the realization that some biomolecules fold upon binding to their complementary targets, and therefore can link recognition power to signal to transduce. Single-stranded DNA (ssDNA) for example is fully flexible in motional dynamics, in that it is unfolded in the absence of its target (e.g., complementary strand), which, in turn, folds into a rigid well-structured double helix upon hybridization (or vice-versa)<sup>45,46</sup>. The authors immobilized the thiolated functionalized aptamers, via self-assembled monolayers (SAMs). Aptamers were covalently labeled with a redox molecule to induce electrochemical signal upon conformational changes. This is a mechanism that mimics the behavior of naturally occurring chemoreceptors in our body<sup>47,48</sup>. Beyond achieving specific molecular detection, E-AB sensors enable detection of any arbitrary target for which the aptamer is available<sup>48</sup>. This was an unprecedented achievement in the field of electroanalytical chemistry, as previously only potentiometry or direct

electrochemical/biocatalytic measurements<sup>49</sup> relying on specific chemical activity would enable specific target measurements in complex environments.

### **1.2.2 E-AB signal and the gain**

In E-AB sensor development, the signal gain, which is defined as the signal changes before and after target introduction divided by the initial signal,  $\left(\frac{I_0-I}{I_0}\right)$ , is critical. As opposed to absolute signaling current, the signal gain has the advantage of normalizing for differences and thus serves well for comparison of different E-AB sensors regardless<sup>50</sup>. Furthermore, signaling gain is a strong function of the sensor architecture, the electrochemical interrogating parameters, and the sample matrix. More specifically, the surface organization of the monolayer, the secondary structure of the aptamer, and the inherent electron transfer rate of the electrochemical tag, all affect the signaling gain<sup>50</sup>. This impact is usually justified by changing the time constant of electron transfer between the electrochemical tag and the electrode surface. since the signal is measured electrochemically, changes in time constants (bound and un-bound aptamers) must be matched by the frequency of the electrochemical method employed. In this section, parameters controlling the chemical and physical nature of the sensor interface, which determine the performance of the E-AB sensor will be thoroughly discussed.

### **1.2.3 Probe packing density**

The probe packing density accounts for the most readily observable variable during optimization process toward highest gain and/or best performance. Several studies have been performed to elucidate the effect of packing density on E-AB sensor performance. In 2001 Georgiadis and his co-workers<sup>50</sup>, explored the DNA surface density based on the kinetics of target capturing using surface plasmon resonance (SPR). They studied the role of electrostatic forces among double-

stranded DNA (dsDNA), and single strand DNA (ssDNA) as a function of the probe density and the kinetics of monolayer film formation<sup>50</sup>. In this work, the kinetics of monolayer film formation showed to have a more pronounced effect on packing density and that ssDNA exhibited greater kinetics and higher density in surface coverage. They demonstrated that the probe density strongly affects target hybridization efficiencies, with a higher density value leading to lower hybridization efficiency<sup>51,52</sup>. This was later confirmed by Benight and co-workers<sup>53</sup>. They chose two targets: cocaine and thrombin, to show the effects of surface density in the signaling gain. In the case of cocaine, low probe density exhibited the highest gain, while an intermediate density for thrombin achieved the best signal gain. This discrepancy was attributed to the probe-probe spacing characteristic between aptamers as a function of their spatial size<sup>54,55</sup>. For the cocaine<sup>56,57</sup>, a diminution of frictions and lower steric hindrances, which in turn, allows higher freedom in structural changes, was justified. Whereas the negative effect of high packing density seen for thrombin, was explained by the reduction of target affinity due to an over-crowded surface at higher densities. It was, however, confirmed that the controlling of probe aptamer concentration during sensor fabrication, was shown to successfully control the surface density of DNA molecules across an order of magnitude<sup>50</sup>. Motivated by such phenomena, Barton and co-workers<sup>58</sup> demonstrated a totally new approach in controlling the probe packing density via in-situ electrochemical activation of copper (II) catalyst for Huisgen 1,3-dipolar coupling between the aptamer and the backfilling agents<sup>59</sup>. Up to now, this protocol has been proven to offer the best tool for the control of surface packing density, and hence the probe-probe spacing.

Given the negative charge of the phosphate backbone of the DNA, the ionic strength can strongly affect the adsorption behavior of the probe aptamers and ultimately the E-AB signaling. Sykes and his co-workers<sup>60</sup>, for example, recently reported that ionic strength, or more precisely dielectric

permittivity of the solution heavily influences the spatial conformation surface bound DNA sequence. They demonstrated that decreasing permittivity causes alteration in distance between distal termini redox reports and the electrode surface, thereby altering the reporter's electron transfer rate. Similarly, decreasing the ionic strength will result in an increase in the electrode surface-DNA backbone interactions which in turn alters the relative proximity between the redox molecule and the electrode surface, impacting the rate of electron transfer <sup>61</sup>. The matrix composition, for example, in the presence of stabilizing cations has been shown to influence the performances of the E-AB sensors <sup>62</sup>. Considering that the aptamer's structure is altered by the concentration and presence of certain ions in the matrix, the relative position of the redox reporter with respect to the electrode surface will be affected, thus influencing the electron transfer kinetics of the platform. Xiao et al <sup>63</sup> investigated the dependence of signal change of thrombin E-AB sensors based on the ionic strength and composition. They determined that at a high ionic strength (e.g., 300-mM Tris base, 420-mM NaCl, 60-mM KCl, and 60-mM MgCl<sub>2</sub>) the apparent binding affinity of an E-AB sensor for thrombin is 50 nM. At the opposite, at low ionic strength, without the presence of potassium (100-mM Tris base), the sensor exhibits an apparent binding affinity of 21 nM with an increase in sensitivity as well <sup>63</sup>. Without potassium, the aptamer is unfolded and thus likely exhibits a larger conformation change in the presence of thrombin, which leads to better sensitivity.

Overall, packing density is perceived as one of the most critical parameters that controls the signal gain of the E-AB sensor. being the characteristic of the 3D organization of the monolayer and the aptamer-target complex, it must be optimized for each single target to ensure the best performance.

### 1.2.4 Backfilling agents and surface homogeneity

Since chemisorption of thiols to the gold surface is an oxidative process by nature, the application of positive potentials has shown promise for enhancing the quality of adsorption in terms of homogeneity and packing density<sup>64,65</sup>. Ma and Lennox reported a faster kinetics while featuring far fewer defects for surface coverage in preparing a mixed-composition SAM via alkanethiol deposition on gold by the application of constant positive potentials versus the assembly resulted from open circuit potential (OCP)<sup>66</sup>. Another study showed the influence of the applied potential<sup>67</sup> on the gain with a mixed SAM of fluorophore-labeled DNA and alkylthiol. They showed that a positive applied potential ( $>0$ /SCE) resulted in ten times higher density compared to deposition at the open circuit potential (OCP) over the same 60 min time-period (**Figure 1-4**) Similarly, it was demonstrated that pulsing the potential in the course of thiolated aptamer SAM formation, led to faster DNA monolayer formation when compared to constant potential<sup>68,69</sup>.

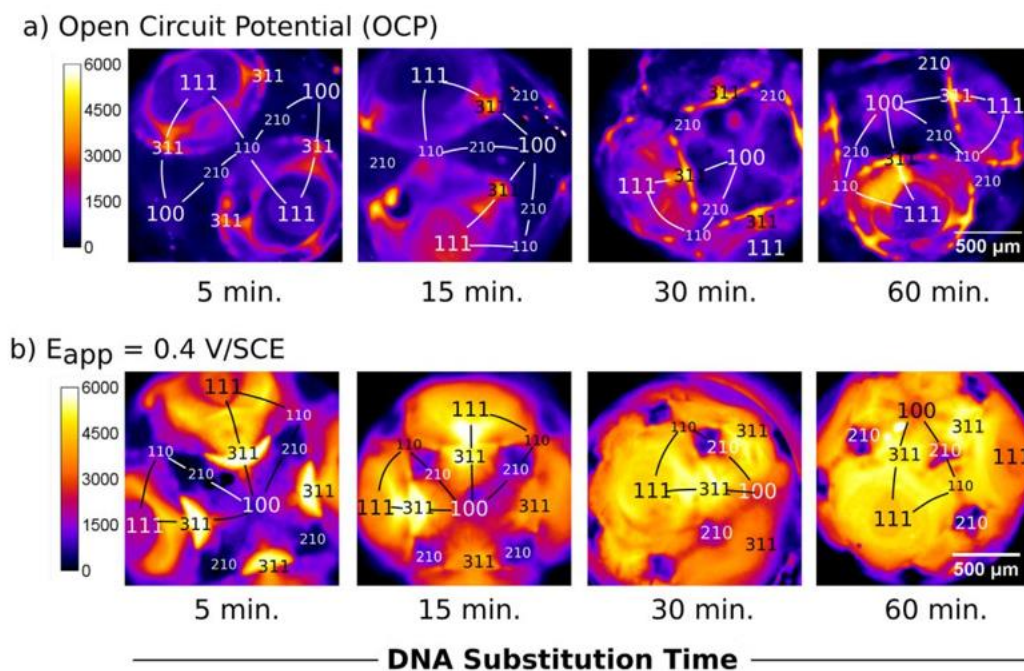


**Figure 1-4.** Fluorescence images taken of MCH/DNA layers prepared a) at OCP (no applied potential) and b) at  $E_{app} 0.40$  V/SCE. Images from left to right correspond to increasing time in the deposition solution. Each image is from a different electrode resulting in a different orientation. The stereographic triangle and crystallographic regions analyzed are shown on the images. All images are false colored to represent intensity. Reproduced from <sup>67</sup>.

Another approach based on chemisorption was used to assemble thiol-terminated single-stranded DNA (HS-ssDNA) onto a gold surface, mixed with a short hydroxyl-terminated alkyl thiol surface diluent (e.g., mercaptohexanol (MCH)) <sup>70-72</sup>. The effect of diluent combined with passivation time on surface composition, density, and orientation of HS-ssDNA oligomers was studied by utilizing X-ray photoelectron spectroscopy (XPS), near-edge absorption X-ray absorption fine structure spectroscopy (NEXAFS), and the fluorescence intensity measurements. It was concluded that longer diluent exposure times (namely >2h) promote the displacement of the DNA molecules on the surface, and that, the DNA aptamer strands in the backfilled surface tend to be more perpendicular to the surface <sup>73</sup>. Therefore, the molecular orientations of immobilized DNA can be easily manipulated via their surface densities, MCH diluent addition, and varying exposure time.

### 1.2.5 The length and the chemistry of the backfilling agents

The length and the charge (chemistry) of SAM comprised of the alkanethiol backfilling agents have been shown to impact the E-AB signaling behavior (**Figure 1-5**). Ricci et al <sup>74</sup> conducted one of the first studies to explore the impact of the alkanethiol length and charge of the SAM passivation layer on the E-AB sensor performances. They observed that the best signaling gain was obtained for an intermediate length of C<sub>6</sub>-OH compared to short (C<sub>2</sub>-OH,) and long (C<sub>11</sub>-OH). A short length of C<sub>2</sub>-OH was associated with enhanced random collision dynamics for probe-target duplex whereas the C<sub>11</sub>-OH co-adsorbate was long enough to reduce the collision efficiency for the single-stranded probe.

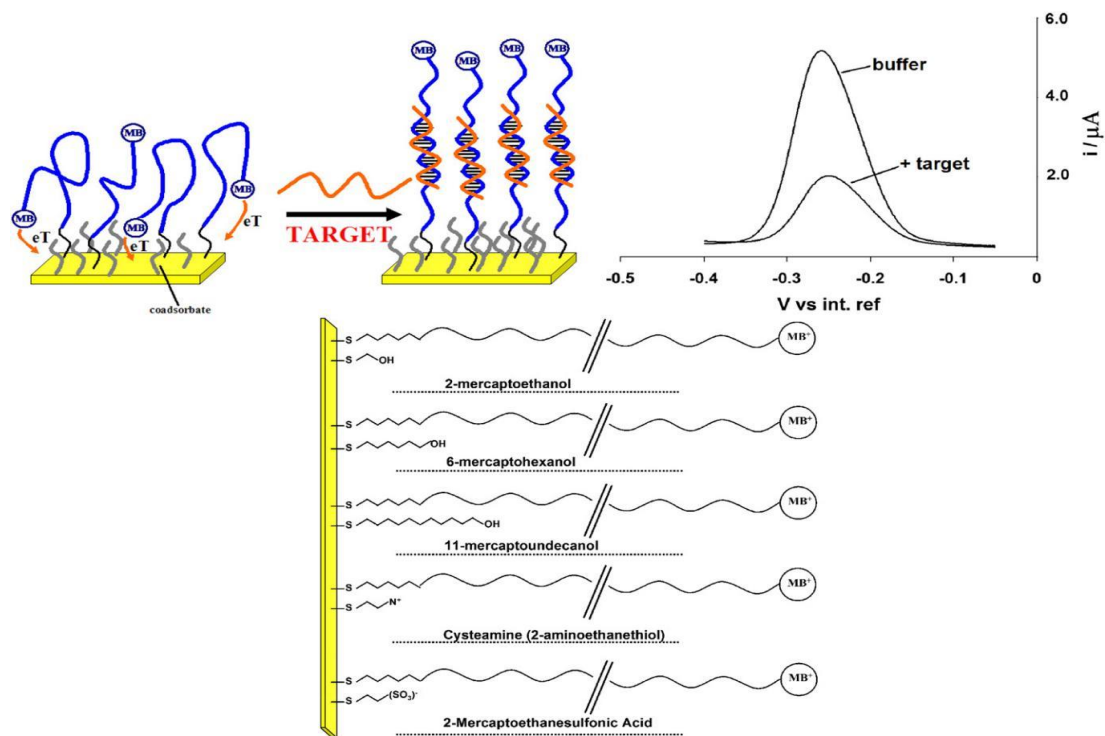


**Figure 1-5.** E-AB sensor fabrication and varying lengths of co-adsorbates: Here the authors have employed linear probe (top left) as a test bed with which to characterize the effects of surface chemistry on the properties of an E-AB sensor. Because hybridization reduces the rate with which the terminal redox tag collides with the electrode surface and transfers electrons the Faradaic current arising from such linear probes is significantly reduced in the presence of a complementary target sequence (top, right). It is thus likely that this suppression and the motion of the unbound and bound probe will be linked to the nature, steric hindrance and charge of the co-adsorbate used for sensor fabrication. They have tested the effects of a range of thiol co-adsorbates (bottom) differing in their length and/or terminal functional groups and chosen to cover a range of charges and steric effects (bottom). Reproduced from <sup>74</sup>.

An additional challenge that directly affects the E-AB signaling is related to the terminal charge (chemistries) of the SAM. This effect was studied using different terminal functionalities - e.g. hydroxyl, amine, and sulfonate groups (**Figure 1-6**)<sup>74</sup>. It was observed that both amine and sulfonate groups on C-2 monolayers produced the highest signal gain with saturating concentrations of target. Interestingly, the surface stability, though only tested in static solutions, was enhanced with short amine-terminated monolayer, due to the electrostatic interactions between positively charged amine group and negatively charged DNA backbone. Furthermore, the extent, to which an E-AB sensor can withstand a physiological environment such as blood, before

they lose their functionality over the formation of a non-specific adsorption layer, is defined as the biocompatibility of the sensor. The biocompatibility of the surface of E-AB sensors is another area that can be, at least partially, managed through the application of suitable SAM alkanethiol. Whiteside et al <sup>75</sup> have extensively studied the impact of different alkylthiol monolayer on surface bio-fouling against fibrinogen and lysozyme proteins via surface plasmon resonance spectroscopy (SPR). Here, a single component SAM alkanethiol layer carrying single charge (either positive or negative) resulted in a full monolayer formation of surface fouling proteins, whereas a monolayer constituted from a mixture of two opposite charges acquired less than 1% monolayer of such proteins<sup>75,76</sup>. This result opened the door to the use of zwitterionic monolayer of phosphatidylcholine terminal groups for the fabrication of E-AB sensors <sup>76, 77</sup> and led to improved signaling in blood despite a strong sensitivity to pH and ionic strength variations<sup>78</sup>. However, since their long-term stability, tested in continuous electrochemical applications, has not been reported, and owing to the fact the acknowledges the progressive desorption of charged monolayers from E-AB sensors<sup>78</sup>, more substantial works need to be done to identify a suitable monolayer that affects stability as well as biocompatibility.

It should be noted that, despite many endeavors in the assessment and identification of an ideal backfilling agent, 6-mercaptohexanol (C<sub>6</sub>-OH) constitutes the most widely used SAM for surface passivation.

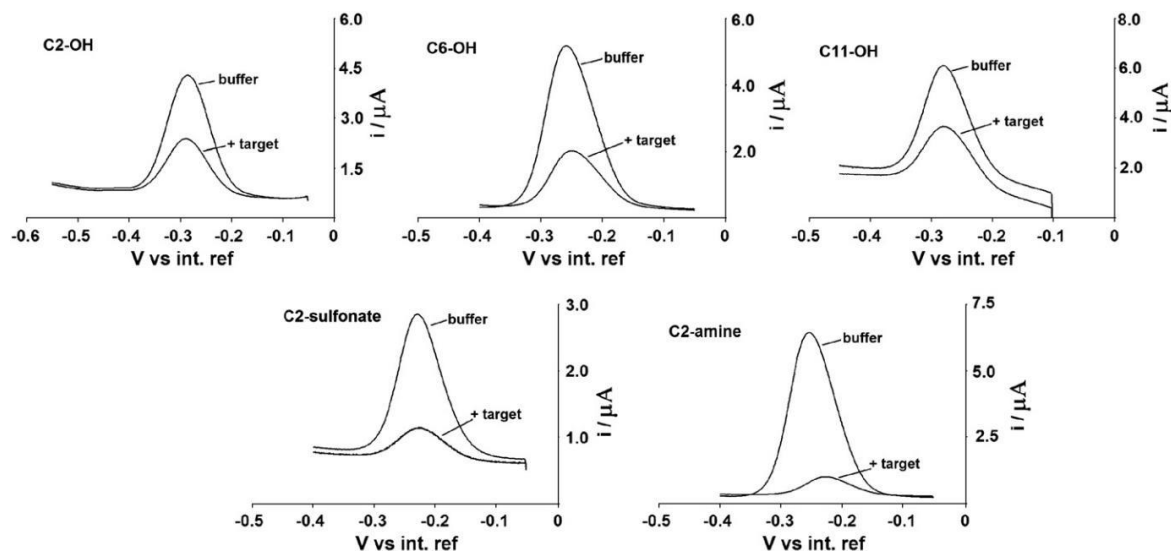


**Figure 1-6.** Co-adsorbate effect on E-AB sensor signaling behavior: Because E-DNA signaling is linked to a binding-specific change in the collision efficiency of the probe-bound redox tag with the electrode surface, the nature (i.e., length and charge) of the co-adsorbate used for sensor production is a determining factor in the performance of E-DNA sensors. Shown are SW voltammograms of sensors fabricated with each of five co-adsorbates before and after the addition of the relevant 17-base target. here, they find that, among the thiols tested, the positively charged C2-amine (cysteamine) gives rise to the largest and most rapid response to target. Reproduced from <sup>74</sup>.

### 1.2.6 The length of the aptamer

DNA length is another fundamental variable that will impact the organization of surface bound DNA layers. In 2000 Tarlov et al examined the influence of oligonucleotide's length on the surface coverage and the corresponding desorption capacity<sup>79</sup>. The findings indicated that the thiol anchoring DNA strongly enhances the immobilization capacity. Moreover, they observed that surface density for shorter strands was higher than longer ones <sup>80-82</sup>. Similarly, the desorption phenomenon is more pronounced as the DNA length increases. Short and long ssDNAs assembly models on the surface are represented in **Figure 1-7**. A higher surface density was anticipated with organized alignment and rod-like configuration for short strands, whereas the longer strands were expected to exhibit a low density with flat configuration and multiple contacts with the substrate.



**Figure 1-7.** Cartoon of two packing configurations for ssDNA probes at a surface with a sticky end-group for specific immobilization. Short probes are envisioned to pack in extended configurations. Longer probes are expected to exist in more flexible, polymeric-like configurations. Reproduced from <sup>79</sup>.

They concluded that oligonucleotides shorter than 24 bases are not strictly length- dependant and therefore organize surface density nearly independent of length variations. Furthermore, the associated surface density, in this regime, reaches to maximum due to the rod-like surface organization. On the other hand, in the case of longer oligonucleotides, surface density is more impacted by the length as the polymeric nature of the strands start to present themselves.

### 1.2.7 The redox reporters and stability

Given the small electrochemical window available on a gold electrode, the number of functional redox labels to be utilized in E-AB sensors is limited. Electrochemical behavior of most relevant redox molecules that can be used as a label candidate has been illustrated in **Figure 1-8** <sup>83</sup>. To date according to the literature, widely used reporters are methylene blue<sup>84</sup> ( $E^{\circ'} = -260$  mV vs. Ag | AgCl), and anthraquinone ( $E^{\circ'} = -440$  mV vs. Ag | AgCl) <sup>85</sup>. These two molecules can undergo a reversible two-electron and one proton electrochemical reactions. One caveat of these redox labels is that their electrochemical functioning (redox potential) alters with varying pH <sup>86</sup>. For example, their application in biological fluids with fluctuating pH like sweat will meaningfully influence their electrochemistry, and thus affecting E-AB signaling current. Ferrocene ( $E^{\circ'} = +220$

mV vs. Ag | AgCl) in contrast exhibits a pH-insensitive one-electron transfer reaction but can be chemically affected by pH<sup>87</sup>. More importantly, it has been shown that the oxidized ferrocenium form is susceptible for nucleophilic reaction with even weak nucleophilic agents like chlorides which are normally abundant in biological fluids<sup>88</sup>. Furthermore, as far as the protein and corresponding charges are concerned, the application of positive potential on ferrocene may increase the non-specific adsorption and contribute to the gold surface etching<sup>89</sup>. For these reasons, the use of ferrocene not recommended in common E-AB sensor fabrication<sup>90</sup>. Anthraquinone provides good chemical stability particularly in chloride media, but has a reduction potential that overlaps with the onset of oxygen reduction on gold<sup>83</sup>. Methylene blue, unlike ferrocene and anthraquinone, undergoes an electrochemically stable electron transfer reaction and has a reduction potential distinct from background electrochemical processes<sup>83</sup> the only compromise that needs to be taken into account is the pH variation control to ensure reproducibility in its electrochemical behavior.

Signal drifting is one of most common characteristics of the redox molecules used as reporters regardless of the matrices whether it is simple buffer or human serum. Recently, a survey on a large set of potential redox reporters (more than a dozens) was conducted jointly by Ricci and Plaxco<sup>83</sup> in order to find out which one demonstrates long-duration stability. Their work demonstrates that the performance of methylene blue-based E-AB sensor is unmatched where the sensor's stability against repeated scanning even in complex environments was significantly superior to its alternatives (**Figure 1-9**), and so, has proven to be the most commonly used reporter in the fabrication of E-AB sensors<sup>84</sup>.

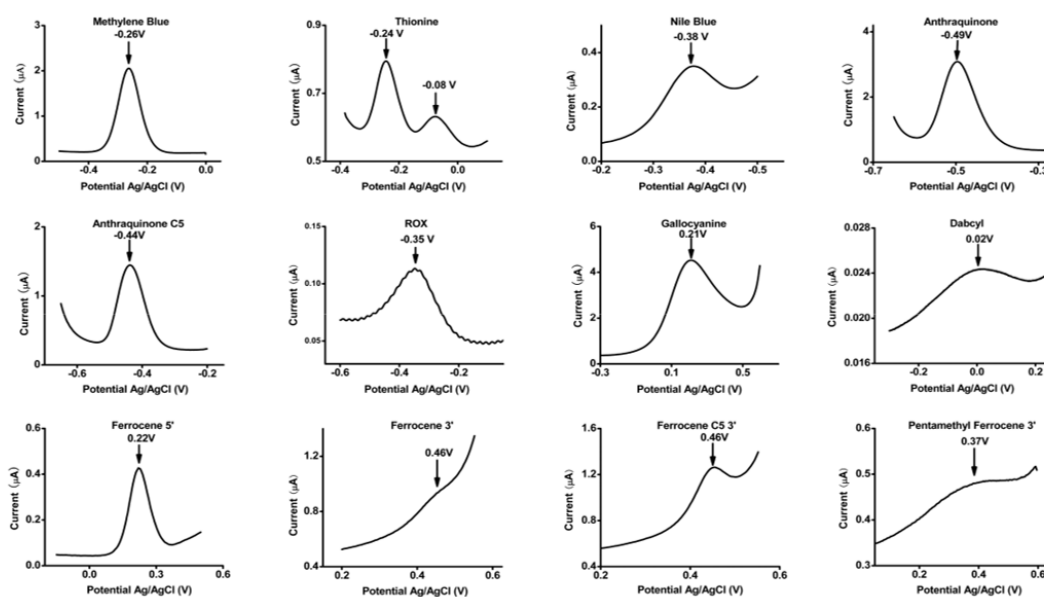


**Figure 1-8.** electrochemical behavior of different redox candidate. As one can see, Dabcyl and ROX, for example, fail to produce clear oxidation and reduction peaks when conjugated to DNA and interrogated using standard square wave voltammetry parameters, and thionine exhibits two peaks in the relevant potential window. In case of ferrocene, three ferrocene-containing constructs were employed: one in which the ferrocene is conjugated directly on to an amine appended to the 5' end of the DNA, a second in which the ferrocene is conjugated directly on to an amine appended to the 3' end of the DNA, and a third, ferrocene C5, in which there is an additional spacer between ferrocene and the amide linkage to the DNA. The highly sloping baselines observed at potentials below  $-0.5$  V and above  $0.5$  V (vs Ag/AgCl) are due to the reduction of oxygen and the subsequent generation of reactive oxygen species (at low potentials) and the oxidation of gold (at high potentials). These same effects cause significant degradation of the thiol-on-gold SAM; that is, some redox reporters fail because they, themselves fail, and others fail because they report at potentials at which SAM stability is poor. Reproduced from <sup>83</sup>.

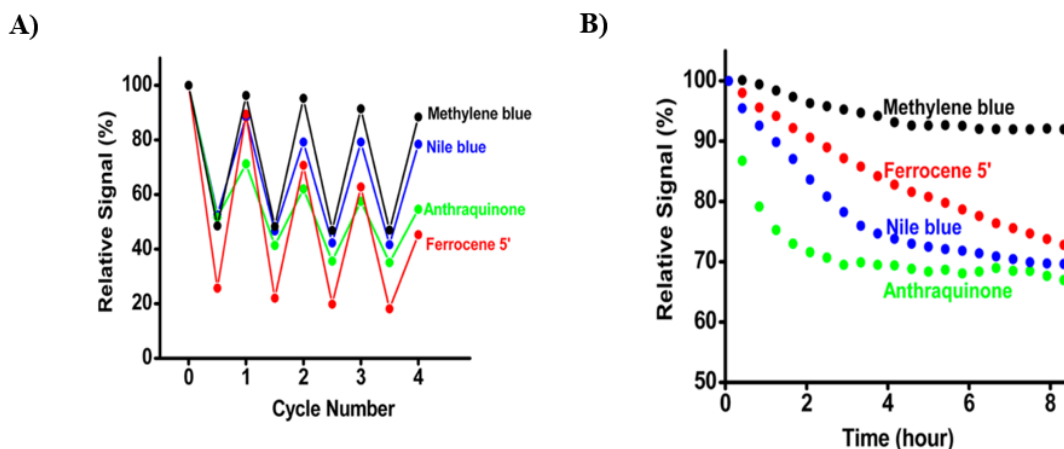


**Figure 1-9.** (a) Sensors fabricated with methylene blue, ferrocene, anthraquinone, or Nile blue exhibit similar signal gain in response to target binding whether deployed in simple buffer solutions or in 20% blood serum. (b) They all drift significantly, however, when repeatedly scanned in 20% serum over the course of hours, with methylene blue exhibiting the least drift. (c) Methylene blue-based sensors are likewise the most stable when the sensors are challenged with multiple cycles of hybridization (with saturating target) and regeneration (via di-water wash) in 20% blood serum. Reproduced from<sup>83</sup>.

The mechanism of target-induced signaling in E-AB sensors is based on the collision frequency of the redox tag and the electrode surface<sup>91</sup>, consequently it seems to be reasonable to argue that the spatial position of the redox reporter within the DNA strand should be critical in its signaling behavior. To elucidate this, Lai et al<sup>92</sup> carried out a detailed quantitative comparative experiment based on three aptamer probes each labeled with methylene blue in the distal end, middle, and proximal end (**Figure 1-10**). They examined the sensor stability, the detection limit, the reusability, and the selectivity and were able to show that a redox reporter positioned at the distal end of the aptamer probe generated the best performances for this sensor design without interfering with monolayer formation and target binding. Furthermore, they argued that the internally conjugated methylene blue is not advantageous as it not only affects the probe structure but also imposes a potential interference in target binding. Therefore, the proximal attached

methylene blue tends to negatively impact the monolayer formation, which can compromise the stability thereby the performances of E-AB sensor.

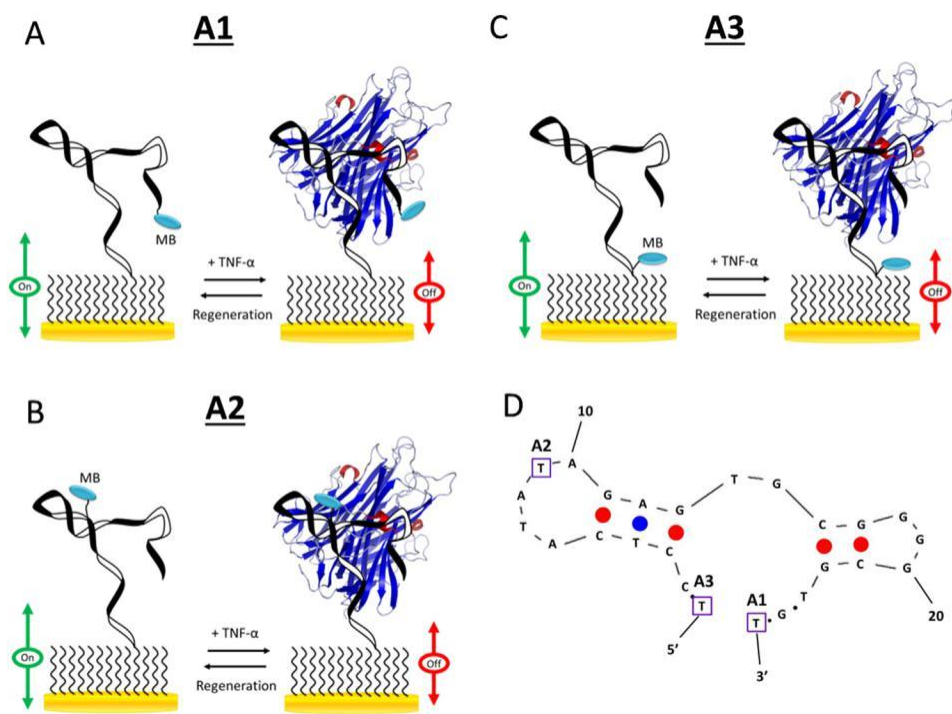


**Figure 1-10.** (A–C) Schematic illustrations of the three E-AB sensors. (D) The optimal (minimum energy) structure of the aptamer predicted by Mfold under the following conditions: 0.1 M Na(I), 22 °C. Also included are the locations of the MB redox label in the three different sensor architectures. Reproduced from <sup>92</sup>.

### 1.3 Operational parameters

The signal changes upon target binding are not only dependant on the sensor fabrication but also are impacted by the electrochemical methods parameters. Given that the motional dynamics and the change in dynamics of the probe aptamer play a pivotal role in the signaling current behavior, it is reasonable to argue that the time scale of the voltametric interrogation is a key parameter to the sensor optimization and fabrication<sup>91</sup>. Most of the techniques featuring frequency element in their current data acquisition including cyclic, alternating-current (ACV), square-wave voltammetry (SWV), and differential-pulse voltammetry are all suitable methods for monitoring

aptamer conformation changes and the resulting changes in corresponding charge transfer rate. The signal evolution from E-AB sensor involves two different striking dynamics (bound and unbound states) which is disturbed with target binding. E-AB sensors will have an optimum interrogation frequency range where the measured current exclusively originated from the faradic conversion of aptamer-bound reporters<sup>93</sup>. At interrogation frequencies below 10 Hz, the current evolution is sensitive to non-faradic currents originating for example from side reactions from metal impurities or gases (e.g., the reduction of oxygen) and vibrational or electronic noise. At frequencies higher than 1000 Hz the contribution of the double layer<sup>94</sup> and electronic noise are more pronounced<sup>95</sup>. As shown in the **Figure 1-11**, plotting the peak current/frequency vs log frequency before and after target addition gives a map that helps navigation of the optimal interrogation frequency where the current is solely acquired from the bound and unbound probe electrons transfer. Here it shows a maximum electron transfer rate of 60 Hz for the unbound and of 500 Hz for target-bound states of the E-AB sensor<sup>93</sup>. Therefore, the development of a map, in which the signal gain is plotted against large ranges of interrogating frequencies is highly recommended which allows one to identify the frequency range that achieves the largest signal difference between zero target and saturation

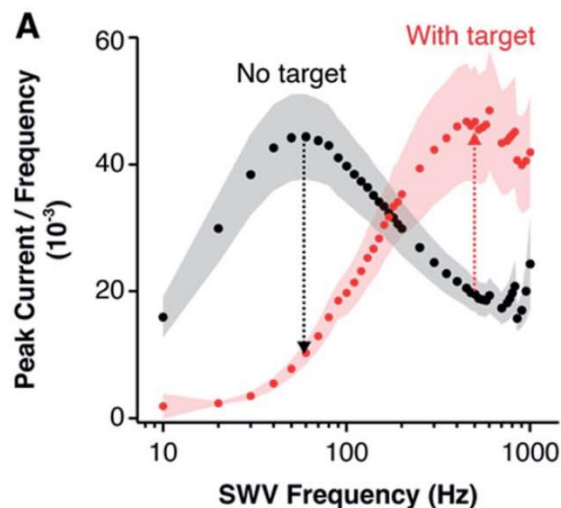


**Figure 1-11.** E-AB sensors have an optimal interrogation frequency range irrespective of interrogation technique. Here, one can determine the frequency ranges in which the bound and un-bound probe aptamer each produces the highest faradic signal current. Reproduced from <sup>93</sup>.

We have discussed the parameters influencing the E-AB sensor in terms of fabrication and operational parameters with no emphasis on any specific target. In the following section, however, we will highlight the importance of interfacial design and molecular architecture in the fabrication E-AB sensor to show how such delicate manipulations can meet new demands. We will focus on the proof-of-the-concept demonstrations of diagnostic devices that have proposed for early monitoring of breast cancer biomarkers.

## 1.4 Breast cancer

Breast cancer is the most diagnosed cancer among women, with nearly 1.7 million new cases diagnosed worldwide in 2012 <sup>96</sup> leading to 551,334 deaths in 2015, and the highest prevalence of metastasis<sup>97</sup>. The total number of cases is predicted to increase by 49% from 1,534,500 (2015) to 2,286,300 annual cases (2050)<sup>98</sup>. The concept of early detection of various forms of cancer before they expand to metastatic state and become practically incurable has garnered much attention

among scientist and physicians<sup>99</sup>. Over the past 20 years the survival rate in breast cancer when diagnosed at early stages have drastically improved with the existing therapies<sup>100</sup>.

Biomarkers include species and substances released from the cancer cells themselves or by other tissues as a result of the response to tumors as well as physiological indicators that can be traced and visualized by imaging technology or detected by molecular technology<sup>101</sup>. Therapeutic biomarkers for cancer ranges from macromolecules such as DNA, genetic mutation, RNA, and protein, to whole cells. They can exist in the blood as circulating mRNA, free DNA, and tumor cells, making liquid biopsies attractive for clinical use<sup>102</sup>. Two categories of biomarkers are frequently used to inform cancer treatment. Prognostic biomarkers which are mainly associated with clinical results and tend to give information about the necessity of the treatment, and predictive biomarkers that serves to better navigate an effective treatment for a subtype of breast cancer<sup>103</sup>. Surprisingly, so far, despite many scientific endeavors, only 9 breast cancer biomarkers have been approved by the Food and Drug Administration (FDA) for clinical applications<sup>104</sup>. These biomarkers are all glycosylated proteins, and a modification in the glycan composition of these glycoproteins may serve as additional information for cancer diagnostics and/or prognosis. The following glycoprotein-based biomarkers have been published in the literature for breast cancer management: HER2/NEU, CA15-3, CA27.29, MAM, galectin 3 binding protein, nectin 4, and fibronectin 1 with a typical concentration in human serum of 1–50 ng/ml<sup>105</sup>. **Table 1-2** lists fundamental characteristics of such biomarkers.

CA15-3 represents a soluble form of mucin 1 (MUC1), a transmembrane protein on the apical cellular surface. MUC1 is a glycoprotein with three domains. The association between breast cancer and elevated expression of CA15-3 has been experimentally confirmed<sup>106</sup>. The CA15-3 has constantly been employed as the clinical biomarker for the prediction of the disease outcome and

monitoring of chemotherapy treatment modalities or even the relapse of the disease. In another word, the CA15-3 accounts for the standard practical serum biomarker of the breast cancer<sup>107</sup>.

**Table 1-2.** Candidate breast cancer biomarkers (BRCA1, BRCA2, CA27.29, CA 15-3, CEA, HER-2, VEGF, tPA, CIFRA-21-1, PDGF, OPN), reprinted from <sup>104</sup>.

Biomarker	Size/kDa	Incidence in Cancer	Level in Serum
<i>BRCA1</i>	207–220	breast, ovarian, prostate, pancreatic	ND
<i>BRCA2</i>	384	Fanconi anemia, breast, ovarian, lung, prostate, pancreatic	ND
<b>CA27.29</b>	250–1000	breast	≤37 U/mL
<b>CA15-3</b>	290–400	breast	3–30 U/mL
<b>CEA</b>	180–200	gastric, pancreatic, lung, breast, medullary thyroid	2–4 ng/mL
<b>HER-2</b>	185	breast, ovarian, gastric, prostate	15 ng/mL
<b>VEGF</b>	18–27	brain, lung, gastrointestinal, hepatobiliary, renal, breast, ovarian	~220 pg/mL
<b>TPA</b>	20–45	breast, lung, pancreatic	109 U/L
<b>CIFRA-21-1</b>	40	breast, lung, pancreatic	50 ng/mL
<b>PDGF</b>	35	glioblastoma, lung, colorectal, breast, liver and ovarian	(7.5 ± 3.1) ng/mL
<b>OPN</b>	41–75	breast, colon, liver, lung, ovarian, prostate	16 ng/mL

## 1.5 Breast cancer biomarkers and clinical utility

Despite recent advances in cancer research, routine clinical practice in breast cancer diagnosis and treatment still relies on a limited set of molecular markers (see **Table 1-3**). There are currently no well-established markers for early diagnosis. Among the serum tests with prognostic value after diagnosis, CA15-3, which measures shed forms of the MUC-1 glycoprotein <sup>108,109</sup>, is not considered useful for early diagnosis due to its low sensitivity and poor specificity <sup>110</sup>, and its value in monitoring after surgery is questionable. Carcinoembryonic antigen (CEA) and CA 27.29, which measure mucin-associated antigens, also have poor sensitivity and specificity and are therefore of questionable utility for early diagnosis, although they can be useful for monitoring advanced disease <sup>111</sup>. It has been suggested that metabolite profiling, which involves analyzing

metabolic products in the body, may have the potential to improve early diagnosis and staging of breast cancer compared to methods based on measuring serum proteins <sup>112,113</sup>.

Estrogen receptor (ER) and the type 2 human epidermal growth factor receptor (HER2 or erbB-2) are not diagnostic markers but are among the most useful for predicting outcomes in breast cancer. For instance, a meta-analysis of data from 20 trials involving over 20,000 patients found that ER status was the only known factor that could predict responsiveness to adjuvant tamoxifen therapy <sup>114</sup>, regardless of other factors such as nodal status. HER2 is also a key predictor of response to targeted therapies such as trastuzumab. In contrast, other tissue marker proteins such as progesterone receptor (PR) and Ki-67 have less predictive value. Overall, the evaluation of tissue marker proteins is an important part of breast cancer diagnosis and treatment planning.

The status of estrogen receptor (ER) and human epidermal growth factor receptor 2 (HER2) can be used to divide breast cancer patients into four therapeutic and prognostic risk groups: triple negative, HER2-positive, and two classes of ER-positive/HER2-negative: low or high proliferation, as defined by Ki-67 or other additional tests <sup>115</sup>. This has been endorsed by an international expert panel. While there are currently no established protein-based tests to determine the mutational status of BRCA1 or BRCA2, these genes are important to mention as they are strong predictive markers of breast cancer. Inheriting a mutation in either gene carries a 50-80% lifetime risk of developing breast cancer <sup>116,117</sup>, the highest risk among breast cancer susceptibility genes. The evaluation of tissue marker proteins is an important part of breast cancer diagnosis and treatment planning, particularly in determining the appropriate use of chemotherapy.

**Table 1-3:** Breast cancer biomarker proteins in common clinical use.

Breast cancer biomarker proteins in common clinical use.	
<i>Cancer marker</i>	
<b><i>Tissue-based markers</i></b>	
<i>ER</i>	Predicting response to hormone therapy in both early and advanced breast cancer In combination with other factors, assessing prognosis in breast cancer
<i>PR</i>	Usually combined with ER for predicting response to hormone therapy
<i>HER2</i>	Determining prognosis, most useful in node-positive patients Conflicting data in node-negative patients for selecting patients with either early or metastatic breast cancer for treatment with trastuzumab
<i>uPA</i>	Determining prognosis in breast cancer, including the subgroup with axillary node-negative disease In clinical use in parts of Europe.
<i>PAI-1</i>	Usually assayed in combination with uPA, that is, for determining prognosis in breast cancer including the subgroup with node-negative disease Provides prognostic information additional to that of uPA
<b><i>Serum-/plasma-based markers</i></b>	
<i>CA 15-3/CA 27.29</i>	Postoperative surveillance in patients with no evidence of disease Monitoring therapy in advanced disease
<i>CEA</i>	Postoperative surveillance in patients with no evidence of disease Overall, appears to be less sensitive than CA 15-3/BR 27.29
<i>TPA</i>	Postoperative surveillance in patients with no evidence of disease

*CA: Carcinoma antigen; CEA: Carcinoembryonic antigen; ER: Estrogen receptor; HER2: Human epidermal growth factor receptor 2; PAI-1: Plasminogen activator inhibitor-1; PR: Progesterone receptor; TPA: Tissue plasminogen activator; uPA: Urokinase plasminogen activator*<sup>118</sup>.

## **1.6 Liquid biopsy: the general concept:**

Liquid biopsy is a non-invasive method for collecting tumor-derived materials, such as DNA, RNA, cells, or extracellular vesicles, from body fluids like blood, urine, or saliva. This technique can be done through a blood draw or urine collection and is seen as an attractive option compared to traditional biopsies which involve removing tissue from a tumor. Liquid biopsy can potentially overcome the issue of tumor heterogeneity by examining the genomic landscape of the entire tumor in the patient's body <sup>119</sup>, and it can be repeated over time to monitor the tumor's response to treatment. It may also have the potential for early cancer detection, prognostication, and predicting treatment response. The development of sensitive assays that can detect small amounts of tumor-derived material in body fluids has made liquid biopsy a viable alternative to traditional biopsies<sup>120-124</sup>.

## **1.7 Liquid biopsy: package of tumor-derived materials**

According to the literature, liquid biopsy involves collecting a sample of body fluid that contains various materials derived from a tumor, including DNA, RNA, intact circulating tumor cells (CTCs), tumor-educated platelets, and extracellular vesicles. These samples can be collected through a blood draw or urine collection, but different technologies are needed to isolate the different tumor-derived materials, such as CTCs and circulating tumor DNA (ctDNA), from the body fluid sample <sup>125</sup>. The concept of liquid biopsy likely dates back to 1948 when cell-free DNA (cfDNA) was first discovered in the bloodstream <sup>126</sup>. Unlike ctDNA, which is released by tumor cells, cfDNA is present in both healthy <sup>127</sup> and sick individuals and can be found in higher quantities during trauma, heart attacks, strokes, or autoimmune conditions<sup>128</sup>. ctDNA is a portion of cfDNA that is released by tumor cells either at the site of the tumor or from CTCs in the bloodstream. CTCs are tumor cells that either actively enters the body's circulation or are shed

from primary or metastatic tumors <sup>129</sup>. Other materials derived from tumors include circulating RNA such as cell-free messenger RNA and microRNA, which are small noncoding RNA molecules of 19 to 24 nucleotides in length <sup>130</sup>. These may be found in extracellular vesicles in the circulation, which are small, membrane-bound vesicles that are shed either by plasma membrane shedding from cells like tumor-educated platelets or by tumor cells through exocytosis (the resulting extracellular vesicles are called exosomes). These vesicles can contain tumor DNA and RNA, as well as tumor-associated proteins and lipids <sup>131</sup>, which protect their contents from enzymes such as plasma nucleases. Tumor-educated platelets are platelets that have taken up tumor RNA from the circulation and may have enhanced functions promoting tumor metastasis<sup>132</sup>.

CTCs and ctDNA are two of the most well-studied materials found in a liquid biopsy. The US Food and Drug Administration recently approved the Therascreen PIK3CA RGQ polymerase chain reaction (PCR) assay as a companion diagnostic test to detect PIK3CA mutations in patients with hormone receptor-positive, human epidermal growth factor receptor 2 (HER2)-negative, PIK3CA-mutated, advanced, or metastatic breast cancer. This approval followed a clinical trial that found patients with these characteristics who were treated with Alpelisib in combination with endocrine therapy Fulvestrant had significantly prolonged progression-free survival compared to those treated with Fulvestrant alone <sup>133</sup>. The companion diagnostic assay can be used on both tissue and liquid biopsies, bringing liquid biopsy closer to being used in the treatment of breast cancer.

CTCs collected from the blood can be analyzed for their contents, such as protein, DNA, mRNA, miRNA, and other properties <sup>134,135</sup>. One example of a protein marker found in CTCs is cancer antigen 15-3 (CA15-3), which is encoded by the Mucin 1 (MUC1) gene. Higher than normal levels of CA15-3 expression is often used as an indicator of primary breast cancer and early detection of relapse <sup>136</sup>.

## **1.8 Liquid biopsy vs. tissue biopsy**

Tissue biopsy is a valuable diagnostic tool that provides information about the tissue's structure and allows for the analysis of hormone receptors and HER2 status. However, it has limitations because it only provides a snapshot of the tumor at one point in time from one specific location, which may not accurately reflect the entire tumor. Cancers are often heterogeneous and can change over time and in response to treatment. A study by Gerlinger et al <sup>137</sup> found that different parts of a primary tumor and its metastases can have different characteristics. While serial longitudinal tissue biopsies could potentially provide a more complete picture of the tumor and its changes, they are impractical in the clinical setting because they are invasive and can have complications. They are also not possible in cases where the tumor is in a difficult-to-access location or if the patient is too sick for an invasive procedure. It is also not feasible to obtain tissue samples from every metastatic deposit in a patient with multiple metastases. The heterogeneity of tumors can make it challenging to determine the best course of treatment based on a single tissue biopsy, as it may not accurately reflect the complexity of the tumor's genomic landscape.

In contrast to tissue biopsy, liquid biopsy has the potential to provide a more comprehensive view of the tumor's genomic landscape, both across all metastatic sites and over time. However, there are challenges in implementing this technology in the clinical setting. For example, circulating tumor DNA is often of poor quality, highly fragmented, and present in low concentrations in the blood. To improve the yield of ctDNA, methods for extracting ctDNA need to be improved or DNA analysis assays need to be made more sensitive to detect ctDNA at very low allele frequencies. At present, tissue biopsy is still considered the reference standard for molecular analysis of tumors in clinical guidelines and recommendations.

The National Comprehensive Cancer Network treatment guidelines <sup>138</sup> for non-small cell lung cancer do not recommend using liquid biopsy in place of tissue diagnosis because of a false-negative rate of 30% for ctDNA testing. Therefore, if a liquid biopsy for EGFR mutations is negative, it is recommended that a tissue biopsy be performed for repeat molecular testing. While PCR-based methods such as ddPCR, BEAMing, and amplification-refractory mutation system are highly sensitive and can detect ctDNA at very low allele frequencies of less than 1%, they can only test for specific genetic changes that are predetermined. Targeted, massively parallel sequencing or next-generation sequencing of multiple genes can provide a wider scope of molecular analysis of the tumor, but it requires specialized bioinformatics support and can have issues with specificity when trying to distinguish low-allele-frequency variants (which is often the case with liquid biopsy) from background noise due to DNA polymerase errors. There is also a lack of standardization in the techniques used for liquid biopsy analysis, including the type of analyte (CTC or ctDNA), the sample used for extraction (serum or plasma for ctDNA testing), the method of quantification (spectrophotometry or fluorescence-based techniques for ctDNA), and the assay itself (ddPCR, amplification-refractory mutation system, BEAMing, or next-generation sequencing). **Table 1-4** compares different attributes of liquid biopsy vs tumor biopsy.

**Table 1-4** : Advantages and drawbacks of tumor liquid biopsies compared to standard tissue-based biopsies<sup>139</sup>.

<b>Circulating biomarkers</b>	<b>Tumor biopsy</b>
<b>Advantages</b>	<b>Advantages</b>
<ul style="list-style-type: none"> <li>• Diagnosis</li> <li>• Prognosis</li> <li>• Real-time therapy follow-up</li> <li>• Low cost</li> <li>• Minimally invasive—higher compliance</li> </ul>	<ul style="list-style-type: none"> <li>• Diagnosis</li> <li>• Prognosis</li> <li>• Material obtained from the primary lesion (high specificity)</li> </ul>
<b>Drawbacks</b>	<b>Drawbacks</b>
<ul style="list-style-type: none"> <li>• Lack of well-defined bio-panels</li> <li>• Relatively overall lower specificity/sensitivity, especially if considered singularly</li> </ul>	<ul style="list-style-type: none"> <li>• Highly invasive—lower compliance</li> <li>• Relatively expensive</li> <li>• Outcome strictly dependent on the correctness of the procedure</li> </ul>

### **1.9 The mucins : family of glycosylated proteins**

There is a lot of research being done to identify markers that have biological and therapeutic importance in breast cancer. Mucins are a large group of glycoproteins that are produced by various types of epithelial cells and their cancerous counterparts. They are divided into two main categories: membrane-bound mucins, including MUC1, MUC3A, MUC3B, MUC4, MUC12, MUC13, and MUC17, and secreted or gel-forming mucins, including MUC2, MUC5AC, MUC5B, and MUC6<sup>140</sup>. All mucins have similar structural features, but they differ in the repeating peptides that they contain<sup>141</sup>. Abnormal expression of mucins has been linked to cancer. Mucins have been shown to play a role in cancer development and to affect cell growth, differentiation, transformation, adhesion, invasion, and immune surveillance<sup>142</sup>. Many studies have found that

MUC1 is overexpressed in breast cancer, as well as in other types of cancer such as colon and pancreatic cancer <sup>143</sup>.

MUC1 is involved in cell signaling, immune regulation, and the inhibition of cell-cell and cell-matrix adhesion <sup>144</sup>. The cytoplasmic domain of MUC1 has been found to interact with  $\beta$ -catenin through a motif similar to that found in E-cadherin, which prevents the formation of the E-cadherin- $\beta$ -catenin complex <sup>145</sup>. This finding has been confirmed in a study using a breast cancer cell line <sup>146,147</sup>. MUC1 may therefore play a role in the detachment, invasion, and metastasis of tumor cells, which is associated with aggressive tumor behavior and a poor prognosis. The cytoplasmic domain of MUC1 also has the ability to bind to Grb2/SOS, which are signaling mediators for tyrosine kinase receptors, when it is phosphorylated <sup>148</sup>.

MUC1 has also been found to colocalize with and interact with members of the epidermal growth factor receptor (EGFR) family <sup>149</sup>. MUC1 mucin is typically found on the top surface of secretory epithelial cells, but in cancerous tissue, its expression can vary in terms of the amount and location within the cell <sup>150</sup>. High levels of abnormal MUC1 expression in breast cancer and other types of cancer leads to the creation of antigenically recognizable regions on the MUC1 molecule, which can stimulate an immune response. This makes MUC1 a potential target for immunotherapy<sup>151</sup>.

MUC2, MUC5AC, and MUC6 are important proteins that help produce the mucus that protects and lubricates epithelial surfaces. MUC2 is a major glycoprotein that is produced in large quantities by intestinal and airway epithelial cells <sup>152</sup>. Its expression is a common feature of all mucinous carcinomas, which are types of cancer that arise from different organs including the breast, colon, and prostate, and it may serve as a potential prognostic indicator <sup>153-155</sup>. MUC2 is expressed in mucinous breast cancer and may help prevent tumor invasion <sup>156</sup>. Its expression is

also associated with aggressive tumor behavior in other types of invasive and intraductal carcinomas of the breast<sup>141,157</sup>.

MUC5AC is mainly found in the mucosal layer of the cardia, fundus, and antrum of the stomach, while MUC6 is found in the pyloric glands<sup>158,159</sup>. Both MUC5AC and MUC6 have similar properties in protecting epithelial tissue and are not usually detected in normal breast tissue<sup>160</sup>. Schmitt et al<sup>160</sup> have found a correlation between MUC6 expression and mucinous carcinoma of the breast. Previous studies have not found any association between MUC5AC or MUC6 and tumor size, histological grade, lymph node status, or estrogen receptor (ER) status<sup>160</sup>.

MUC3 is found in the intestine and is made up of two distinct genes called MUC3A and MUC3B. It has been shown that MUC3 can be upregulated by steroids in Vitro, which suggests that there may be a link between abnormal hormonal mechanisms and the loss of controlled expression of mucin genes in breast cancer. In gastric carcinoma, or cancer of the stomach, MUC3 expression has been associated with a poor prognosis<sup>161</sup>.

MUC4 normally provides a protective layer of mucus for the epithelial cells in the breast. The ability of MUC4 to create an antiadhesive, antirecognition barrier may potentially be used as a mechanism to prevent apoptosis and indirectly increase tumor proliferation<sup>162</sup>. It has also been shown to modulate the c-erbB-2 receptor tyrosine kinase through two epidermal growth factor-like domains in the transmembrane portion of the complex (ASGP-2)<sup>163</sup>. Overexpression of MUC4 has been shown to block cell-cell and cell-matrix interactions, protect tumor cells from immune surveillance, and promote metastasis. In addition, as a ligand for ErbB2, MUC4 can increase the phosphorylation of ErbB2 and potentially alter the signals generated by this receptor

<sup>164</sup>. The deregulation of MUC4 may contribute to tumor progression and altered expression of MUC4 has been found in many types of carcinoma <sup>165,166</sup>.

### **1.10 The structure of MUC1**

Mucins are a type of protein that is heavily glycosylated, meaning that they are decorated with complex sugars <sup>167</sup>. They are found in many different tissues in the body, including the mucous membranes that line various internal surfaces such as the respiratory and digestive tracts. Mucins play important roles in various processes such as lubrication, protection, and immune defense<sup>168,169</sup>.

There are three main types of mucins: transmembrane (e.g., MUC1, MUC4, and MUC6), secreted (Gel-forming) (e.g., MUC2, MUC5AC, MUC6), and soluble (not gel-forming) (e.g., MUC7, MUC8, MUC9, and MUC20) <sup>170,171</sup>. Transmembrane mucins are anchored to the cell membrane and extend outwards from the surface of the cell. Secreted mucins are produced by certain cells and are released into the surrounding tissue, where they form a protective gel-like layer. Soluble mucins are not anchored to the cell membrane and are found in the extracellular space.

MUC1 is a well-studied transmembrane mucin that is expressed on the surface of many types of cells, including epithelial cells. It is characterized by a variable number of tandem repeats (VNTRs), which are short sequences of amino acids that are repeated many times in the protein. MUC1 also has a sperm protein-enterokinase-agarin (SEA) domain, which is an extracellular domain, and a transmembrane domain. The cytoplasmic tail domain of MUC1 extends up to 200-500 nm out of the cell surface. MUC1 plays various roles in the body, including acting as a tumor marker and mediating cell-cell and cell-matrix interactions <sup>172,173</sup>.

In cancer, the structure of MUC1 is altered due to overexpression caused by the loss of polarity in epithelial cells. This change results in the carbohydrate side chain becoming incomplete and

forming new carbohydrate side chains, such as Thomsen-Friedenreich (TF or T), Tn, and sialyl-Tn (STn)<sup>174,175</sup>. MUC1's core peptide is also more exposed to cancer, as shown in the **Figure 1-12**.

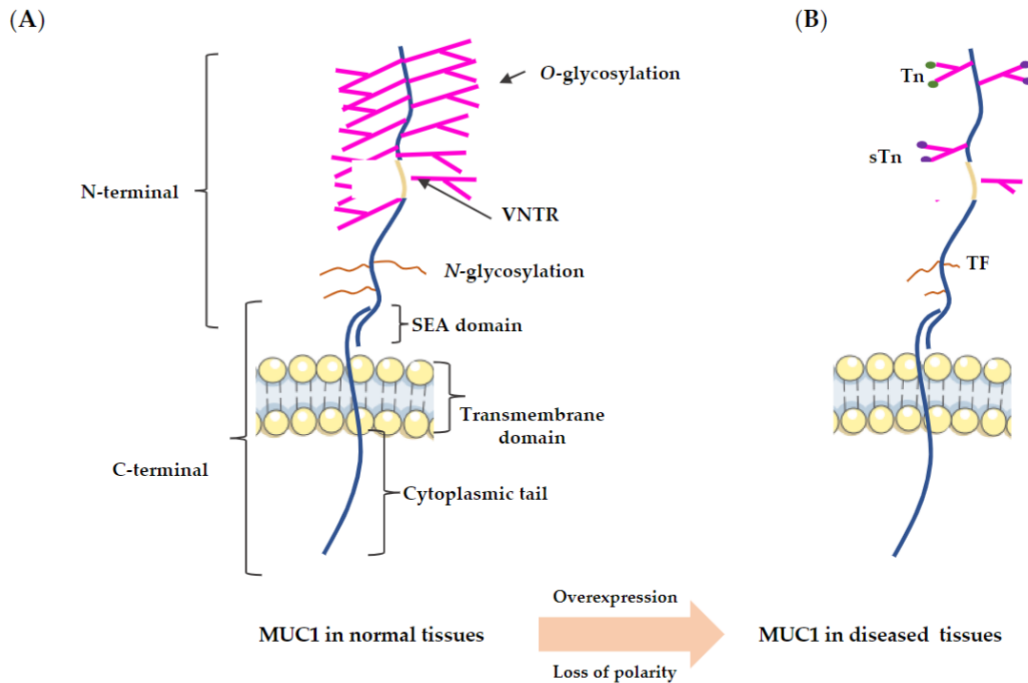


**Figure 1-12** Structure of MUC1 in normal tissues and diseased tissues. (A) The structure of MUC1 in normal tissues; (B) The structure of MUC1 in diseased tissues<sup>176</sup>.

### 1.11 Significance of MUC1 (CA15-3)

Circulating tumor cells (CTCs) can be detected in about 50-80% of patients with metastatic breast, colon, or prostate cancer<sup>177,178</sup>. It is not currently known why CTCs are not detected in some patients, whether it is because they are too rare to be captured, do not have surface markers that allow for the capture, or are not present in the bloodstream (e.g., the metastatic cells are only in the tissue or lymphatics). For patients with detectable CTCs, the surface antigens currently used to identify them are epithelial cell adhesion molecule (EpCAM), cytokeratin-19<sup>179</sup>, and MUC1<sup>180</sup>.

MUC1 is often used as a capture antigen because it is frequently overexpressed on CTCs. It is typically found to be expressed in more than 60% of captured CTCs from patients with metastatic breast, lung, pancreatic, and colon cancer<sup>181-183</sup>. The detection of MUC1 (also known as serum antigens CA 15-3, KL-6, and BM7<sup>184,185</sup>) in patient blood is currently used clinically to evaluate response to therapy and as a prognostic indicator for survival. The serum antigen CA 15-3 is one of the most widely used serum antigens in breast cancer, and high CA 15-3 levels are associated with higher-grade tumors, lymph node involvement, and the presence of distant metastases<sup>186</sup>. The location of MUC1 within cells is also important.

CA15-3, a high molecular weight glycoprotein (300-450 k Da), is synthesized by the apical surface of epithelial ducts and acinic breast cells and is then secreted in milk normally. In cancer, CA15-3 may enter the bloodstream due to changes in the structure of the breast. High levels of CA15-3 may indicate the presence of metastases, especially in the bones. It appears that CA15-3 could be a useful factor in predicting the likelihood of bone metastases in these patients. According to bone scans, about 2%, 10%, and 20% of patients with breast cancer in stages 1, 2, and 3, respectively, will experience bone metastasis<sup>187</sup>.

In a study about the prognostic value of the preoperative CA 15-3 and CEA levels, Park et al<sup>188</sup> reported that, Out of a group of 1681 patients, 176 had high levels of the CA15-3 tumor marker and 131 had high levels of the CEA marker before surgery. Higher levels of these markers were linked to larger tumors, cancer that had spread to the lymph nodes, and advanced cancer stages. Patients with elevated levels of these markers had worse survival rates, even when comparing people with the same cancer stage. Patients with normal levels of both markers had better survival rates than those with elevated levels of one or both markers. In a statistical analysis that took into account other factors, high levels of these markers were found to be independent predictors of

survival. This association between high marker levels and poor survival was confirmed with longer follow-up and a larger group of patients.

In another work, performed by Incoronato et al <sup>189</sup>, whose aim was to examine the value of CA15-3 for the diagnostic integration of molecular imaging findings performed with hybrid positron emission tomography and computed tomography (PETCT) technology, a cohort of 45 people with a median age of 65 years (ranging from 39-85 years old) with history of breast cancer who had already been treated via surgery and other methods were chosen. Before undergoing a PETCT examination, three measurements of CA15-3 were taken over a period of one year, at intervals of 0-3 months, 3-6 months, and 6-9 months. Disease relapse was determined by either a prolonged clinical outcome or imaging follow-up. The sensitivity and specificity of both the PETCT and the CA15-3 measurements were evaluated based on their ability to predict disease relapse in comparison to the clinical outcome.

The results indicated that in breast cancer patients undergoing follow-up, serial increases in CA15-3 levels can be used to predict positive PETCT results. Elevated CA15-3 levels may serve as an early warning sign for patients who are at a higher risk of recurrence and in need of accurate molecular imaging evaluations, as they may indicate the presence of multiple lesions or liver involvement. Additionally, patients receiving chemotherapy or anti-hormonal treatment who have negative PETCT scans, but increased CA15-3 levels should be considered at risk for relapse, as the presence of a tumor as indicated by elevated CA15-3 levels can predict positive metabolic imaging.

Elsewhere, Al-Azawi et al <sup>190</sup> retrospectively examined the role of CA15-3 in conjunction with other clinicopathological variables as a predictor of response and time to disease recurrence in

patients with locally advanced breast cancer (LABC) following treatment. The researchers reviewed pre- and post-primary chemotherapy concentrations of CA15-3 along with other variables and analyzed their relationship to four outcomes following primary chemotherapy: clinical response, pathological response, time to recurrence, and time to progression. Persistently elevated CA 15-3 after primary chemotherapy (PC) was defined as consecutively high levels above the cut-off point during and after PC. Eventually, they concluded that an elevated CA 15-3 level is a predictor of a poor response to chemotherapy. Furthermore, persistently elevated CA 15-3 levels in combination with lymph vascular invasion and HER2 status after chemotherapy predicts reduced disease-free survival in patients with locally advanced breast cancer.

There is an ongoing debate about the usefulness of measuring CA15-3 levels in patients with breast cancer. While the European Group on Tumor Markers has recommended using CA15-3 and CEA levels to predict prognosis, detect disease progression, and monitor treatment in breast cancer, the American Society of Clinical Oncology and the National Comprehensive Cancer Network does not currently recommend using these markers for breast cancer screening or treatment decisions<sup>191</sup>. These controversies may be partly due to the conflicting conclusions of research<sup>192–194</sup>.

### **1.12 Relationship between CA 15-3 and tumor and patient characteristics**

According to a substantial research work that has evaluated the preoperative CA15-3 serum levels prospectively in 600 patients<sup>195</sup>, it has been shown that CA15-3 concentrations were meaningfully higher in patients suffering from larger tumors, and in patients with an increasing nodal burden. Cuzick's test for trend demonstrated a significant increase in CA15-3 across these groups for tumor size and for nodal burden. Moreover, no significant difference was found in patients with ER positive or negative, however, concentrations were significantly higher in patients 50 years or older

compared with those younger than 50. Additionally, levels were higher in patients with positive axillary nodes compared to those with negative axillary nodes. Results are shown in **Table 1-5**. Of note, it has been shown that the CA15-3 cut-off concentration has been estimated as 30-35 U/ml (which is approximately equivalent to 5  $\mu$ M of the target) <sup>196,197</sup>.

**Table 1-6** Median and mean CA 15-3 concentrations in different subgroups <sup>194</sup>

Variables		CA15-3, units/L	
<b>Tumor size, cm</b>	n	median	Mean
0-2	208	20	20.8
2-5	341	21	24.2
5	51	26	37.2
<b>Age at diagnosis</b>			
50years	209	19	22.8
50years	391	21	24.9
<b>Axillary node status</b>			
Negative	290	19	21.2
Positive	310	21	26.9
<b>ER status(n 505)</b>			
Negative	161	20	24.1
Positive	344	21	24.5

### 1.12.1 Relationship between CA 15-3 and overall survival

As shown in **Figure 1-13** and **Table 1-6**, patients with high CA15-3 (>30 units/L) had a worse overall survival pattern than those with low concentrations of the marker.

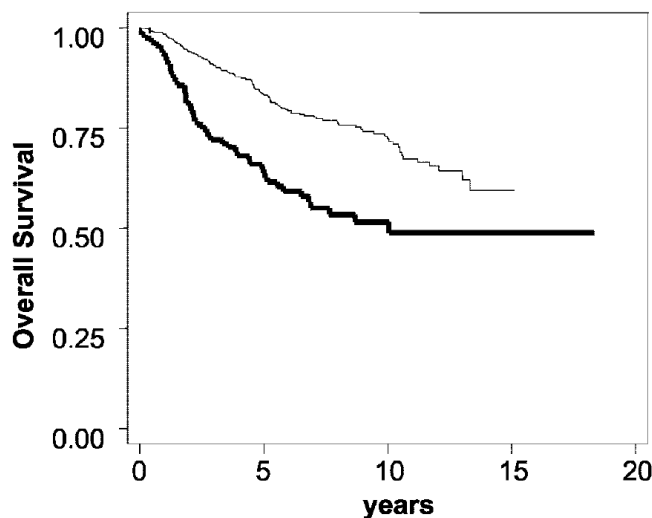


**Figure 1-13** Overall survival according to serum CA 15-3 concentrations in 600 patients with breast cancer. Thin line, CA 15-3  $\leq$  30 units/L (n =489); thick line, CA 15-3  $\geq$  30 units/L (n =111). HR = 2.16 (CI, 1.55–3.03);  $P < 0.0001$  <sup>194</sup>.

### 1.13 Current use

Currently, the primary use of CA 15-3 is to monitor treatment progress in patients with advanced breast cancer, particularly in cases where the disease is not evaluable <sup>108</sup>. Most expert panels do not enthusiastically recommend using CA 15-3 for routine surveillance of asymptomatic women who have had surgery for breast cancer <sup>108</sup>. However, as more therapies become available for recurrent or metastatic disease, this may change in the future. The main limitation of CA 15-3 as a marker for breast cancer is its lack of sensitivity for detecting early-stage disease. The challenge with using serum markers for breast cancer is to find a marker that is both sensitive and specific for detecting small or early tumors in women.

## 1.14 Vascular Endothelial Growth Factor (VEGF) Protein

The VEGF gene family includes six proteins, known as VEGF-A, VEGF-B, VEGF-C, VEGF-D, VEGF-E, and placenta growth factor PlGF-1 and -2, that play a role in the growth of blood vessels and lymph vessels<sup>198-200</sup>. VEGF-A, also known as VEGF or VPF, was first identified as a factor secreted by tumor cells that can increase the permeability of blood vessels. Later, Ferrara et al<sup>201</sup> isolated and cloned VEGF-A as a protein that stimulates the growth of blood vessels in the endothelium, or the inner lining of blood vessels. VEGF-A is a 45-kDa protein that exists as a dimer and has various angiogenic properties. The VEGF-A gene can produce different isoforms, or variations, through a process called alternative splicing<sup>88</sup>. These isoforms include VEGF<sub>121</sub>, VEGF<sub>165</sub>, VEGF<sub>189</sub>, and VEGF<sub>206</sub><sup>89</sup>. There are also some less common isoforms, such as VEGF<sub>145</sub> and VEGF<sub>183</sub><sup>202</sup>. VEGF<sub>121</sub> is secreted freely, while the larger isoforms, VEGF<sub>189</sub> and VEGF<sub>206</sub>, are trapped in the extracellular matrix and must be activated by proteases, or proteins that break down other proteins. VEGF<sub>165</sub> exists in both a soluble form and a form that is bound to the extracellular matrix<sup>203</sup>. The isoforms of VEGF-A, VEGF-C, and VEGF-D that are bound to the extracellular matrix can be made active by being cleaved at the C-terminus by plasmin, or they can be released from the extracellular matrix by matrix metalloproteinase 9 (MMP-9). VEGF<sub>165</sub> is the most common isoform and is often found at high levels in different types of human cancerous tumors. Recent research suggests that the expression patterns of these isoforms may be important in cancer progression and angiogenesis. Recent research indicates that the expression of certain VEGF isoforms is specific to certain tissues, which suggests that these isoforms have defined roles in the formation of new blood vessels (vasculogenesis) and possibly in the growth of new blood vessels in tumors (tumor angiogenesis)<sup>204-206</sup>.

It is well-established in cancer biology that tumor growth relies on the development of new blood vessels, a process known as angiogenesis<sup>207</sup>. This is important for supplying oxygen, nutrients, growth factors and hormones, proteolytic enzymes, and influencing hemostatic factors that regulate the coagulation and fibrinolytic system. Additionally, angiogenesis allows for the dissemination of tumor cells to other parts of the body. The angiogenic process is a complex, dynamic process regulated by both pro- and antiangiogenic molecules. The "switch" to an angiogenic phenotype, where proangiogenic mechanisms overpower negative regulators of angiogenesis, is considered a hallmark of the malignancy process<sup>208</sup>. In general, increased tumor vascularization (e.g., increased microvessel density) and tumor expression of proangiogenic factors have been associated with advanced tumor stage and poor prognosis in a variety of human cancers<sup>209-211</sup>.

Decades of research on the molecular basis of angiogenesis have identified several growth factor receptor pathways that stimulate the formation of new blood vessels in tumors. One of the major pathways involved in this process is the vascular endothelial growth factor (VEGF) family of proteins and receptors<sup>212</sup>.

VEGF<sub>165</sub> is the most common isoform of VEGF and is frequently overexpressed in various types of human solid tumors. Recent studies suggest that the expression patterns of certain VEGF isoforms are specific to certain tissues, indicating that these isoforms may have defined roles in both vasculogenesis and tumor angiogenesis. Notably, VEGF<sub>165</sub> exists in both a soluble and an ECM-bound form<sup>204,205,207</sup>.

### **1.15 Significance of VEGF<sub>165</sub>**

Vascular endothelial growth factor (VEGF) is a protein that promotes angiogenesis and is associated with negative clinical outcomes in breast cancer. In one study evaluation of different angiogenic markers in breast cancer patients with positive hormone receptors has been examined<sup>213</sup>. The authors analyzed serum and tumor samples from 71 patients with operable primary breast cancer that was hormone receptor-positive to determine the expression of VEGF and the possible relationship between circulating serum VEGF levels, tumor VEGF expression, microvessel density (MVD), and other immunohistochemical parameters. They found that basal VEGF serum levels were significantly higher in breast cancer patients than in healthy controls. There was also a significant correlation between basal VEGF serum concentrations, MVD, and p53 status. Intratumoral VEGF expression was significantly associated with neoplastic embolization and circulating VEGF levels. These results confirm that in primary hormone receptor-positive breast cancer, serum VEGF levels are elevated and show a positive relationship with tumor VEGF and p53 overexpression.

In another study<sup>214</sup>, conducted on a large cohort consisting of 253 patients with metastatic breast cancer, in which the clinical relevance of serum VEGF was assessed to explore the relationship between VEGF and another blood-based biomarker, the author concluded that in metastatic breast cancer patients with elevated levels of VEGF have a significantly worse clinical outcome. This finding supports the biological role of VEGF in breast cancer.

There is a significant amount of research indicating that VEGF is overexpressed in many human tumors and is strongly associated with intratumoral microvessel density (MVD) and prognosis in breast cancer<sup>215</sup>. Studies have shown that the immunocytochemically assessed VEGF in human

primary breast tumors has a close correlation with MVD <sup>216-218</sup>. Several investigations have also reported that higher levels of VEGF in tumor cytosols are linked to a poorer course of the disease in breast cancer patients. Some studies have found that high VEGF levels are correlated with poor relapse-free and overall survival in patients without lymph node infiltration, while others have found that high VEGF expression in breast tumors is indicative of poor survival in lymph node-positive patients <sup>219,220</sup>. However, a study by Linderholm et al <sup>221</sup> demonstrated that VEGF predicted poor outcomes in both lymph node-positive and lymph node-negative patients with primary breast carcinomas. While the negative impact of VEGF is well-documented and accepted, more research is needed to validate its prognostic significance in specific subgroups of patients.

### **1.16 To determine the relationship between preoperative serum VEGF and to compare serum VEGF with two established tumor markers for breast cancer, namely, CEA and CA15.3**

in 2001 Heer et al <sup>222</sup>, conducted a series of experiments to evaluate the clinical relevance of serum levels of VEGF<sub>165</sub> on various prognostic indices in breast cancer. Additionally, to have a better grasp in a broader context, the author has compared the results with two well-established breast cancer tumor markers, that is, CEA and CA15-3. Their findings are as follows:

Serum levels of VEGF are significantly elevated in ductal but not lobular carcinoma. This is consistent with the findings of Dvorak et al<sup>223</sup>, who observed significant VEGF mRNA expression in various types of carcinoma tissues except for lobular carcinoma of the breast and papillary carcinoma of the bladder. This suggests that the tumor is the main source of VEGF in the serum. This has implications for understanding the pathogenesis and progression of lobular carcinoma and may also be relevant for the future management of this type of cancer. Experimental studies have shown that animals treated with neutralizing antibodies against VEGF exhibit reduced tumor and metastasis growth when inoculated with tumor cells, compared to untreated animals. This has opened the possibility of using antiangiogenic treatment as adjuvant therapy. The different angiogenic responses of different types of breast cancer may allow for the selection of patients who may benefit from such adjuvant therapy, similar to the selection of patients for tamoxifen therapy based on their estrogen receptor status

In the previous study, performed by the same author, on serum VEGF in colorectal cancer they found a good correlation between VEGF levels, cancer stage, and nodal status. However, this correlation was not observed in the present study of breast cancer, which may be due to the influence of the female hormonal environment in the pathogenesis of breast cancer. The correlation between serum VEGF and estrogen receptor status supports this possibility. Further long-term follow-up studies are needed to determine if preoperative serum VEGF levels have prognostic significance, as has been shown for tumor VEGF levels, and whether serum VEGF can be used to detect early recurrence in breast cancer.

This study found that serum VEGF has a higher sensitivity of 62.1% for detecting breast cancer compared to the commonly used tumor markers CA15.3 (13.6%) and CEA (10.3%), with a specificity of 74%. Therefore, it may be useful to include serum VEGF in the preoperative

diagnostic toolkit, especially in cases where it is difficult to distinguish between benign changes and ductal carcinoma in situ on mammography. Overall, this study shows that serum VEGF is elevated in patients with breast cancer and that its relation to cancer type and estrogen receptor status may provide insights into tumor biology and have therapeutic implications in the future.

## **1.17 Current technologies available in liquid biopsy**

### **1.17.1 DNA**

circulating tumor DNA (ctDNA) has been found in the blood of cancer patients since the 1970s, but recent technological advancements have allowed for its detection and analysis to be more precise. Clinical trials have demonstrated its usefulness for identifying mutations that can be targeted with specific treatments and for monitoring the effectiveness of treatment. ctDNA is typically extracted from plasma, rather than serum, using manual or automated techniques (e.g. Qiagen, Siemens, Promega). In laboratory settings, automated methods are often preferred due to their consistency and cost-effectiveness.

There are several PCR-based kits available that can detect ctDNA by identifying the size of LINE1 or ALU repeats to determine the fragment size<sup>224,225</sup>. A commercial version of this technique is in development. To confirm that the ctDNA is specifically derived from a tumor (ctDNA), it must be shown to contain mutations present in the tumor or to be methylated at certain tumor gene locations (e.g. RASSF1A)<sup>226</sup>. These characteristics can be identified using PCR methods, and commercial PCR-based mutation detection systems can detect some patients with known tumor mutations. There are also improved methods under development that can detect as little as 0.01% mutant DNA in wild-type DNA and are being evaluated for clinical use. These methods have shown good concordance with the presence of tumor in the plasma<sup>227</sup>. Methylated DNA can also be detected using ELISA methods (Volition SA, Belgium).

### **1.17.2 RNA**

PCR-based techniques have been used to detect microRNAs (miRNAs) in plasma, and some studies have suggested that this is a reliable method for detecting cancer relapse or even early cancer detection <sup>228–230</sup>. One study found that Droplet Digital PCR technology improved the reproducibility of measuring miRNA levels in patient serum by seven-fold compared to qPCR <sup>231</sup>. However, other groups have had less success with this approach, and the need for special handling of blood samples for miRNA analysis may make it challenging to use this technology routinely in clinical settings

### **1.17.3 Proteins**

Measuring protein tumor markers in patient serum is a standard practice in most hospitals for monitoring patient progress and serves as the gold standard for comparison with other methods <sup>232</sup>. Most hospitals have tests available for a variety of tumor markers, including AFP, CA125, CEA, CA15-3, CA19-9, and PSA. Some hospitals may also offer tests for additional markers such as CA72-4, HE-4, CYFRA21-1, S100, NSE, SCCA, sHER2, and ProGRP, which can be measured using ELISA assays. Other biomarkers such as thymidine kinase, circulating nucleosomes, HMGB1, sRAGE, and DNase activity have also been suggested as useful indicators <sup>233</sup>, but multiplex measurement and analysis can be challenging. The advantage of these methods is that they are simple and relatively inexpensive

### **1.17.4 Cells**

A simple search on PubMed for "circulating tumor cells in blood" returns 9179 references. There are many methods available for isolating and analyzing circulating tumor cells (CTCs), which are based on physical properties such as size or shape, or biological characteristics such as adhesion molecule expression <sup>234–236</sup>. Isolation methods include CTC microchips, filtration systems, and

bead-based capture, while PCR and cytological techniques are used for analysis. Veridex (now part of Janssen) is a leading company in this field and offers CellSearch™, a widely used technology for CTC analysis in research studies and clinical trials. CellSearch™ has been FDA-approved for use in breast cancer to monitor treatment <sup>237,238</sup>.

There are limitations to the use of CTC analysis, including the inability to obtain living cells and the difficulty of conducting molecular studies. CellSearch, a commonly used technology, tends to identify fewer CTCs than other methods, and there is concern that some of these may be non-neoplastic cells such as macrophages that express similar markers. Studies have also shown that CTCs have a high degree of molecular heterogeneity, making it challenging to identify and capture cells with altered phenotypes and to determine which are clinically relevant. Efforts to improve sensitivity and usefulness in detecting low volume disease may decrease specificity for CTCs. Many other CTC detection methods are available or under development, and some are being commercialized for research use only <sup>239</sup>.

## **1.18 E-AB sensor fabrication and interfacial engineering**

### **1.18.1 Single-target electrochemical aptasensor**

In 2013, Ma et al <sup>240</sup> developed a simple E-AB sensor for the quantitative detection of MUC1 in static buffer solution which achieved target detection only by relying on target-induced conformational changes of the MUC1 probe aptamer that has been immobilized on the surface of gold electrode via gold-thiol chemistry with a MB reporter being tethered at the distal end of the probe for electrochemical signal transduction (**Figure 1-14**). In the absence of MUC1 target, the ssDNA aptamers are folded into their inherent hairpin conformation, allowing the electron transfer from the MB reporter to the gold surface (state one). Upon addition of MUC1 target, and as a result of a binding event, the aptamer's conformation changes to un-folded structure, moves the MB

reporter away from the electrode surface (second state) preventing electron to flow to the electrode. With a surface density of  $3.5 \pm 0.5 \times 10^{12}$  molecule/cm<sup>2</sup> (corresponding to probe-to-probe spacing of  $\sim 6$  nm), they managed with this very simple interfacial manipulation to achieve a limit of detection (LOD) of 50 nM and linear dynamic range (LDR) up to 1.5  $\mu$ M in buffer solution, respectively. according to **Table 1-2**, the corresponding LDR permits MUC1 quantification in buffer with meaningful clinical relevance. This simple architecture, however, generally suffers from a low signal-to-noise and doesn't permit miniaturization and simultaneous analysis.

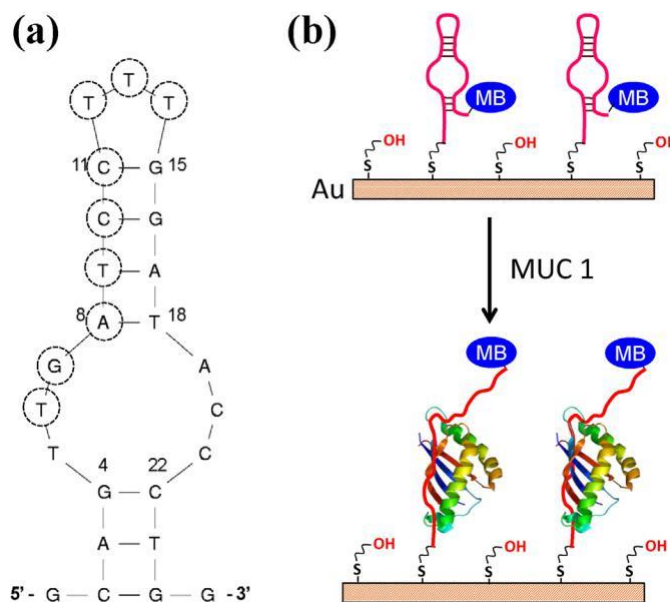


**Figure 1-14** The secondary structure of the anti-MUC1 DNA aptamer (a) and the possible conformational change of MB-anti-MUC1-aptamer (immobilized on gold electrode) upon target binding. Reproduced from <sup>240</sup>

### 1.18.2 Dual target electrochemical aptasensor

Other aptasensors have been developed to simultaneously detect more than just one analyte. For example, Li et al, in 2010 <sup>241</sup> developed a sensing strategy based on concomitant expression of different biomarkers on the cell surface. They proposed a cytosensor using a sandwich structure based immune-aptasensor for the quantification of the carcinoembryonic antigen (CEA) and

MUC1 in buffer solution. The MUC1 aptamers were first immobilized to the gold electrode to capture the target cell upon which the CEAs are located. Secondly, the cadmium nanoparticles decorated anti-CEA are introduced to capture specifically the CEA on the cell membrane. The presence of CEA and MUC1 are then monitored via stripping the Cd ions from the electrode (Figure 1-15). When MUC1 is not overexpressed on the cell surface, no signal of Cd<sup>2+</sup> cations can be measured. This cytosensor could specially monitor MCF-7 cells in a wide range from 10<sup>4</sup> to 10<sup>7</sup> cells ml<sup>-1</sup>.

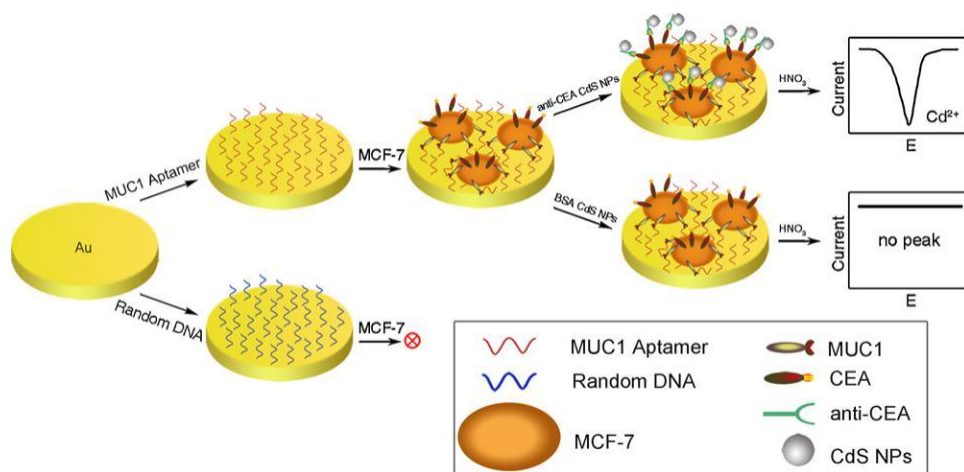


**Figure 1-15** Schematic illustration of the method to detect breast cancer cells through simultaneous recognition of two different tumor markers. Reproduced from <sup>241</sup>

Combination of the affinity-based recognition element in immune-aptasensor with the electrochemical signal generation happened to result in a very impressive sensitivity. Theoretically this sensing strategy can afford LDR with clinical relevance, nonetheless, since no real sample application has been performed, no realistic prediction can be made. More recently, a regenerable electrochemical aptasensor for parallel and continuous detection was fabricated to monitor MUC1 and CEA <sup>242</sup> in static buffer solution. The signal generation is a two-step reaction based on relative

spatial positioning of the distal-tagged MB from surface of electrode, which is initially distant from the electrode caused by the hybridization of MUC1 Aptamer and CEA Aptamer and the hybridization between CEA aptamer and DNA1 (**Figure 1-16**).

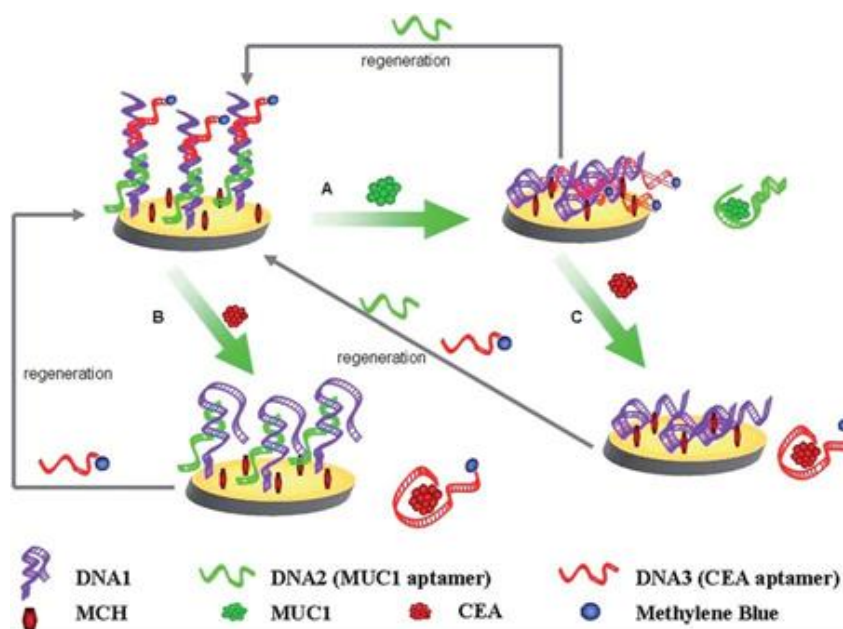


**Figure 1-16.** Schematic routines for the parallel or the continuous detection of MUC1 and CEA, and the regeneration of this present. Reproduced from <sup>242</sup>.

When the MUC1 target is introduced, MUC1 aptamer is detached and the structure loses its stiffness and the distal tagged MB reporter partially folds to the electrode leading to a primary signal occurrence<sup>242</sup>. The introduction of CEA causes a denaturation of the two aptamers (CEA and DNA1), which contributes to a further signal reduction. Considering the concentration of linker MUC1 aptamer is constant, incubation of the sensor with the aptamers allows for another hybridization and so another measurement, i.e., the reusability. This smart interfacial architecture manipulation enables multiple quantification, but cannot be empirically employed, as it requires a

sequential exposure by the analytes, which is unrealistic in physiological environment and therefore is not clinically relevant. On the other hand, it has the potential guidance for multiplexed target analysis with good accuracy and reproducibility which can accommodate the task within clinical range of the MUC1 biomarker in the buffer solution.

Another dual target electrochemical aptasensor for the simultaneous detection of MUC1 and CEA based on  $[\text{Ru}(\text{NH}_3)_6]^{3+}$  electronic wires and metal ion electrochemical labels has been reported by Ma <sup>243</sup> (**Figure 1-17**). Accordingly, when subjected to MUC1 and CEA, the interaction between biomarkers and their relevant aptamers leads to the dissociation of the double-stranded DNA (dsDNA) into ssDNA which makes them available for a secondary hybridization (**Figure 1-17**). The latter aptamer is conjugated with unique metal ions ( $\text{Pb}^{2+}$  and  $\text{Cd}^{2+}$ ), which are later detected by differential pulse voltammetry (DPV). To maximize  $\text{Pb}^{2+}$  and  $\text{Cd}^{2+}$ , Au/bovine serum albumin (Au/BSA) nanospheres were used as carriers to prepare Au/BSA-metal ions ( $\text{Pb}^{2+}$  and  $\text{Cd}^{2+}$ ) which were conjugated with two aptamers. After embedding of  $[\text{Ru}(\text{NH}_3)_6]^{3+}$  complexes into dsDNA and formation of electronic wires, the electron transfer and electrical conductivity were significantly improved, which lead to a high sensitivity with a LOD of 3.33 fM, and LDR ranging from 0.01 pM to 100 nM for MUC1.

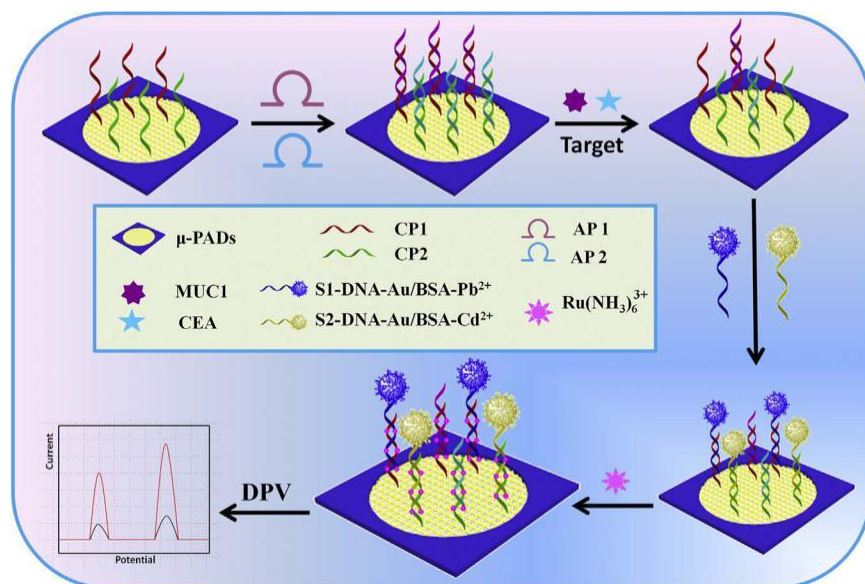


**Figure 1-17.** Schematic representation of the dual-target electrochemical aptasensor for the detection of CEA and MUC1 based on metal ion electrochemical labels and  $\text{Ru}(\text{NH}_3)_6^{3+}$  electronic wires. Reproduced from <sup>243</sup>.

In this work, the molecular design can be easily translated to other target as opposed to the previous study. Apart from the use of critical metal ions, their utilization alleviates the concerns of pH induced variations observed with molecular redox MB reporter. Furthermore, the “cut-off concentration” of MUC1 for a normal healthy woman is generally accepted to be around 35 U/mL which corresponds to approximately 5  $\mu\text{M}$  MUC1 (Table 1-2), therefore, the proposed sensing platform should be able to accommodate such a test. Zhao et al <sup>244</sup> reported an electrochemical aptasensor, using a ferrocene-labeled aptamer-cDNA as DNA probe, for the simultaneous detection of MUC1 and vascular endothelial growth factor ( $\text{VEGF}_{165}$ ). The schematic of the strategy is shown in **Figure 1-18**.

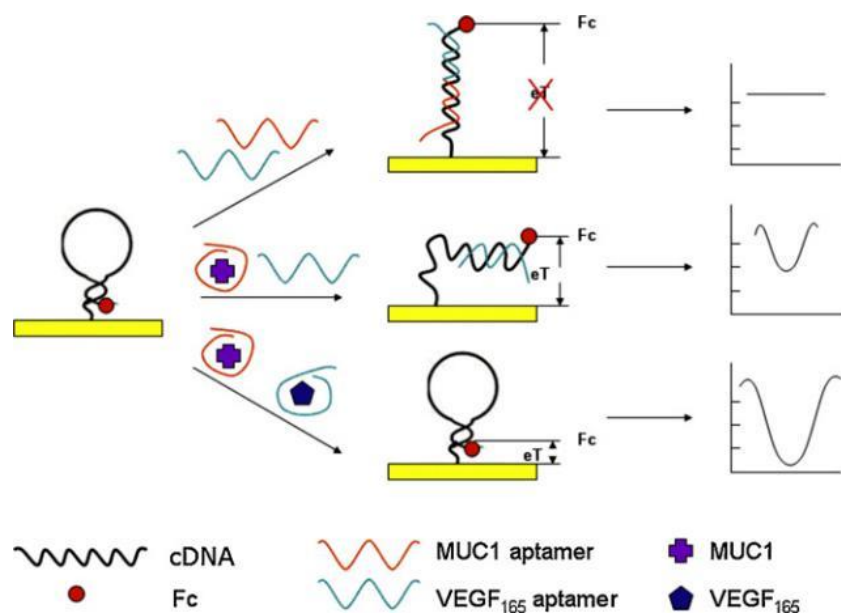


**Figure 1-18.** Schematic illustration of the method to simultaneously detect two tumor markers. Reproduced from <sup>244</sup>.

In this “signal-on” electrochemical biosensing assay, the immobilized complementary DNA (cDNA) on the electrode surface can be partially hybridized with both MUC1-specific and VEGF<sub>165</sub>-specific aptamers to form a long double stranded standing upright DNA structure with ferrocene reporter away from the electrode resulting in no significant electrochemical signal generation. However, in the presence of the two biomarkers, hybridization of cDNA with aptamers is inhibited and subsequently, the distance between the electrode surface and the ferrocene is reduced, resulting in an electrochemical signal which is reported to be proportional to the target concentrations. The increase of the electrochemical signal is proportional to the addition of either of the biomarkers, but the highest is obtained when both are present. Here, MUC1, or VEGF<sub>165</sub> were found to be individually detected in a linear range from 1nM to 20 nM, and a detection limit of 0.33 nM. However, given that the clinical mean serum value of the VEGF<sub>165</sub> in patients and healthy volunteers are 434 pg/mL (11.42 pM) and 256 pg/mL (6.7 pM), respectively<sup>245</sup>, the E-AB

sensor is not clinically relevant. Additionally, the proposed signaling behavior is relying on the collision efficiency of the cDNA, which in turn is known to be heavily dependent on the viscosity and the ambient temperature. therefore, the lack of real sample application for the final interpretation is critical.

For simultaneous detection of the MUC1 and CEA, Xiang et al <sup>246</sup> reported an integrated signal probe/gold nanoparticle [(ISP)/AuNPs-based] aptasensor consisting of two probe aptamers (sp1 and sp2) labeled with different redox labels of MB and Fc were combined into one DNA structure as shown in **Figure 1-19**. This ISP-based design constitutes a straightforward signal-off type of sensor. In this platform, target-induced conformational changes of the corresponding probe aptamers act as the source of signal generation while using MB and Fc redox labels enable independent and simultaneous detection making the signal generation for target not bound to the other. The proposed aptasensor, when properly optimized, yields a LDR from 10 pM to 1  $\mu$ M with LOD of 4 pM of MUC1. The latter detection system possesses such advantages as simplicity in design, good reproducibility and accuracy, high sensitivity, and selectivity with a theoretical clinical relevance based on static buffer results. Yet, due to repetitive washing steps needed for signal generation, the application is relatively labour intensive. Furthermore, application of Fc, due to its susceptibility for chemical changes, may be fatal for sensor continuous performance.

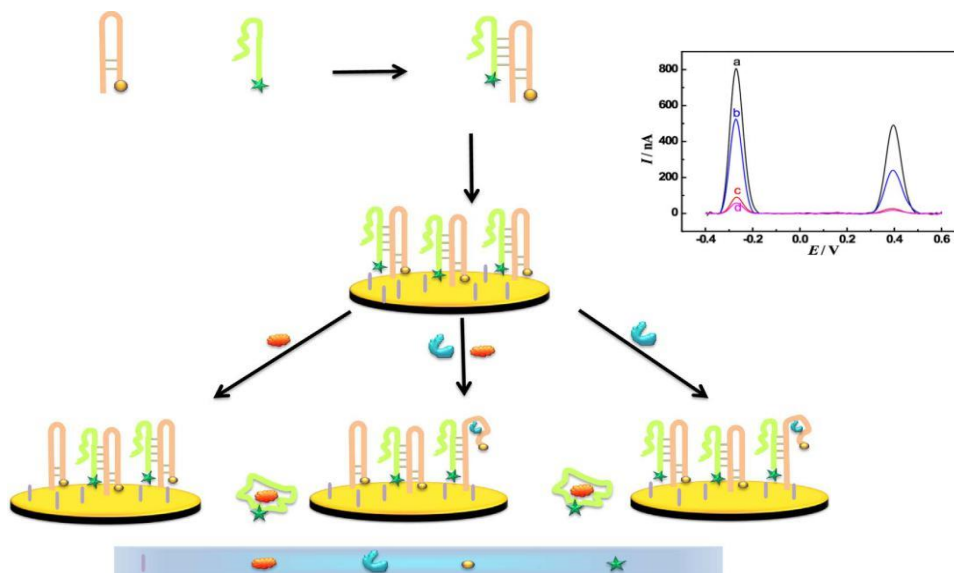


**Figure 1-19.** A) Schematic representation of the ISP-based aptasensor for dual-analyte detection. B) SWV responses of MCH/ISP4/AuNPs/GCE (a, b) and MCH/ISP4/gold electrode (c, d) in PBS (10 mM, pH 7.4) before and after introduction of solution containing 100 ng mL<sup>-1</sup> CEA and 100 nM MUC1. Reproduced from <sup>246</sup>.

### 1.18.3 Signal amplification strategy

Motivated by high sensitivity brought about by signal amplification, Wen et al <sup>247</sup>, proposed an exonuclease enzyme-assisted target recycling amplification strategy for their aptasensor. Here, the initial electrochemical signal is generated by dsDNA structure composed of S1 and S2 aptamers modified with MB (**Figure 1-20**). The signal reduction and amplification were carried out by introduction of MUC1 and an exonuclease, respectively. After MUC1 target addition, S2 is dissociated from S1 and the exonuclease can digest ssDNA.

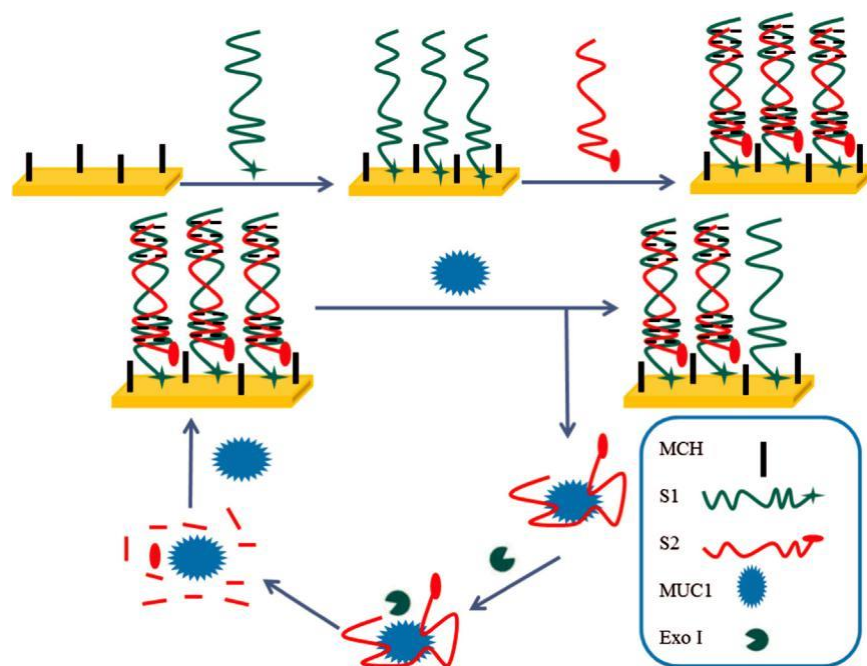


**Figure 1-20.** Schematic diagram of aptasensor fabrication process for the MUC1 detection based on insertion approach and Exo I-assisted recycling. Reproduced from <sup>247</sup>.

The digestion of the S2 releases MUC1, which can once again hybridize with S2. This design allowed multiple rounds of target hybridization and exhibited a LDR from 10 pM to 1  $\mu$ M associated to a LOD of 4 pM. This method is a smart strategy for high amplification factor but is labour intensiveness to generate analytical signal and due to the inverse relationship between the signal current and concentration of the target, the signal amplification capacity is limited.

Alternatively, another sensitive electrochemical aptasensor with a DNA bulge-loop (as a L-DNA probe) was fabricated through hybridization of the MUC1 aptamer with methylene blue labeled complementary aptamer with high-efficient exonuclease I (Exo I)-assisted target recycling amplification strategy (**Figure 1-21**)<sup>248</sup>. Due to the existing electrostatic repulsion between negatively charged ITO and the L-DNA, only a small electrochemical signal was initially detected. However, upon addition of MUC1 as the target, the L-DNA structure is dissociated due to the

MUC1/ aptamer affinity. By adding Exo I, the liberated cDNA-MB was digested into nucleotides resulting in the production of short MB-labeled mononucleotides fragments MB-MFs). Given the low negative charges of MB-MFs, they diffused to the negatively charged ITO electrode surface and produced a stronger electrochemical signal which then is used as analytical current.

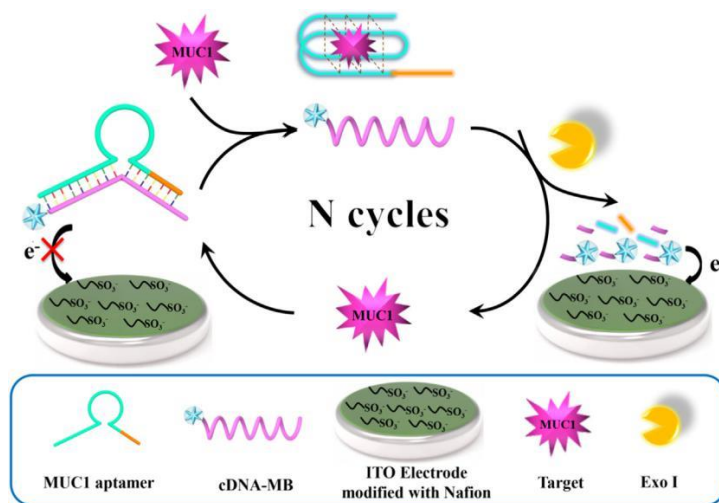


**Figure 1-21.** Schematic illustration of the proposed homogeneous electrochemical aptasensor for MUC1 detection based on Exo I-assisted target recycling amplification. Reproduced from <sup>248</sup>.

This enhanced electrochemical signal was linearly proportional to the log of [MUC1] concentration in the range of 1.0 pg ml<sup>-1</sup> – 50 ng ml<sup>-1</sup> and the LOD for this assay was as low as 0.40 pg ml<sup>-1</sup>. The proposed strategy has the potential to detect other tumor biomarkers by only changing the corresponding aptamer sequence of target. Since this is a signal-on type of biosensor, the amplification capacity is theoretically limitless, the clinical relevance is doubtful since the but given that the signal generation mostly relies on electrostatic forces between the ITO surface and the prob aptamer, the corresponding application in real samples where there are abundant of charged particles faces a real challenge.

Inspired by the ongoing progress in molecular design and interfacial strategies, to address low signal-to-noise, and hence high sensitivity in E-AB sensor application while sticking to simplicity in the signal generation and the performance, we have developed a novel and versatile strategy by judiciously combining an elaborated molecular redox tag with a so-called screening effect derived by backfilling passivation layer, and applied it for the detection the MUC1 and VEGF<sub>165</sub> biomarkers in huma serum. To do this, a lysine molecule, as linker, was conjugated with two MB molecules, tethered to 5'- end terminus of the surface-bound DNA probe aptamer backfilled with a 9-carbon thick alkyl thiol SAM passivating layer (**Figure 1-22**). Increasing the passivating layer thickness up to 9 carbon was proved to be critical in the optimal signal generation. results showed that the synergy effect between SAM thickness, and the augmented redox assembly can lead to 60% gain enhancement for MUC1 detection in the signal-off, and up to 195%. in the signal-on type of E-AB sensor for the detection of VEGF<sub>165</sub>. which in turn led to an order of magnitude improvement in LOD i.e., from 3.7 nM to 0.32 nM in detection of the MUC1 biomarker, and from 6.4 pM to 0.56 pM in the case of VEGF<sub>165</sub> biomarker when employed in human serum samples (comparisons were made with conventional mode of fabrication). Considering the LDR, ranging from 1nM to 500 nM for MUC1, and also from 2 pM to 300 pM for the VEGF<sub>165</sub> biomarker, both E-AB sensors revealed a meaningful clinical relevance which makes them potentially liable for diagnostic devices. thus, we have developed a simple, and truly reagentless sensing platform that can address high sensitivity and readily circumvent the low signal-to-noise. The latter attribute potentially qualifies the strategy for miniaturization applications. where the lack of high surface area disrupts the sensitivity. furthermore, being reagentless, the outline doesn't demand for additional steps in signal generation. **Figure 1-22** illustrates different stages in conjugation and sensor fabrication. One caveat of such an application is that the signal amplification is somehow

limited to the number of redox tags tethered to the probe aptamer. Also, there is always a chance that such inclusion would disrupt the natural dynamics of the probe aptamer and hence could impact the affinity. Though the latter effect was not observed, such validation is highly encouraged.

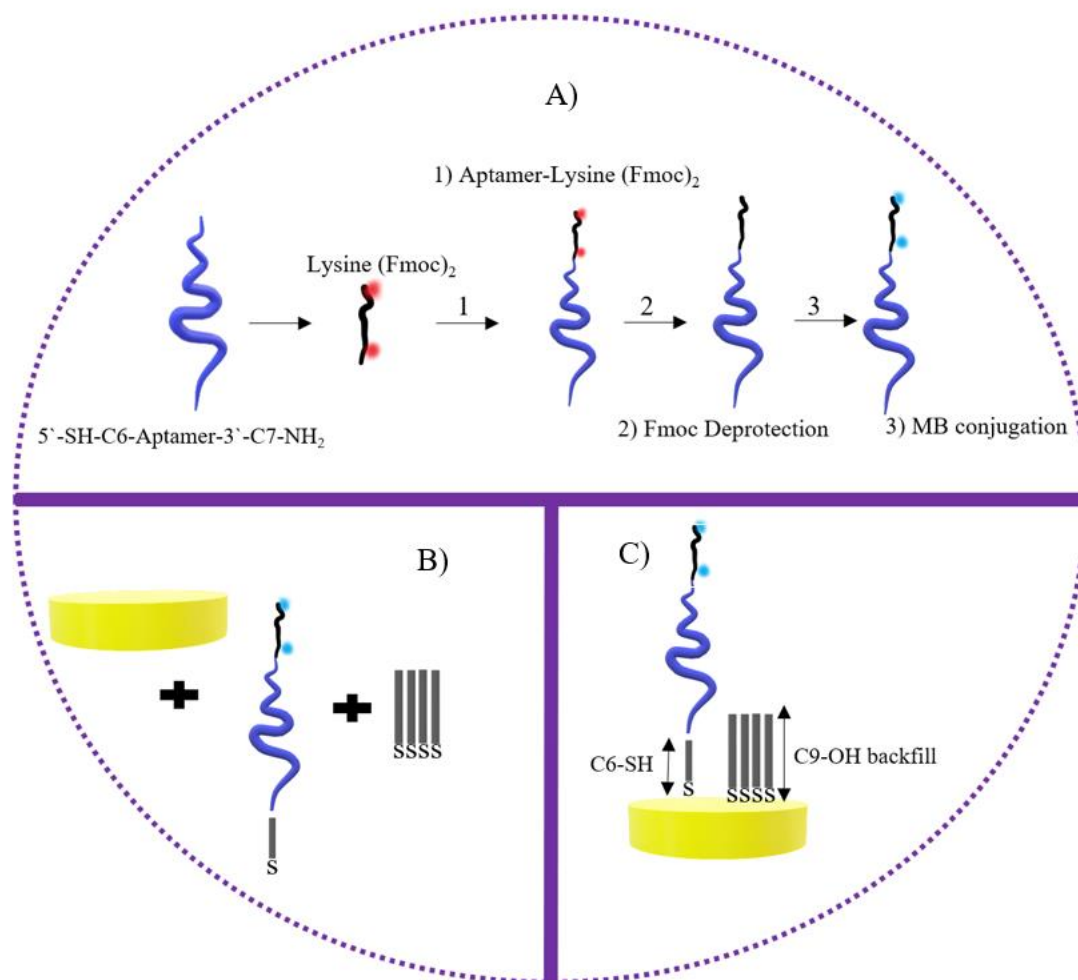


**Figure 1-22.** schematic illustration of reaction steps (A). fabrication elements (B). the final sensing platform is based on a modified aptamer chemisorbed on a gold electrode, backfilled with C9-OH alkylatiol (C). Fmoc represents the fluorenyl methoxycarbonyl protecting group for amino functionalities on the lysine molecule to facilitate selective conjugation.

## Conclusion

To this date, E-AB sensors have shown to be promising in the development of diagnostic tools for real-world applications allowing real-time measurement of a great variety of targets ranging from small molecules to proteins even in unprocessed biological fluids without depending on the chemical reactivity of their targets. Here, we have critically discussed the most influential parameters on the E-AB sensor performance in terms of fabrication and operational parameters. It is evident that a whole set of essential optimizations is required to identify the best interrogation parameters during the development of next-generation DNA-based sensors. On the other hand, with enough acknowledgment of these parameters, objectively, they cannot address many of the challenges. Such as the solution for simultaneous target analysis, the way we can impart amplification to signal generation, or for example, how it is possible to delay surface non-specific adsorption.

In addition, in the second part of this review, we highlighted the importance of how new approaches regarding molecular design in the bioelectrochemical interface can meet further demands. In doing so, to avoid confusion and in the meantime, to stick with rational comparison we tried to incorporate MUC1 as one of the approved biomarkers in breast cancer treatment navigation. Accordingly, it is safe to say that only rigorous duplication in the fabrication/application of an E-AB sensor is likely to end up with the same results. As a small variation in temperature, buffer composition, ionic strength, and solvents or biofluids, can affect the E-AB sensor's performance.

In the end, it can be concluded that the realm of biosensors is still in its inchoate stages as the true translation from laboratory-bound proof-of-the-concept demonstrations to a versatile device for a closely relevant clinical application awaits further developments.

## References

- 1 W. H. Organization, WHO Report on Cancer: Setting Priorities, Investing Wisely and Providing Care for All. 2020.
- 2 Surveys and statistical programs - Canadian Cancer Registry (CCR), <https://www23.statcan.gc.ca/imdb/p2SV.pl?Function=getSurvey&SDDS=3207&lang=en&db=imdb&adm=8&dis=2>, (accessed 6 August 2022).
- 3 Cancer Research UK, <https://www.cancerresearchuk.org/>, (accessed 6 August 2022).
- 4 E. L. Bird-Lieberman and R. C. Fitzgerald, *Br. J. Cancer*, 2009, **101**, 1–6.
- 5 S. Abati, C. Bramati, S. Bondi, A. Lissoni and M. Trimarchi, *Int. J. Environ. Res. Public Heal.* 2020, Vol. 17, Page 9160, 2020, **17**, 9160.
- 6 T. Baykul, H. H. Yilmaz, Ü. Aydin, M. A. Aydin, M. Ç. Aksoy and D. Yildirim, *J. Int. Med. Res.*, 2010, **38**, 737–749.
- 7 S. Lam and H. Shibuya, *Clin. Chest Med.*, 1999, **20**, 53–61.
- 8 J. Austoker, *BMJ*, 1994, **308**, 1682–1686.
- 9 A. M. Lutz, J. K. Willmann, C. W. Drescher, P. Ray, F. V. Cochran, N. Urban and S. S. Gambhir, *Radiology*, 2011, **259**, 329–345.
- 10 C. Coleman, *Semin. Oncol. Nurs.*, 2017, **33**, 141–155.
- 11 W. Hamilton, F. M. Walter, G. Rubin and R. D. Neal, *Nat. Rev. Clin. Oncol.*, 2016, **13**, 740–749.
- 12 S. S. Raab and D. M. Grzybicki, *CA. Cancer J. Clin.*, 2010, **60**, 139–165.
- 13 M. P. Coleman, D. Forman, H. Bryant, J. Butler, B. Rachet, C. Maringe, U. Nur, E. Tracey, M. Coory, J. Hatcher, C. E. McGahan, D. Turner, L. Marrett, M. L. Gjerstorff, T. B. Johannesen, J. Adolfsson, M. Lambe, G. Lawrence, D. Meechan, E. J. Morris, R. Middleton, J. Steward and M. A. Richards, *Lancet*, 2011, **377**, 127–138.
- 14 B. Crew, *Nature*, 2020, **580**, S5–S7.
- 15 J. Feng, B. Li, J. Ying, W. Pan, C. Liu, T. Luo, H. Lin and L. Zheng, *Small Struct.*, 2020, **1**, 2000063.
- 16 D. Crosby, *Br. J. Cancer* 2021 1263, 2022, **126**, 313–315.
- 17 A. K. Mattox, C. Bettegowda, S. Zhou, N. Papadopoulos, K. W. Kinzler and B. Vogelstein, *Sci. Transl. Med.*, , DOI:10.1126/SCITRANSLMED.AAY1984.
- 18 G. Siravegna, S. Marsoni, S. Siena and A. Bardelli, *Nat. Rev. Clin. Oncol.* 2017 149, 2017, **14**, 531–548.
- 19 J. Marrugo-Ramírez, M. Mir and J. Samitier, *Int. J. Mol. Sci.*, , DOI:10.3390/IJMS19102877.
- 20 M. Bahassi, J. Mol Biomark Diagn and E. Mustapha Bahassi, *J Mol Biomark Diagn*, 2013, **4**, 157.
- 21 M. L. Wroclawski, A. Serpa-Neto, F. L. A. Fonseca, O. Castro-Neves-Neto, A. S. F. L. Pompeo, M. T. Machado, A. C. L. Pompeo and A. Del Giglio, *Tumor Biol.* 2013 345, 2013, **34**, 2921–2927.
- 22 H. Schwarzenbach, J. Stoehlmacher, K. Pantel and E. Goekkurt, *Ann. N. Y. Acad. Sci.*, 2008, **1137**, 190–196.
- 23 Analysis of circulating tumor DNA in plasma at diagnosis and during follow-up of lung cancer patients - PubMed, <https://pubmed.ncbi.nlm.nih.gov/11406535/>, (accessed 6 August 2022).
- 24 T. Frisk, N. Sandström, L. Eng, W. Van Der Wijngaart, P. Månsson and G. Stemme, *pubs.rsc.org*, ,

DOI:10.1039/b800487k.

- 25 T. Sakata and Y. Miyahara, *ChemBioChem*, 2005, **6**, 703–710.
- 26 H. J. Park, S. K. Kim, K. Park, H. K. Lyu, C. S. Lee, S. J. Chung, W. S. Yun, M. Kim and B. H. Chung, *FEBS Lett.*, 2009, **583**, 157–162.
- 27 M. Gouzy, M. Keß, P. K.-B. and Bioelectronics and undefined 2009, *Elsevier*.
- 28 R. Rich, G. Papalia, P. Flynn, ... J. F.-A. and undefined 2009, *Elsevier*.
- 29 Y. Du, B. Li, H. Wei, Y. Wang and E. Wang, *Angew. Chem., Int. Ed.*, 1990, **346**, 5110–5117.
- 30 A. Bogomolova, E. Komarova, K. Reber, T. Gerasimov, O. Yavuz, S. Bhatt and M. Aldissi, *Anal. Chem.*, 2009, **81**, 3944–3949.
- 31 N. S. Que-Gewirth and B. A. Sullenger, *Gene Ther. 2007 144*, 2007, **14**, 283–291.
- 32 S. Song, L. Wang, J. Li, C. Fan and J. Zhao, *TrAC Trends Anal. Chem.*, 2008, **27**, 108–117.
- 33 C. M. Dollins, S. Nair and B. A. Sullenger, <https://home.liebertpub.com/hum>, 2008, **19**, 443–450.
- 34 R. Reid, B. Chatterjee, S. J. Das, S. Ghosh and T. K. Sharma, *Anal. Biochem.*, 2020, **593**, 113574.
- 35 K. Han, L. Chen, Z. Lin and G. Li, *Electrochem. commun.*, 2009, **11**, 157–160.
- 36 J. Liu and Y. Lu, *Angew. Chemie Int. Ed.*, 2006, **45**, 90–94.
- 37 W. Zhao, W. Chiuman, J. C. F. Lam, S. A. McManus, W. Chen, Y. Cui, R. Pelton, M. A. Brook and Y. Li, *J. Am. Chem. Soc.*, 2008, **130**, 3610–3618.
- 38 Y. Xiao, A. A. Lubin, A. J. Heeger and K. W. Plaxco, *Angew. Chemie*, 2005, **117**, 5592–5595.
- 39 J. Wang, W. Meng, X. Zheng, S. Liu and G. Li, *Biosens. Bioelectron.*, 2009, **24**, 1598–1602.
- 40 J. H. T. Luong, K. B. Male and J. D. Glennon, *Biotechnol. Adv.*, 2008, **26**, 492–500.
- 41 Y. Xiao, A. A. Lubin, A. J. Heeger and K. W. Plaxco, *Angew. Chemie Int. Ed.*, 2005, **44**, 5456–5459.
- 42 L. Bock, L. Griffin, J. Latham, E. Vermaas, J. T.- Nature and undefined 1992, *nature.com*.
- 43 A. Ellington, J. S.- nature and undefined 1990, *nature.com*, , DOI:10.1038/346818a0.
- 44 L. Gold, *J. Mol. Evol.*, 2015, **81**, 140–143.
- 45 J. Kohn, K. P. the N. A. of Sciences and undefined 2005, *Natl. Acad. Sci.*
- 46 K. J. Oh, K. J. Cash and K. W. Plaxco, *Chem. - A Eur. J.*, 2009, **15**, 2244–2251.
- 47 A. A. Lubin and K. W. Plaxco, *Acc. Chem. Res.*, 2010, **43**, 496–505.
- 48 F. Ricci, A. Vallée-Bélisle, A. J. Simon, A. Porchetta and K. W. Plaxco, *Acc. Chem. Res.*, 2016, **49**, 1884–1892.
- 49 F. L. Kiechle, *Diabetes Technol. Ther.*, 2001, **3**, 647–650.
- 50 R. J. White, N. Phares, A. A. Lubin, Y. Xiao and K. W. Plaxco, *Langmuir*, 2008, **24**, 10513–10518.
- 51 L. M. Demers, C. A. Mirkin, R. C. Mucic, R. A. Reynolds, R. L. Letsinger, R. Elghanian and G. Viswanadham, *Anal. Chem.*, 2000, **72**, 5535–5541.
- 52 A. B. Steel, T. M. Herne and M. J. Tarlov, *Anal. Chem.*, 1998, **70**, 4670–4677.
- 53 P. V. Riccelli, F. Merante, K. T. Leung, S. Bortolin, R. L. Zastawny, R. Janeczko and A. S. Benight, *Nucleic*

- Acids Res.*, 2001, **29**, 996–1004.
- 54 A. Meller, L. Nivon and D. Branton, *Phys. Rev. Lett.*, 2001, **86**, 3435–3438.
- 55 A. Reuter, W. U. Dittmer and F. C. Simmel, *Eur. Phys. J. E*, 2007, **22**, 33–40.
- 56 Q. Zhou, K. Son, Y. Liu and A. Revzin, *Annu. Rev. Biomed. Eng.*, 2015, **17**, 165–190.
- 57 Y. Liu, Z. Matharu, M. C. Howland, A. Revzin and A. L. Simonian, *Anal. Bioanal. Chem.*, 2012, 404, 1181–1196.
- 58 A. L. Furst, M. G. Hill and J. K. Barton, *Langmuir*, 2015, **31**, 6554–6562.
- 59 A. Z. Bradley, M. G. Kociolek and R. P. Johnson, *J. Org. Chem.*, 2000, **65**, 7134–7138.
- 60 K. S. Sykes, L. F. L. Oliveira, G. Stan and R. J. White, *Langmuir*, 2019, **35**, 12962–12970.
- 61 L. Qi, H. Tian and H. Z. Yu, *Anal. Chem.*, 2018, **90**, 9174–9181.
- 62 L. R. Schoukroun-Barnes, F. C. Macazo, B. Gutierrez, J. Lottermoser, J. Liu and R. J. White, *Annu. Rev. Anal. Chem.*, 2016, **9**, 163–181.
- 63 Y. Xiao, T. Uzawa, R. J. White, D. DeMartini and K. W. Plaxco, *Electroanalysis*, 2009, **21**, 1267–1271.
- 64 D. E. Weisshaar, B. D. Lamp and M. D. Porter, *J. Am. Chem. Soc.*, 1992, 114, 5860–5862.
- 65 H. Ron and I. Rubinstein, *J. Am. Chem. Soc.*, 1998, **120**, 13444–13452.
- 66 A. Peterson, R. H.-N. acids research and undefined 2001, *academic.oup.com*.
- 67 K. Leung, A. Gaxiola, H. Yu, D. B.-E. Acta and undefined 2018, *Elsevier*.
- 68 D. Jambrec, M. Gebala, F. La Mantia and W. Schuhmann, *Angew. Chemie Int. Ed.*, 2015, **54**, 15064–15068.
- 69 D. Jambrec, F. Conzuelo, A. Estrada-Vargas and W. Schuhmann, *ChemElectroChem*, 2016, **3**, 1484–1489.
- 70 R. Levicky, T. M. Herne, M. J. Tarlov and S. K. Satija, *J. Am. Chem. Soc.*, 1998, **120**, 9787–9792.
- 71 T. M. Herne and M. J. Tarlov, *J. Am. Chem. Soc.*, 1997, **119**, 8916–8920.
- 72 K. A. Peterlinz, R. M. Georgiadis, T. M. Herne and M. J. Tarlov, *J. Am. Chem. Soc.*, 1997, **119**, 3401–3402.
- 73 C. Y. Lee, P. Gong, G. M. Harbers, D. W. Grainger, D. G. Castner and L. J. Gamble, *Anal. Chem.*, 2006, **78**, 3316–3325.
- 74 F. Ricci, N. Zari, F. Caprio, S. Recine, A. Amine, D. Moscone, G. Palleschi and K. W. Plaxco, *Bioelectrochemistry*, 2009, **76**, 208–213.
- 75 E. Ostuni, R. G. Chapman, M. N. Liang, G. Meluleni, G. Pier, D. E. Ingber and G. M. Whitesides, *ACS Publ.*, 2001, **17**, 6336–6343.
- 76 R. E. Holmlin, X. Chen, R. G. Chapman, S. Takayama and G. M. Whitesides, *Langmuir*, 2001, **17**, 2841–2850.
- 77 H. Li, P. Dauphin-Ducharme, N. Arroyo-Currás, C. H. Tran, P. A. Vieira, S. Li, C. Shin, J. Somerson, T. E. Kippin and K. W. Plaxco, *Angew. Chemie Int. Ed.*, 2017, **56**, 7492–7495.
- 78 X. Xu, A. Makaraviciute, S. Kumar, C. Wen, M. Sjödin, E. Abdurakhmanov, U. H. Danielson, L. Nyholm and Z. Zhang, *Anal. Chem.*, , DOI:10.1021/acs.analchem.9b03946.
- 79 A. Steel, R. Levicky, T. Herne, M. T.-B. journal and undefined 2000, *Elsevier*.
- 80 D. Rekish, Y. Lyubchenko, L. S.-B. journal and undefined 1996, *Elsevier*.

- 81 C. A. Mirkin, R. L. Letsinger, R. C. Mucic and J. J. Storhoff, *Nature*, 1996, **382**, 607–609.
- 82 \* Bernard Tinland, Alain Pluen, and Jean Sturm and G. Weill, , DOI:10.1021/MA970381+.
- 83 D. Kang, F. Ricci, R. J. White and K. W. Plaxco, *Anal. Chem.*, 2016, **88**, 10452–10458.
- 84 D. Kang, X. Zuo, R. Yang, F. Xia, K. W. Plaxco and R. J. White, *Anal. Chem.*, 2009, **81**, 9109–9113.
- 85 H. Li, N. Arroyo-Currás, D. Kang, F. Ricci and K. W. Plaxco, *J. Am. Chem. Soc.*, 2016, **138**, 15809–15812.
- 86 E. González-Fernández, N. Avlonitis, A. F. Murray, A. R. Mount and M. Bradley, *Biosens. Bioelectron.*, 2016, **84**, 82–88.
- 87 R. Prins, A. R. Korswagen and A. G. T. G. Kortbeek, *J. Organomet. Chem.*, 1972, **39**, 335–344.
- 88 R. Prins, A. R. Korswagen and A. G. T. G. Kortbeek, *J. Organomet. Chem.*, 1972, **39**, 335–344.
- 89 E. E. Ferapontova and K. V. Gothelf, *Electroanalysis*, 2009, **21**, 1261–1266.
- 90 E. E. Ferapontova and K. V. Gothelf, *Electroanalysis*, 2009, **21**, 1261–1266.
- 91 P. Dauphin-Ducharme and K. W. Plaxco, *Anal. Chem.*, 2016, **88**, 11654–11662.
- 92 M. D. Mayer and R. Y. Lai, *Talanta*, 2018, **189**, 585–591.
- 93 S. D. Curtis, K. L. Ploense, M. Kurnik, G. Ortega, C. Parolo, T. E. Kippin, K. W. Plaxco and N. Arroyo-Currás, *Anal. Chem.*, 2019, **91**, 12321–12328.
- 94 P. Dauphin-Ducharme, N. Arroyo-Currás, R. Adhikari, J. Somerson, G. Ortega, D. E. Makarov and K. W. Plaxco, *J. Phys. Chem. C*, 2018, **122**, 21441–21448.
- 95 R. J. White and K. W. Plaxco, *Anal. Chem.*, 2010, **82**, 73–76.
- 96 L. A. Torre, F. Bray, R. L. Siegel, J. Ferlay, J. Lortet-Tieulent and A. Jemal, *CA. Cancer J. Clin.*, 2015, **65**, 87–108.
- 97 F. Cardoso, D. Spence, S. Mertz, D. Corneliussen-James, K. Sabelko, J. Gralow, M. J. Cardoso, F. Peccatori, D. Paonessa, A. Benares, N. Sakurai, M. Beishon, S. J. Barker and M. Mayer, *Breast*, 2018, **39**, 131–138.
- 98 H. K. Weir, T. D. Thompson, S. L. Stewart and M. C. White, *Prev. Chronic Dis.*, 2021, **18**, 1–8.
- 99 R. Etzioni, N. Urban, S. Ramsey, M. McIntosh, S. Schwartz, B. Reid, J. Radich, G. Anderson and L. Hartwell, *Nat. Rev. Cancer* 2003 34, 2003, **3**, 243–252.
- 100 A. Jemal, R. Siegel, E. Ward, Y. Hao, J. Xu, T. Murray and M. J. Thun, *CA. Cancer J. Clin.*, 2008, **58**, 71–96.
- 101 S. Y. Loke and A. S. G. Lee, *Eur. J. Cancer*, 2018, **92**, 54–68.
- 102 S. A. Eccles, E. O. Aboagye, S. Ali, A. S. Anderson, J. Armes, F. Berditchevski, J. P. Blaydes, K. Brennan, N. J. Brown, H. E. Bryant, N. J. Bundred, J. M. Burchell, A. M. Campbell, J. S. Carroll, R. B. Clarke, C. E. Coles, G. J. R. Cook, A. Cox, N. J. Curtin, L. V. Dekker, I. dos Santos Silva, S. W. Duffy, D. F. Easton, D. M. Eccles, D. R. Edwards, J. Edwards, D. G. Evans, D. F. Fenlon, J. M. Flanagan, C. Foster, W. M. Gallagher, M. Garcia-Closas, J. M. W. Gee, A. J. Gescher, V. Goh, A. M. Groves, A. J. Harvey, M. Harvie, B. T. Hennessy, S. Hiscox, I. Holen, S. J. Howell, A. Howell, G. Hubbard, N. Hulbert-Williams, M. S. Hunter, B. Jasani, L. J. Jones, T. J. Key, C. C. Kirwan, A. Kong, I. H. Kunkler, S. P. Langdon, M. O. Leach, D. J. Mann, J. F. Marshall, L. A. Martin, S. G. Martin, J. E. Macdougall, D. W. Miles, W. R. Miller, J. R. Morris, S. M. Moss, P. Mullan, R. Natrajan, J. P. B. O’Connor, R. O’Connor, C. Palmieri, P. D. P. Pharoah, E. A. Rakha, E. Reed, S. P. Robinson, E. Sahai, J. M. Saxton, P. Schmid, M. J. Smalley, V. Speirs, R. Stein, J. Stingl, C. H. Streuli, A. N. J. Tutt, G. Velikova, R. A. Walker, C. J. Watson, K. J. Williams, L. S. Young and A. M. Thompson, *Breast Cancer Res.* 2013 155, 2013, **15**, 1–37.

- 103 R. Simon, *JNCI J. Natl. Cancer Inst.*, 2015, **107**, 153.
- 104 V. Gajdosova, L. Lorencova, P. Kasak and J. Tkac, *Sensors (Switzerland)*, 2020, **20**, 1–37.
- 105 S. Mittal, H. Kaur, N. Gautam and A. K. Mantha, *Biosens. Bioelectron.*, 2017, **88**, 217–231.
- 106 S. Akbari Nakhjavani, B. Khalilzadeh, P. Samadi Pakchin, R. Saber, M. H. Ghahremani and Y. Omid, *Biosens. Bioelectron.*, 2018, **122**, 8–15.
- 107 M. J. Duffy, *Ann. Clin. Biochem.*, 1999, **36**, 579–586.
- 108 M. J. Duffy, D. Evoy and E. W. McDermott, *Clin. Chim. Acta*, 2010, **411**, 1869–1874.
- 109 M. J. Duffy, *Clin. Chem.*, 2006, **52**, 345–351.
- 110 M. Brooks, *Methods Mol. Biol.*, 2009, **472**, 307–321.
- 111 M. Gion, R. Mione, A. E. Leon and R. Dittadi, *Clin. Chem.*, 1999, **45**, 630–637.
- 112 V. M. Asiago, L. Z. Alvarado, N. Shanaiah, G. A. N. Gowda, K. Owusu-Sarfo, R. A. Ballas and D. Raftery, *Cancer Res.*, 2010, **70**, 8309–8318.
- 113 C. Denkert, E. Bucher, M. Hilvo, R. Salek, M. Orešič, J. Griffin, S. Brockmöller, F. Klauschen, S. Loibl, D. K. Barupal, J. Budczies, K. Iljin, V. Nekljudova and O. Fiehn, *Genome Med.*, 2012, **4**, 1–9.
- 114 P. L. Bedard and F. Cardoso, *Nat. Rev. Clin. Oncol.* 2011 85, 2011, **8**, 272–279.
- 115 M. Kaufmann and L. Pusztai, *Cancer*, 2011, **117**, 1575–1582.
- 116 R. Roy, J. Chun and S. N. Powell, *Nat. Rev. Cancer* 2012 121, 2011, **12**, 68–78.
- 117 S. Bayraktar and S. Glück, *Breast Cancer Res. Treat.*, 2012, **135**, 355–366.
- 118 C. M. Sturgeon, M. J. Duffy, U. H. Stenman, H. Lilja, N. Brünner, D. W. Chan, R. Babaian, R. C. Bast, B. Dowell, F. J. Esteva, C. Haglund, N. Harbeck, D. F. Hayes, M. Holten-Andersen, G. G. Klee, R. Lamerz, L. H. Looijenga, R. Molina, H. J. Nielsen, H. Rittenhouse, A. Semjonow, I. M. Shih, P. Sibley, G. Sölétormos, C. Stephan, L. Sokoll, B. R. Hoffman and E. P. Diamandis, *Clin. Chem.*, 2008, **54**, e11–e79.
- 119 A. Ziegler, U. Zangemeister-Wittke and R. A. Stahel, *Cancer Treat. Rev.*, 2002, **28**, 255–271.
- 120 M. Murtaza, S. J. Dawson, K. Pogrebniak, O. M. Rueda, E. Provenzano, J. Grant, S. F. Chin, D. W. Y. Tsui, F. Marass, D. Gale, H. R. Ali, P. Shah, T. Contente-Cuomo, H. Farahani, K. Shumansky, Z. Kingsbury, S. Humphray, D. Bentley, S. P. Shah, M. Wallis, N. Rosenfeld and C. Caldas, *Nat. Commun.* 2015 61, 2015, **6**, 1–6.
- 121 E. Heitzer, P. Ulz and J. B. Geigl, *Clin. Chem.*, 2015, **61**, 112–123.
- 122 N. Eigeliene, J. Saarenheimo and A. Jekunen, *Oncology*, 2019, **96**, 115–124.
- 123 L. De Mattos-Arruda and C. Caldas, *Mol. Oncol.*, 2016, **10**, 464–474.
- 124 E. Crowley, F. Di Nicolantonio, F. Loupakis and A. Bardelli, *Nat. Rev. Clin. Oncol.* 2013 108, 2013, **10**, 472–484.
- 125 C. Bettgowda, M. Sausen, R. J. Leary, I. Kinde, Y. Wang, N. Agrawal, B. R. Bartlett, H. Wang, B. Luber, R. M. Alani, E. S. Antonarakis, N. S. Azad, A. Bardelli, H. Brem, J. L. Cameron, C. C. Lee, L. A. Fecher, G. L. Gallia, P. Gibbs, D. Le, R. L. Giuntoli, M. Goggins, M. D. Hogarty, M. Holdhoff, S. M. Hong, Y. Jiao, H. H. Juhl, J. J. Kim, G. Siravegna, D. A. Laheru, C. Lauricella, M. Lim, E. J. Lipson, S. K. N. Marie, G. J. Netto, K. S. Oliner, A. Olivi, L. Olsson, G. J. Riggins, A. Sartore-Bianchi, K. Schmidt, I. M. Shih, S. M. Oba-Shinjo, S. Siena, D. Theodorescu, J. Tie, T. T. Harkins, S. Veronese, T. L. Wang, J. D. Weingart, C. L. Wolfgang, L. D. Wood, D. Xing, R. H. Hruban, J. Wu, P. J. Allen, C. M. Schmidt, M. A. Choti, V. E. Velculescu, K. W. Kinzler, B. Vogelstein, N. Papadopoulos and L. A. Diaz, *Sci. Transl. Med.*, ,

- 126 K. Uzawa, T. Baba, F. Uchida, M. Yamatoji, A. Kasamatsu, Y. Sakamoto, K. Ogawara, M. Shiiba, H. Bukawa and H. Tanzawa, *Oncotarget*, 2012, **3**, 670–677.
- 127 V. Swarup and M. R. Rajeswari, *FEBS Lett.*, 2007, **581**, 795–799.
- 128 V. Swarup and M. R. Rajeswari, *FEBS Lett.*, 2007, **581**, 795–799.
- 129 B. Bystricky and M. Mego, *Neoplasma*, 2016, **63**, 18–29.
- 130 P. S. Mitchell, R. K. Parkin, E. M. Kroh, B. R. Fritz, S. K. Wyman, E. L. Pogossova-Agadjanian, A. Peterson, J. Noteboom, K. C. O'Briant, A. Allen, D. W. Lin, N. Urban, C. W. Drescher, B. S. Knudsen, D. L. Stirewalt, R. Gentleman, R. L. Vessella, P. S. Nelson, D. B. Martin and M. Tewari, *Proc. Natl. Acad. Sci. U. S. A.*, 2008, **105**, 10513–10518.
- 131 H. Valadi, K. Ekström, A. Bossios, M. Sjöstrand, J. J. Lee and J. O. Lötvall, *Nat. Cell Biol.* 2007 96, 2007, **9**, 654–659.
- 132 T. Miyashita, H. Tajima, I. Makino, H. Nakagawara, H. Kitagawa, S. Fushida, J. W. Harmon and T. Ohta, *J. Surg. Res.*, 2015, **193**, 289–294.
- 133 F. André, E. Ciruelos, G. Rubovszky, M. Campone, S. Loibl, H. S. Rugo, H. Iwata, P. Conte, I. A. Mayer, B. Kaufman, T. Yamashita, Y.-S. Lu, K. Inoue, M. Takahashi, Z. Pápai, A.-S. Longin, D. Mills, C. Wilke, S. Hirawat and D. Juric, *N. Engl. J. Med.*, 2019, **380**, 1929–1940.
- 134 E. Fina, M. Callari, C. Reduzzi, F. D'Aiuto, G. Mariani, D. Generali, M. A. Pierotti, M. G. Daidone and V. Cappelletti, *Clin. Chem.*, 2015, **61**, 278–289.
- 135 G. Kallergi, S. Agelaki, M. A. Papadaki, D. Nasias, A. Matikas, D. Mavroudis and V. Georgoulis, *Breast Cancer Res.*, 2015, **17**, 1–11.
- 136 M. J. Duffy, S. Shering, F. Sherry, E. McDermott and N. O'Higgins, <https://doi.org/10.1177/172460080001500410>, 2018, **15**, 330–333.
- 137 M. Gerlinger, A. J. Rowan, S. Horswell, J. Larkin, D. Endesfelder, E. Gronroos, P. Martinez, N. Matthews, A. Stewart, P. Tarpey, I. Varela, B. Phillimore, S. Begum, N. Q. McDonald, A. Butler, D. Jones, K. Raine, C. Latimer, C. R. Santos, M. Nohadani, A. C. Eklund, B. Spencer-Dene, G. Clark, L. Pickering, G. Stamp, M. Gore, Z. Szallasi, J. Downward, P. A. Futreal and C. Swanton, *N. Engl. J. Med.*, 2012, **366**, 883–892.
- 138 H. Aoki, R. Ogura, Y. Tsukamoto, M. Okada, M. N. Sumeda, M. Isogawa, S. Yoshida and Y. Fujii, *Cent. Nerv. Syst. Cancers Version*, 2011, **2**, 19–21.
- 139 A. Ravelli, J. M. Reuben, F. Lanza, S. Anfossi, M. R. Cappelletti, L. Zanotti, A. Gobbi, C. Senti, P. Brambilla, M. Milani, D. Spada, P. Pedrazzoli, M. Martino, A. Bottini and D. Generali, *Tumor Biol.*, 2015, **36**, 6653–6665.
- 140 F. J. V. L and S. D, *Front. Biosci.*, 2001, **6**, d1207-1215.
- 141 L. K. Diaz, E. L. Wiley and M. Morrow, *Breast J.*, 2001, **7**, 40–45.
- 142 M. A. Hollingsworth and B. J. Swanson, *Nat. Rev. Cancer* 2004 41, 2004, **4**, 45–60.
- 143 Y. Masaki, M. Oka, Y. Ogura, T. Ueno, K. Nishihara, A. Tangoku, M. Takahashi, M. Yamamoto and T. Irimura, *Hepatology*, 1999, **46**, 2240–2245.
- 144 J. Wesseling, S. W. Van Der Valk and J. Hilkens, <https://doi.org/10.1091/mbc.7.4.565>, 2017, **7**, 565–577.
- 145 M. Yamamoto, A. Bharti, Y. Li and D. Kufe, *J. Biol. Chem.*, 1997, **272**, 12492–12494.
- 146 S. Z. Yang, N. Kohno, A. Yokoyama, K. Kondo, H. Hamada and K. Hiwada, *Int. J. Oncol.*, 2001, **18**, 541–548.

- 147 Decreased MUC1 Expression Induces E-Cadherin-mediated Cell Adhesion of Breast Cancer Cell Lines1 | Cancer Research | American Association for Cancer Research, <https://aacrjournals.org/cancerres/article/58/9/2014/505124/Decreased-MUC1-Expression-Induces-E-Cadherin>, (accessed 1 January 2023).
- 148 Association of the DF3/MUC1 Breast Cancer Antigen with Grb2 and the Sos/Ras Exchange Protein1 | Cancer Research | American Association for Cancer Research, <https://aacrjournals.org/cancerres/article/55/18/4000/501392/Association-of-the-DF3-MUC1-Breast-Cancer-Antigen>, (accessed 1 January 2023).
- 149 J. A. Schroeder, M. C. Thompson, M. M. Gardner and S. J. Gendler, *J. Biol. Chem.*, 2001, **276**, 13057–13064.
- 150 J. J. Rahn, L. Dabbagh, M. Pasdar and J. C. Hugh, , DOI:10.1002/1097-0142.
- 151 S. J. Gendler, *J. Mammary Gland Biol. Neoplasia*, 2001, **6**, 339–353.
- 152 J. R. Gum, J. W. Hicks, N. W. Toribara, B. Siddiki and Y. S. Kim, *J. Biol. Chem.*, 1994, **269**, 2440–2446.
- 153 M. Osako, S. Yonezawa, B. Siddiki, J. Huang, J. J. L. Ho, Y. S. Kim and E. Sato, , DOI:10.1002/1097-0142.
- 154 Expression of MUC1 and MUC2 mucins in gastric carcinomas: its relationship with the prognosis of the patients. | Clinical Cancer Research | American Association for Cancer Research, <https://aacrjournals.org/clincancerres/article/4/11/2605/12649/Expression-of-MUC1-and-MUC2-mucins-in-gastric>, (accessed 1 January 2023).
- 155 Selection of tumor antigens as targets for immune attack using immunohistochemistry: protein antigens. | Clinical Cancer Research | American Association for Cancer Research, <https://aacrjournals.org/clincancerres/article/4/11/2669/12479/Selection-of-tumor-antigens-as-targets-for-immune>, (accessed 1 January 2023).
- 156 F. Clayton, *Hum. Pathol.*, 1986, **17**, 34–38.
- 157 M. D. Walsh, M. A. McGuckin, P. L. Devine, B. G. Hohn and R. G. Wright, *J. Clin. Pathol.*, 1993, **46**, 922–925.
- 158 C. De Bolós, M. Garrido and F. X. Real, *Gastroenterology*, 1995, **109**, 723–734.
- 159 Mucin Gene Expression in Normal, Preneoplastic, and Neoplastic Human Gastric Epithelium1 | Cancer Research | American Association for Cancer Research, <https://aacrjournals.org/cancerres/article/55/12/2681/501420/Mucin-Gene-Expression-in-Normal-Preneoplastic-and>, (accessed 1 January 2023).
- 160 M. B. Pereira, A. J. Dias, C. A. Reis and F. C. Schmitt, *J. Clin. Pathol.*, 2001, **54**, 210–213.
- 161 R. Q. Wang and D. C. Fang, *J. Clin. Pathol.*, 2003, **56**, 378–384.
- 162 K. L. Carraway, S. A. Price-Schiavi, M. Komatsu, S. Jepson, A. Perez and C. A. Carothers Carraway, *J. Mammary Gland Biol. Neoplasia*, 2001, **6**, 323–337.
- 163 K. L. Carraway, E. A. Rossi, M. Komatsu, S. A. Price-Schiavi, D. Huang, P. M. Guy, M. E. Carvajal, N. Fregien, C. A. Carothers Carraway and K. L. Carraway, *J. Biol. Chem.*, 1999, **274**, 5263–5266.
- 164 S. A. Price-Schiavi, S. Jepson, P. Li, M. Arango, P. S. Rudland, L. Yee and K. L. Carraway, *Int. J. Cancer*, 2002, **99**, 783–791.
- 165 P. L. Nguyen, G. A. Niehans, D. L. Cherwitz, Y. S. Kim and S. B. Ho, *Tumor Biol.*, 1996, **17**, 176–192.
- 166 J. S. Chu and K. J. Chang, *Cancer Lett.*, 1999, **142**, 121–127.
- 167 S. Nath and P. Mukherjee, *Trends Mol. Med.*, 2014, **20**, 332–342.
- 168 M. Bose and P. Mukherjee, *Trends Mol. Med.*, 2020, **26**, 324–336.

- 169 T. Gao, Q. Cen and H. Lei, *Biomed. Pharmacother.*, , DOI:10.1016/J.BIOPHA.2020.110888.
- 170 M. Marczynski, B. Winkeljann and O. Lieleg, *Biopolym. Biomed. Biotechnol. Appl.*, 2021, 181–208.
- 171 A. Kasprzak and A. Adamek, *Int. J. Mol. Sci.* 2019, Vol. 20, Page 1288, 2019, **20**, 1288.
- 172 C. L. Hattrup and S. J. Gendler, <https://doi.org/10.1146/annurev.physiol.70.113006.100659>, 2008, **70**, 431–457.
- 173 M. S. Syrkina, A. A. Maslakova, D. M. Potashnikova, V. P. Veiko, Y. S. Vassetzky and M. A. Rubtsov, *J. Cell. Biochem.*, 2017, **118**, 4002–4011.
- 174 R. Singh and D. Bandyopadhyay, <http://dx.doi.org/10.4161/cbt.6.4.4201>, 2007, **6**, 481–486.
- 175 D. M. Beckwith and M. Cudic, *Semin. Immunol.*, 2020, **47**, 101389.
- 176 W. Chen, Z. Zhang, S. Zhang, P. Zhu, J. K. S. Ko and K. K. L. Yung, *Int. J. Mol. Sci.* 2021, Vol. 22, Page 6567, 2021, **22**, 6567.
- 177 L. Sanislo, K. B. Vertakova, P. Kuliffay, J. Brtko, A. Galbava and S. Galbavy, *Endocr. Regul.*, 2011, **45**, 113–124.
- 178 D. Marrinucci, K. Bethel, A. Kolatkar, M. S. Luttgen, M. Malchiodi, F. Baehring, K. Voigt, D. Lazar, J. Nieva, L. Bazhenova, A. H. Ko, W. M. Korn, E. Schram, M. Coward, X. Yang, T. Metzner, R. Lamy, M. Honnatti, C. Yoshioka, J. Kunken, Y. Petrova, D. Sok, D. Nelson and P. Kuhn, *Phys. Biol.*, 2012, **9**, 016003.
- 179 M. Y. Sha, H. Xu, M. J. Natan and R. Cromer, *J. Am. Chem. Soc.*, 2008, **130**, 17214–17215.
- 180 A. De Albuquerque, S. Kaul, G. Breier, P. Krabisch and N. Fersis, *Breast Care*, 2012, **7**, 7–12.
- 181 J. F. Rovet, *Endocr. Dev.*, 2014, **26**, 26–43.
- 182 A. De Albuquerque, I. Kubisch, D. Ernst, G. Breier, G. Stamminger, N. Fersis, U. Stölzel, J. Boese-Landgraf, A. Eichler and S. Kaul, *Clin. Lab.*, 2012, **58**, 373–384.
- 183 B. Aktas, V. Müller, M. Tewes, J. Zeitz, S. Kasimir-Bauer, C. R. Loehberg, B. Rack, A. Schneeweiss and T. Fehm, *Gynecol. Oncol.*, 2011, **122**, 356–360.
- 184 L. Karthik, G. Kumar, T. Keswani, A. Bhattacharyya, S. Sarath Chandar and K. V. Bhaskara Rao, *PLoS One*, 2014, **9**, e90972.
- 185 J. C. Grutters, .
- 186 A. González-Sistal, J. I. Arias and Á. Ruibal, <https://doi.org/10.5301/JBM.2011.8591>, 2018, **27**, 47–52.
- 187 A. Fakhari, E. Gharepapagh, S. Dabiri, A. Fakhari, E. Gharepapagh, S. Dabiri and N. Gilani, *Med. J. Islam. Repub. Iran*, 2019, **33**, 142.
- 188 J. S. Lee, S. Park, J. M. Park, J. H. Cho, S. I. Kim and B. W. Park, *Ann. Oncol.*, 2013, **24**, 1225–1231.
- 189 M. Incoronato, P. Mirabelli, O. Catalano, M. Aiello, C. Parente, A. Soricelli and E. Nicolai, *BMC Cancer*, 2014, **14**, 1–6.
- 190 D. Al-Azawi, G. Kelly, E. Myers, E. W. McDermott, A. D. K. Hill, M. J. Duffy and N. O. Higgins, *BMC Cancer*, 2006, **6**, 1–7.
- 191 W. G. Chu and D. W. Ryu, *Ann. Surg. Treat. Res.*, 2015, **90**, 57–63.
- 192 A. Berruti, M. Tampellini, M. Torta, T. Buniva, G. Gorzegno and L. Dogliotti, *Eur. J. Cancer*, 1994, **30**, 2082–2084.
- 193 P. Bliss, R. C. F. Leonard, J. Fiskens and J. Roulsten, *Dis. Markers*, 1993, **11**, 45–48.

- 194 I. A. Darwish, T. A. Wani, N. Y. Khalil and D. A. Blake, *Talanta*, 2012, **97**, 499–504.
- 195 M. J. Duffy, C. Duggan, R. Keane, A. D. K. Hill, E. McDermott, J. Crown and N. O’Higgins, *Clin. Chem.*, 2004, **50**, 559–563.
- 196
- 197 F. G. Ebeling, P. Stieber, M. Untch, D. Nagel, G. E. Konecny, U. M. Schmitt, A. Fateh-Moghadam and D. Seidel, *Br. J. Cancer* 2002 868, 2002, **86**, 1217–1222.
- 198 N. Ferrara, H. P. Gerber and J. LeCouter, *Nat. Med.* 2003 96, 2003, **9**, 669–676.
- 199 K. A. Houck, N. Ferrara, J. Winer, G. Cachianes, B. Li and D. W. Leung, *Mol. Endocrinol.*, 1991, **5**, 1806–1814.
- 200 E. Tischer, R. Mitchell, T. Hartman, M. Silva, D. Gospodarowicz, J. C. Fiddes and J. A. Abraham, *J. Biol. Chem.*, 1991, **266**, 11947–11954.
- 201 D. W. Leung, G. Cachianes, W. J. Kuang, D. V. Goeddel and N. Ferrara, *Science* (80-. ), 1989, **246**, 1306–1309.
- 202 G. NEUFELD, T. COHEN, S. GENGRINOVITCH and Z. POLTORAK, *FASEB J.*, 1999, **13**, 9–22.
- 203 B. A. Keyt, L. T. Berleau, H. V. Nguyen, H. Chen, H. Heinsohn, R. Vandlen and N. Ferrara, *J. Biol. Chem.*, 1996, **271**, 7788–7795.
- 204 N. Ferrara, *J. Mol. Med.*, 1999, **77**, 527–543.
- 205 N. Ferrara, K. Mayo, J. Cidlowski, N. Kochupillai and G. Cutler, *Recent Prog. Horm. Res.*, 2000, **55**, 15–35; discussion 35.
- 206 M. J. Cross, J. Dixelius, T. Matsumoto and L. Claesson-Welsh, *Trends Biochem. Sci.*, 2003, **28**, 488–494.
- 207 I. J. Fidler and L. M. Ellis, *Cell*, 1994, **79**, 185–188.
- 208 D. Hanahan and R. A. Weinberg, *Cell*, 2000, **100**, 57–70.
- 209 V. Permeability, F. Endothelial, G. Factor, M. Hyperpermeability, A. Harold, F. Dvorak, L. F. Brown, M. Detmar and A. M. Dvorak, *Am. J. Pathol.*, 1995, **146**, 1029.
- 210 H. F. Dvorak, J. A. Nagy, D. Feng, L. F. Brown, A. M. Dvorak, H. Yoshiji, S. R. Harris and U. P. Thorgeirsson, *Curr. Top. Microbiol. Immunol.*, 1999, **237**, 98–132.
- 211 N. Reinmuth, A. A. Parikh, S. A. Ahmad, W. Liu, O. Stoeltzing, F. Fan, A. Takeda, M. Akagi and L. M. Ellis, *Microsc. Res. Tech.*, 2003, **60**, 199–207.
- 212 S. Rafii, D. Lyden, R. Benezra, K. Hattori and B. Heissig, *Nat. Rev. Cancer* 2002 211, 2002, **2**, 826–835.
- 213 F. Iovino, F. Ferraraccio, M. Orditura, G. Antonioli, F. Morgillo, T. Cascone, M. R. Diadema, G. Aurilio, G. Santabarbara, R. Ruggiero, C. Belli, E. Irlandese, M. Fasano, F. Ciardiello, E. Procaccini, F. Lo Schiavo, G. Catalano and F. De Vita, <http://dx.doi.org/10.1080/07357900701560612>, 2009, **26**, 250–255.
- 214 M. Banyś-Paluchowski, I. Witzel, S. Riethdorf, K. Pantel, B. Rack, W. Janni, P. A. Fasching, B. Aktas, S. Kasimir-Bauer, A. Hartkopf, E. F. Solomayer, T. Fehm and V. Müller, *Breast Cancer Res. Treat.*, 2018, **172**, 93–104.
- 215 M. Toi, T. Matsumoto and H. Bando, *Lancet Oncol.*, 2001, **2**, 667–673.
- 216 M. Toi, K. Inada, H. Suzuki and T. Tominaga, *Breast Cancer Res. Treat.*, 1995, **36**, 193–204.
- 217 F. De Paola, A. M. Granato, E. Scarpi, F. Monti, L. Medri, S. Bianchi, D. Amadori and A. Volpi, *Int. J. Cancer*, 2002, **98**, 228–233.

- 218 E. Zhong, E. Brogi, T. M. D'Alfonso, H. Wen, D. Frosina, N. K. Cheung, A. A. Jungbluth and D. S. Ross, *Appl. Immunohistochem. Mol. Morphol.*, , DOI:10.1097/PAI.0000000000000974.
- 219 K. Grankvist, M. Johansson and B. Tavelin, *Artic. J. Clin. Oncol.*, , DOI:10.1200/JCO.2000.18.7.1423.
- 220 G. Gasparini, M. Toi, R. Miceli, P. B. Vermeulen, R. Dittadi, E. Biganzoli, A. Morabito, M. Fanelli, C. Gatti, H. Suzuki, T. Tominaga, L. Y. Dirix and M. Gion, *Cancer J. Sci. Am.*, 1999, **5**, 101–111.
- 221 B. Linderholm, B. Lindh, B. Tavelin, K. Grankvist and R. Henriksson, *Int. J. Cancer (Pred. Oncol.)*, 2000, **89**, 51–62.
- 222 Serum Vascular Endothelial Growth Factor in Breast Cancer | Clinical Cancer Research | American Association for Cancer Research, <https://aacrjournals.org/clincancerres/article/7/11/3491/288564/Serum-Vascular-Endothelial-Growth-Factor-in-Breast>, (accessed 2 January 2023).
- 223 V. Permeability, F. Endothelial, G. Factor, M. Hyperpermeability, A. Harold, F. Dvorak, L. F. Brown, M. Detmar and A. M. Dvorak, *Am. J. Pathol.*, 1995, **146**, 1029.
- 224 R. Mead, M. Duku, P. Bhandari and I. A. Cree, *Br. J. Cancer 2011 1052*, 2011, **105**, 239–245.
- 225 E. Sunami, A. T. Vu, S. L. Nguyen, A. E. Giuliano and D. S. B. Hoon, *Ann. N. Y. Acad. Sci.*, 2008, **1137**, 171–174.
- 226 E. Sunami, A. T. Vu, S. L. Nguyen and D. S. B. Hoon, *Methods Mol. Biol.*, 2009, **507**, 349–356.
- 227 A. R. Thierry, F. Mouliere, S. El Messaoudi, C. Mollevi, E. Lopez-Crapez, F. Rolet, B. Gillet, C. Gongora, P. Dechelotte, B. Robert, M. Del Rio, P. J. Lamy, F. Bibeau, M. Nouaille, V. Lorient, A. S. Jarrousse, F. Molina, M. Mathonnet, D. Pezet and M. Ychou, *Nat. Med. 2014 204*, 2014, **20**, 430–435.
- 228 E. Zandberga, V. Kozirovskis, A. Abols, D. Andrejeva, G. Purkalne and A. Line, *Genes, Chromosom. Cancer*, 2013, **52**, 356–369.
- 229 P. Ulivi, G. Foschi, M. Mengozzi, E. Scarpi, R. Silvestrini, D. Amadori and W. Zoli, *Int. J. Mol. Sci. 2013, Vol. 14, Pages 10332-10342*, 2013, **14**, 10332–10342.
- 230 C. Sanfiorenzo, M. I. Ilie, A. Belaid, F. Barlési, J. Mouroux, C. H. Marquette, P. Brest and P. Hofman, *PLoS One*, 2013, **8**, e54596.
- 231 C. M. Hindson, J. R. Chevillet, H. A. Briggs, E. N. Gallichotte, I. K. Ruf, B. J. Hindson, R. L. Vessella and M. Tewari, *Nat. Methods 2013 1010*, 2013, **10**, 1003–1005.
- 232 R. Molina, S. Holdenrieder, J. M. Auge, A. Schalhorn, R. Hatz and P. Stieber, *Cancer Biomarkers*, 2010, **6**, 163–178.
- 233 C. Wittwer, S. Boeck, V. Heinemann, M. Haas, P. Stieber, D. Nagel and S. Holdenrieder, *Int. J. Cancer*, 2013, **133**, 2619–2630.
- 234 C. Alix-Panabières and K. Pantel, *Clin. Chem.*, 2013, **59**, 110–118.
- 235 P. Gao, S. C. Jiao, L. Bai, H. Wang, F. F. Jing and J. L. Yang, *J. Int. Med. Res.*, 2013, **41**, 923–933.
- 236 K. Pantel and C. Alix-Panabières, *Cancer Res.*, 2013, **73**, 6384–6388.
- 237 F. Bidard, D. Peeters, T. Fehm, F. N.-T. lancet oncology and undefined 2014, *Elsevier*.
- 238 S. Riethdorf, H. Fritsche, V. Müller, T. Rau, C. Schindlbeck, B. Rack, W. Janni, C. Coith, K. Beck, F. Jänicke, S. Jackson, T. Gornet, M. Cristofanilli and K. Pantel, *Clin. Cancer Res.*, 2007, **13**, 920–928.
- 239 B. Hong and Y. Zu, *Theranostics*, 2013, **3**, 377–394.
- 240 F. Ma, C. Ho, A. K. H. Cheng and H. Z. Yu, *Electrochim. Acta*, 2013, **110**, 139–145.

- 241 T. Li, Q. Fan, T. Liu, X. Zhu, J. Zhao and G. Li, *Biosens. Bioelectron.*, 2010, **25**, 2686–2689.
- 242 C. Liu, X. Liu, Y. Qin, C. Deng and J. Xiang, *RSC Adv.*, 2016, **6**, 58469–58476.
- 243 C. Ma, H. Liu, L. Zhang, H. Li, M. Yan, X. Song and J. Yu, *Biosens. Bioelectron.*, 2018, **99**, 8–13.
- 244 J. Zhao, X. He, B. Bo, X. Liu, Y. Yin and G. Li, *Biosens. Bioelectron.*, 2012, **34**, 249–252.
- 245 S. Zhao, W. Yang and R. Y. Lai, *Biosens. Bioelectron.*, 2011, **26**, 2442–2447.
- 246 J. Xiang, X. Pi, X. Chen, L. Xiang, M. Yang, H. Ren, X. Shen, N. Qi and C. Deng, *Biosens. Bioelectron.*, 2017, **96**, 268–274.
- 247 W. Wen, R. Hu, T. Bao, X. Zhang and S. Wang, *Biosens. Bioelectron.*, 2015, **71**, 13–17.
- 248 C. Lin, H. Zheng, Y. Huang, Z. Chen, F. Luo, J. Wang, L. Guo, B. Qiu, Z. Lin and H. Yang, *Biosens. Bioelectron.*, 2018, **117**, 474–479.



## **Chapter 2.**

# **Engineering the interface of an electrochemical aptamer-based sensor to detect MUC 1 tumor marker in serum.**

Ashkan Koushanpour, Edward J. Harvey, Geraldine Merle\*

A. Koushanpour,

Experimental Surgery, Faculty of Medicine, McGill University, Montreal, H3A 0C5, Canada

Dr. E. Harvey

Department of Surgery, Faculty of Medicine, McGill University, Montreal, H3A 0C5, Canada

Dr. G. E. Merle

Department of Chemical Engineering, Polytechnique, Montreal, H3T 1J4, Canada

**KEYWORDS** Cancer biomarker MUC 1; Aptamer; interfacial design; Biosensor; Diagnostic

To be submitted.

## **Abstract**

A new concept for the design and construction of an electrochemical aptamer (E-AB) sensor is reported where double redox tags (methylene blue) are tethered on an aptamer via the inclusion of a lysine linker. The effect of the passivation layer thickness was studied to further polarize the aptamer's population in equilibrium with the target and surface density and the interrogating frequency was studied. The analytical performances of this new E-AB sensor were measured and compared with a conventional single-tagged E-AB sensor towards the detection of MUC1 in buffer and serum. Greater performance for the double-tagged aptamer combined with lysine linker was measured with a limit of detection (LOD) of 0.32 nM and a linear dynamic range (LDR) from 1 nM to 500 nM, whereas the conventional counterpart exhibits ten times higher LOD (3.7nM) and a LDR from 10 nM to 500 nM. This synthetic strategy is the solution to build sensitive E-AB sensors on microelectrodes to compensate for the poor signal-to-noise ratio where normal performance is critically hindered by the limited geometric surface area.

## **2.1 Introduction**

The detection of transmembrane proteins, involved in cell adhesion, is an important goal as it can potentially be a predictive marker of malignant cancer cells. MUC1, a heavily O-glycosylated heterodimeric protein from the mucin family, has a key role in forming a protective mucus on the apical cell surface of most normal secretory epithelial cells and also to some extent on hematopoietic cells<sup>1</sup>. This transmembrane glycoprotein is normally expressed at low levels (3-30 U/ml, **Table 1-2**) on the apical surface of cells but in cancer, its expression level is greatly increased, which in turn affects the invasion, proliferation, and survival of cancer cells by preventing cell-cell and cell-extracellular matrix adhesion<sup>2</sup>. Many adenocarcinomas including

cancers of the pancreas, gastric<sup>3</sup>, lung<sup>4</sup>, breast<sup>5</sup>, ovary<sup>6</sup>, colon<sup>7,8</sup>, and other tissues overexpress the mucin proteins.<sup>7,9-14</sup>

Mucin proteins are overexpressed in several malignant tumors and identified as a key biomarker in cancer dissemination and metastasis. Thus, their detection and quantification could be important in cancer diagnosis and treatment information. Traditional techniques including immunohistochemistry,<sup>15</sup> Western blotting,<sup>16</sup> enzyme-linked immunosorbent assay (ELISA)<sup>17-19</sup>, dot blotting, and immunofluorescence<sup>20</sup> have been applied in detection of MUC1 (in blood and tissue where applicable). These methods are highly reliable and sensitive, however require expert manpower, expensive and complex instrumentations, which limiting their use in real-time clinical diagnostics. To meet these drawbacks, electrochemical techniques have been explored for the rapid and sensitive analysis of biomolecules<sup>21-24</sup>. They offer unique characteristics such as simple instrumentation, low cost, ease of use, selectivity and sensitivity, miniaturization,<sup>25</sup> and portability.<sup>26</sup> Among the various mode of detection, aptamers as the recognition element, have gained more interest as a result of high specificity and selectivity to specific target molecules and easier synthesis protocols, lower cost, and higher stability compared to antibodies. E-AB sensors are redox-tag modified short single-stranded DNA, immobilized on the surface of electrode most commonly on Au electrode via self-assembled monolayer (SAMs) chemistry<sup>27,28</sup>. The detection is based on conformational changes (folding and unfolding of the oligonucleotide secondary structure) of the aptamer following the binding with its target. The target-induced conformational change in the structure of the aptamer leads to an electrochemical signal (loss or gain)<sup>29,30</sup>. Biosensors with various aptamers have been designed with different biointerface molecular strategies for stressing the induced-conformational changes of the aptamer at a low concentration of biomolecules. For example, Immoos et al designed a self-complementary DNA aptamer using

single stranded oligodeoxynucleotide intervened by a poly (ethylene glycol) linker- leading to a 6-fold increase in the signaling current<sup>31</sup>. Similarly, a binding-induced strand displacement strategy was applied to the detection of complementary DNA- leading to 7-fold increase in gain (which is defined as the signal changes before and after target introduction divided by the initial signal,  $\left(\frac{I_0-I}{I_0}\right)$ ) compared to the control<sup>27</sup>. A DNA pseudoknot reported by Xiao<sup>32</sup> consisting of DNA structure containing two stem-loops, was developed to minimize collisions between the redox tag and the electrode- increasing the gain by 100%. This strategy improves the signaling, but also jeopardizes the generation of the sensor and their stability in real samples. Moreover, an additional auxiliary aptamer hybridization (such as capture probe and signaling probe) inherently complicates the sensor fabrication particularly when high surface coverage of the aptamer is favorable<sup>33,34</sup>, or in the case of a DNA pseudoknot, the manipulation can't afford high sensitivity. Furthermore, none of the above interfacial manipulations address the issue of low signal to noise (S/N) more particularly when miniaturization is essential (as for microelectrodes). In response to the above concerns, we report a new strategy in biointerfacial molecular design to increase the gain in a simple signal-off architecture based on the MUC1 introduction. Our strategy is schematically illustrated in **Figure 2-1**. To increase sensitivity, the improved signal-off architecture consists of two redox modified DNA sequence to augment the electronic source combined with an optimized screening effect of alkylthiol SAMs. To create higher degree of freedom while boosting the electronic source, a lysine molecule acts as a linker, upon which two spatially resolved methylene blue (MB) molecules are appended. Characterization and optimization of this simple sensing approach are described and compared with the specificity of the conventional corresponding E-AB sensors in simple buffer and human serum.

## 2.2 Experimental

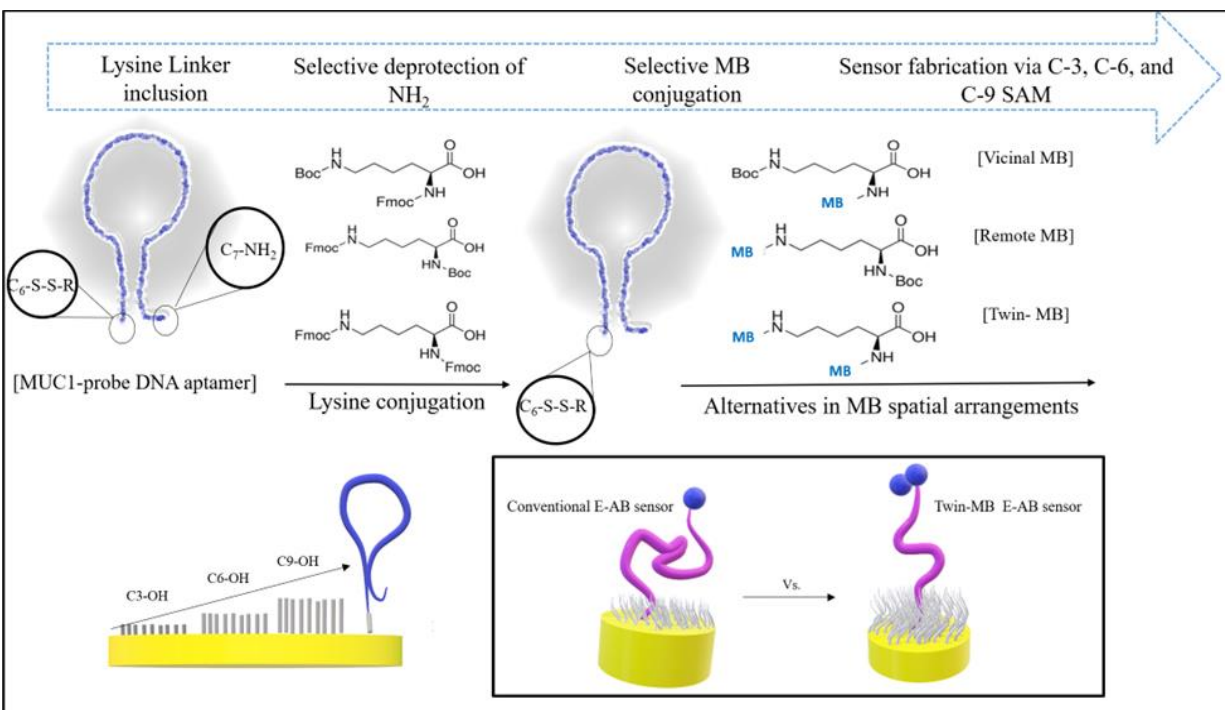


**Figure 2-1** Schematic illustration of aptamer manipulation with lysine and further spatially selective arrangement of MB conjugations.

### 2.2.1 Reagents

The following reagents were used as received (all from Sigma-Aldrich unless otherwise stated): human male AB plasma, USA origin, sterile-filtered, 2-(N-Morpholino) ethanesulfonic acid (MES), N $\alpha$ , N $\epsilon$ -di-Fmoc-L-lysine (Fmoc-lysine(Fmoc)-OH), N $\alpha$ -Fmoc-N $\epsilon$ -Boc-L-lysine (Fmoc-lysine(Boc)-OH), N $\alpha$ -Boc-N $\epsilon$ -Fmoc-lysine (Boc-lysine(Fmoc)-OH), Hexahydropyridine, Piperidine (all reagent grade), 3-Mercaptopropanol (C3-OH), 6-mercapto-1-hexanol (C6-OH), 9-Mercapto-nonan-1-ol (C9-OH), tris-(2-carboxyethyl) phosphine hydrochloride (TCEP), N-Ethyl-N'-(3-dimethylaminopropyl) carbodiimide (EDC), Hydroxy-2,5-dioxopyrrolidine-3-sulfonic acid sodium salt (Sulfo-NHS). 3-(N,N-dimethylamino)-7-[N-(3-(N-succinimidyl)-carboxyethyl)-N-

(methyl)-amino] phenothiazin-5-ium perchlorate (MB-NHS ester) was purchased from Glen research. The HPLC-purified and desalted anti-MUC1 DNA aptamers are as follows:

- HO-(CH<sub>2</sub>)<sub>6</sub>-SS-(CH<sub>2</sub>)<sub>6</sub>-O-5'-GCA GTT GAT CCT TTG GAT ACC CTG G-3'-(CH<sub>2</sub>)<sub>7</sub>-NHCO-(CH<sub>2</sub>)<sub>3</sub>-MB referred to as Control aptamer.
- HO-(CH<sub>2</sub>)<sub>6</sub>-SS-(CH<sub>2</sub>)<sub>6</sub>-O-5'-GCA GTT GAT CCT TTG GAT ACC CTG G-3'-(CH<sub>2</sub>)<sub>7</sub>-NH<sub>2</sub> referred to as aptamer-NH<sub>2</sub>.

These were purchased from Biosearch Technologies Inc. (Novato, CA). The sequence was reported by Ferreira et al as the S1.3/S2.2.<sup>35</sup> Also, the 60-mer 3× VTR MUC1 peptide (PDT RPA PGS TAP PAH GVT SAP DTR PAP GST APP AHG VTS APD TRP APG STA PPA HGV TSA) was purchased from PL Laboratories Inc. (Vancouver, Canada). The peptides were suspended in a phosphate buffer (137 mM NaCl, 10 mM Na<sub>2</sub>HPO<sub>4</sub>, 1.4 mM KH<sub>2</sub>PO<sub>4</sub>, 2.7 mM KCl, pH 7.4) and stored at -20°C.

## **2.3 Chemical synthesis of lysine-MB and corresponding DNA aptamer conjugation**

### **2.3.1 Synthesis of DNA aptamer-Fmoc-lysine(Fmoc)-OH**

All materials were used as purchased from Sigma-Aldrich. 8.9 mg of Fmoc-lysine(Fmoc)-OH (5.0 mM) was suspended into 3 ml of DMF, to which 1 ml of 50 mM MES buffer, pH 6.2, was added. To activate the carboxylic group on Fmoc-lysine(Fmoc)-OH, 30 mM of EDC/ NHS was added (17.25 mg, and 10.35 mg respectively). After 10 min in RT, 50 µl of the latter mixture, was mixed with 50 µl of 0.5 mM DNA aptamer-NH<sub>2</sub>. This reaction was left for 4 h with moderate shaking. To isolate the labeled aptamers from excess reactants we used precipitation method, in which 20µl of 4-M LiCl and 500 µl of ethanol (chilled to -20°C) were mixed well with DNA solution (100 µl) and was stored at -20°C for at least 3h. The aptamers were then separated from the supernatant

via centrifugation at 12,000 *g*. The pellet was washed with 70% and 100% ethanol, centrifuging after each wash.

### **2.3.2 De-protection of aptamer-Fmoc-lysine (Fmoc)-OH**

The pellet (aptamer-lysine(Fmoc)<sub>2</sub>) was then suspended in a 80%:20% mixture of DMF : piperidine solution and was left to react for 30 min. The aptamer-lysine (NH<sub>2</sub>)<sub>2</sub> was precipitated from the mixture following the same precipitation method described previously.

### **2.3.3 Methylene blue labeling of aptamer-lysine**

Lastly, the aptamer-lysine (aptamer-lysine(NH<sub>2</sub>)<sub>2</sub>) was labelled with MB redox reporters. The previous aptamer-lysine (NH<sub>2</sub>)<sub>2</sub> pellet was then suspended in 100 µl of 50 mM MES buffer solution, pH 6.2. 0.30 mg of MB-NHS ester salt (3.71 mM) was dissolved in 50 µl of DMF and added to the aptamer solution. After 4 h at RT at a moderate shaking, 30 mM of EDC/NHS was added to the solution and the mixture was left overnight. After the primary mixture aptamer retrieval, the final round of product isolation from the crude mixture was performed through high-performance liquid chromatography (HPLC) equipped with size-exclusion column, Phenomenex-BioSep-SEC-S 3000, 300×7.8 mm 5 micron, under the mobile phase condition of 50 mM Phosphate and 100 mM NaCl, pH 6.8. The product's mass was confirmed by liquid chromatography mass spectrometry (LC-MS). The mass of 9537,1416 *m/z* was found for DNA-lysine-(MB)<sub>2</sub> (Twin-MB).

## **2.4 Electron transfer kinetics**

Kinetic assessments were performed according to Laviron formalism using the following set of equations:<sup>36</sup>

$$E_{p,c} = E^{o'} - \frac{2.3RT}{\alpha nF} \log \left[ \frac{\alpha nFv}{RTk_{app}} \right] \quad (\text{Eq 2-1})$$

$$E_{p,a} = E^{o'} - \frac{2.3RT}{(1-\alpha)nF} \log \left[ \frac{(1-\alpha)nFv}{RTk_{app}} \right] \quad (\text{Eq 2-2})$$

where  $E_{p,a}$  is the potential of the anodic peak,  $E_{p,c}$  is the potential of the cathodic peak,  $E^{o'}$  is the formal potential calculated by averaging the anodic and cathodic potentials at slow scan rates,  $v$  is the scan rate,  $\alpha$  is the electron-transfer coefficient,  $k_{app}$  is the apparent rate constant,  $R$  is the ideal gas constant,  $T$  is the absolute temperature,  $F$  is the Faraday constant, and  $n$  is the number of electrons transferred.

## 2.5 Preparation of E-AB sensor

Regardless of whether it is Control aptamer or Twin-MB, the E-AB sensor was fabricated using gold disk electrode (1.6 mm diameter; BAS, West Lafayette, IN). The electrodes were treated with polishing on Buehler alumina slurry (1 and 0.05  $\mu\text{m}$ ) for 5 minutes, after 2 minutes sonication they were transferred to “piranha” solution consisting of a 3:1 ratio of 30% w/v aqueous solutions of  $\text{H}_2\text{SO}_4$  and  $\text{H}_2\text{O}_2$  for 5 minutes. Then they were subject to electrochemical polishing in 0.1 M  $\text{H}_2\text{SO}_4$  solution cycled from 1.4 V to 0.1 V for 25 cycles. afterwards, the electrodes were incubated with 100% ethanol for another 5 minutes. To fabricate the E-AB sensor, the relevant aptamer (Control or Twin-MB) was diluted to 70 nM in PBS saline buffer (described below). A cleaned electrode was immersed in this solution and incubated for 2 h. Next, to passivate the surface and displace the none-specific adsorbed aptamers, the electrode was subject to another round of 2 h incubation with 2 mM relevant alkyl thiol dissolved in PBS saline (either C-3, or C-6). To carry out the passivation with C-9, however, the incubation was done in MES buffer 50 mM, pH 6.5 for the same duration. This immobilization technique is essential for a proper E-AB sensor function.

Surface probe density ( $\Gamma$ ) of each electrode was calculated by the area under the reductive peaks of CVs at 0.2 V/s (eq 3).

$$\Gamma = \frac{Q}{nFA} \quad (\text{Eq 2-3})$$

In eq 3, Q is the area of the reductive signal, n is the number of electrons per redox event (n = 2 for MB), F is Faraday's constant, and A is the area of the gold electrode ca. 0.020 cm<sup>2</sup>.

## 2.6 Electrochemical characterization of E-AB sensors

Electrochemical measurements were made using a potentiostat / galvanostat (VersaSTAT 4, Princeton Applied Research) with a three-electrode system consisting of an Ag/AgCl (saturated KCl), Pt wire, and gold (1.6 mm diameter; BAS, West Lafayette, IN) as reference, counter and working electrodes, respectively. Electrochemical measurements were performed in phosphate buffer saline (PBS) (containing 2.92 g of NaCl, 0.0690 g of NaH<sub>2</sub>PO<sub>4</sub>, 0.071 g of Na<sub>2</sub>HPO<sub>4</sub> plus 50  $\mu$ l of 1M MgCl<sub>2</sub> in 25 ml of deionized water, Millipore, nanopure water, 17.5 M $\Omega$  cm<sup>-1</sup>), pH 7.2, using Square Wave Voltammetry (SWV) featuring amplitude of 50 mV, step potential of 5 mV and frequency of 20 Hz or 80 Hz for Control aptamer and Twin-MB featuring E-AB sensors, respectively. Electrochemical interrogations were recorded from 0.1 V to -0.5 V versus Ag/AgCl (saturated KCl) reference electrode.

## 2.7 Results and discussion

This investigation explored a new interfacial design using a specific DNA aptamer that has been modified at its 5'-terminus with a thiol group and at its 3'-terminus with lysine molecule bearing two redox active methylene blues. Sensors were built by immobilizing these modified aptamers via self-assembly alkanethiol chemistry to 0.02 cm<sup>2</sup> gold electrodes (**Figure 2-1**). In contrast to

the conventional commercially available single MB tagged aptamers (Control aptamer) which uses a C7-NH<sub>2</sub> alkane linker, the redox probe was further away from the distal end of 26-mer aptamer due to the lysine group (Twin-MB). To confirm that the incorporation of the lysine group did not alter the electrochemical behavior of the redox probe attached to the aptamer, cyclic voltammetry technique is then employed to monitor the four-electron, two-proton reduction of two methylene blues. As can be seen in **Figure 2-2**, CV exhibits strong pair of reductive and oxidative peaks with a midpoint potential at -0.238 V versus Ag/AgCl for both control and experimental electrodes. It can be also noted that the reductive current emerged from the Twin-MB is significantly higher than the control with a ratio of 2.16 ( $I_{red, modified} / I_{red, control}$ ).

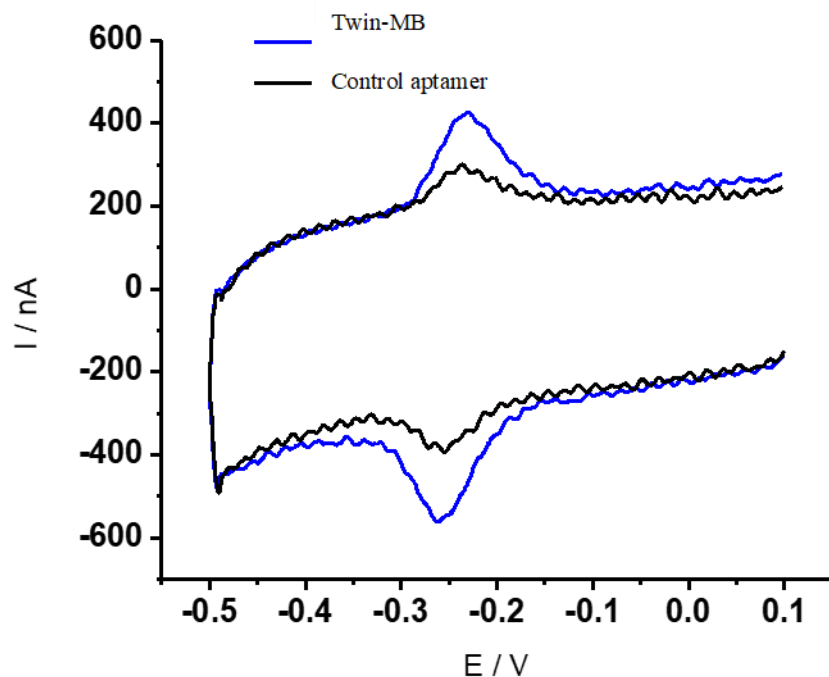


**Figure 2-2.** CVs of the control E-AB and Twin-MB sensors at 0.2 V/s, in PBS, pH 7.2. Both electrodes were prepared with 70 nM of corresponding aptamers and passivated with a C-6 mercaptohexanol agent.

The peak current is proportional to the number of methylene blue groups undergoing electron transfer. This finding indicates the presence of two MB on the Twin-MB electrode. Given that both control and Twin-MB exhibit same redox peak, the chemical synthesis, and the loading of two MB with lysine do not affect the electrochemical properties of the sensor.

We then studied the effects of varying E-AB sensor fabrication and operational parameters on the signal suppression. Among them, the packing density of aptamers on the electrode surface was studied and controlled by simply varying the concentration of probe DNA employed during sensor fabrication. To normalize the performances of the Twin-MB E-AB sensor with the control one, the probe density was only investigated for the control E-AB sensor and kept as a constant value over the course of study for control and Twin-MB sensors. Using fabrication concentrations of 0.01  $\mu\text{M}$  to 1.5  $\mu\text{M}$  DNA, we reproducibly reached probe densities from  $0.06 \times 10^{12}$  to  $8.2 \times 10^{12}$  molecule /  $\text{cm}^2$ . According to the diagram **Figure 2-3**, the optimal probe density is achieved at  $4.7 \times 10^{12}$  molecule /  $\text{cm}^2$  built from an aptamer solution of 70 nM. Findings indicate that the MUC1 sensor is optimal with an intermediate probe density. This corresponds to a mean probe-probe spacing of  $\sim 6.3$  nm.

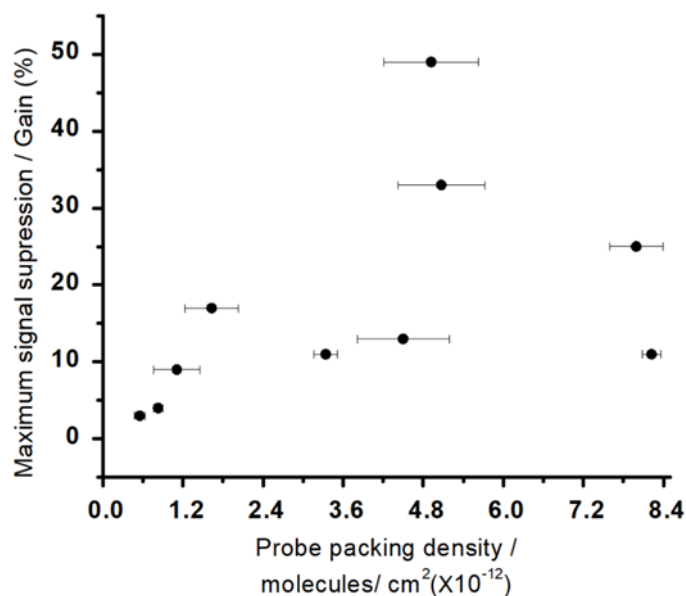


**Figure 2-3.** Probe density versus gain. The experiment was carried out with amplitude 50 mV, step 5 mV, and the frequency of 20 Hz in PBS solution pH = 7.2. Values are the average and standard deviations from three independent sensors at each probe density.

Given the effect of the probe density on signal suppression, it is anticipated that the collision dynamics of the redox tag has a key role, which suggests that the frequency used to interrogate the sensor has an impact by changing the electron transfer efficiency between the redox reporter and the electrode. In **Figure 2-4 A**, the frequency parameter was examined in the range of 10 Hz to 800 Hz (plot of signal/Hz vs log(Hz)) by plotting the signal suppression versus frequency (Hz) before and after of MUC 1 for control E-AB sensor. We see that a frequency of 20 Hz yields comparatively the highest signal suppression (49%) (**Figure 2-4 B**). However, the frequency interrogations for the Twin-MB E-AB sensor (**Figure 2-4 C**), revealed that 80 Hz is associated with the highest gain of 52% (**Figure 2-4 D**). The similar behavior of SWV profiles with and without MUC1 target imply that the mechanism of this E-AB sensor design is probably the result of MUC1-binding induced conformational changes, which quantitatively reduces the electron transfer. We believe that this apparent shift in frequency from 20 Hz to 80 Hz, is likely attributed

to the lysine inclusion. Since maximum % signal suppression was obtained at a frequency of 80 Hz, all the other experiments in this study were performed at this frequency for Twin-MB E-AB sensor.

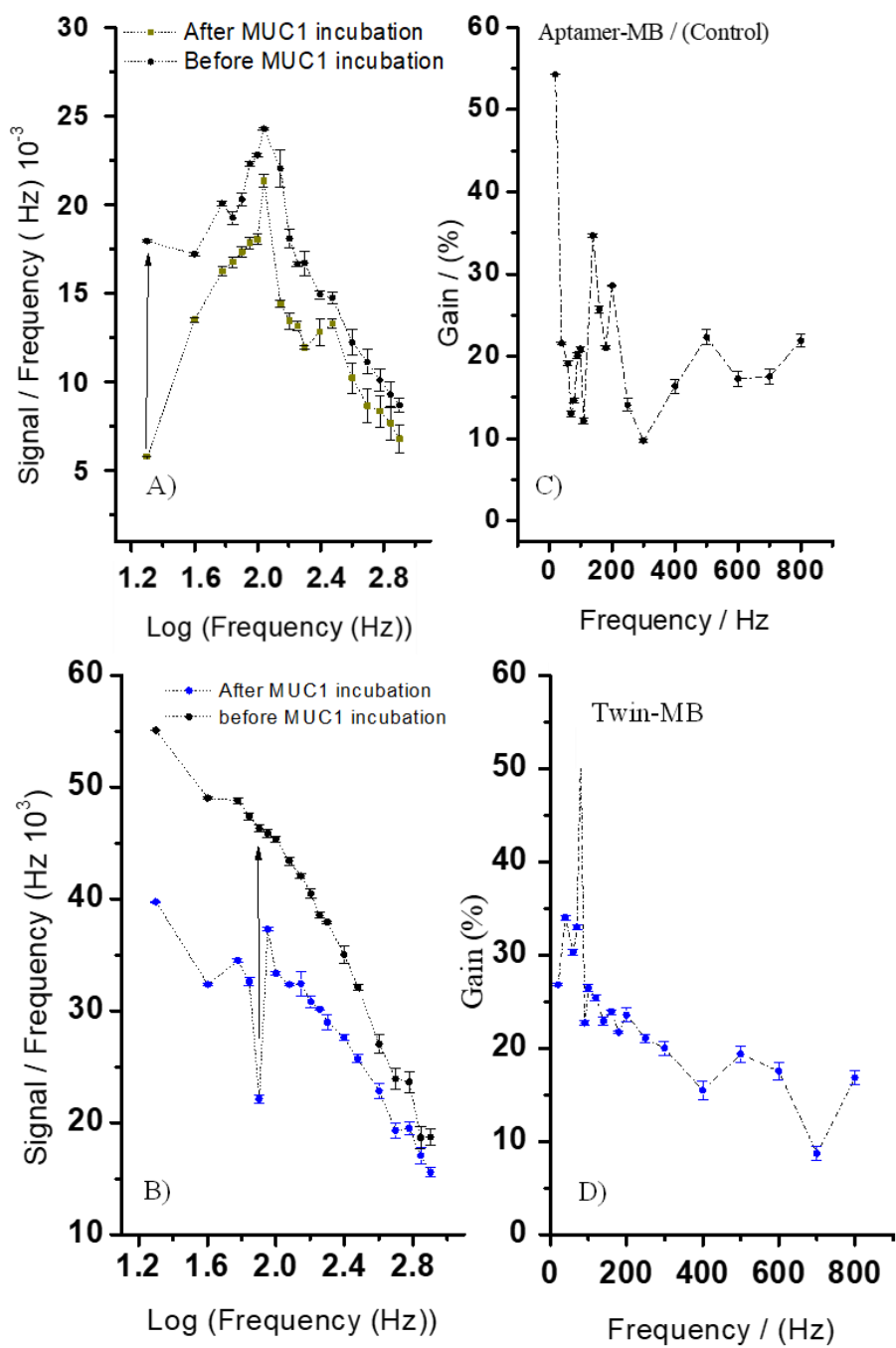


**Figure 2-4.** Plot of Log (Hz) vs signal/Hz A) control, B) Twin-MB. And plot of frequency variations (Hz) versus gain. C) for Control aptamer, and D) for Twin-MB.

The fabrication of the passivation layer on the electrodes is critical. If not adequately insulated faradic currents will lower or eliminate the capacitive signal. Because the gain of an aptasensor greatly varies with the conductivity of the SAM, it was essential in this work to combine the ideal SAM thickness with our new aptamer design. Therefore, we have first characterized the performance of MUC1 E-AB sensors with three different SAMs by varying the thickness and conductivity. 3-, 6- and 9-carbon, hydroxyl-terminated thiols were tested to evaluate the electron transfer efficiency, hybridization kinetics, and finally the gain. To do so, we have characterized the performance of sensors fabricated using control and Twin-tagged MB, and progressively increased the length of the SAM passivation layer. **Figure 2-5** displays the gain fluctuations characterized by control (A) and Twin-MB E-AB sensors (B), relative to progressively increasing thickness of SAM. As can be seen in **Figure 2-5 A, B**, the application of C-3 is associated with the lowest gain for both control and Twin-MB sensors at about 20%, and 17% respectively. Applying a C-6 passivation layer yields a gain enhancement of approximately 50% for both E-AB sensors **Figure 2-5 A, B**. The origin of the differences observed for the C-3 and C-6 gains is unclear, but we believe that it is likely due to an increase in the fraction of aptamers unfolded in the absence of MUC1 caused by a strong negative electric field at gold surface in operating condition that pushes farther away the aptamer and forces it to adopt an unfolded state<sup>37</sup> and/or possibly from a poor surface organization which in the case of C-3, seems to be more critical. Additionally, the observed gain enhancement for C-6 could be attributed to the longer length of the SAM improving the overall organization of the aptamers<sup>30,38</sup>. Surprisingly, using a C-9 SAM for the Twin-MB E-AB sensor led to a gain enhancement up to 78% (**Figure 2-5 B**) whereas the control results in gain suppression down to ~ca. 17% (**Figure 2-5 A**). While the complete reasons

are unclear, this difference can be attributed to the longer “lysine” linker incorporated in the Twin-MB E-AB sensor construct.

The variations of the electron transfer kinetics (from C-3 to C-9) for the control E-AB sensor demonstrates a growing kinetic limitation particularly in the case of C-9 MCH of  $183\text{ s}^{-1}$ ,  $147\text{ s}^{-1}$  and  $81\text{ s}^{-1}$ , corresponding to  $y = -0.0628x + 0.0438$ ,  $y = -0.0656x + 0.0408$ , and  $y = -0.0719x + 0.0391$ , respectively. At the opposite, the apparent electron transfer rates for the Twin-MB E-AB sensor, were  $198\text{ s}^{-1}$ ,  $161\text{ s}^{-1}$ , and  $127\text{ s}^{-1}$  (corresponding to  $y = -0.0592x + 0.0417$ ,  $y = -0.0641x + 0.0418$ , and  $y = -0.0686x + 0.0397$ ). In addition to increasing the signal to noise for Twin-MB E-AB sensor, it appears that the incorporation of lysine linker improves the diffusion of the redox probe into the passivation layer or cavities<sup>39</sup>, which in turn facilitates the electronic transmission<sup>30,38,40,41</sup>.

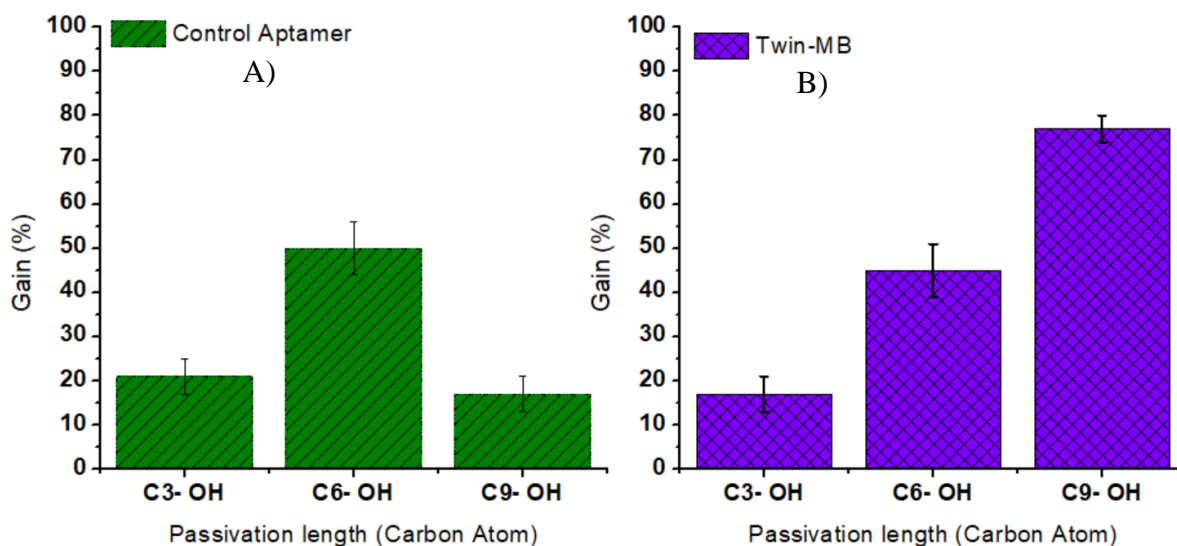


**Figure 2-5.** demonstrates the gain variations relative to systematic changes in SAMs layer thickness from C-3 to C-9. A) control E-AB sensor, and B) E-AB sensor built upon Twin-MB aptamer.

Since the gain is defined as an equilibrium between the folded and unfolded aptamers, one can argue that utilization of the C-9, relative to C-3, and C-6, is likely to create a better gap resolution between folded and unfolded aptamers. Twin-MB contributes to a higher signaling current. The results show an ideal balance between the length of SAM layer and the intensified electronic source (lysine inclusion and spatially resolved MBs). Here, a thicker passivation layer (C-9 for Twin-MB) contributes to gain enhancement by shifting the equilibrium toward the folded state enabling a higher variation in current between with and without until the point at which the insulating nature of the SAM passivation layer get the upper hand and reduces the signaling current. Here, we have proven that by simply varying the SAM thickness in E-AB fabrication significantly improve sensor performance. Hybridization kinetics measurements demonstrate the signal gain vs hybridization time for control and Twin-MB E-AB sensors in **Figure 2-6**. After 80 min incubation in MUC1 solution, the gain measured for both sensing systems have reached a plateau, which suggests a very similar dynamics in the formation of the aptamer/MUC1 complex.

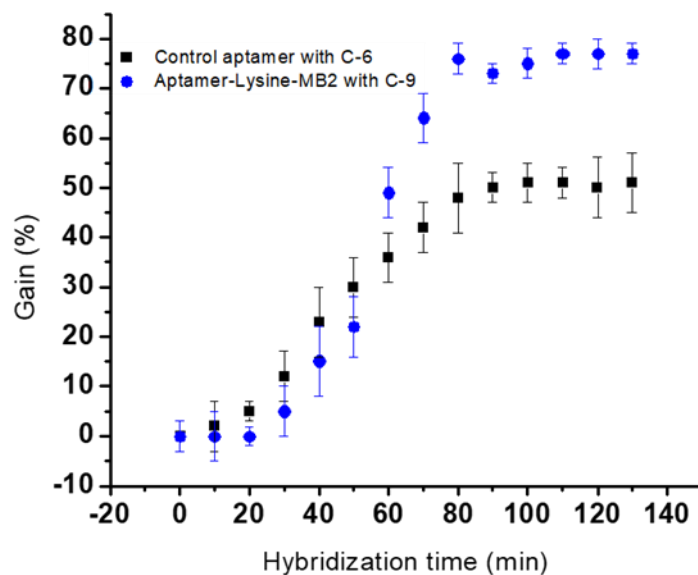


**Figure 2-6.** Response time comparison between Twin-MB E-AB sensor on C-9 (blue curve), and control E-AB sensor on C-6 (black curve). Comparison was made among the strongest alternatives.

The electron-transfer kinetic findings suggest that increasing the thickness of SAMs probably affect the aptamer organization (as we go from C-3 to C-6), up to a point when the electron transfer kinetic limitation becomes a critical issue, such as C-9 versus C6 for the control E-AB construct. However, this limitation appears to be overcome in the Twin-MB E-AB sensor likely due to a higher signal to noise. Since maximum signal suppression (gain) was obtained with C6 and C9 SAMs for control and Twin-MB E-AB sensors, respectively, all the other experiments in this study were performed with these construction parameters.

The sensitivity of the Twin-MB E-AB sensor for detection of MUC1 biomarker both in PBS solution and in serum samples was investigated by SWV technique (**Figure 2-7**) and compared with a control E-AB sensor (shown in **Figure S 2-1**). As shown in **Figure 2-7 A**, the linear relationship between the signal suppression and the MUC1 concentration ranges from 1 nM to 500

nM (**Figure 2-7 A inset**) with a linear regression equation of  $y = 0.923x + +106.51$  and a corresponding LOD of 0.32 nM (defined as  $(3s_{y/x})/m$ , where  $s_{y/x}$  is the standard error of regression and  $m$  is the slope ( $n = 3$ )).

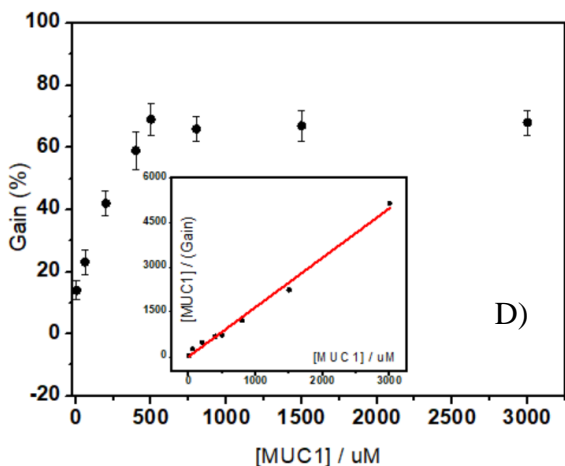
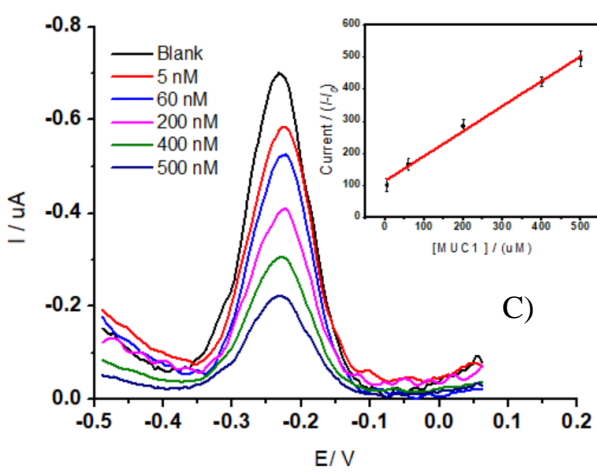
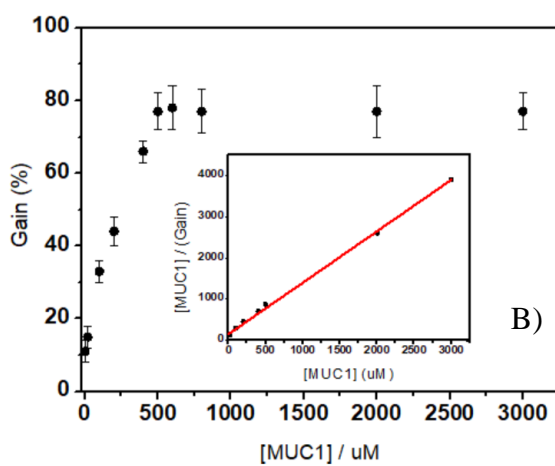
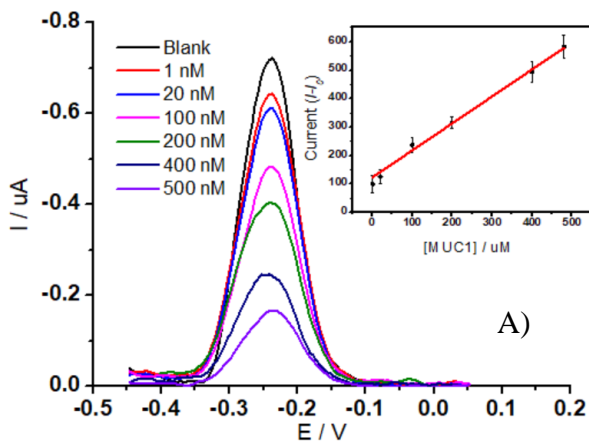
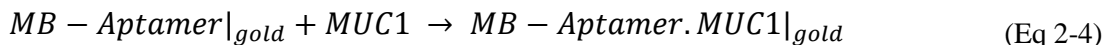


**Figure 2-7.** A) SWV responses of Twin-MB E-AB sensor (C-9) at different concentration of MUC1 in PBS buffer. Inset (A) shows the calibration curve: from 1.0 nM to 500 nM in buffer, (B) Dose-response curves of the Twin-MB E-AB sensor on C-9 in buffer. Inset in (B), shows linearized adsorption isotherm in buffer. C) SWV responses of Twin-MB E-AB sensor (C-9) at different concentration of MUC1 in 50% human serum. Inset (C) shows the calibration curve: from 1.0 nM to 500 nM in 50% human serum, (D) Dose-response curves of the Twin-MB E-AB sensor (C-9) in 50% human serum. (D). The experiments were carried out with amplitude of 50 mV, step 5 mV, and the frequency of 80 Hz (n=3).

The Control aptamer covers a MUC 1 concentration range from 10 nM to 500 nM with a linear regression equation of  $y = 0.1918x + 65.79$  and a LOD of 3.70 nM (**Figure S 2-1 A,B**), approximately 10 times higher than Twin-MB E-AB sensor. **Figure 2-7. B** displays the correlation between the relative gain, given by  $\Delta I/I_0$  (the change in the SWV peak current divided by the initial value, i.e., before the addition of MUC1) and the concentration of MUC1 (in nM). We assume that the binding process meets the requirements of the Langmuir isotherm<sup>42</sup>, thus the dissociation constant ( $K_D$ ) can be calculated from the equations:



$$K_D = \frac{[MB - Aptamer|_{gold}] [MUC1]}{[MB - Aptamer \cdot MUC1|_{gold}]} \quad (\text{Eq 2-5})$$

where  $[MB - Aptamer|_{gold}]$ ,  $[MUC1]$ , and  $[MB - Aptamer \cdot MUC1|_{gold}]$  represent the surface concentration of probe aptamers, the solution concentration of MUC1, and the surface concentration of the aptamer-MUC1 complex, respectively. Thus, the relationship between the relative gain ( $\Delta I/I_0$ ),  $[\Delta I/I_0]_{sat}$  (the saturated sensor signal), the solution concentration of MUC1, and the  $K_D$  can be described as following:

$$[\Delta I/I_0] = [\Delta I/I_0]_{sat} \frac{[MUC1]}{K_D + [MUC1]} \quad (\text{Eq 2-6})$$

$$\frac{[MUC1]}{[\Delta I/I_0]_{sat}} + \frac{K_D}{[\Delta I/I_0]_{sat}} = \frac{[MUC1]}{\Delta I/I_0} \quad (\text{Eq 2-7})$$

Accordingly, the  $K_D$  from the linear parts are 71.33 nM (**Figure 2-7. B.** inset) and 105.80 nM (**Figure S 2-1 C, D**) for Twin-MB and control E-AB sensors in PBS buffer, respectively. Given that the probe densities are unchanged and nucleotide sequences are identical, the corresponding decrease in  $K_D$  (from 105.80 to 71.33) and hence higher affinity are most likely attributed to the orientation and better access to the binding sequence on the unfolded aptamer.

The physiologically relevant MUC 1 concentrations are often cited as 34 U/mL<sup>43-45</sup>, which corresponds to approximately 5  $\mu$ M. Low levels of MUC1 (usually less than 31 U/mL) can be found in the serum of healthy individuals<sup>43</sup>. However, the normal range of MUC1 in serum can vary depending on the assay used. In cancer antigen detection tests, levels of CA 15-3 (soluble form of MUC1) lower than 25-30 U/mL are generally considered normal in serum<sup>44</sup>. Whereas, a 100-fold increase in MUC1 levels is a strong indicator of cancer<sup>45</sup>.

We evaluated the sensitivity and dynamic range of the Twin-MB E-AB sensor across the physiological concentrations of MUC1 in diluted human serum sample (diluted 1:1 with PBS buffer). As shown in **Figure 2-7 C**, the LOD towards spiked amounts of MUC1 in diluted human serum was calculated as of 0.4 nM, for which we obtained the value of  $K_D = 79.0$  (**Figure 2-7 D**). According to the LOD and the LDR, the developed Twin-MB sensor demonstrates clinical relevance for MUC1 concentration range in serum.

Regeneration performance was evaluated at both low and saturated concentrations of the MUC1 target. After one minute incubation in 8 Guanidine-HCl, 97% of the signal of the Twin-MB E-AB sensor was recovered at 200 nM of MUC1 (**Figure 2-8 A**). The regeneration in saturated concentrations of 550 nM, causes approximately 87% loss of the initial signal associated with small shift in potential (**Figure 2-8 B**).

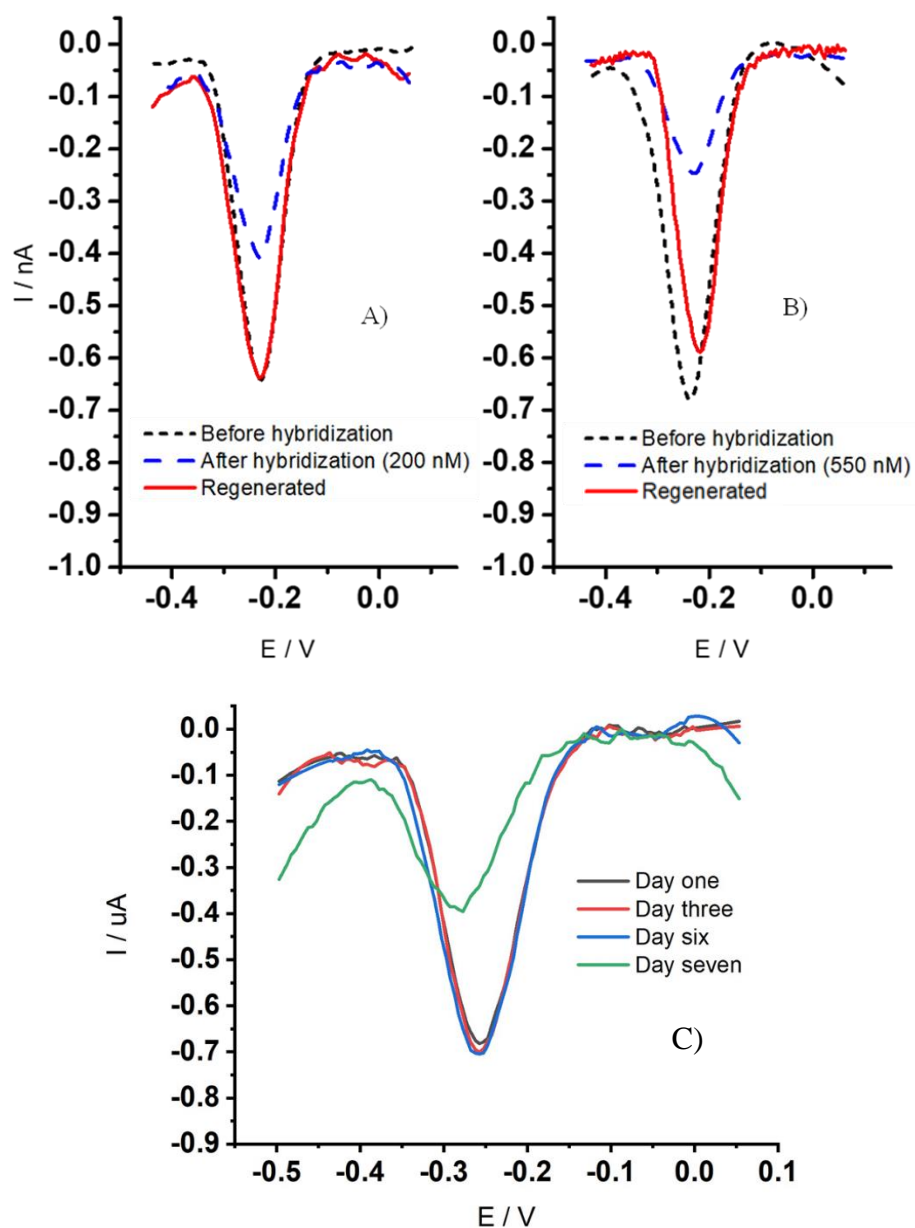


**Figure 2-8.** Regeneration of the Twin-MB E-AB sensor for 200 nM (A), and 550 nM (B), of MUC1 biomarker (C) Stability test of Tein-MB E-AB sensor for 7 days. The experiments were carried out with amplitude 50 mV, step 5 mV, and the frequency of 80 Hz in 50% diluted serum.

Finally, a stability test of the Twin-MB E-AB sensor after storage at 4°C was performed. The Twin-MB E-AB sensor exhibits a very stable current up to 6 days with less than 4% variation in absolute current (**Figure 2-8 C**) and a robust performance in 50% diluted serum for 3 h without significant deviation in corresponding response.

Over the past two decades, a substantial number of interfacial strategies have been reported to address some critical concerns related to electrochemical aptasensors for the detection of MUC1 biomarker. Recently, Zhao et al <sup>46</sup> manipulated the electrochemical biointerface of an E-AB sensor for multi-target (MUC1 and VEGF<sub>165</sub>) detection in a sequential format. They used the strand-displacement approach for each target to induce partial folding in the ferrocene-tagged signaling aptamer strand. This signal-on. type of sensor exhibits an outstanding sensitivity of 0.33 nM for MUC1, but a LDR (1 nM to 20 nM) is unfortunately not applicable for real samples for quantitative target detection, it requires essential washing steps for data acquisition, and this design cannot be miniaturized. Wang et al, reported the detection of MUC1 with a LOD of 0.1 nM, and a LDR ranging from 0.5 nM to 20 nM of MUC1. This was achieved through enzymatically assisted signal generation validated in blood serum. This enzymatic amplified strategy yields the most sensitive result for MUC1 biomarker, however, the restricted LDR, and multi- intervening washing -steps strongly limit further use. Additionally, it was established that the use of a positive potential for electrochemical detection promotes the biofouling of the surface by potential assisted protein recruitment on to the surface. In this work we have introduced a molecular assembly in the interfacial layer, combining an optimized SAM length, with amplifying redox system. We demonstrate a strong improvement of the S/N ratio with one of the lowest LOD (0.4 nM) reported so far for which the LDR ranges from 1 nM to 500 nM, validated in physiologically related samples. Compared to previously reported methods, our approach offers higher or comparable

results in terms of sensitivity and reliability but in addition it is easily scalable, allows long-term operation in real sample and miniaturization with potential application to protein and nucleotide targets.

**Table 2.1** Literature overview on aptamer featuring biosensors for detection of MUC1 biomarker.

Analytical method	Biorecognition element	LOD	Physiological sample	Reuse	Ref.
Aptasensor-based quantum dots	DNA aptamer	250 nM	serum	-	42
GO-based fluorescence aptasensor	DNA aptamer	0.04 $\mu$ M	serum	-	47
Electrochemical aptasensor	DNA aptamer	0.1 nM	serum	-	48
QD-based FRET aptasensor	DNA aptamer	50 nM	No	-	49
Aptamer-Antibody ELISA	DNA aptamer-Antibody	0.12 $\mu$ M	No	-	50
GO-based ERET aptasensor	DNA Aptamer	40 nM	serum	-	51
E-AB sensor	DNA aptamer	50 nM	No	-	52
E-AB sensor	DNA aptamer	0.33 nM	No	-	46
E-AB sensor	DNA aptamer	0.4 nM	serum	Yes	This work

## Conclusion

Here, we have demonstrated that a simple variation in design of the biointerface skeleton could significantly improve sensor performance. Relying on the equilibrium significance in the concept of gain, and maintaining the simplicity of the fabrication, we have shown the synergy effect between SAM monolayer passivation length and augmented redox reporters leading to 60% gain enhancement. The MUC1 sensors exhibit a LOD of 3.7 and a LDR from 10 nM to 500 nM in serum. We have for the first time revealed the existence of a delicate dynamic between different parts of the biointerface. This work on augmented electronic source is one step towards a smart solution to address the insufficient signal-to-noise in the case of microelectrodes without having to “increase” surface area” or roughness. Although the magnitude of the effects and improvements

may slightly vary with the couple target/probe, this concept can serve as a basic outline for the future fabrication of E-AB sensors.

## **Supporting information**

### **Engineering the interface of an electrochemical aptamer-based sensor to detect MUC 1 tumor marker in serum.**

Ashkan Koushanpour, Edward J. Harvey, Geraldine Merle\*

A. Koushanpour,

Experimental Surgery, Faculty of Medicine, McGill University, Montreal, H3A 0C5, Canada

Dr. E. Harvey

Department of Surgery, Faculty of Medicine, McGill University, Montreal, H3A 0C5, Canada

Dr. G. E. Merle

Department of Chemical Engineering, Polytechnique, Montreal, H3T 1J4, Canada

**KEYWORDS:** Cancer biomarker MUC 1; Aptamer; interfacial design; Biosensor; Diagnostic

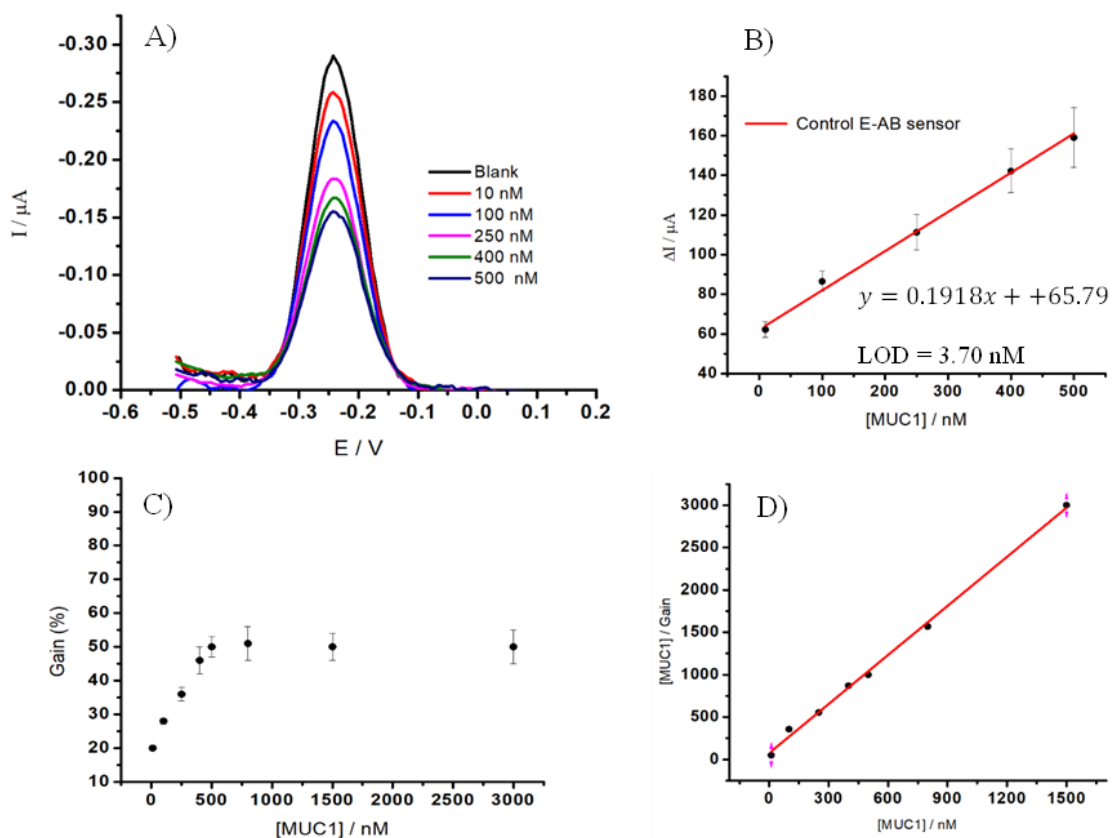


**Figure S 2-1** A) displays SWV responses of the control E-AB sensor, on C-6, with progressively increasing concentrations of MUC1 in PBS buffer. B) shows the calibration curves: from 10.0 nM to 500 nM in the buffer. C) Dose-response curves of the control E-AB sensor in the buffer. The illustrated error bars represent the standard deviation of three measurements obtained at each MUC1 concentration. D) shows linearized adsorption isotherm in buffer. The solid line is the best fit to the experimental data from which the dissociation constant  $K_D$  was determined. The incubation time was 80 min. These data were collected with three electrodes prepared in parallel. The experiments were carried out with amplitude 50 mV, step 5 mV, and the frequency of 20 Hz in corresponding environments

## 2.8 Methods and materials

The following reagents were used as received (all from Sigma-Aldrich, unless otherwise stated): human male AB plasma, USA origin, sterile-filtered, 4-Morpholineethanesulfonic acid, 2-(N-Morpholino) ethanesulfonic acid (MES),  $\text{N}\alpha$ ,  $\text{N}\epsilon$ -di-Fmoc-lysine (Fmoc-lysine (Fmoc)-OH),  $\text{N}\alpha$ -Fmoc- $\text{N}\epsilon$ -Boc-L-lysine (Fmoc-lysine (Boc)-OH),  $\text{N}\alpha$ -Boc- $\text{N}\epsilon$ -Fmoc-lysine (Boc-lysine (Fmoc)-

OH), Hexahydropyridine, Piperidine (all reagent grade), 9-Mercapto-nonan-1-ol (C9-OH), tris-(2-carboxyethyl) phosphine hydrochloride (TCEP), N-Ethyl-N'-(3-dimethylaminopropyl) carbodiimide (EDC), Hydroxy-2,5-dioxopyrrolidine-3-sulfonicacid sodium salt (Sulfo-NHS), MB-NHS ester was purchased from Glen research.

The HPLC-purified and desalted anti-MUC1 DNA aptamers,

HO-(CH<sub>2</sub>)<sub>6</sub>-SS-(CH<sub>2</sub>)<sub>6</sub>-O-5'-GCA GTT GAT CCT TTG GAT ACC CTG G-3'-(CH<sub>2</sub>)<sub>7</sub>-NH<sub>2</sub>  
(aptamer-NH<sub>2</sub>)

was purchased from Biosearch Technologies Inc. (Novato, CA). the sequence was reported by Ferreira et al as the S1.3/S2.2. Also, the 60-mer 3× VTR MUC1 peptide (PDT RPA PGS TAP PAH GVT SAP DTR PAP GST APP AHG VTS APD TRP APG STA PPA HGV TSA) was purchased from PL Laboratories Inc. (Vancouver, Canada). The peptides were suspended in a phosphate buffer (137 mM NaCl, 10 mM Na<sub>2</sub>HPO<sub>4</sub>, 1.4 mM KH<sub>2</sub>PO<sub>4</sub>, 2.7 mM KCl, pH 7.4) and stored at -20°C.

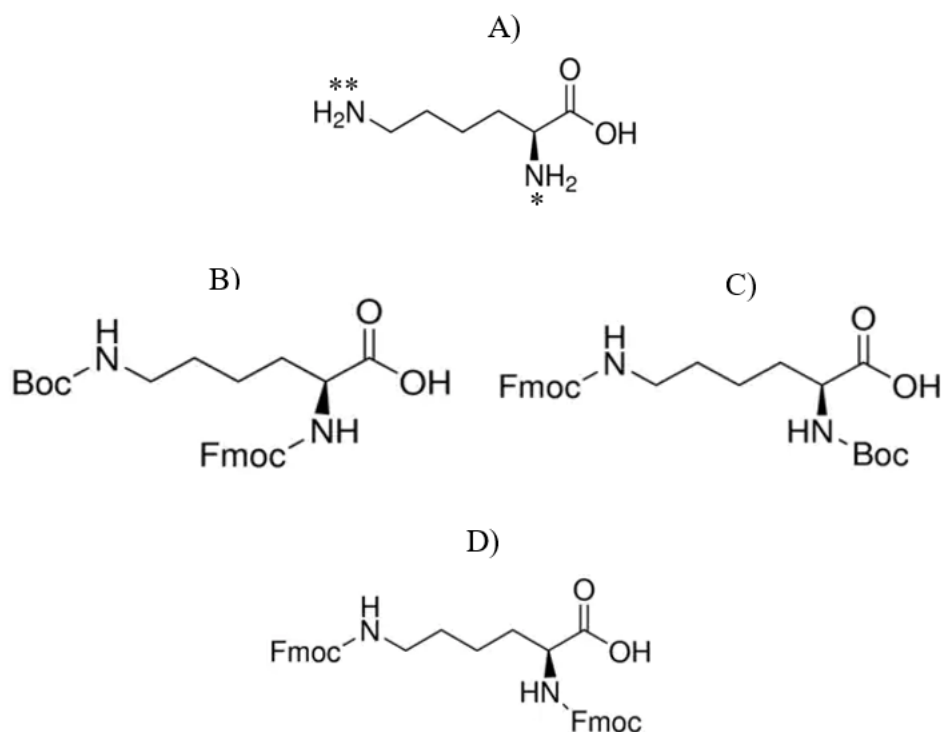


**Figure S 2-2** molecular structure of lysine (A), Fmoc-lysine(Boc)-OH (used in the synthesis of remote MB)(B), Boc-lysine(Fmoc)-OH (used in the synthesis of vicinal MB) (C), and Fmoc- lysine(Fmoc)-OH (used for the synthesis of Twin-MB). \* and \*\* specify the vicinal and the remote amino groups, respectively.

## 2.9 DNA modification and purification:

### 2.9.1 Synthesis of DNA-Fmoc-lysine(Boc)-OH

All materials were used as purchased from Sigma-Aldrich.

7.02 mg of Fmoc-lysine(Boc)-OH (5.0 mM) was suspended into 3 ml of DMF to which 1 ml of 50 mM MES buffer, PH 6.2, was added to buffer the reaction. To activate the carboxylic group on Fmoc-lysine(Boc)-OH, 30 mM of EDC/ NHS was added (17.25 mg, and 10.35 mg respectively).

after 10 min in RT, 50  $\mu$ l of the latter mixture, was mixed with 50  $\mu$ l of 0.5 mM DNA-aptamer-NH<sub>2</sub>. This reaction was left for 4 h with moderate shaking.

To Purify the labeled DNA from excess reactants we used the precipitation method, in which 20  $\mu$ l of 4-*M* LiCl and 500  $\mu$ l of ethanol (chilled to  $-20^{\circ}\text{C}$ ) were mixed with crude reaction (100  $\mu$ l) well and stored at  $-20^{\circ}\text{C}$  for at least 3h. then the DNA was separated from the supernatant via centrifugation at 12,000 *g*. the pellet was washed with 70% and 100% ethanol, centrifuging after each wash.

### **2.10 Deprotection of Fmoc group**

The pellet (DNA-aptamer-lysine (Fmoc)(Boc)) was then suspended in a 80%:20% mixture of DMF: piperidine solution and was left to react for 30 min. to retrieve the DNA (DNA-aptamer-lysine) it was precipitated from the mixture following the same method described in the paper. Through this, the Boc protecting group will largely remain intact to ensure desired arrangement of MB.

### **2.11 Synthesis of DNA-MB-lysine(Boc)-OH (referred to as remote MB)**

To synthesize the DNA-aptamer-lysine with MB redox reporter (remote MB), the pellet recovered from the last step was suspended in 100  $\mu$ l of 50 mM MES buffer solution, pH 6.2. 0.30 mg of MB-NHS ester salt (3.71 mM) was dissolved in 50  $\mu$ l of DMF and added to the DNA solution. This solution was left for 4h at RT on moderate shaking. after 4 h, to further push the reaction forward, 30 mM of EDC/NHS was added to the solution and the mixture was left overnight. The crude DNA products were retrieved via ethanol/LiCl precipitation (described in the paper).

### **2.12 Synthesis of DNA-Boc-lysine(MB)-OH (referred to as Vicinal MB)**

The same procedure was followed for the synthesis of DNA-Aptamer with vicinal MB.

### **2.13 Synthesis of DNA-MB-lysine(MB)-OH (referred to as Twin-MB).**

Twin-MB was synthesized according to the procedure described in the experimental section.

### **2.14 Purification and isolation of the DNA products**

The product isolations were carried out by high-performance liquid chromatography (HPLC) equipped with a size-exclusion column, Phenomenex-BioSep-SEC-S 3000, 300×7.8 mm 5 microns, under the mobile phase condition of 50 mM Phosphate and 100 mM NaCl at pH 6.8. The masses of the products were confirmed by liquid chromatography-mass spectrometry (LC-MS). A mass of 9117.338 and  $m/z$  and 9537.1416  $m/z$  were found for DNA-lysine-MB (both remote and vicinal MB), and Twin-MB, respectively.

### **2.15 The various spatial arrangement of MB on the lysine linker attached to the DNA-aptamer will influence the gain fluctuations**

To ensure the selectivity in the reactions, we employed lysine linkers whose amino groups were distinctively protected by different protecting groups (Fmoc and Boc) in an alternative way as shown **Figure S 2-2**.

According to the assumption, the desired result on the gain fluctuations would not be observed unless the thickness of the SAM (MCH) is also taken into consideration concomitantly. As shown in **Figure 2-5**, the C-3 and C-6 MCH lacked any discriminating effect. Thus, all the following experiments were designed and carried out based on C-9 passivating alkyl thiol layers (**Figure S 2-3**)

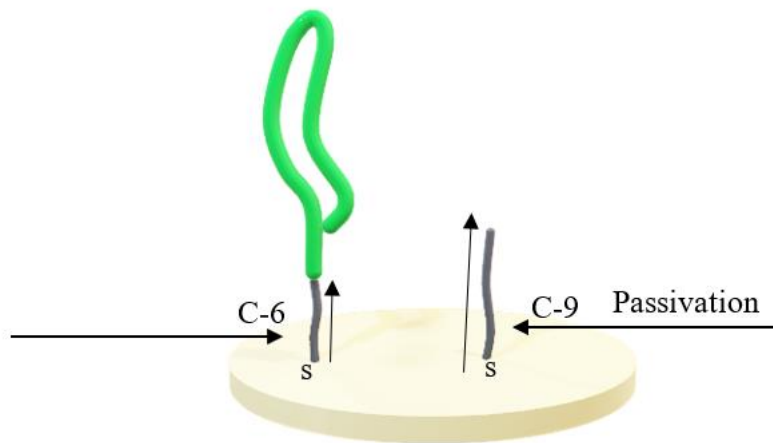


**Figure S 2-3 .** E-AB sensor fabricated by the self-assembly of redox/s tagged DNA with C-6 alkyl thiol modification (5') embedded with C-9 alkyl thiol monolayer.

To verify the effect of spatially different single MB of lysine on the gain fluctuations, three individual sets of each modification, that is, DNA-aptamer with vicinal MB, remote MB, and the one bearing Twin-MB were subjected to the saturated concentration of MUC1 protein (550 nM). the results shown in **Figure S 2-4.** represent the averages of three individual experiments.

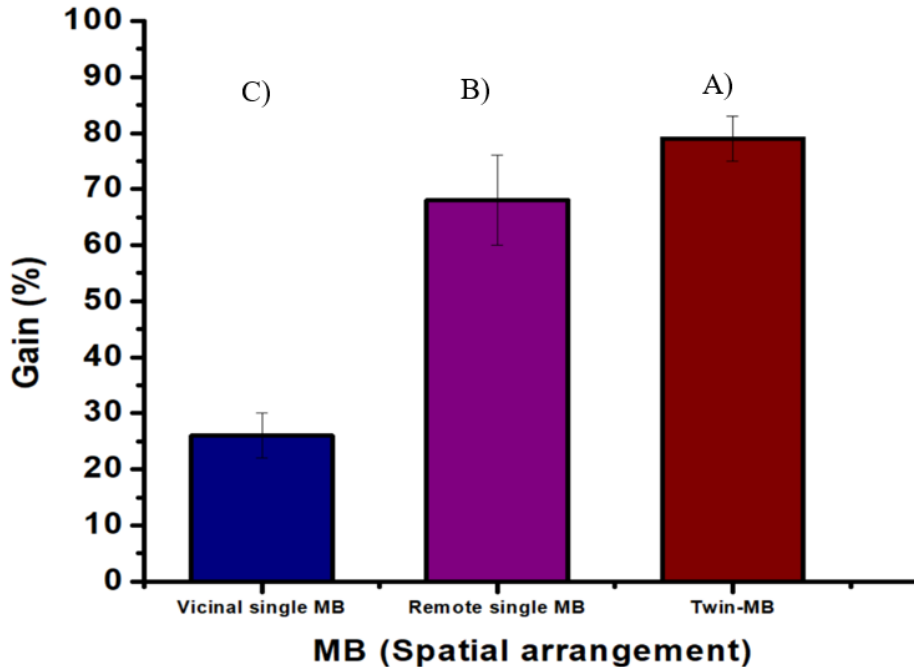


**Figure S 2-4 .** Gain fluctuations resulted from different spatial MB arrangements on probe aptamer, A) the Twin-MB, B) remote single MB, C) and Vicinal single MB, respectively experiments were carried out on E-AB sensors passivated by C-9 MCH. The results are averages of three individual experiments. Sensors were allowed to hybridize with 500 nM of MUC1 for 80 min in PBS buffer. The experiments were carried out with amplitude 50 mV, step 5 mV, and the frequency of 80 Hz in corresponding environments.

**Figure S 2-4** represents the results of gain variations relative to single MB spatial arrangements on the lysine linker (Vicinal and remote MB) and the one with two MBs (Twin-MB). One can see the superior effect belongs to the Twin-MB (**Figure S 2-4 A**). Owing to the fact that the inherent electron transfer kinetics of MB stays relatively constant in all three experiments (**Figure S 2-4 A, B, and C**), the gain variations can be likely known to be correlated with the structural synergy effects among lysine linker, MB spatial arrangement, and the thickness of the passivating layer (C-9).

We assumed that the longer linker inclusion (lysine) provides a higher degree of freedom and thus a higher probability of random diffusions into the SAM's cavities, this effect is noticeable for the furthest site of MB (remote site), particularly in the folded state (initial state). Whereas in the probe aptamer with a single vicinal MB (**Figure S 2-4 C**), this diffusion is less likely to happen. This argument is in good agreement with results obtained in the electron transfer kinetics study. Furthermore, after hybridization, the longer SAM (C-9) seems to be contributing to a further aptamer's population polarization at equilibrium by more effectively pushing the aptamers outward meanwhile acting as a momentary shield against random back-strikes of aptamers in their unfolded states. This is particularly noticeable compared with C-6 SAM, shown in **Figure S 2-4**, where there seems to be no such contribution and eventually yields similar gains ( ca. %50 ).

The lowest gain was observed in the case of vicinal MB (**Figure S 2-4 C**, 26%) which can be thought of as being resulted from the lack of diffusion, longer electron transfer barrier, and lastly weak initial signal current (folded state).

The gain observed in the probe aptamer with remote single MB (**Figure S 2-4 B**, 69%) can be viewed as the in-between condition. That is, unlike the vicinal MB (**Figure S 2-4 C**, 26%), MB in the remote one is more prone to random diffusions while population depolarization is supported by the thicker SAM. In the meantime, to argue its lower gain relative to Twin-MB (**Figure S 2-4 A**, 78%), we will have to take the back-strikes into account. Besides, compared to the Twin-MB, the initial signal generated by the remote single MB is remarkably weaker, and hence the offsetting effect is more pronounced.

## References

- 1 D. J. Thornton, K. Rousseau and M. A. McGuckin, *Annu. Rev. Physiol.*, 2008, **70**, 459–486.
- 2 Increased invasiveness of MUC11 cDNA-transfected human gastric cancer MKN74 cells, <https://onlinelibrary.wiley.com/doi/epdf/10.1002/%28SICI%291097-0215%2819980504%2976%3A3%3C377%3A%3AAID-IJC15%3E3.0.CO%3B2-8>, (accessed 9 August 2022).
- 3 N. W. Toribara, A. M. Robertson, S. B. Ho, W. L. Kuo, E. Gum, J. W. Hicks, J. R. Gum, J. C. Byrd, B. Siddiki and Y. S. Kim, *J. Biol. Chem.*, 1993, **268**, 5879–5885.
- 4 A. Ohgami, T. Tsuda, T. Osaki, T. Mitsudomi, Y. Morimoto, T. Higashi and K. Yasumoto, *Ann. Thorac. Surg.*, 1999, **67**, 810–814.
- 5 D. F. Hayes, R. Mesa-Tejada, L. D. Papsidero, G. A. Croghan, A. H. Korzun, L. Norton, W. Wood, J. A. Strauchen, M. Grimes, R. B. Weiss, H. J. Ree, A. D. Thor, F. C. Koerner, M. A. Rice, M. Barcos and D. W. Kufe, <https://doi.org/10.1200/JCO.1991.9.7.1113>, 2016, **9**, 1113–1123.
- 6 C. H. M. J. Van Elssen, P. W. H. Frings, F. J. Bot, K. K. Van De Vijver, M. B. Huls, B. Meek, P. Hupperets, W. T. V. Germeraad and G. M. J. Bos, *Histopathology*, 2010, **57**, 597–606.
- 7 W. M. C. Mulder, M. J. Stukart, E. De Windt, J. Wagstaff, R. J. Scheper and E. Bloemena, *Cancer Immunol. Immunother.* 1996 426, 1996, **42**, 351–356.
- 8 R. Aoki, S. Tanaka, K. Haruma, M. Yoshihara, K. Sumii, G. Kajiyama, F. Shimamoto and N. Kohno, *Dis. Colon Rectum* 1998 4110, 1998, **41**, 1262–1272.
- 9 F. Marin, P. Corstjens, B. De Gaulejac, E. De Vrind-De Jong and P. Westbroek, *J. Biol. Chem.*, 2000, **275**, 20667–20675.
- 10 M. Retz, J. Lehmann, C. Röder, B. Plötz, J. Harder, J. Eggers, J. Pauluschke, H. Kalthoff and M. Stöckle, *Cancer Res.*
- 11 A. L. Beautrais, P. R. Joyce and R. T. Mulder, *J. Am. Acad. Child Adolesc. Psychiatry*, 1996, **35**, 1174–1182.
- 12 C. Alarcón, A. I. Zaromytidou, Q. Xi, S. Gao, J. Yu, S. Fujisawa, A. Barlas, A. N. Miller, K. Manova-Todorova, M. J. Macias, G. Sapkota, D. Pan and J. Massagué, *Cell*, 2009, **139**, 757–769.
- 13 V. P. Balachandran, M. J. Cavnar, S. Zeng, Z. M. Bamboat, L. M. Ocuin, H. Obaid, E. C. Sorenson, R. Popow, C. Ariyan, F. Rossi, P. Besmer, T. Guo, C. R. Antonescu, T. Taguchi, J. Yuan, J. D. Wolchok, J. P. Allison and R. P. Dematteo, *Nat. Med.* 2011 179, 2011, **17**, 1094–1100.
- 14 F. Demichelis, K. Fall, S. Perner, O. Andrés, F. Schmidt, S. R. Setlur, Y. Hoshida, J. M. Mosquera, Y. Pawitan, C. Lee, H. O. Adami, L. A. Mucci, P. W. Kantoff, S. O. Andersson, A. M. Chinnaiyan, J. E. Johansson and M. A. Rubin, *Oncogene* 2007 2631, 2007, **26**, 4596–4599.
- 15 C. F. Qu, Y. Li, Y. J. Song, S. M. A. Rizvi, C. Raja, D. Zhang, J. Samra, R. Smith, A. C. Perkins, C. Apostolidis and B. J. Allen, *Br. J. Cancer*, 2004, **91**, 2086–2093.
- 16 G. A. Dent, C. J. Civalier, M. E. Brecher and S. A. Bentley, *Am. J. Clin. Pathol.*, 1999, **111**, 741–747.
- 17 C. S. M. Ferreira, K. Papamichael, G. Guilbault, T. Schwarzacher, J. Garipey and S. Missailidis, *Anal. Bioanal. Chem.* 2007 3904, 2007, **390**, 1039–1050.
- 18 S. Von Mensdorff-Pouilly, M. M. Gourevitch, P. Kenemans, A. A. Verstraeten, G. J. Van Kamp, A. Kok, K. Van Uffelen, F. G. M. Snijdwint, M. A. Paul, S. Meijer and J. Hilgers, *Tumor Biol.*, 1998, **19**, 186–195.
- 19 B. Jezeršek, J. Červek, Z. Rudolf and S. Novaković, *Cancer Lett.*, 1996, **110**, 137–144.

- 20 C. A. Harrop, D. J. Thornton and M. A. McGuckin, *Methods Mol. Biol.*, 2012, **842**, 49–66.
- 21 B. J. Privett, J. H. Shin and M. H. Schoenfisch, *Anal. Chem.*, 2010, **82**, 4723–4741.
- 22 N. J. Ronkainen, H. B. Halsall and W. R. Heineman, *Chem. Soc. Rev.*, 2010, **39**, 1747–1763.
- 23 E. Bakker and E. Pretsch, *TrAC Trends Anal. Chem.*, 2008, **27**, 612–618.
- 24 J. Wang, *Chem. Rev.*, 2008, **108**, 814–825.
- 25 B. Derkus, *Biosens. Bioelectron.*, 2016, **79**, 901–913.
- 26 J. Yoon, H. Y. Cho, M. Shin, H. K. Choi, T. Lee and J. W. Choi, *J. Mater. Chem. B*, 2020, **8**, 7303–7318.
- 27 Y. Xiao, A. A. Lubin, B. R. Baker, K. W. Plaxco and A. J. Heeger, *Proc. Natl. Acad. Sci.*, 2006, **103**, 16677–16680.
- 28 Y. C. Lim, A. Z. Kouzani and W. Duan, *J. Biomed. Nanotechnol.*, 2010, **6**, 93–105.
- 29 A. A. Lubin and K. W. Plaxco, *Acc. Chem. Res.*, 2010, **43**, 496–505.
- 30 R. J. White, N. Phares, A. A. Lubin, Y. Xiao and K. W. Plaxco, *Langmuir*, 2008, **24**, 10513–10518.
- 31 C. E. Immoos, S. J. Lee and M. W. Grinstaff, *J. Am. Chem. Soc.*, 2004, **126**, 10814–10815.
- 32 Y. Xiao, X. Qu, K. W. Plaxco and A. J. Heeger, *J. Am. Chem. Soc.*, 2007, **129**, 11896–11897.
- 33 F. Ricci, R. Y. Lai, A. J. Heeger, K. W. Plaxco and J. J. Sumner, *Langmuir*, 2007, **23**, 6827–6834.
- 34 A. Peterson, R. H.-N. acids research and undefined 2001, *academic.oup.com*.
- 35 C. S. M. Ferreira, C. S. Matthews and S. Missailidis, *Tumor Biol.*, 2006, **27**, 289–301.
- 36 E. Laviron, *J. Electroanal. Chem. Interfacial Electrochem.*, 1979, **101**, 19–28.
- 37 Electrochemical Methods: Fundamentals and Applications - Allen J. Bard, Larry R. Faulkner, Henry S. White  
- Google Books,  
[https://books.google.ca/books?hl=en&lr=&id=4ShuEAAAQBAJ&oi=fnd&pg=PT44&ots=SIFyBQUxqD&sig=5llmS\\_iIGM4ahdGCfruTt4ex5bA&redir\\_esc=y#v=onepage&q&f=false](https://books.google.ca/books?hl=en&lr=&id=4ShuEAAAQBAJ&oi=fnd&pg=PT44&ots=SIFyBQUxqD&sig=5llmS_iIGM4ahdGCfruTt4ex5bA&redir_esc=y#v=onepage&q&f=false), (accessed 19 August 2022).
- 38 D. Li, S. Song and C. Fan, *Acc. Chem. Res.*, 2010, **43**, 631–641.
- 39 K. K. Leung, A. D. Gaxiola, H. Z. Yu and D. Bizzotto, *Electrochim. Acta*, 2018, **261**, 188–197.
- 40 T. M. Herne and M. J. Tarlov, *J. Am. Chem. Soc.*, 1997, **119**, 8916–8920.
- 41 C. Y. Lee, P. Gong, G. M. Harbers, D. W. Grainger, D. G. Castner and L. J. Gamble, *Anal. Chem.*, 2006, **78**, 3316–3325.
- 42 A. K. H. Cheng, H. Su, Y. A. Wang and H. Z. Yu, *Anal. Chem.*, 2009, **81**, 6130–6139.
- 43 M. Moreno, H. J. Bontkes, R. J. Scheper, P. Kenemans, R. H. M. Verheijen and S. von Mensdorff-Pouilly, *Cancer Lett.*, 2007, **257**, 47–55.
- 44 A. Rughetti, A. Fama, S. von Mensdorff-Pouilly, F. Taurino, H. Rahimi, M. Ribersani, F. Natalino, G. M. D’Elia, L. Bizzoni, R. Latagliata, M. Breccia, R. Foà, G. Alimena, G. Girelli, L. Frati, M. Nuti and A. Tafuri, *Blood*, 2008, **112**, 5237.
- 45 E. Gheybi, J. Amani, A. H. Salmanian, F. Mashayekhi and S. Khodi, *Tumor Biol.*, 2014, **35**, 11489–11497.
- 46 J. Zhao, X. He, B. Bo, X. Liu, Y. Yin and G. Li, *Biosens. Bioelectron.*, 2012, **34**, 249–252.
- 47 Y. He, Y. Lin, H. Tang and D. Pang, *Nanoscale*, 2012, **4**, 2054–2059.

- 48 Z. Wang, N. Xia, J. Shi, S. Li, Y. Zhao, H. Wang and L. Liu, <http://dx.doi.org/10.1080/00032719.2014.905953>, 2014, **47**, 2431–2442.
- 49 S. Shin, H. Y. Nam, E. J. Lee, W. Jung and S. S. Hah, *Bioorg. Med. Chem. Lett.*, 2012, **22**, 6081–6084.
- 50 C. S. M. Ferreira, K. Papamichael, G. Guilbault, T. Schwarzacher, J. Garipey and S. Missailidis, *Anal. Bioanal. Chem.* 2007 3904, 2007, **390**, 1039–1050.
- 51 W. Wei, D. F. Li, X. H. Pan and S. Q. Liu, *Analyst*, 2012, **137**, 2101–2106.
- 52 F. Ma, C. Ho, A. K. H. Cheng and H. Z. Yu, *Electrochim. Acta*, 2013, **110**, 139–145.



## **The relevance and the contribution to the bigger picture**

Throughout chapter 2, we reported a novel E-AB sensor for sensitive quantification of MUC1 in human serum samples. we underlined an adoption of a new strategy in the manipulation of the electrochemical interfacial layer during the fabrication of E-AB sensors and outlined the systematic engineering as well as corresponding comparisons with the conventional E-AB sensors. briefly, unlike the commercially available single redox-tagged probe aptamers, we employed a MUC1 probe aptamer tethered to two spatially resolved redox tags (methylene blue) via the inclusion of a lysine linker. Furthermore, to induce further polarization between folded and unfolded states at equilibrium, that is, the aptamer's conformational changes, we have concomitantly probed the effect of various thicknesses of the thiolated self-assembly monolayers (SAMs) that are commonly used for surface passivation. We found that there is a positive combined effect in the form of synergy leading to a significant improvement in the performance of E-AB sensors (signal gain). And showed that the adaptation of such interfacial manipulation in the fabrication of an E-AB sensor (signal-off) completely supports a sensitive, and reagentless sensing platform. However, since the interfacial manipulation and its functioning are rigorously dependant to the signaling behavior/characteristics of the sensing platform, we continued to further probe the potential and applicability of the proposed strategy in the context of the signal-on type of E-AB sensor. to do so, we chose the VEGF165 biomarker which among other isoforms, has been recognized as one of the most abundantly overexpressed biomarkers in breast cancer. As well as a 30-mer probe aptamer which has been reported to possess signal-on characteristics if employed in E-AB sensors. Chapter 2, considers the feasibility of such manipulation in the format

of a signal-on type of sensor, as well as its advantages over the conventional protocol of fabrication

## **Chapter 3.**

### **Amplifying VEGF signal-on multi-tagged probe aptamer**

Ashkan Koushanpour, Edward J. Harvey, Geraldine E. Merle\*

A. Koushanpour,

Experimental Surgery, Faculty of Medicine, McGill University, Montreal, H3A 0C5, Canada

Dr. E. Harvey

Department of Surgery, Faculty of Medicine, McGill University, Montreal, H3A 0C5, Canada

Dr. G. E. Merle

Department of Chemical Engineering, Polytechnique, Montreal, H3T 1J4, Canada

**KEYWORDS** Vascular endothelial cell growth factors (VEGF<sub>165</sub>); Aptamer; Biosensor;  
Diagnostic

to be submitted.

## **Abstract**

We report an electrochemical aptamer-based sensor (E-AB) for the detection of vascular endothelial growth factor (VEGF<sub>165</sub>) biomarker directly in serum samples. Here, a E-AB approach employs a signal amplification strategy based on the synergy effect of the alky thiol passivation self-assembled layer (SAM) and the terminally tethered lysine twin methylene blue (Modified aptamer) to the distal end of probe aptamer as the redox tags. The new reagent-less sensing system yields a gain enhancement up to 195%, that can readily detect VEGF<sub>165</sub> biomarker in diluted human serum samples down to 2.0 pM offering the limit of detection (LOD) of 0.56 pM. This strategy is particularly promising for miniaturized sensing platforms where the low signal-to-noise (S/N) severely hampers the sensitivity of detection. The spatially resolved MB redox tags enhances the S/N, and the amplification capability also contributes to a greater amount of sensitivity. Given these advantages, this approach is particularly suitable for implementation in portable microdevices for the direct detection of proteins and small molecules in complex clinical samples.

## **3.1 Introduction**

2.3 million women are diagnosed with breast cancer according to World Health Organization (WHO), and there were 685,000 deaths globally, making it the world's most prevalent cancer <sup>1</sup>. Statistics show that 90% of the death are related to cancer metastasis<sup>2</sup>, which strongly implies the importance of early diagnosis. Early cancer diagnosis techniques rely on clinical tests or biopsy and imaging systems <sup>3,4</sup>, but they are discomforting, mostly invasive and not accessible for real-time monitoring. To facilitate an early detection and proper treatment, other diagnostic tools from traditional ones are required in terms of cost, accessibility, and time.

Cancer biomarkers are signature biomolecules usually referring to proteins, genes, and other molecules which can be used to screen and identify whether a patient has a specific disease or cancer<sup>5</sup>. Among them, a vascular endothelial growth factor (VEGF), a signal protein secreted by both endothelial and tumor cells, acts as a key regulator of angiogenesis and vascular development processes. VEGF<sub>165</sub> one of the most dominating isoforms, has been isolated with the highest incidence in breast cancer as it regulates vigorously angiogenesis in cancer development and metastasis<sup>6,7</sup>. When solid tumors reach around 0.2–2.0 mm in diameter, independent blood supplies for oxygen and nutrients and metastasis are required, VEGF<sub>165</sub> is overexpressed to stimulate vascularization<sup>8</sup>. Given its key role in tumor growth and metastasis, screening VEGF<sub>165</sub> in blood has also been regarded as a significant biomarker for cancer diagnosis in clinical<sup>9</sup>

Having the ability to quickly and inexpensively detect specific biomolecules can have a significant impact on patient care and the identification of infectious disease transmission patterns, as well as other goals related to health. Enzyme Linked Immunosorbent Assay (ELISA)<sup>6</sup> is the gold standard method for detecting and measuring protein biomarkers. Most sensitive mode of detection in ELISA is achieved through a sandwich assay, which involves binding an antibody with an additional substance that can be used as a label or to produce small, detectable molecules. However, this method often requires multiple washing steps to remove background signal, which increases the duration of the assay and the risk of errors. A faster, cheaper method with specific detectable capabilities would help to make assay development more accessible and widespread. To date various VEGF detection techniques have been reported including radioimmunoassay<sup>10</sup>, and mass spectrometry<sup>11</sup>. Nevertheless, challenges associated to complexity, speed of detection make them less ideal for real-time clinical diagnostics.

Over the last two decades, the E-AB sensors have gained much attention<sup>12</sup>. Aptamers are oligonucleotides or peptide that have high affinity, specificity, and selectivity to specific target molecules. Traditionally one extremity is immobilized onto an electrode surface while the other is modified with a redox tag. The electrochemical signal is generated when target recognized aptamer and induced a conformational change making the biosensor reagentless and readily reusable<sup>13</sup>. Various E-AB sensors have been reported to date with architectural related signal amplification methodologies<sup>14</sup>. but so far the S/N ratio remains low and high sensitivity is still challenging to improvement<sup>15</sup>. Despite a relatively large number of E-AB sensors reported to date, architectural related methodologies including triblock DNA polymer with intervening poly ethylene glycol<sup>16</sup>, strand displacement mechanism<sup>17</sup> and DNA pseudoknot approach<sup>18</sup>, have been successfully developed for signal amplification. However, they are complex and not tested in real samples<sup>14,16,17</sup>. Immoos et al<sup>16</sup> introduced the first signal amplification in a signal-on DNA sensor, which employed a polyethylene glycol bridge (PEG) separating probe and capture aptamer strands, in which oligonucleotide target hybridization prompted a loop formation with the aptamers. This pushes the terminally tagged ferrocene to the proximity of the electrode surface increasing the signaling current by 600%. Given that the specificity of the design for this oligonucleotide target, this methodology cannot be applied for every protein targets unless being appropriately tailored, and as such, it lacks versatility<sup>15</sup>. Another approach is based on the strand displacement<sup>17</sup>, which involves a rigidity- caused by double stranded element resulted from hybridization between capturing and signaling aptamer- that keeps the terminally tagged MB away from the surface. The oligonucleotide target competitive hybridization with the immobilized aptamer, triggers the release of the signalling strand, and causes a significant current increase, reaching the fM detection (gain ~ 700% )( which is defined as the signal changes before and after target introduction divided

by the initial signal,  $\left(\frac{I_0-I}{I_0}\right)$ ). The major drawback for this multiple strand hybridization-dependant signal generation, is the complicated fabrication process and the lack of regenerability particularly in real samples<sup>19,20</sup>. Lastly, a pseudoknot DNA approach was developed<sup>18</sup>. In this architecture, a pseudoknot pulls apart the methylene blue redox compound from the surface in the absence of target. When hybridized, the DNA sequence changes into a single strand DNA allowing the electron transfer to the electrode and thus an increase of signalling current. This approach showed a great stability and regenerability even in blood, yet with a modest gain (~100%) , and relatively a low sensitivity.

General approaches to improve the surface area either through surface roughness or via nanoparticle decorations have failed to properly address the signal amplification as the increase of surface rarely generates a proportional boost in the analytical signal<sup>21</sup>. Meanwhile, since the signaling mechanism in this class arises from the changes in electron transfer efficiency followed by target induced changes in conformation/flexibility of the aptamer probe, biomedical engineering of the aptamer sequence, though rarely, has also been used to enhance the analytical attributes. For example, White and his coworkers<sup>22</sup> successfully demonstrated that by rational engineering of the aptamer sequence they could tune a ranges of affinity from 220 nM to 42  $\mu$ M, and could improve the LOD as much as 100-fold. In addition, biosensors that employ surface roughness to increase their microscopic surface area offer another strategy to fighting with loss in signal. However, poor wettability of the surface has been demonstrated to counteract with the real amplification. In an attempt to enhance the S/N, and the signaling gain, Plaxco and his co-workers<sup>23</sup> developed a simple, low-cost method for creating high roughness through shrink-induced high surface area of the electrode for which they observed exceptional signal strength, and gain amplification up to 330% that accounts nearly more than two-fold greater than that of seen

previously on its planar alternative (150%). To accomplish this, they manage to exclude air pockets from the meniscus of the roughened surface by using a solution prepared with a mass ratio of 6% polyvinyl pyrrolidone (PVP10) and 0.01% non-polar surfactant (Triton X100). This modification allows sample to access more electrode surface and maximize the electrochemical active surface area gain achieved by shrinking. In the final assessment, rational engineering of the aptamer structure since directly influence the affinity of the aptamer to its target, is probably the most effective measure in order to enhance analytical performance. However, it should be noted that, the significant know-how, non-trivial cost associated with the experiments, and significant time investment to carry out such engineering, make it not readily available and widely practiced.

Recently, we have introduced an interfacial manipulation that not only enables a high signal amplification, but also can readily address the low S/N ratio specially when the surface area is becoming an issue e.g., microelectrodes. To do so, we boost the electronic source, i.e. methylene blue (MB), by modifying the probe with a 2 MB- grafted lysine. Also, we found that by varying the width of the alkylthiol passivation layer, a higher resolution of the signaling current was produced leading to significant gain enhancement, and hence sensitivity. Furthermore, this strategy improves the stability and reusability of the aptasensing platform in human serum samples. In this work, we have employed this strategy in developing a signal-on type of E-AB sensor for the detection of VEGF<sub>165</sub> biomarker in human serum sample and compared the analytical performance with the conventional counterpart E-AB sensor. Eventually the evaluation of the regenerability and stability of the sensing platform are presented.

## 3.2 Experimental

### 3.2.1 Reagents

The following reagents were purchased from Sigma-Aldrich (unless otherwise stated) and used as received: human male AB plasma, USA origin, sterile-filtered, 4-Morpholineethanesulfonic acid, 2-(N-Morpholino) ethanesulfonic acid (MES), N $\alpha$ ,N $\epsilon$ -di-Fmoc-L-lysine, Fmoc-lysine(Fmoc)-OH (Fmoc-lysine(Fmoc)-OH), Hexahydropyridine, Piperidine (all reagent grade), 3-Mercaptopropanol (C3-OH), 6-mercapto-1-hexanol (C6-OH), 9-Mercapto-nonan-1-ol (C9-OH), tris-(2-carboxyethyl) phosphine hydrochloride (TCEP), N-Ethyl-N'-(3-dimethylaminopropyl) carbodiimide (EDC), Hydroxy-2,5-dioxopyrrolidine-3-sulfonic acid sodium salt (Sulfo-NHS). MB-NHS ester was purchased from Glen research. The HPLC-purified and desalted anti-VEGF DNA aptamers are as follows:

HO-(CH<sub>2</sub>)<sub>6</sub>-SS-(CH<sub>2</sub>)<sub>6</sub>-O-5'-TTT-TCC-CGT-CTT-CCA-GAC-AAG-AGT-GCA-GGG-3'-(CH<sub>2</sub>)<sub>7</sub>-NHCO-(CH<sub>2</sub>)<sub>3</sub>-MB. referred to as Control aptamer.

HO-(CH<sub>2</sub>)<sub>6</sub>-SS-(CH<sub>2</sub>)<sub>6</sub>-O-5'-TTT-TCC-CGT-CTT-CCA-GAC-AAG-AGT-GCA-GGG-3'-(CH<sub>2</sub>)<sub>7</sub>-NH<sub>2</sub>. Referred to as anti-VEGF aptamer-NH<sub>2</sub>.

These were purchased from Biosearch Technologies Inc. (Novato, CA). Also, Recombinant Human VEGF Protein CF (isoform 165), was purchased from Bio-technie Canada. The protein was suspended in a sterile PBS and stored at -20°C.

## 3.3 Chemical synthesis of lysine-MB and aptamer conjugation

### 3.3.1 Modification of aptamer-NHCO-lysine-(Fmoc)<sub>2</sub>

8.9 mg of Fmoc-lysine(Fmoc)-OH (5.0 mM) was suspended in 2 ml of DMF to which 1 ml of 50 mM MES buffer, PH 6.2, was added to buffer the reaction. To activate the carboxylic group on

Fmoc-lysine(Fmoc)-OH, 30 mM of EDC/ NHS was added (17.25 mg, and 10.35 mg respectively). After 10 min at RT, 50  $\mu$ l of the solution was mixed with 50  $\mu$ l of 0.5 mM Anti-VEGF aptamer. This reaction was left for 4 h under moderate stirring. To extract the labeled DNA from excess reactants, 20  $\mu$ l of 4-*M* LiCl and 500  $\mu$ l of ethanol (chilled to  $-20^{\circ}\text{C}$ ) were thoroughly mixed with DNA solution (100  $\mu$ l) and stored at  $-20^{\circ}\text{C}$  for at least 3 h. Then, the DNA was isolated from the solution via centrifugation at 12,000 *g*. The precipitate was washed and centrifuged with 70% and 100% ethanol.

### **3.3.2 De-protection of aptamer-lysine (Fmoc)<sub>2</sub>**

The anti-aptamer-lysine (Fmoc)<sub>2</sub> precipitate was suspended in an 80% : 20% mixture of DMF: piperidine solution and left to react for 30 min at RT. The anti-aptamer-lysine was retrieved after the deprotection and precipitation following the previous method.

### **3.3.3 Labeling aptamer-lysine-(COOH)<sub>2</sub> with methylene blue (Modified aptamer)**

The anti-aptamer-lysine precipitate was suspended in 100  $\mu$ l of 50 mM MES buffer solution at pH 6.2. Then, 0.30 mg of MB-NHS ester salt (3.71 mM) was dissolved in 50  $\mu$ l of DMF and added to the DNA solution. This solution was left 4h at RT at a moderate shaking. After 4 h, 30 mM of EDC/NHS was added to the solution and the mixture was left overnight in fridge at RT . To purify and isolate the reacted DNA, a high-performance liquid chromatography (HPLC) using a size-exclusion column, Phenomenex BioSep-SEC-S 3000, 300  $\times$  7.80 mm, 5 micron was used with phosphate buffer (50 mM PBS, 100 mM NaCl, pH = 6.8) as the mobile phase. The DNA-lysine-(MB)<sub>2</sub> (Modified aptamer) mass was confirmed with liquid chromatography mass spectrometry (LC-MS). A mass of 10701.664 *m/z* was found for Modified aptamer, corroborating a calculated mass of 10719.638 *m/z*.

### 3.4 Preparation of E-AB sensor

Control and Modified aptamer electrodes were fabricated using gold disk electrode (1.6 mm diameter; BAS, West Lafayette, IN). The electrodes were treated with polishing on Buehler alumina slurry (1 and 0.05  $\mu\text{m}$ ) for 5 minutes, after 2 minutes of sonication they were transferred to “piranha” solution consisting of a 3:1 ratio of 30% w/v aqueous solutions of  $\text{H}_2\text{SO}_4$  and  $\text{H}_2\text{O}_2$  for 5 minutes. Then, the electrodes were subject to electrochemical polishing in 0.1 M  $\text{H}_2\text{SO}_4$  solution cycled from 1.4 V to 0.1 V for 25 cycles. Afterwards, the electrodes were incubated with 100% ethanol for another 5 minutes. To fabricate the E-AB sensor, the relevant aptamer was diluted in 0.07  $\mu\text{M}$  of PBS saline buffer (**Figure S 3-1**). A cleaned electrode was immersed in this solution and incubated for 2 h. Next, to passivate the surface and displace the none-specific adsorbed aptamers, the electrode was subject to another round of 2h incubation with 2mM relevant alkyl thiol dissolved in PBS saline (C-3 and C-6 hydroxyl alkyl thiol). To carry out the passivation with C-9, however, the incubation was done in MES 50 mM, pH 6.5 for the same duration. This immobilization technique is essential for a proper E-AB sensor function. Surface probe density ( $\Gamma$ ) of each electrode was calculated by the area under the reductive peaks of CVs at 200 mV/s (Eq 3-1).

$$\Gamma = \frac{Q}{(nFA)} \quad (\text{Eq 3-1})$$

In Eq 3-1, Q is the area of the reductive signal, n is the number of electrons per redox event (n = 2 for MB), F is Faraday's constant, and A, is the area of the gold electrode ca. 0.020  $\text{cm}^2$ .

Kinetic assessments were performed according to Laviron formalism using the following set of equations:

$$E_{p,c} = E^{o'} - \frac{2.3RT}{\alpha nF} \log \left[ \frac{\alpha nFv}{RTk_{app}} \right] \quad (\text{Eq 3-2})$$

$$E_{p,a} = E^{o'} - \frac{2.3RT}{(1-\alpha)nF} \log \left[ \frac{(1-\alpha)nFv}{RTk_{app}} \right] \quad (\text{Eq 3-3})$$

where  $E_{p,a}$  is the potential of the anodic peak,  $E_{p,c}$  is the potential of the cathodic peak,  $E^{o'}$  is the formal potential calculated by averaging the anodic and cathodic potentials at slow scan rates,  $v$  is the scan rate,  $\alpha$  is the electron-transfer coefficient,  $k_{app}$  is the apparent rate constant,  $R$  is the ideal gas constant,  $T$  is the absolute temperature,  $F$  is the Faraday constant, and  $n$  is the number of electrons transferred.

### 3.5 Electrochemical characterization

Electrochemical measurements were carried out with a potentiostat/galvanostat (VersaSTAT 4, Princeton Applied Research) and a three-electrode system consisting of an Ag/AgCl (saturated KCl), Pt wire, and gold disk electrodes (1.6 mm diameter; BAS, West Lafayette, IN) as reference, counter and working electrodes, respectively. Electrochemical measurements were performed in phosphate buffer saline (PBS) (10 mM phosphate containing 2.92 g of NaCl, 0.0690 g of NaH<sub>2</sub>PO<sub>4</sub>, 0.071 g of Na<sub>2</sub>HPO<sub>4</sub> plus 50  $\mu$ l of 1M MgCl<sub>2</sub> in 25 ml of deionized water, Millipore, nanopure water, 17.5 M $\Omega$  cm<sup>-1</sup>), pH 7.2, using SWV featuring amplitude of 50 mV, step potential of 5 mV and frequency of 40 Hz (**Figure S 3-2**). Electrochemical interrogations were recorded from 0.1 V to -0.5 V versus Ag/AgCl (saturated KCl) reference electrode.

### 3.6 Results and discussions

A new interfacial design using a VEGF specific DNA sequence modified with a thiol group at 5'- and with two redox active methylene blues grafted lysine at 3'- (Modified aptamer), whereas the conventional commercially available single MB tagged aptamers (Control aptamer) which presents a C7-NH<sub>2</sub> alkane linker (**Figure 3-1**). In our experimental group, the redox probe was further away from the distal end of 30-mer aptamer due to the lysine group. The Modified aptamer

electrode is constructed by tethering two spatially resolved MB conjugated aptamer to a C-OH passivated gold electrode via self-assembled monolayer chemistry<sup>24</sup> **Figure 3-1**). In the absence of a target, the aptamer is believed to assume an unfolded structure holding the redox tags away from the electrode and thus undergoes the minimum amount of electron transfer with the electrode. Upon target binding, the aptamer is thought to fold into a configuration that forces the redox tags (MBs) further to the proximity of the electrode, leading to improved electron-transfer efficiency (signal-on)<sup>25,26</sup>.

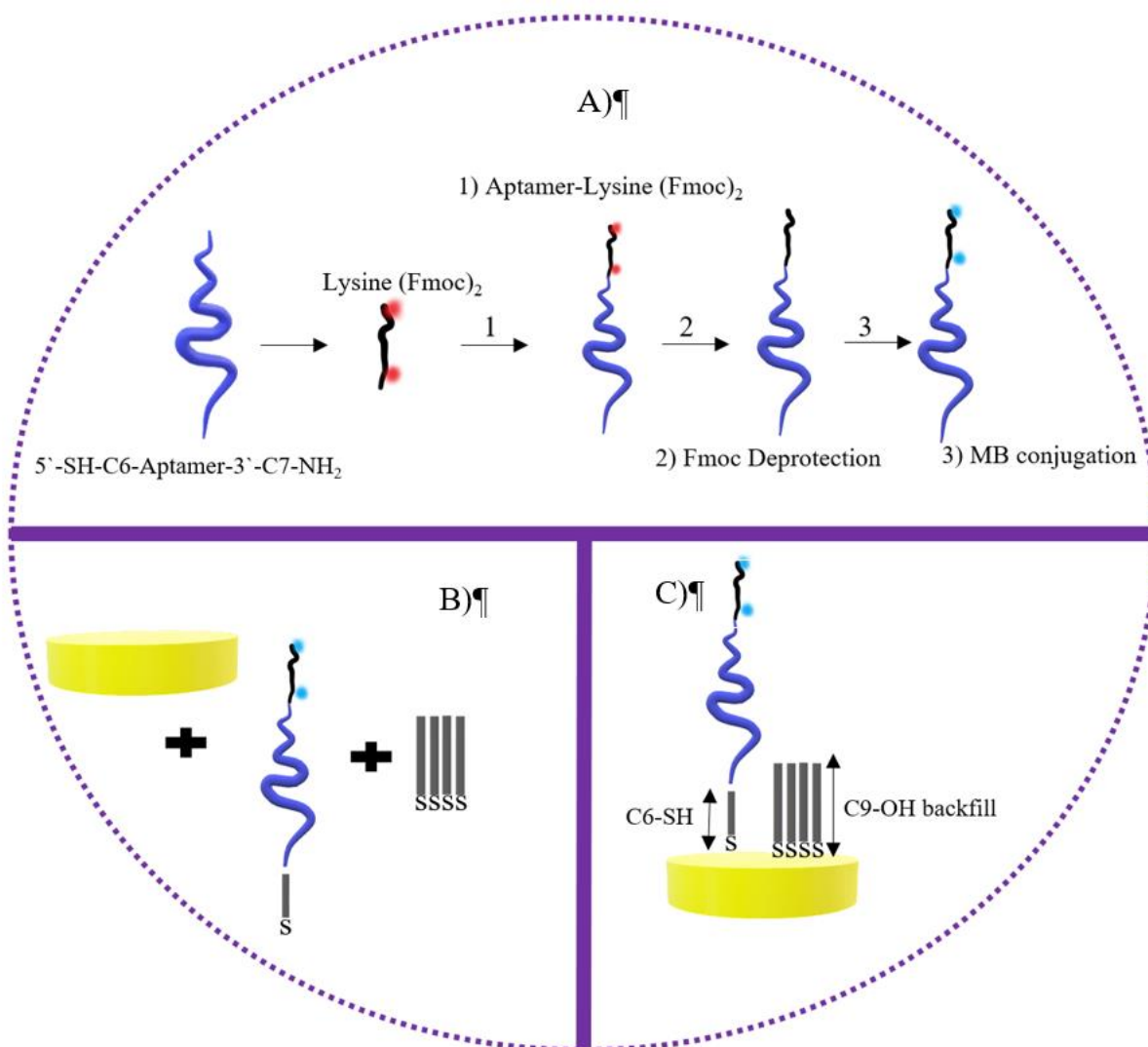


**Figure 3-1.** schematic illustration of reaction steps (A). fabrication elements (B). the final sensing platform based on Modified aptamer chemisorbed on gold electrode (C).

Electrochemical characterization along with hybridization kinetic analysis were carried out to establish that the lysine group did not change the electrochemical signature of MB and the results were compared to the Control aptamer. As can be seen in **Figure 3-2**, the cyclic voltammogram demonstrates strong reductive and oxidative peaks with a midpoint at -0.23 V vs. Ag/AgCl, similar to the Control aptamer. Furthermore, the reductive current generated by Modified aptamer is significantly higher than the Control aptamer with a ratio of 2.16 ( $I_{red, Modified} / I_{red, Control}$ ). Given that peak current is proportional to the number of methylene blue groups undergoing electron transfer, this result confirms the incorporation of 2 MB on the Modified aptamer electrode.

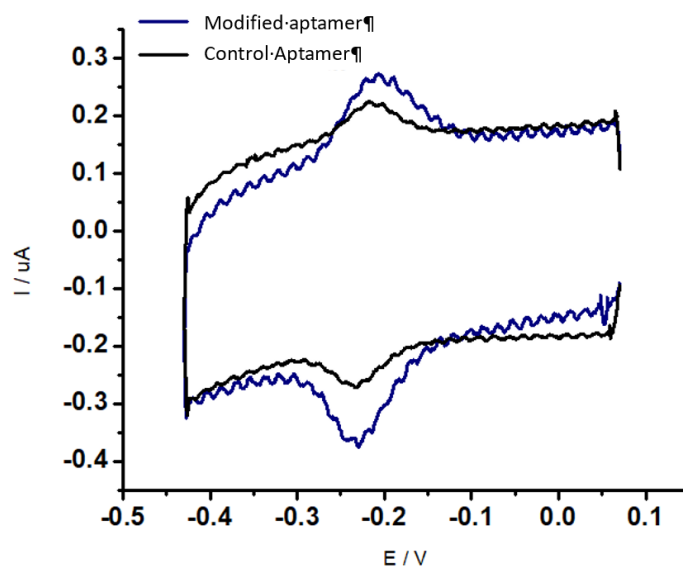


**Figure 3-2.** CVs of the Modified and the Control aptamer in 10 mM PBS buffer at pH 7.2 , and a scan rate of 0.2 Vs<sup>-1</sup>

Adding a passivation layer on the surface of electrodes is essential for insulating against the faradic currents and preventing a decrease of the capacitive signal. We investigated three different layers (thickness and conductivity), i.e. 3-, 6- and 9-carbon, hydroxyl-terminated thiols and assessed the

gain of the aptasensor (**Figure 3-3**). After 50 min incubation in target solution, the electrodes fabricated with C-3 exhibited the lowest gain for Control aptamer (50%) and the modified one (34%). The gain increased gradually with the thickness of the passivation layer for both electrodes (Control aptamer gain of 103%, and 113% and Modified aptamer gain of 125%, and 195% for C-6 OH, and C-9 OH respectively). The steady increase observed in gain values for both alternatives was attributed to the progressively thicker passivation layer, which probably improved the surface organization of aptamers leading to higher accessibility and offered a greater binding ability to the VEGF165 target or a better ratio between folded and unfolded structures.<sup>27,28</sup>

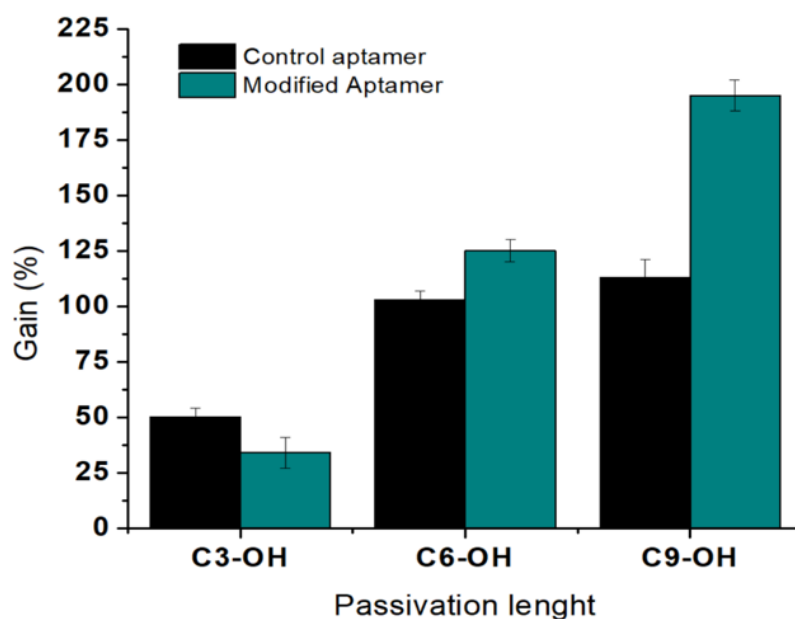


**Figure 3-3.** Gain measurement function of the passivation layer, i.e. C-3 to C-9. SWV was carried out in PBS hybridization buffer after 50 min incubation with the VEGF165 target.

In **Table 3.1** apparent electron transfer rate for Control and Modified aptamers are calculated as function of the passivation layer. The apparent electron transfer kinetics ( $K_{app}$ ) for the Control

aptamer were  $177.82\text{ s}^{-1}$ ,  $139.40\text{ s}^{-1}$ , and  $69.90\text{ s}^{-1}$  for C-3, C-6, and C-9 passivation layers, respectively. Accordingly, the same descending trend was obtained for the Modified aptamer in the Kapp along with a widening in passivation layer. This finding confirmed that a thicker passivation layer might create a higher barrier towards the electron transfer ability. However, as can be seen in **Table 3.1**, the Modified aptamer showed to be relatively less sensitive against such effect, probably due to the fine equilibrium between the thick passivation layer and electronic boost generated by the 2-methylene blue redox probe. In this case, a thicker passivation layer causes a better spatial resolution between folded and unfolded aptamer populations at the equilibrium and the presence of the 2 redox molecules can compensate for the higher charge transfer barrier resulted from the longer alky thiols.

**Table 3.1.** Apparent electron transfer rate for Control and Modified anti-VEGF<sub>165</sub> probes.

<i>Alkyl-thiol passivation length</i>	<i>K<sub>app</sub> for VEGF<sub>165</sub> Control aptamer / s<sup>-1</sup></i>	<i>K<sub>app</sub> for VEGF<sub>165</sub> Modified aptamer / s<sup>-1</sup></i>
<i>C3-OH</i>	183.03	189.3
<i>C6-OH</i>	139.40	158.6
<i>C9-OH</i>	69.90	118

The latter effect is more noticeable when the aptamer is in the folded state, i.e., after target hybridization, because the distance of MB to the electrode caused by the lysine inclusion enhances the diffusion of the redox probe into the passivation layer or cavities, thus facilitates the electronic transmission<sup>29</sup>. The hybridization kinetics for E-AB sensor composed of Control and M aptamers were plotted in **Figure 3-4**. The electrodes exhibited a similar trend for the signal gain with an increase with the incubation time followed by a plateau after 50 min incubation in VEGF<sub>165</sub> solution suggesting similar dynamics in the hybridization of the aptamer with VEGF<sub>165</sub> molecule.

Nevertheless, the kinetics for Modified aptamer was faster with 100% of signal gain after only 15 min compared to 40 minutes for the control electrode. Given that both electrodes share the same surface density along with other fabrication parameters, a faster rate is likely attributed to the lysine-(MB)<sub>2</sub> moiety on the modified aptamer. This was supported by the  $K_D$  values of 13.29 and 15.74 pM for Modified and Control aptamer, respectively calculated from Eq-3-7)(see below).

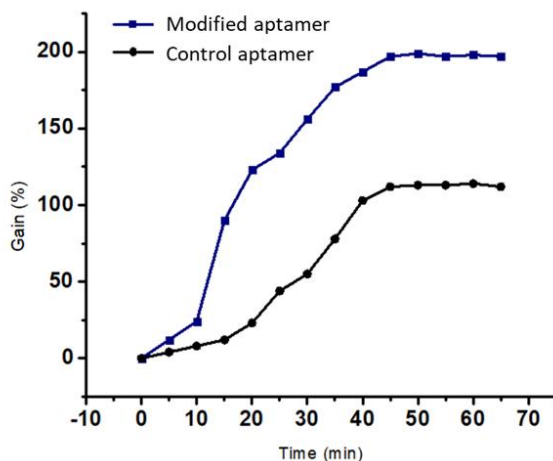


**Figure 3-4.** Hybridization kinetics of E-AB sensor composed of Modified aptamer and Control aptamer. SWV performed in a saturated concentration of VEGF<sub>165</sub> with amplitude of 50 mV, step potential of 5 mV, and frequency of 40 Hz. Electrodes were fabricated with 0.07 μM of aptamers and with C9-OH passivation layer.

### 3.7 The E-AB sensor performance in diluted human serum

The E-AB sensor signaling behaviour was evaluated in both PBS and human serum samples (**Figure S 3-3**). A well-defined peak, characteristic of MB reduction, was observed at 0.238 V vs Ag/AgCl. The analytical performance of the modified E-AB sensor against VEGF<sub>165</sub> biomarker was investigated in 50% diluted human serum samples (**Figure 3-5 A,B**) and the results were compared with the control E-AB sensor concomitantly (**Figure 3-5 C,D**). The Modified aptamer E-AB sensor's responses were assessed toward a range of VEGF<sub>165</sub> concentrations (from 0 pM to 2000 pM) in 50% diluted human serum via SWV. As shown in **Figure 3-5 A**, under the optimized experimental conditions, the Modified aptamer E-AB sensor exhibited a reliably sensitive response

toward its target. A linear relationship between the signal and the VEGF<sub>165</sub> concentration was measured from 2 pM to 300 pM (**Figure 3-5 A**) with a linear regression equation of ( $y = 1.426x + 61.50$ ,  $R^2 = 0.987$ ) which corresponds to a LOD of 0.56 pM (defined as  $(3s_{y/x})/m$ , where  $s_{y/x}$  is the standard error of regression and  $m$  is the slope ( $n = 3$ )) (**Figure 3-5 B**). The control E-AB sensor displays an inferior sensitivity against the VEGF<sub>165</sub> target (**Figure 3-5 C**), where a linear relationship from 20 pM to 150 pM with linear regression equation of ( $y = 0.664x + 24.0$ ,  $R^2 = 0.991$ ) corresponding to the LOD of 6.4 pM of the VEGF<sub>165</sub> was calculated (**Figure 3-5 D**).

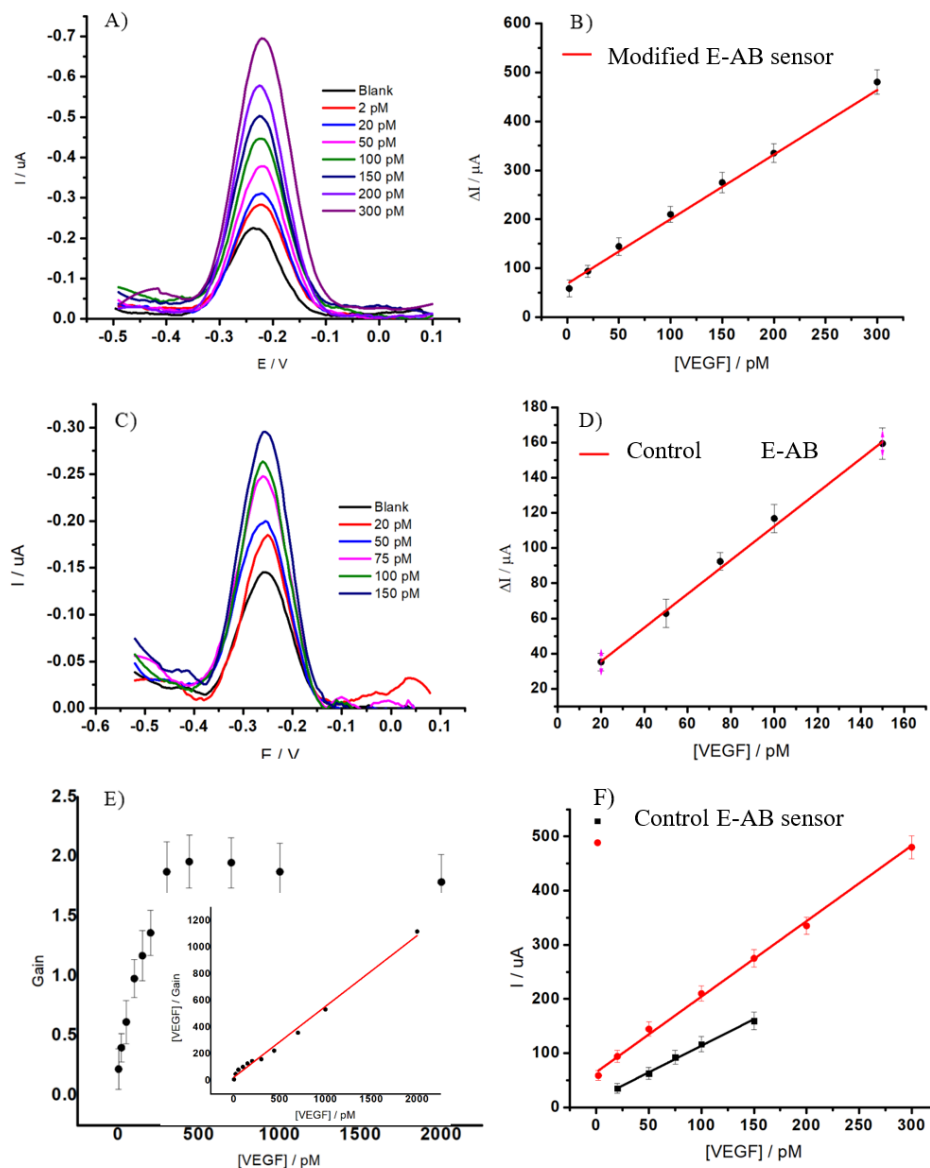
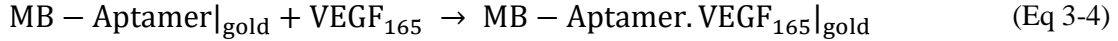


**Figure 3-5.** A) displays the SWV responses of Modified aptamer E-AB sensor on C-9 OH, with varying concentrations of VEGF165 biomarker. B) the corresponding LDR. C) calibration curve corresponding to control E-AB sensor and D) the corresponding LDR. E) represents the Dose-response curves of the Modified aptamer E-AB sensor. Inset in (E) shows linearized adsorption isotherm. The solid line is the best fit to the experimental data from which the dissociation constant  $K_D$  was determined. F) represents a comparison of the calibration curve slopes resulting from Modified aptamer and Control aptamers incorporated E-AB sensors, respectively. The experiments were carried out with amplitude 50 mV, step 5 mV, and the frequency of 40 Hz in corresponding environments with 50 min incubation time in 50% diluted human serum. The illustrated error bars represent the standard deviation of three measurements obtained at each VEGF165 concentration. These data were collected with three electrodes prepared in parallel.

In **Figure 3-5 E**, the correlation between signal change (gain) and the VEGF<sub>165</sub> concentration (in pM) was analysed and the gain variation reached a plateau beyond 300 pM of VEGF<sub>165</sub>.

Given the 1:1 binding stoichiometry between VEGF<sub>165</sub> : Aptamer<sup>26</sup> and assuming the Langmuir isotherm<sup>30</sup>, a  $K_D$  was obtained through (Eq 3-7)).



$$K_D = \frac{[\text{MB - Aptamer}|_{\text{gold}}] [\text{VEGF}_{165}]}{[\text{MB - Aptamer} \cdot \text{VEGF}_{165}|_{\text{gold}}]} \quad (\text{Eq 3-5})$$

$$\Delta I/I_0 = [\Delta I/I_0]_{\text{Sat}} \frac{[\text{VEGF}_{165}]}{K_D + [\text{VEGF}_{165}]} \quad (\text{Eq 3-6})$$

, where  $[\text{MB - Aptamer}|_{\text{gold}}]$ ,  $[\text{VEGF}_{165}]$ , and  $[\text{MB - Aptamer} \cdot \text{VEGF}_{165}|_{\text{gold}}]$  represent the surface concentration of MB-anti-VEGF<sub>165</sub> aptamers, the solution concentration of VEGF<sub>165</sub>, and the surface concentration of the aptamer-VEGF<sub>165</sub> complex, respectively. Thus, the relationship between the relative gain ( $\Delta I/I_0$ ),  $[\Delta I/I_0]_{\text{sat}}$  (the saturated sensor signal), the solution concentration of VEGF<sub>165</sub>, and the  $K_D$  can be described as following:

$$\frac{[\text{VEGF}_{165}]}{[\Delta I/I_0]_{\text{Sat}}} + \frac{K_D}{[\Delta I/I_0]_{\text{Sat}}} = \frac{[\text{VEGF}_{165}]}{\Delta I/I_0} \quad (\text{Eq 3-7})$$

Accordingly, the  $K_D$  calculated from the linear part is equal to 13.29 pM for modified E-AB sensor (**Figure 3-5 E, inset**), and the one for control E-AB sensor was obtained as 15.74 pM (data not shown). The data in **Figure 3-5 D** showed that the new strategy resulted in an increase of more than twice (2.1 times) in the slope of the calibration curve compared to that of the control E-AB sensor, ( $y = 1.426x + 61.50$ ) and of ( $y = 0.664x + 24.0$ ), respectively. Furthermore, the improvement in LDR (**Figure 3-5 F, red line**) is beyond to what was achieved for the control E-AB sensor, and is most likely attributed to a higher S/N ratio<sup>31</sup>. The advantage of higher S/N creates a broader signal resolution before and after the target hybridization and contributes to a higher

signal capacity. In contrast to the conventional mode of sensor preparation, this interfacial manipulation offers great advantages particularly in terms of S/N and sensitivity. Indeed, the corresponding span particularly for the modified E-AB sensor successfully cover the clinical cut-off concentration of VEGF<sub>165</sub> biomarker in the serum (i.e., 3 pM to 12 pM and more) As reported<sup>32</sup>, the mean value of serum VEGF<sub>165</sub> for control is 201.7 pg/ml (~5.3 pM) (median, 167.5 pg/ml; with range of 101.5–245.3 pg/ml), vs significantly elevated amount in cancer patients (median, 305.9 pg/ml; with range of 156.7–451.6 pg/ml) with cut-off value of 241.02 pg/ml (~6.4 pM).

Finally, the regeneration of the signal and reusability of the sensor were evaluated using 8-M Guanidine HCl and VEGF<sub>165</sub> concentration at saturated level in 50% diluted serum (**Figure 3-6 A, B** respectively). To assess the signal regeneration, i.e. to retrieve the initial signal after each hybridization, the sensor was incubated in 8-M Guanidine HCl for 100 s followed by soaking with water for 150 s. The data show that the mean signal regeneration for the modified E-AB sensor was 94% (RSD = 4.43% for 3 individual sensors). The reusability of the sensor was also examined under the same VEGF<sub>165</sub> removal protocol. Data reveal that the gain value calculated after the second trial decrease gradually to 172% compared to its initial gain value (195%). This means that this sensor in optimal condition can be reused no more than twice. The sensor demonstrated a high surface stability up 3 days in buffer with a mean value of 95.2% of its initial signal value (RSD 3.91%, n= 3 electrodes), as opposed to 87.0% (RSD of 3.77%) for the control one (data not shown).

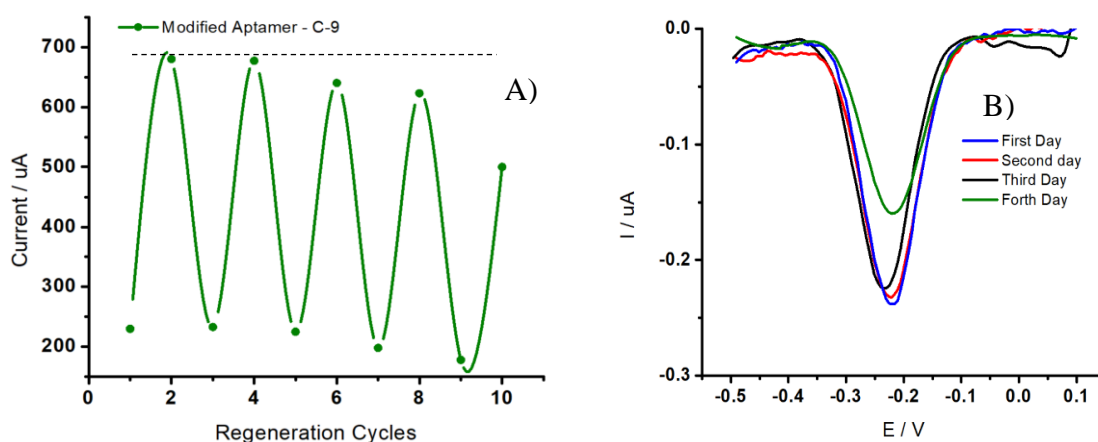


**Figure 3-6.** (A) Regeneration of the modified E-AB sensor for 350 pM of VEGF<sub>165</sub> biomarker (B) Stability test of modified E-AB sensor. The experiment was carried out with amplitude 50 mV, step 5 mV, and the frequency of 40 Hz. in 50% diluted serum sample.

The performance of interfacial manipulation in this work has been compared with previously reported electrochemical assays for the detection of VEGF<sub>165</sub> (**Table 3.2**). So far, one of the best method, in terms of stability and regenerability, has been reported by Feng et al,<sup>33</sup>. They have employed electrochemically triggered aptamer immobilization that takes place within 30 min with outstanding outcome in regenerability (reaching ~84% of initial current after two times of applications). Compared to their data, using C-9 alkyl thiol is highly comparable as only 11% decay in its initial signal after three times of application was measured. Furthermore, LOD measurements were performed in buffer whereas in this work, diluted human serum was used. According to the literature, the lowest LOD in VEGF<sub>165</sub> detection has been reported by Jang et al,<sup>34</sup> as of 100 fM of VEGF<sub>165</sub> in buffer solution with wide LDR (from 10 fM to 10 nM). A graphene-based field effect transistor (FET) was obtained by growing the Polypyrrole-converted nitrogen-doped few-layer graphene (PPy-NDFLG) on Cu substrate by chemical vapor deposition combined with vapor deposition polymerization. which then incorporated this into a liquid-ion gated FET. The FET sensor fabrication is complex, data lacks verification in physiological fluids and the

regenerability of the sensor mostly relies on the re-fabrication of at least the whole monolayer of biorecognition element, and therefore doesn't address the robustness of the monolayer itself after its hybridization with the target, whereas in our work the corresponding evaluation directly refers interfacial layer composing of the biorecognition. Overall, the results show a greater performance with previously reported works and because of the ease of the fabrication steps, it make this interfacial manipulation a very fast and versatile method suitable both for macro and microelectrode applications. The use of a lysine-(MB)<sub>2</sub> as the redox tag assembly, has proven to be rewarding in the generation of a robust signal current with improvement of S/N even with microelectrode applications. The reagentless process of VEGF<sub>165</sub> detection, which is free of multi-step washing and addition of exogenous reagent stand out among previously reported work<sup>34-36</sup>.

**Table 3.2.** Literature overview on DNA/RNA biosensors for detection of VEGF165 detection

Method	Biorecognition element	LOD	serum sample	Repeat ability	Ref.
E-AB sensor	DNA aptamer	6.2 nM	No	Yes	33
Optical detection via QDs modified probe aptamer	DNA aptamer	12nM	Yes	No	37
Porosity induced hydrogel microspheres	Capturing-Antibody	0.13 pM	Yes	No	38
AuNPs/ITO	Capturing-Antibody	2.6 PM	Yes	No	39
Surface plasmon resonance imaging	RNA aptamer	1PM	No	No	36
Rolling circle amplification SPR	DNA aptamer	2.6 PM	No	No	35
E-AB sensor	DNA aptamer	5PM	Yes	Yes	24
Chemiluminescence linked aptamer catalysis	DNA aptamer	50 PM	Yes	No	40
Polypyrrole nanotube biosensor	RNA aptamer	0.4 pM	No	Yes	41
N-doped Graphene transistor	RNA aptamer	0.1 pM	No	Yes	34
E-AB sensor	DNA aptamer	0.56 pM	Yes	Yes	Present work

## Conclusion

Precise monitoring of physiologically and clinically important targets heavily rely on the suitable signal amplification strategies that are easily incorporated with the sensing platforms. In this work, we have shown a new approach in signal amplification that is directed towards VEGF<sub>165</sub> biomarker measurement in 50% serum which achieves physiologically relevant sensitivity and specificity for prognostic purposes. Our data show that this strategy is implementable both with signal-off and signal-on type of E-AB sensors. Moreover, the sensing platform integrated with this strategy is perfectly reagent-less and single step. Last, due to the two spatially resolved MB redox tags, this strategy can successfully maintain its significance even in miniaturized sensing platforms where the scantily populated prob aptamers fail to generate enough signal to achieve a desirable sensitivity. The E-AB amplification approach thus appears well suited for convenient point-of-care diagnostics and the field monitoring of proteins and small molecule analytes.

## **Supporting information**

### **Amplifying VEGF signal-on multi-tagged probe aptamer**

Ashkan Koushanpour, Edward J. Harvey, Geraldine E. Merle\*

A. Koushanpour,

Experimental Surgery, Faculty of Medicine, McGill University, Montreal, H3A 0C5, Canada

Dr. E. Harvey

Department of Surgery, Faculty of Medicine, McGill University, Montreal, H3A 0C5, Canada

Dr. G. E. Merle

Department of Chemical Engineering, Polytechnique, Montreal, H3T 1J4, Canada

**KEYWORDS** Vascular endothelial cell growth factors (VEGF<sub>165</sub>); Aptamer; Biosensor;  
Diagnostic

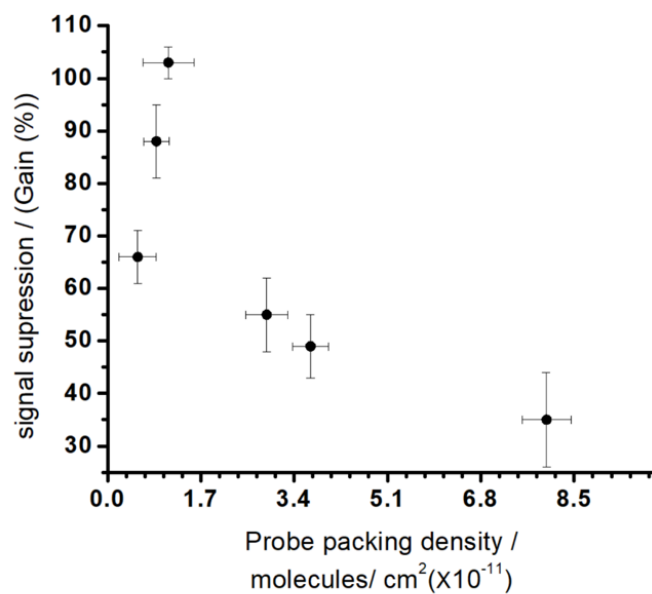


**Figure S 3-1** packing density optimization for varying concentrations of Control aptamer ranging from 0.01  $\mu\text{M}$  up to 0.5  $\mu\text{M}$ . with optimum concentration of 0.07  $\mu\text{M}$  corresponding to  $1.11 \times 10^{11}$  molecule/cm<sup>2</sup> and probe-probe spacing of approximately 33.9 nm.

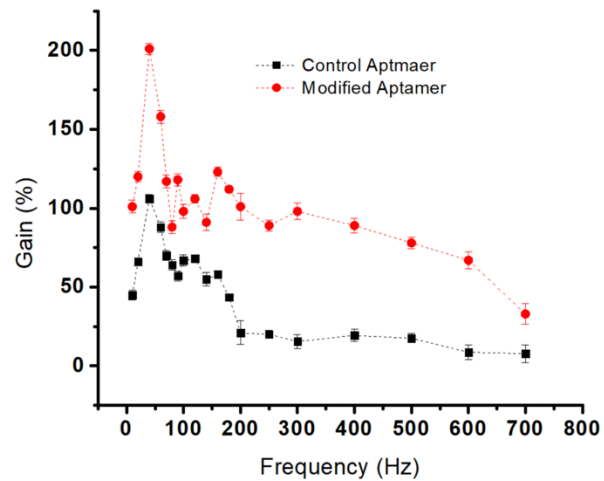


**Figure S 3-2** Plot of the SWV Frequency range (Hz) vs signal gain for the Control aptamer and the Modified aptamer. The best results coincide at 40 Hz.

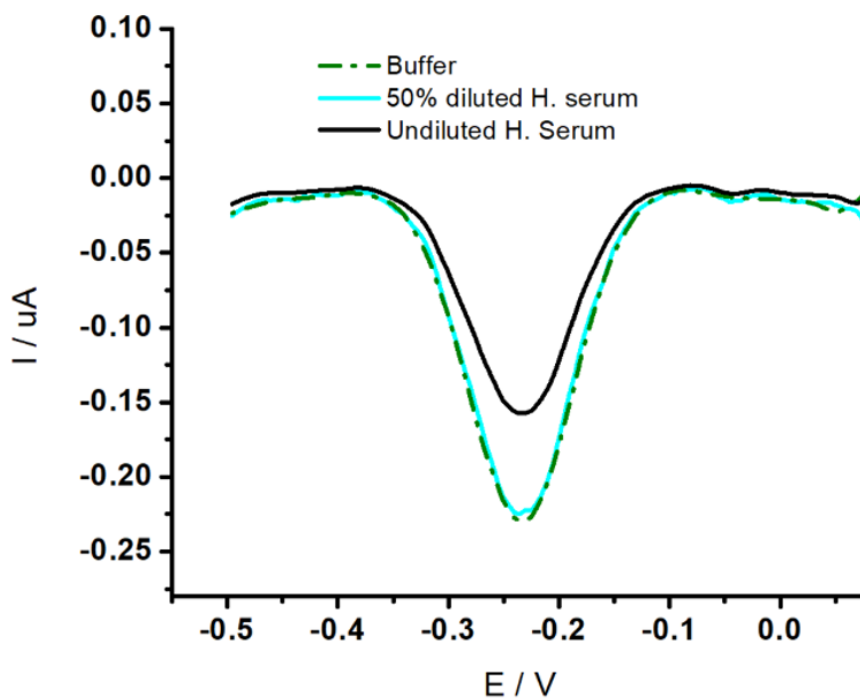


**Figure S 3-3** SWV responses of Modified aptamer E-AB sensor on C-9 OH alkyl thiol passivation layer. in, PBS buffer (dashed green curve), in 50% diluted human serum (solid green curve), and in undiluted human serum (black curve) with 33% signal variation. The experiments were carried out with an amplitude of 50 mV, step 5 mV, and frequency of 40 Hz in corresponding environments.

## References

- 1 L. Jing, C. Xie, Q. Li, M. Yang, S. Li, H. Li and F. Xia, *Anal. Chem.*, 2022, **94**, 269–296.
- 2 S. Herath, S. Razavi Bazaz, J. Monkman, M. Ebrahimi Warkiani, D. Richard, K. O’Byrne and A. Kulasinghe, *Expert Rev. Mol. Diagn.*, 2020, **20**, 1139–1147.
- 3 E. S. McDonald, A. S. Clark, J. Tchou, P. Zhang and G. M. Freedman, *J Nucl Med*, 2016, **57**, 9–16.
- 4 E. A. Krupinski and Y. Jiang, *Med. Phys.*, 2008, **35**, 645–659.
- 5 L. Hartwell, D. Mankoff, A. Paulovich, S. Ramsey and E. Swisher, *Nat. Biotechnol.*, 2006, **24**, 905–908.
- 6 M. Banys-Paluchowski, I. Witzel, S. Riethdorf, K. Pantel, B. Rack, W. Janni, P. A. Fasching, B. Aktas, S. Kasimir-Bauer, A. Hartkopf, E. F. Solomayer, T. Fehm and V. Müller, *Breast Cancer Res. Treat. 2018 1721*, 2018, **172**, 93–104.
- 7 S. Li, L. Wang, Y. Meng, Y. Chang, J. Xu, Q. Zhang, S. Li, L. Wang, Y. Meng, Y. Chang, J. Xu and Q. Zhang, *Oncotarget*, 2017, **8**, 41282–41293.
- 8 R. Roskoski, *Crit. Rev. Oncol. Hematol.*, 2007, **62**, 179–213.
- 9 M. Toi, H. Bando, T. Ogawa, M. Muta, C. Hornig and H. A. Weich, *Int. J. Cancer*, 2002, **98**, 14–18.
- 10 G. C. McKeeman, J. E. S. Ardill, C. M. Caldwell, A. J. Hunter and N. McClure, *Am. J. Obstet. Gynecol.*, 2004, **191**, 1240–1246.
- 11 S. R. Piersma, U. Fiedler, S. Span, A. Lingnau, T. V. Pham, S. Hoffmann, M. H. G. Kubbutat and C. R. Jiménez, *J. Proteome Res.*, 2010, **9**, 1913–1922.
- 12 A. A. Lubin and K. W. Plaxco, *Acc. Chem. Res.*, 2010, **43**, 496–505.
- 13 D. Li, S. Song and C. Fan, *Acc. Chem. Res.*, 2010, **43**, 631–641.
- 14 F. Ricci and K. W. Plaxco, *Microchim. Acta 2008 1633*, 2008, **163**, 149–155.
- 15 Y. Xiao, X. Qu, K. W. Plaxco and A. J. Heeger, *J. Am. Chem. Soc.*, 2007, **129**, 11896–11897.
- 16 C. E. Immoos, S. J. Lee and M. W. Grinstaff, *J. Am. Chem. Soc.*, 2004, **126**, 10814–10815.
- 17 Y. Xiao, A. A. Lubin, B. R. Baker, K. W. Plaxco and A. J. Heeger, *Proc. Natl. Acad. Sci.*, 2006, **103**, 16677–16680.
- 18 Y. Xiao, X. Qu, K. W. Plaxco and A. J. Heeger, *J. Am. Chem. Soc.*, 2007, **129**, 11896–11897.
- 19 Y. Xiao, A. A. Lubin, B. R. Baker, K. W. Plaxco and A. J. Heeger, *Proc. Natl. Acad. Sci. U. S. A.*, 2006, **103**, 16677–16680.
- 20 Y. Gao, L. K. Wolf and R. M. Georgiadis, *Nucleic Acids Res.*, 2006, **34**, 3370–3377.
- 21 N. Arroyo-Currás, K. Scida, K. L. Ploense, T. E. Kippin and K. W. Plaxco, *Anal. Chem.*, 2017, **89**, 12185–12191.
- 22 L. R. Schoukroun-Barnes, S. Wagan and R. J. White, *Anal. Chem.*, 2014, **86**, 1131–1137.
- 23 A. Hauke, L. S. S. Kumar, M. Y. Kim, J. Pegan, M. Khine, H. Li, K. W. Plaxco and J. Heikenfeld, *Biosens. Bioelectron.*, 2017, **94**, 438–442.
- 24 S. Zhao, W. Yang and R. Y. Lai, *Biosens. Bioelectron.*, 2011, **26**, 2442–2447.
- 25 J. Nick Taylor, Q. Darugar, K. Kourentzi, R. C. Willson and C. F. Landes, *Biochem. Biophys. Res. Commun.*, 2008, **373**, 213–218.

- 26 A. S. R. Potty, K. Kourentzi, H. Fang, G. W. Jackson, X. Zhang, G. B. Legge and R. C. Willson, *Biopolymers*, 2009, **91**, 145–156.
- 27 R. Levicky, T. M. Herne, M. J. Tarlov and S. K. Satija, *J. Am. Chem. Soc.*, 1998, **120**, 9787–9792.
- 28 X. Zhang and V. K. Yadavalli, *Biosens. Bioelectron.*, 2011, **26**, 3142–3147.
- 29 C. M. A. Brett, S. Kresak, T. Hianik and A. M. Oliveira Brett, *Electroanalysis*, 2003, **15**, 557–565.
- 30 F. Ma, C. Ho, A. K. H. Cheng and H. Z. Yu, *Electrochim. Acta*, 2013, **110**, 139–145.
- 31 Z. gang Yu, A. L. Sutlief and R. Y. Lai, *Sensors Actuators, B Chem.*, 2018, **258**, 722–729.
- 32 Serum Vascular Endothelial Growth Factor in Breast Cancer | Clinical Cancer Research | American Association for Cancer Research, <https://aacrjournals.org/clincancerres/article/7/11/3491/288564/Serum-Vascular-Endothelial-Growth-Factor-in-Breast>, (accessed 3 January 2023).
- 33 L. Feng, Z. Lyu, A. Offenhäusser and D. Mayer, *Eng. Life Sci.*, 2016, **16**, 550–559.
- 34 O. S. Kwon, S. J. Park, J. Y. Hong, A. R. Han, J. S. Lee, J. S. Lee, J. H. Oh and J. Jang, *ACS Nano*, 2012, **6**, 1486–1493.
- 35 H. Chen, Y. Hou, F. Qi, J. Zhang, K. Koh, Z. Shen and G. Li, *Biosens. Bioelectron.*, 2014, **61**, 83–87.
- 36 Y. Li, J. L. Hye and R. M. Corn, *Anal. Chem.*, 2007, **79**, 1082–1088.
- 37 R. Freeman, J. Girsh, A. Fang-Ju Jou, J. A. A. Ho, T. Hug, J. Dervedde and I. Willner, *Anal. Chem.*, 2012, **84**, 6192–6198.
- 38 M. A. Al-Ameen and G. Ghosh, *Biosens. Bioelectron.*, 2013, **49**, 105–110.
- 39 G. Il Kim, K. W. Kim, M. K. Oh and Y. M. Sung, *Biosens. Bioelectron.*, 2010, **25**, 1717–1722.
- 40 W. Li, Q. Zhang, H. Zhou, J. Chen, Y. Li, C. Zhang and C. Yu, *Anal. Chem.*, 2015, **87**, 8336–8341.
- 41 O. S. Kwon, S. J. Park and J. Jang, *Biomaterials*, 2010, **31**, 4740–4747.



## **The relevance and the contribution to the bigger picture**

So far, we have shown that the molecular manipulation of the interfacial layer is consistent with both signal-off and signal-on types of E-AB sensors. We have also been able to show how useful such an adaptation could be in the fabrication of a reagentless, sensitive sensing platform. This chapter relates to the role of gold nano-dimensionality of the electrode surface.

In chapter 4, we have emphasized the role of morphological dimensions on the E-AB sensor's performance for the detection of MUC1 (breast cancer biomarker) in the human serum sample. To accomplish this, bottom-up approaches were utilized for the synthesis of one- and three-dimensional gold substrates that were used in the construction of E-AB sensors, and the results were benchmarked with the regular gold electrode (two-dimensional) based E-AB sensor. The data revealed that, contrary to the general perception, increasing the surface area won't always lead to higher signal gain if there is a morphological mal effect in play. Also, data suggested that the surface/orientation of aptamers, on top of the alkanethiols SAM, may strongly rely on the surface morphology features and eventually affect the sensor performance/sensitivity. the insight gained from this work can be used to further probe the role of dimensionality/morphology in the signaling behavior of E-AB sensors. In this study, the role of aptamer's length was not included. this inclusion can further complement our statement regarding the role of surface nano-dimensionality on the aptamer's surface organization and its dynamics.

## **Chapter 4.**

# **Nano-dimensionality effect on the electrochemical aptamer-based sensor performance for serological MUC1 detection.**

Ashkan Koushanpour, Edward J. Harvey, Geraldine E. Merle\*

A. Koushanpour,

Experimental Surgery, Faculty of Medicine, McGill University, Montreal, H3A 0C5, Canada

Dr. E. Harvey

Department of Surgery, Faculty of Medicine, McGill University, Montreal, H3A 0C5, Canada

Dr. G. E. Merle

Department of Chemical Engineering, Polytechnique, Montreal, H3T 1J4, Canada

**KEYWORDS:** Gold dimensionality effect, MUC1 Biomarker, Aptamer; Biosensor.

To be submitted.

## Abstract

The modularity of the electrochemical aptamer-based (E-AB) sensors has made them useful candidates for a real-time, and specific determination of molecular targets (irrespective of their chemical reactivity). This, however, can hardly be achieved without certain considerations being applied to the interfacial region. In this work, we have emphasized the role of the electrode surface's morphological dimensions on the E-AB sensor's performance for the detection of MUC1 (breast cancer biomarker) in the human serum sample. To accomplish this, bottom-up approaches were utilized for the synthesis of one- and three-dimensional gold substrates (with  $0.072\text{ cm}^2$  and  $0.079\text{ cm}^2$  ECSA, respectively) that were later used in the construction of E-AB sensors, and the results were compared to the planar gold electrode (two-dimensional with ECSA of  $0.02\text{ cm}^2$ ). The selection of the regular gold electrode as the two-dimensional substrate was essential to make the study relevant and comparable with the widely used type of electrode that is commonly used in the fabrication of E-AB sensors. Our data show that the E-AB sensor based on the three-dimensional gold substrate with a limit of detection (LOD) of  $6.8\text{ nM}$  literally didn't make any improvement relative to the regular electrode (two-dimensional) with a LOD of  $7.8\text{ nM}$ . Whereas the one-dimensional gold substrate proved to be the most sensitive one with a LOD of  $3.5\text{ nM}$ . this enhancement is likely due to the attributes of the surface organization. Therefore, our findings suggest that a large surface area alone does not necessarily guarantee a better sensitivity unless causing a fruitful contribution to the aptamers' surface organization.

## 4.1 Introduction

Aptamers have attracted much attention in diagnostic medicine due to their easy synthesis protocols, low cost, great stability, and ability to recognize and bind a broad range of target analytes<sup>1-3</sup>. These short, single-stranded DNA or RNA molecules have been endorsed as recognition elements in biosensors, more particularly in E-AB sensors<sup>4</sup>. E-AB sensors are comprised of a surface-bound redox-modified probe aptamer (stem-loop) that is immobilized on the surface of a gold electrode via self-assembled monolayer chemistry (SAM). In absence of a target, the redox entity is found at the proximity of the electrode where a large current flows. After target addition, the hybridization-induced secondary-structure change will take the redox moiety away from the surface decreasing the current. This change in the current is readily measurable and is relatable to the target concentration.

The properties that define the interfacial region's characteristics are key in the performance of E-AB sensors<sup>5-7</sup>. Generally the SAM of the oligonucleotides on the electrode surface is considered the most well-defined building block in the construction of an E-AB sensor, and therefore has been tremendously employed to immobilize different probes on Au surface<sup>8</sup>. In addition, the goal in optimization of an E-AB sensor is to find a condition that affords the largest conformational changes<sup>9</sup> of the aptamer, as well as optimum strand-to-strand interspace<sup>10,11</sup>. As the interfacial recognition layer develops, several properties have been shown to be impactful such as aptamer organization/orientation<sup>12-14</sup>, aptamer length<sup>15</sup>, chemistry<sup>16</sup>, and spatial location of the electrochemical tag<sup>17</sup>, surface density, and backfilling strategies<sup>18,19</sup>. Incorporation of nanostructures can significantly contribute to the progress of many of these features<sup>20</sup>. For example, it can stabilize the DNA or RNA strands<sup>21</sup>, enhances the sensitivity<sup>22</sup> and enables a rapid electron transfer<sup>23</sup>. Nanomaterials possess a large number of unique physical and chemical

properties emerging from their nano size (e.g., varying in electrical conductivity and optical characteristics compared to their bulk alternatives)<sup>24,25</sup>. Interestingly, these attributes can be tailored and optimized for specific applications by manipulation of their properties including size, surface area, dimensionality, and porosity<sup>26</sup>. There are many reports showing the influence of size and shape of nanostructures on the SAM quality, target binding, and surface chemistry<sup>27-29</sup>.

Among metal nanostructures, gold is the most widely used<sup>30</sup> due to its ease of synthesis, biocompatibility, excellent conductive properties, and strong electron carriers. Given that they tend to display size, shape, and composition-dependent properties<sup>31</sup> such as morphologies (e.g., shape and surface structure) and distance-dependent properties (e.g., plasmonic and quantum confinement effect) Au nanomaterials have been studied and applied to biomedical applications<sup>32-34</sup>. Recently, surface's nano-effects have received considerable attentions in the fabrication of E-AB sensors as they provide superior analytical performance, because not only can they significantly increase the loading amount of DNA probes, but also may serve as a medium to bolster the electrochemical response in hybridization reaction<sup>35-37</sup>. Plaxco et al have shown the application of nanoporous gold for the miniaturization of an in Vivo E-AB sensor and concluded that such incorporation can lead to 100-fold increase in macroscopic surface area of the electrode<sup>38</sup>. Other works have shown that these nanomaterials were key to enable a precise long-term measurement of specific molecular target in Vivo<sup>39</sup>. In addition, Kelley et al have demonstrated that utilization of nanostructured gold surface dramatically enhances the hybridization efficiency compared to the same probe molecules when tethered to smoother surface<sup>40</sup>. Moreover, Shahrokhian and his co-workers<sup>41</sup> developed a label-free aptasensor based in nanoporous gold for the detection of salmonella by selective removal of the Cu from Au-Cu alloy. They have observed

that nanoporous gold morphology is more efficient in formation of SAM in comparison with planar gold electrode.

So far, there has been very few attempts in addressing the impact of the dimensionality of gold nanostructures on the E-AB sensor's analytical performance. In this study, we aim to identify the impact of the gold substrate nano-dimensionality on the performance of E-AB biosensor. To do so, bottom-up approaches were employed to synthesise one-dimensional (1D) and three-dimensional (3D) gold substrates- which later serve as substrates for the aptamer functionalization. Fabricated E-AB biosensors were then employed in the detection of MUC1 (breast cancer biomarker) in human serum samples and ultimately compared with the gold-standard regular gold electrode (2D) as the benchmark of the comparison.

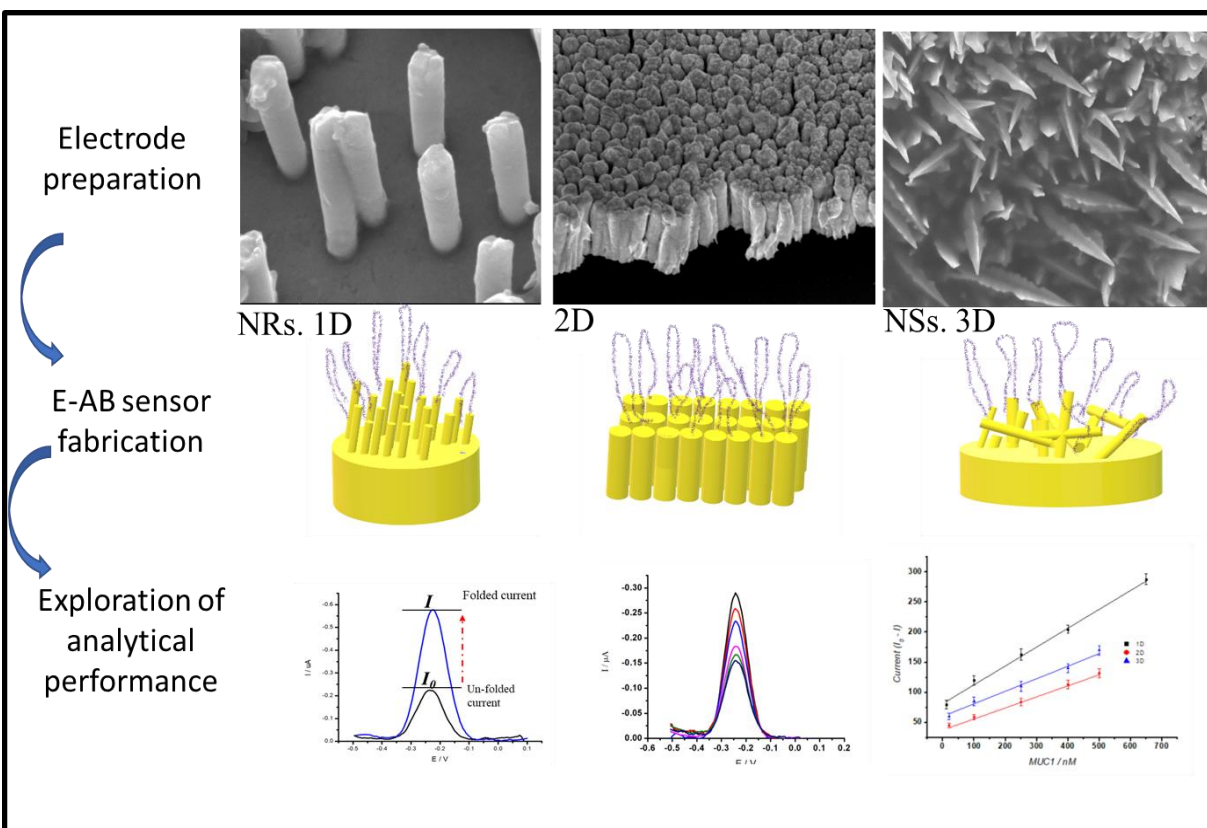


**Figure 4-1.** Schematic illustration of this work.

## 4.2 Experimental

### 4.2.1 Reagents

The following reagents were used as received (all reagents are by Sigma-Aldrich unless otherwise stated): human male AB plasma, USA origin, sterile-filtered, 6-mercapto-1-hexanol (C6-OH), tris-(2-carboxyethyl) phosphine hydrochloride (TCEP). The HPLC-purified and desalted anti-MUC1 DNA aptamers,

HO-(CH<sub>2</sub>)<sub>6</sub>-SS-(CH<sub>2</sub>)<sub>6</sub>-O-5'-GCA GTT GAT CCT TTG GAT ACC CTG-G-3'-(CH<sub>2</sub>)<sub>7</sub>-NHCO-(CH<sub>2</sub>)<sub>3</sub>-MB referred to as MB-anti-MUC1 aptamer.

The products were purchased from Biosearch Technologies Inc. (Novato, CA). The sequence was reported by Ferreira et al as the S1.3/S2.2<sup>42</sup>.

The 60-mer 3× VTR MUC1 peptide (PDT RPA PGS TAP PAH GVT SAP DTR PAP GST APP AHG VTS APD TRP APG STA PPA HGV TSA) was purchased from PL Laboratories Inc. (Vancouver, Canada). The peptides were suspended in a phosphate buffer (137 mM NaCl, 10 mM Na<sub>2</sub>HPO<sub>4</sub>, 1.4 mM KH<sub>2</sub>PO<sub>4</sub>, 2.7 mM KCl, pH 7.2) and stored at -20°C.

### 4.3 Preparation of E-AB sensor

The E-AB sensors (2D) were fabricated using gold disk electrode (1.6 mm diameter; BAS, West Lafayette, IN). The electrodes were polished with Buehler alumina slurry (1 and 0.05 μm) for 5 minutes, sonicated for 2 minutes and then transferred to “piranha” solution (3:1 ratio of H<sub>2</sub>SO<sub>4</sub> : H<sub>2</sub>O<sub>2</sub>) for 5 minutes. Finally, the electrodes were cycled in 0.1 M H<sub>2</sub>SO<sub>4</sub> solution cycled from 1.4 V to 0.1 V for 25 cycles and incubated with 100% ethanol for another 5 minutes. To fabricate the E-AB sensors, the relevant aptamer was diluted in 0.07 μM of PBS buffer (see below). The electrode was immersed and incubated in E-AB solution for 2 h. Passivation of the surface and displacement of the non-specific adsorbed aptamers were performed after 2h incubations in 2mM mercaptohexanol (MCH). The surface probe density (Γ) of each electrode was calculated by the area under the reductive peak of CV at 200 mV/s (Eq 4-1).

$$\Gamma = \frac{Q}{(nFA)} \quad (\text{Eq 4-1})$$

where Q is the area of the reductive signal, n is the number of electrons per redox event (n = 2 for MB), F is Faraday’s constant, and A is the area of the gold electrode as 0.020 cm<sup>2</sup>. Accordingly, the probe density was obtained as of 4.7×10<sup>12</sup> molecules/cm<sup>2</sup>. The same fabrication protocol was followed for preparation of other E-AB sensors featuring 1D and 3D gold nanostructures.

Electrochemical optimizations were performed in 10 mM phosphate buffer saline (PBS) (containing 2.92 g of NaCl, 0.0690 g of NaH<sub>2</sub>PO<sub>4</sub>, 0.071 g of Na<sub>2</sub>HPO<sub>4</sub> plus 50 µl of 1M MgCl<sub>2</sub> in 25 ml of deionized water, Millipore, nanopure water, 17.5 MΩ cm<sup>-1</sup>), pH 7.2, using Square Wave Voltammetry (SWV) featuring amplitude of 50 mV, step potential of 5 mV and frequency of 20 Hz. Electrochemical interrogations were recorded from 0.1 V to -0.5 V versus Ag/AgCl (sat. KCl) reference electrode.

## **4.4 Synthesis of gold nanostructures**

### **4.4.1 Gold nanospike synthesis**

The gold nanospike surface was prepared via a shape-controlled electrochemical method<sup>43</sup>. Briefly, gold nano-spikes were electrochemically formed on a gold disk electrode (1.6 mm diameter) from a solution containing 6.9 mM HAuCl<sub>4</sub> and 0.5 mM Pb(CH<sub>3</sub>COO)<sub>2</sub>. The electrochemical deposition was performed for 600 s at 0.05 V using Ag/AgCl (sat. KCl) as reference electrode and a graphite as an auxiliary electrode.

### **4.4.2 Gold nanorods synthesis**

The soft template-assisted electrodeposition method was used to produce gold nanorods in the pores of the track-etched polycarbonate (TEPC) membrane (pore diameter of 200 nm). To achieve this, a 100 nm thick gold layer was created through the sputtering method on one side of the TEPC membrane that served as a conductive substrate. Next, we assembled the TEPC membrane on a carbon with 2% Nafion acetate solution as polyelectrolyte glue (**Figure 4-2**). This unit was then placed in a mixture of 5.8 mM HAuCl<sub>4</sub> and 0.1 M HClO<sub>4</sub> for 2 hours. Then Au nanorod was electrodeposited at a constant potential of 0.18 V for 110 s. The membrane was finally dissolved in dichloromethane for 5 min.

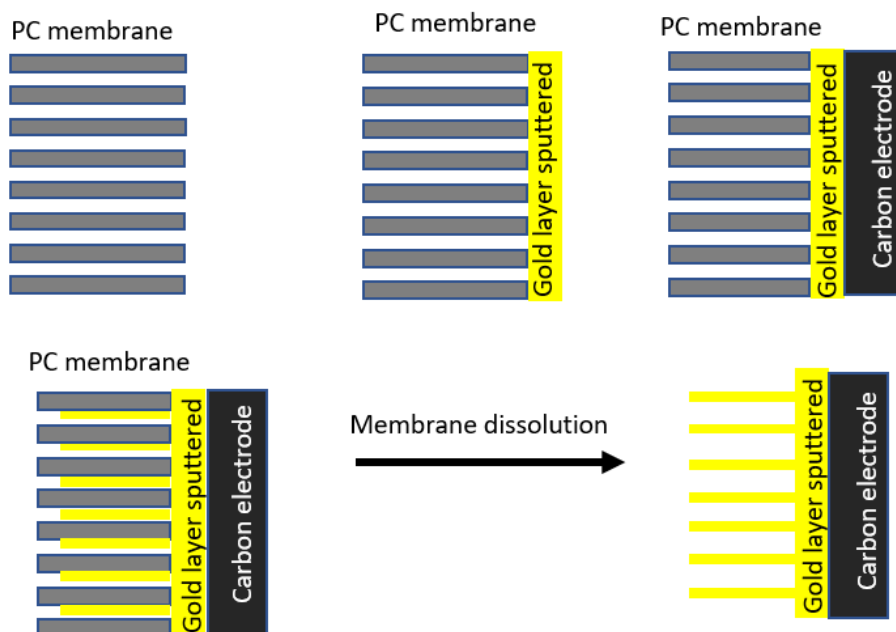


**Figure 4-2.** Schematic representation of template-based synthesis of gold nanorods using TEPC.

#### 4.5 Physico-chemical characterization and electrochemical measurements

The surface morphology was investigated by FEI Quanta 450 environmental scanning electron microscope field-emission scanning electron microscopy (FE-ESEM), and the energy-dispersive X-ray spectroscopy (EDX) was used to determine the chemical composition of the 3D gold substrate surface. Electrochemical measurements were made using a potentiostat/galvanostat (VersaSTAT 4, Princeton Applied Research) with a three-electrode system consisting of an Ag/AgCl (sat. KCl) reference electrode, Pt wire counter electrode, and gold disk electrodes. electrochemical measurements were performed in 50% diluted human serum samples using SWV featuring amplitude of 50 mV, step potential of 5 mV and frequency of 20 Hz, respectively. The electrochemical interrogations were recorded from 0.1 V to -0.5 V versus Ag/AgCl (sat. KCl) reference electrode.

## 4.6 Results and discussion

In this study, we investigated the influence of the gold surface dimensionality on the E-AB sensor's analytical performance in a signal-off sensor directed against the protein MUC1 in diluted human serum samples. Each sensor includes a DNA aptamer (25 nucleotides) that has been attached to the gold surface at its 5' terminus via thiol chemistry and present at its 3' a redox active methylene blue (MB). The E-AB sensors were built by immobilizing these modified aptamers through alkanethiol chemistry on three different nanostructured gold surfaces: control (2D), nanospike (NSs, 3D) and nanorods (NRs, 1D). **Figure 4-3 A-B-C** shows a scanning electron microscopy (SEM) image in top view of a representative TEPC membrane, and the corresponding Au NR electrode after the removal of the TEPC membrane. The electrode surface is fully covered by high-density ( $\sim 5.0 \cdot 10^8 \text{ NWs.cm}^{-2}$ ) and parallel NRs of 200 nm in diameter and 800nm in length, with 300 nm to 700 nm of inter-distance between them.

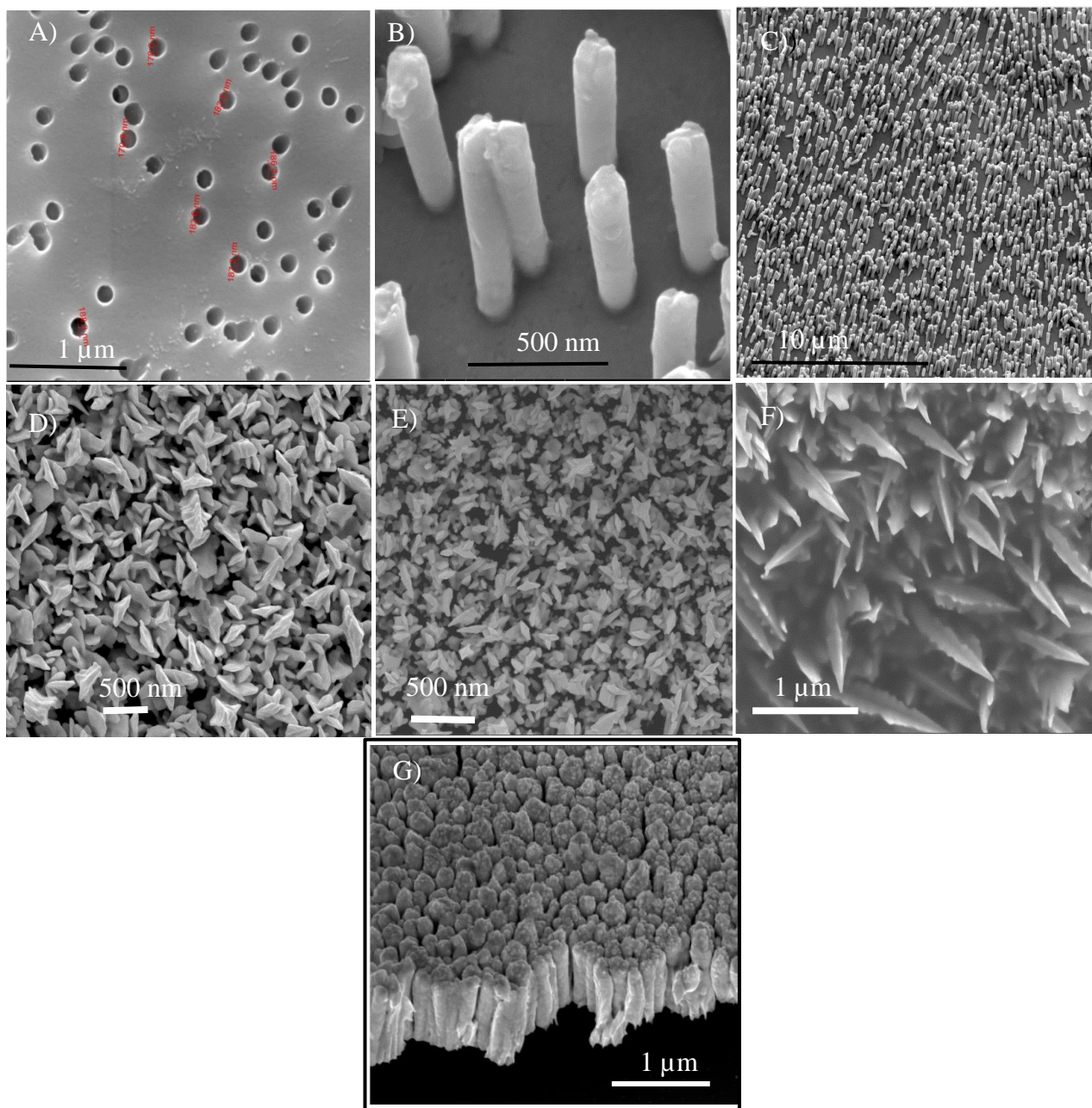


**Figure 4-3.** SEM images of the gold substrates A) surface of TEPC membrane. B) close view of 1D gold nanorods. C) showing the electrode surface with 1D orientation. D) zoomed-in top-view of 3D gold nanopikes. E) zoomed-out top-view of 3D gold nanopikes. F) tilted view of the 3D gold nanopikes. G) side-view of 2D gold surface.

In **Figure 4-3 D-E-F**, the surface of the electrode exhibits a uniform coating of well-defined Au nanospikes as can be seen in a lower-magnification SEM image of the nanospikes (**Figure 4-3 D**) with prismatic tapering ends. The top view of 3D gold nanospikes indicates a base thickness dimension of about ~350 nm (**Figure 4-3 E-F**) and approximately, 500 nm in length. Lastly, in **Figure 4-3 G** one can see the side-view of the 2D sputtered-gold surface. Complete removal of Pb for the NS structure has been confirmed with EDX analysis as shown in **Figure 4-4 A**.

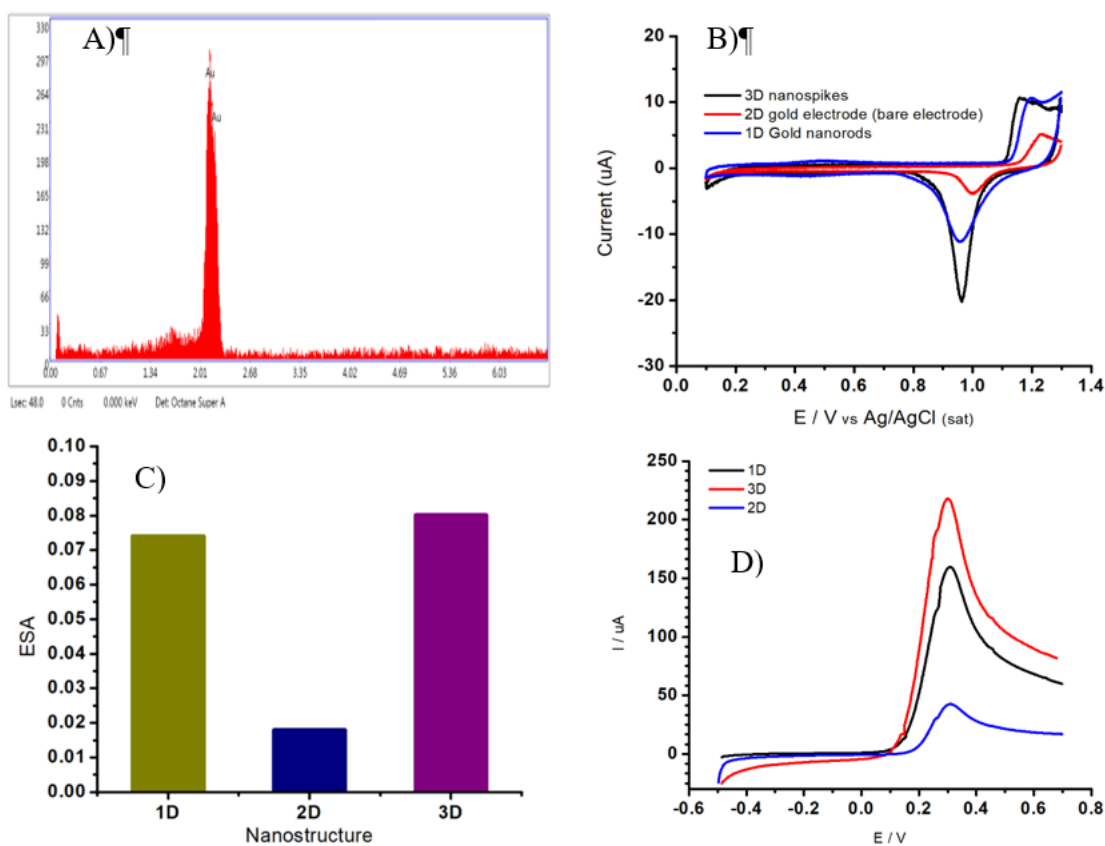


**Figure 4-4.** A) EDX spectrum from 3D gold nanoparticles. B) CV of a gold electrode featuring a various morphological aspect of 1D, 2D, and 3D nanostructures. Cyclic voltammetry was performed in 0.1 H<sub>2</sub>SO<sub>4</sub> solution with sweep rate of 0.05 V.s<sup>-1</sup>. C) ECSA resulted from LSV, and D) the corresponding LSV performed in water solution containing K<sub>4</sub>Fe(CN)<sub>6</sub> (10.0 mM),  $\nu = 0.1$  V.s<sup>-1</sup>

The electrochemical active surface area (ECSA) of the Au control, Au NSs and Au NRs were determined using cyclic voltammetry in 0.1 M H<sub>2</sub>SO<sub>4</sub> solution. **Figure 4-4 B** represents cyclic voltammograms that were taken from each of the Au surfaces. ECSA was calculated from the cathodic peak which is related to the removal of monolayer of oxide formed on the surfaces during the onward scan of the cyclic voltammogram. A cathodic peak was observed in the range of 0.90 to 1.05 V vs. Ag/AgCl. The onset for oxide formation for the Au nanostructures (NSs and NRs) is at a lower potential (1.12 V) than that of the Au-control electrode (1.18 V) confirming the presence

of Au nanostructures on the electrode. As expected, the ECSA of the Au NSs ( $0.079 \text{ cm}^2$ ) and NRs ( $0.072 \text{ cm}^2$ ) revealed higher surface area compared to that of control Au electrode ( $0.04 \text{ cm}^2$ ) as has been shown in **Figure 4-4 C**. Given the geometrical area of the bare electrode ca.,  $0.02 \text{ cm}^2$ , a roughness factor ( $R_f$ , the ratio of real surface area to geometrical area) of 3.95 and 3.6 were calculated for the NSs and NRs, respectively (**Figure 4-4 D**).

Given the MUC1 E-AB sensor's signalling mechanism, the electron transfer rate before and after MUC1 hybridization at the electrode surface is dependent on the SWV frequency used to interrogate the electrode, as well as the packing density. The latter was optimized by measuring the signal response of MUC1 on the aptamer modified gold electrode using various concentrations of the probe aptamer. An optimal probe density was achieved at  $4.7 \times 10^{12} \text{ molecule.cm}^{-2}$ , corresponding to an aptamer solution of 70 nM. Due to the size of surface nanostructures ( $> 80 \text{ nm}$ ), a similar probe surface density of  $4.7 \times 10^{12} \text{ molecule.cm}^{-2}$  was expected for 1D and 3D based E-AB sensors<sup>44</sup>. Given that they will share the same probe surface density, the difference in performance will be only the result of surface dimensionality.

Au nanostructures can influence the diffusion, thus the response time for the E-AB sensor to capture a detectable number of analyte molecules on its surface was determined (**Figure 4-5**). Three electrode configurations with MUC1 were screened and their response time vs signal gain were compared. The results shows that the electrodes exhibited a similar behavior in terms of gain variations vs. time until a plateau is reached. The highest gain ( $\sim 60\%$ ) was achieved for Au NR (1D) electrodes in 70 minutes whereas Au NS (3D) and Au control (2D) required 70 minutes to reach only 40%. These gain variations, in the case of Au NR (1D), started to be measurable only after 10 min in contact with MUC1, whereas Au Ns (3D), and the control electrodes (2D) needed at least 20-30 min. This hybridization kinetic behavior is likely due to the difference between

accumulation of MUC1 on the sensor surface and can be easily influenced by the surface geometry-induced steric hindrances<sup>45</sup>.

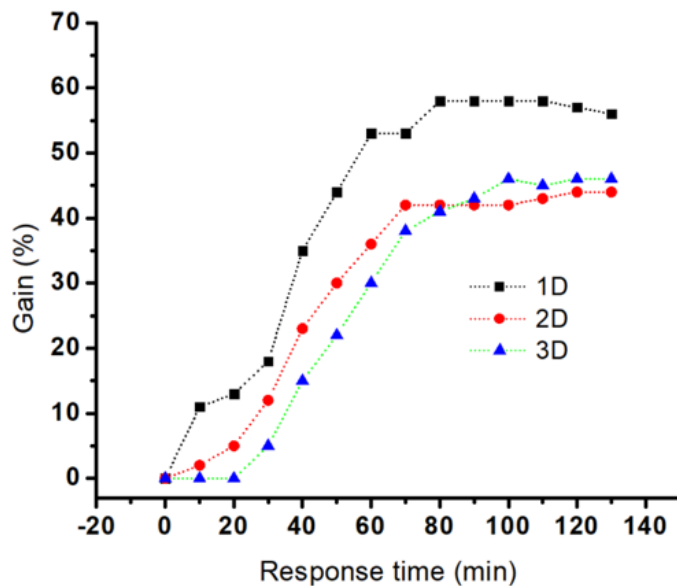


**Figure 4-5.** representation of the typical response time (signal suppression) of the various E-AB sensors featuring 1D, 2D, and 3D gold substrate within 2h incubation with a saturated concentration of MUC1 in 50% diluted human serum. Data points have been collected from a single measurement.

The influence of Au dimensionalities on the analytical performance of the corresponding E-AB sensors were analyzed with increased concentrations from 0 nM to 650 nM of MUC1 in the 50% diluted human serum samples. The corresponding signal changes ( $\Delta i$  = the change of peak current before and after addition of MUC1) were monitored via SWV technique (**Figure 4-6 A.B.C**). The SWV voltammograms showed a proportional decrease of MB current at  $\sim -0.25$  V vs Ag/AgCl with the increase of MUC1 concentrations.

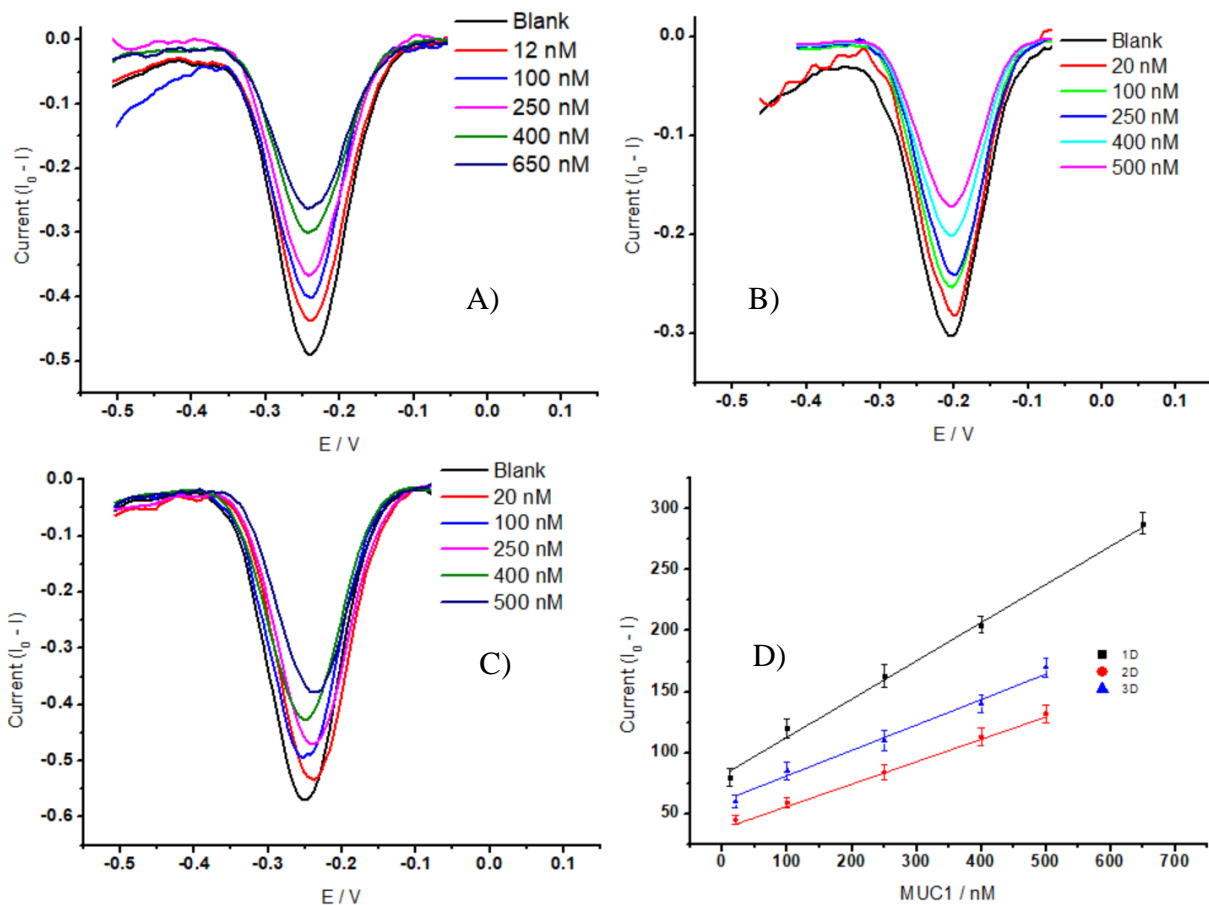


**Figure 4-6.** SWV responses of the E-AB sensors featuring 1D (A), 2D (B), and 3D (C) gold substrates after incubating with MUC1 at different concentrations. (D) collected Calibration curves for the detection of MUC1 based on various dimensionalities. The experiment was carried out with amplitude 50 mV, step 5 mV, and the frequency of 20 Hz in the 50% diluted human serum samples.

The SWV data were converted into calibration curve by plotting the signal suppression vs. concentration of MUC1 (**Figure 4-6 D**). MB redox peak linearly decreased in response to the addition of MUC1 for the three electrodes. We obtained the corresponding regression equations of  $\Delta i = 0.3332x + 81.51$  ( $R^2 = 99.47$ ),  $\Delta i = 0.1833x + 37.72$  ( $R^2 = 99.30$ ), and  $\Delta i = 0.2079x + 60.56$  ( $R^2 = 98.82$ ), for NRs (1D), control (2D) and NSs (3D) featuring E-AB sensors, respectively. A detection limit (LOD) (calculated by  $D_l = \frac{3S_b}{m}$ , where  $S_b$  is the standard deviation of the blank measures and  $m$  is the slope of the calibration curve obtained from the linear

regression analysis) of 3.5 nM, 7.8 nM, and 6.8 nM, was calculated for NRs (1D), 2D control, and NSs (3D) featuring E-AB sensors, respectively. There is an obvious relationship between the sensitivity and the dimensionality of the surface but not only 1D gold substrate was relatively more sensitive, it also yielded a wider LDR (from 12 nM to 650 nM), whereas the performances of 3D gold substrate did not differ from control 2D. The observed behavior can be most likely explained through the influence of surface morphology on the surface organization of aptamers. The large surface area of the 1D gold substrate significantly increased the immobilization sites for the MUC1 probe aptamers, also the properly oriented, and evenly distribution of gold nanorods seem to have facilitated the MUC1 diffusion to the nicely projected probe aptamers. thus, making the electrode readily accessible to the target. At the opposite, it appears that 3D Au produced the opposite effect with either the de-activation of the probe aptamers, or an unfavorable conformational change after target hybridization, which when combined, counterbalanced the positive impact of high surface area.

To investigate the repeatability, we prepared three fresh E-AB sensors and incubated them with saturated concentration of MUC1 in 50% human serum samples. All E-AB sensors exhibited similar signaling behavior with relative standard deviations (RSD) of 4.1% (NR), 4.5% (control), and 3.7% (NS), respectively. These values demonstrate that the repeatability character of the E-AB sensors within the corresponding time frame (90 min) was satisfactory. Moreover, the stability of fabricated E-AB sensors was also examined. Following the storage in the refrigerator at 4 °C for 9 days, NR (1D) and NS (3D) based aptasensors retained 91% and 95% of their initial currents, respectively, whereas the control electrode (2D) lost more than 90% of its initial value after only 3 days. The stabilization of aptamer by nanostructure is a well-documented effect <sup>40-41</sup>.

Nanostructure employment can increase the robustness of the surface which leads to higher stability of surface immobilization.

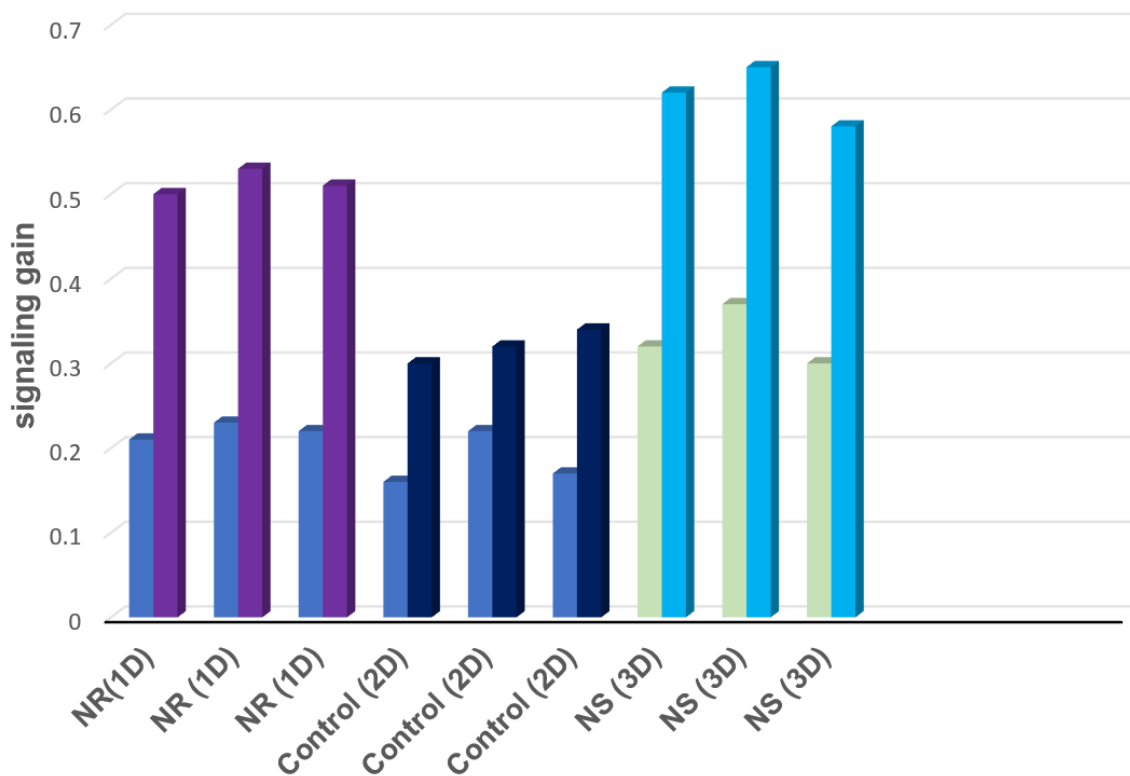


**Figure 4-7.** Shows repeatability results for three freshly prepared E-AB sensors 1D, 2D, and 3D.

## Conclusion

In this work, the surface nano-dimensionality and the corresponding influence on the E-AB sensor performance were investigated. Two bottom-up approaches, a template-based synthesis using TEPC and electrochemical deposition were used to build and synthesize 1D gold nanorods (ECSA =  $0.072 \text{ cm}^2$ ) and 3D gold nanopikes (ECSA =  $0.079 \text{ cm}^2$ ) respectively. After attachment of aptamer on the various Au surfaces using thiol chemistry, the analytical performances were measured and compared to the regular gold electrode (ECSA =  $0.02 \text{ cm}^2$ ) as the benchmark of the study. The highest sensitivity was obtained for 1D nanorods with 3.5 nM versus 6.8 nM for 3D nanopike featuring electrode. while control E-AB sensor only resulted in the LOD of 7.8 nM. our data revealed that, contrary to the general perception, increasing of the surface area won't always lead to higher gain if there is a morphological counterplay. Also, data suggested that the surface/orientation of aptamers, on top of the alkanethiols SAM, may strongly rely on the surface morphology features and eventually affects the sensor performance/sensitivity. on the other hand, surface enhancement on the electrode due to employment of NS, and NR, demonstrated a significant improvement in the shelf-life of the E-AB sensors (~9 days) relative to the control sensor with planar surface (~3 days). Given that the effect of various aptamer's lengths was not included in this study, future works are needed to consider the morphological influences on the aptamer's surface organization and the corresponding target-probe dynamics. In future, we plan to further grow such line of studies to achieve deeper insights into the interfacial properties and corresponding effect on the E-AB sensor performance.

## References

- (1) Que-Gewirth, N. S.; Sullenger, B. A. Gene Therapy Progress and Prospects: RNA Aptamers. *Gene Ther.* **2007**, *14* (4), 283–291. <https://doi.org/10.1038/SJ.GT.3302900>.
- (2) Song, S.; Wang, L.; Li, J.; Fan, C.; Zhao, J. Aptamer-Based Biosensors. *TrAC Trends Anal. Chem.* **2008**, *27* (2), 108–117. <https://doi.org/10.1016/J.TRAC.2007.12.004>.
- (3) Dollins, C. M.; Nair, S.; Sullenger, B. A. Aptamers in Immunotherapy. <https://home.liebertpub.com/hum> **2008**, *19* (5), 443–450. <https://doi.org/10.1089/HUM.2008.045>.
- (4) Xiao, Y.; Lai, R. Y.; Plaxco, K. W. Preparation of Electrode-Immobilized, Redox-Modified Oligonucleotides for Electrochemical DNA and Aptamer-Based Sensing. *Nat. Protoc.* **2007**, *2* (11), 2875–2880. <https://doi.org/10.1038/nprot.2007.413>.
- (5) Sharafeldin, M.; Davis, J. J. Characterising the Biosensing Interface. *Anal. Chim. Acta* **2022**, *1216*, 339759. <https://doi.org/10.1016/J.ACA.2022.339759>.
- (6) Muñoz, J.; Montes, R.; Baeza, M. Trends in Electrochemical Impedance Spectroscopy Involving Nanocomposite Transducers: Characterization, Architecture Surface and Bio-Sensing. *TrAC Trends Anal. Chem.* **2017**, *97*, 201–215. <https://doi.org/10.1016/J.TRAC.2017.08.012>.
- (7) Bizzotto, D.; Burgess, I. J.; Doneux, T.; Sagara, T.; Yu, H. Z. Beyond Simple Cartoons: Challenges in Characterizing Electrochemical Biosensor Interfaces. *ACS Sensors* **2018**, *3* (1), 5–12. [https://doi.org/10.1021/ACSSENSORS.7B00840/ASSET/IMAGES/LARGE/SE-2017-00840G\\_0001.JPEG](https://doi.org/10.1021/ACSSENSORS.7B00840/ASSET/IMAGES/LARGE/SE-2017-00840G_0001.JPEG).
- (8) Gooding, J. J.; Darwish, N. The Rise of Self-Assembled Monolayers for Fabricating Electrochemical Biosensors—an Interfacial Perspective. *Chem. Rec.* **2012**, *12* (1), 92–105. <https://doi.org/10.1002/TCR.201100013>.
- (9) Xiao, Y.; Uzawa, T.; White, R. J.; DeMartini, D.; Plaxco, K. W. On the Signaling of Electrochemical Aptamer-Based Sensors: Collision- and Folding-Based Mechanisms. *Electroanalysis* **2009**, *21* (11), 1267–1271. <https://doi.org/10.1002/ELAN.200804564>.
- (10) Cholko, T.; Chang, C. E. A. Modeling Effects of Surface Properties and Probe Density for Nanoscale Biosensor Design: A Case Study of Dna Hybridization near Surfaces. *J. Phys. Chem. B* **2021**, *125* (7), 1746–1754. [https://doi.org/10.1021/ACS.JPCB.0C09723/SUPPL\\_FILE/JP0C09723\\_SI\\_001.PDF](https://doi.org/10.1021/ACS.JPCB.0C09723/SUPPL_FILE/JP0C09723_SI_001.PDF).
- (11) Lin, M.; Wang, J.; Zhou, G.; Wang, J.; Wu, N.; Lu, J.; Gao, J.; Chen, X.; Shi, J.; Zuo, X.; Fan, C. Programmable Engineering of a Biosensing Interface with Tetrahedral DNA Nanostructures for Ultrasensitive DNA Detection. *Angew. Chemie* **2015**, *127* (7), 2179–2183. <https://doi.org/10.1002/ANGE.201410720>.
- (12) Furst, A. L.; Hill, M. G.; Barton, J. K. DNA-Modified Electrodes Fabricated Using Copper-Free Click Chemistry for Enhanced Protein Detection. *Langmuir* **2013**, *29* (52), 16141–16149. [https://doi.org/10.1021/LA403262V/SUPPL\\_FILE/LA403262V\\_SI\\_001.PDF](https://doi.org/10.1021/LA403262V/SUPPL_FILE/LA403262V_SI_001.PDF).
- (13) Steel, A. B.; Levicky, R. L.; Herne, T. M.; Tarlov, M. J. Immobilization of Nucleic Acids at Solid Surfaces: Effect of Oligonucleotide Length on Layer Assembly. *Biophys. J.* **2000**, *79* (2), 975–981. [https://doi.org/10.1016/S0006-3495\(00\)76351-X](https://doi.org/10.1016/S0006-3495(00)76351-X).
- (14) Herne, T. M.; Tarlov, M. J. Characterization of DNA Probes Immobilized on Gold Surfaces. *J. Am. Chem. Soc.* **1997**, *119* (38), 8916–8920. <https://doi.org/10.1021/JA9719586>.
- (15) Ricci, F.; Lai, R. Y.; Heeger, A. J.; Plaxco, K. W.; Sumner, J. J. Effect of Molecular Crowding on the Response of an Electrochemical DNA Sensor. *Langmuir* **2007**, *23* (12), 6827–6834. <https://doi.org/10.1021/LA700328R/ASSET/IMAGES/MEDIUM/LA700328RN00001.GIF>.
- (16) Ricci, F.; Zari, N.; Caprio, F.; Recine, S.; Amine, A.; Moscone, D.; Palleschi, G.; Plaxco, K. W. Surface Chemistry Effects on the Performance of an Electrochemical Sensor. *Bioelectrochemistry* **2009**, *76* (0), 208–

213. <https://doi.org/10.1016/J.BIOELECHEMA.2009.03.007>.
- (17) Mayer, M. D.; Lai, R. Y. Effects of Redox Label Location on the Performance of an Electrochemical Aptamer-Based Tumor Necrosis Factor-Alpha Sensor. *Talanta* **2018**, *189*, 585–591. <https://doi.org/10.1016/J.TALANTA.2018.07.055>.
- (18) Lee, C. Y.; Gong, P.; Harbers, G. M.; Grainger, D. W.; Castner, D. G.; Gamble, L. J. Surface Coverage and Structure of Mixed DNA/Alkylthiol Monolayers on Gold: Characterization by XPS, NEXAFS, and Fluorescence Intensity Measurements. *Anal. Chem.* **2006**, *78* (10), 3316–3325. <https://doi.org/10.1021/AC052137J>.
- (19) Leung, K. K.; Gaxiola, A. D.; Yu, H. Z.; Bizzotto, D. Tailoring the DNA SAM Surface Density on Different Surface Crystallographic Features Using Potential Assisted Thiol Exchange. *Electrochim. Acta* **2018**, *261*, 188–197. <https://doi.org/10.1016/J.ELECTACTA.2017.12.114>.
- (20) Dimcheva, N. Nanostructures of Noble Metals as Functional Materials in Biosensors. *Curr. Opin. Electrochem.* **2020**, *19*, 35–41. <https://doi.org/10.1016/J.COELEC.2019.09.008>.
- (21) Urmann, K.; Modrejewski, J.; Scheper, T.; Walter, J. G. Aptamer-Modified Nanomaterials: Principles and Applications. *BioNanoMaterials* **2017**, *18* (1–2). <https://doi.org/10.1515/BNM-2016-0012>.
- (22) Shariati, M.; Ghorbani, M.; Sasanpour, P.; Karimizefreh, A. An Ultrasensitive Label Free Human Papilloma Virus DNA Biosensor Using Gold Nanotubes Based on Nanoporous Polycarbonate in Electrical Alignment. *Anal. Chim. Acta* **2019**, *1048*, 31–41. <https://doi.org/10.1016/J.ACA.2018.09.062>.
- (23) Tulli, F.; Gulotta, F. A.; Martino, D. M.; Zanini, V. I. P.; Borsarelli, C. D. Ultrasensitive Amperometric Biosensing of Polyphenols Using Horseradish Peroxidase Immobilized in a Laponite/Au/DNA-Bioinspired Polycation Nanocomposite. *J. Electrochem. Soc.* **2018**, *165* (10), B452–B457. <https://doi.org/10.1149/2.1191810JES/PDF>.
- (24) Kumar, N.; Kumbhat, S. Unique Properties. *Essentials Nanosci. Nanotechnol.* **2016**, 326–360. <https://doi.org/10.1002/9781119096122.CH8>.
- (25) Navya, P. N.; Daima, H. K. Rational Engineering of Physicochemical Properties of Nanomaterials for Biomedical Applications with Nanotoxicological Perspectives. *Nano Conver.* **2016**, *3* (1). <https://doi.org/10.1186/S40580-016-0064-Z>.
- (26) Solanki, P. R.; Kaushik, A.; Agrawal, V. V.; Malhotra, B. D. Nanostructured Metal Oxide-Based Biosensors. *NPG Asia Mater.* **2011**, *31* **2011**, *3* (1), 17–24. <https://doi.org/10.1038/asiamat.2010.137>.
- (27) Zhou, Q.; Kim, T. Review of Microfluidic Approaches for Surface-Enhanced Raman Scattering. *Sensors Actuators B Chem.* **2016**, *227*, 504–514. <https://doi.org/10.1016/J.SNB.2015.12.069>.
- (28) Soleymani, L.; Fang, Z.; Sargent, E. H.; Kelley, S. O. Programming the Detection Limits of Biosensors through Controlled Nanostructuring. *Nat. Nanotechnol.* **2009**, *4* (12), 844–848. <https://doi.org/10.1038/NNANO.2009.276>.
- (29) Sheehan, P. E.; Whitman, L. J. Detection Limits for Nanoscale Biosensors. *Nano Lett.* **2005**, *5* (4), 803–807. <https://doi.org/10.1021/NL050298X>.
- (30) Hammami, I.; Alabdallah, N. M.; jomaa, A. Al; kamoun, M. Gold Nanoparticles: Synthesis Properties and Applications. *J. King Saud Univ. - Sci.* **2021**, *33* (7). <https://doi.org/10.1016/J.JKSUS.2021.101560>.
- (31) Yan, Z.; Taylor, M. G.; Mascareno, A.; Mpourmpakis, G. Size-, Shape-, and Composition-Dependent Model for Metal Nanoparticle Stability Prediction. *Nano Lett.* **2018**, *18* (4), 2696–2704. [https://doi.org/10.1021/ACS.NANOLETT.8B00670/SUPPL\\_FILE/NL8B00670\\_SI\\_001.PDF](https://doi.org/10.1021/ACS.NANOLETT.8B00670/SUPPL_FILE/NL8B00670_SI_001.PDF).
- (32) Taylor, M. G.; Austin, N.; Gounaris, C. E.; Mpourmpakis, G. Catalyst Design Based on Morphology- and Environment-Dependent Adsorption on Metal Nanoparticles. *ACS Catal.* **2015**, *5* (11), 6296–6301. [https://doi.org/10.1021/ACSCATAL.5B01696/SUPPL\\_FILE/CS5B01696\\_SI\\_001.PDF](https://doi.org/10.1021/ACSCATAL.5B01696/SUPPL_FILE/CS5B01696_SI_001.PDF).

- (33) Bratlie, K. M.; Lee, H.; Komvopoulos, K.; Yang, P.; Somorjai, G. A. Platinum Nanoparticle Shape Effects on Benzene Hydrogenation Selectivity. *Nano Lett.* **2007**, *7* (10), 3097–3101. [https://doi.org/10.1021/NL0716000/SUPPL\\_FILE/NL0716000SI20070914\\_111617.PDF](https://doi.org/10.1021/NL0716000/SUPPL_FILE/NL0716000SI20070914_111617.PDF).
- (34) Arenz, M.; Landman, U.; Heiz, U. CO Combustion on Supported Gold Clusters. *ChemPhysChem* **2006**, *7* (9), 1871–1879. <https://doi.org/10.1002/CPHC.200600029>.
- (35) Huang, X. J.; O'Mahony, A. M.; Compton, R. G. Microelectrode Arrays for Electrochemistry: Approaches to Fabrication. *Small* **2009**, *5* (7), 776–788. <https://doi.org/10.1002/SMLL.200801593>.
- (36) Walcarius, A.; Minteer, S. D.; Wang, J.; Lin, Y.; Merkoçi, A. Nanomaterials for Bio-Functionalized Electrodes: Recent Trends. *J. Mater. Chem. B* **2013**, *1* (38), 4878–4908. <https://doi.org/10.1039/C3TB20881H>.
- (37) Shi, L.; Chu, Z.; Dong, X.; Jin, W.; Dempsey, E. A Highly Oriented Hybrid Microarray Modified Electrode Fabricated by a Template-Free Method for Ultrasensitive Electrochemical DNA Recognition. *Nanoscale* **2013**, *5* (21), 10219–10225. <https://doi.org/10.1039/C3NR03097K>.
- (38) Downs, A. M.; Gerson, J.; Hossain, M. N.; Ploense, K.; Pham, M.; Kraatz, H. B.; Kippin, T.; Plaxco, K. W. Nanoporous Gold for the Miniaturization of in Vivo Electrochemical Aptamer-Based Sensors. *ACS Sensors* **2021**, *6* (6), 2299–2306. [https://doi.org/10.1021/ACSSENSORS.1C00354/SUPPL\\_FILE/SE1C00354\\_SI\\_001.PDF](https://doi.org/10.1021/ACSSENSORS.1C00354/SUPPL_FILE/SE1C00354_SI_001.PDF).
- (39) Arroyo-Currás, N.; Scida, K.; Ploense, K. L.; Kippin, T. E.; Plaxco, K. W. High Surface Area Electrodes Generated via Electrochemical Roughening Improve the Signaling of Electrochemical Aptamer-Based Biosensors. *Anal. Chem.* **2017**, *89* (22), 12185–12191. [https://doi.org/10.1021/ACS.ANALCHEM.7B02830/SUPPL\\_FILE/AC7B02830\\_SI\\_001.PDF](https://doi.org/10.1021/ACS.ANALCHEM.7B02830/SUPPL_FILE/AC7B02830_SI_001.PDF).
- (40) Bin, X.; Sargent, E. H.; Kelley, S. O. Nanostructuring of Sensors Determines the Efficiency of Biomolecular Capture. *Anal. Chem.* **2010**, *82* (14), 5928–5931. [https://doi.org/10.1021/AC101164N/SUPPL\\_FILE/AC101164N\\_SI\\_001.PDF](https://doi.org/10.1021/AC101164N/SUPPL_FILE/AC101164N_SI_001.PDF).
- (41) Ranjbar, S.; Shahrokhian, S.; Nurmohammadi, F. Nanoporous Gold as a Suitable Substrate for Preparation of a New Sensitive Electrochemical Aptasensor for Detection of Salmonella Typhimurium. *Sensors Actuators B Chem.* **2018**, *255*, 1536–1544. <https://doi.org/10.1016/J.SNB.2017.08.160>.
- (42) Ferreira, C. S. M.; Matthews, C. S.; Missailidis, S. DNA Aptamers That Bind to MUC1 Tumour Marker: Design and Characterization of MUC1-Binding Single-Stranded DNA Aptamers. *Tumor Biol.* **2006**, *27* (6), 289–301. <https://doi.org/10.1159/000096085>.
- (43) Plowman, B.; Ippolito, S. J.; Bansal, V.; Sabri, Y. M.; O'Mullane, A. P.; Bhargava, S. K. Gold Nanospikes Formed through a Simple Electrochemical Route with High Electrocatalytic and Surface Enhanced Raman Scattering Activity. *Chem. Commun.* **2009**, No. 33, 5039–5041. <https://doi.org/10.1039/B910830K>.
- (44) Hill, H. D.; Millstone, J. E.; Banholzer, M. J.; Mirkin, C. A. The Role Radius of Curvature Plays in Thiolated Oligonucleotide Loading on Gold Nanoparticles. *ACS Nano* **2009**, *3* (2), 418–424. [https://doi.org/10.1021/NN800726E/ASSET/IMAGES/MEDIUM/NN-2008-00726E\\_0010.GIF](https://doi.org/10.1021/NN800726E/ASSET/IMAGES/MEDIUM/NN-2008-00726E_0010.GIF).
- (45) Mahshid, S. S.; Camiré, S.; Ricci, F.; Vallée-Bélisle, A. A Highly Selective Electrochemical DNA-Based Sensor That Employs Steric Hindrance Effects to Detect Proteins Directly in Whole Blood. *J. Am. Chem. Soc.* **2015**, *137* (50), 15596–15599. [https://doi.org/10.1021/JACS.5B04942/SUPPL\\_FILE/JA5B04942\\_SI\\_001.PDF](https://doi.org/10.1021/JACS.5B04942/SUPPL_FILE/JA5B04942_SI_001.PDF).



## Chapter 5.

### Comprehensive scholarly discussion

An electrochemical biosensor is rigorously defined as a self-contained integrated device that serves to translate the information from a biological domain, mostly the activity/concentration of the analyte, into physical output signal with a defined sensitivity<sup>1</sup>. In the realm of medical devices and applications, it is arguable that the last frontier goal of such development is envisioned as implantable bioanalytical sensors that enable precise and continuous monitoring of clinically and physiologically important analytes in the living body for a long period of time<sup>2-4</sup>. E-AB sensors have partially fulfilled the task, by so far allowing the multi-hour in Vivo continuous measurement over the plethora of molecular targets, irrespective of their specific chemical reactivity. These sensors achieve this by employing nucleic acid aptamers as the biorecognition elements that can reversibly bind to their target molecules with selectivity even in a contamination-driven biological environment such as the whole blood<sup>5,6</sup>. Nevertheless, the road from in Vitro proof-of-the-concept demonstrations, i.e., benchtop prototypes, to a truly relevant in Vivo clinical application is still challenging.

One major bottleneck lies in the art of Systematic Evolution of Ligands by Exponential Enrichment (SELEX), which is not primarily directed towards R&D of aptamers for E-AB sensor application. Currently, the biofouling of the surface of E-AB sensors can't withstand non-specific adsorption of inborn protein entities<sup>7</sup> and the low signal-to-noise is a conventional downside of the current fabrication methodology<sup>8</sup>. Consequently, new innovations in the fields of biomedical engineering, interfacial chemistry, material science, and data management are required to tackle current E-AB sensor challenges.

The low signal-to-noise, and lack of signal amplification, thus sensitivity, are the most common issues that have impeded the development of E-AB sensors<sup>8</sup>. With regard to the signal-to-noise, , the most commonly used methodology has been so-called the roughening of the surface of the electrode material for generating microstructures and increase the number of immobilization sites for biorecognition elements<sup>5</sup>. This method is rather simple however the corresponding signal amplification lacks proportionality to surface area enhancement, e.g., a 10X increase in the surface area via roughening, will only yield in a two or three-times boost in the analytical signal. And therefore, fails to meet the real demand for signal amplification. Other innovations such as exploiting biotechnological-derived molecules such as phi29 DNA<sup>9</sup>, a polymerase, which can trigger an intense proliferation of signal-generating elements like G-quadruplex aptamers, fails to address the real challenge in creating a truly reagentless sensing platform as they tend to complex the signal acquisition process by requiring more additional processing steps. Keeping this in mind, these methodologies although interesting and sophisticated, hardly satisfy the requirements for the development of implantable biosensor applications.

The core of the current thesis which is composed of three research papers tends to propose and underline new strategies that help circumvent these issues from an interfacial chemistry point of view. **Figure 5-1** illustrates the general configuration of the E-AB sensing platform vs the one that has been proposed in the current body of research.

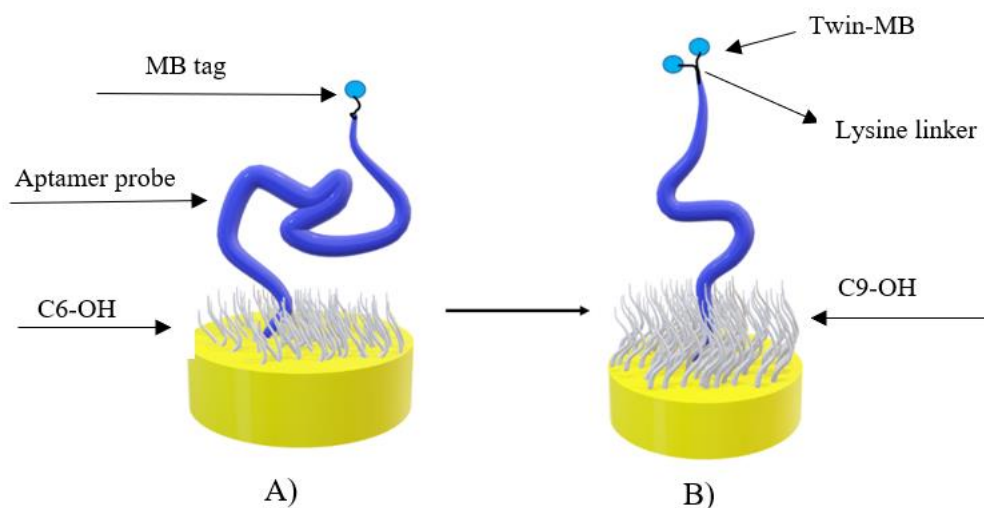


**Figure 5-1.** schematic structure of the E-AB sensor. A) conventional vs. B) modified configuration. Where in A) C<sub>6</sub>-OH is used as a backfilling agent with a single redox-tagged probe aptamer, whereas in B), C<sub>9</sub>-OH as a backfilling agent, and Twin-MB redox-tagged probe aptamer are used.

Unlike conventional sensor configuration, which comprises a C<sub>6</sub>-OH backfilled gold electrode modified with surface-immobilized single-MB redox-tagged DNA aptamer, the proposed setting includes a C<sub>9</sub>-OH backfilled surface combined with a twin-MB tagged DNA aptamer. **Figure 5-2** illustrates the chemical steps needed to synthesize the Twin-MB tagged DNA aptamers, as well as the backfilling agent's length. We have manipulated the interface during the fabrication of E-AB sensors and studied the analytical performances towards the detection of breast cancer biomarkers in human serum samples. To confirm the versatility of this strategy and its effectiveness in electrochemical aptasensors, both signal-off and signal-on types of sensors were investigated with the use of MUC1 and VEGF<sub>165</sub> biomarkers, respectively.

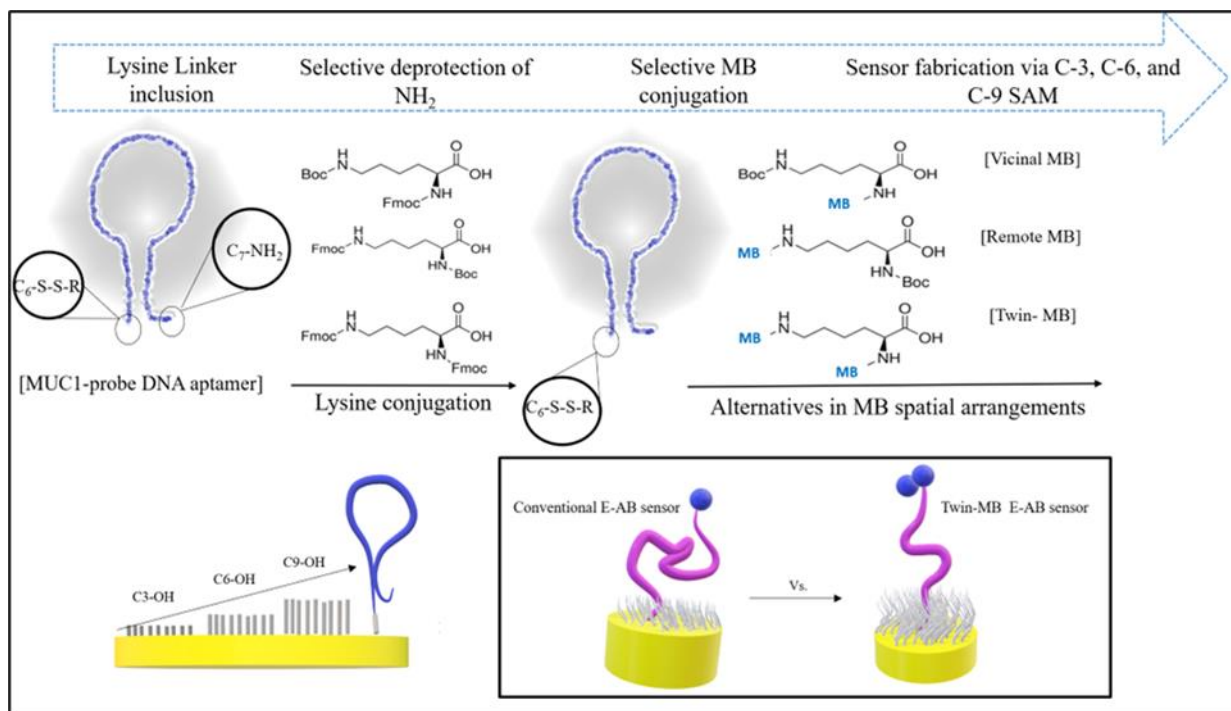


**Figure 5-2.** Schematic illustration of aptamer manipulation with lysine and further spatially selective arrangement of MB conjugations.

The signal gain was studied to normalize the differences for any microscopic changes, and to offer a fair comparison between the different variations used in the fabrication parameters. It must be noted that the signal gain is calculated by the relative changes in the initial peak current induced by the target.

In Chapter 2, the interrogating parameters for MUC1 aptamer probes were optimized and two distinct frequencies of 20 Hz and 80 Hz were chosen as optimum frequencies for the control and the modified DNA aptamers, respectively. This difference in frequency was not attributed to the chemical manipulations on DNA aptamer i.e., conjugation of the lysine (MB)<sub>2</sub>. Based on three observations: 1) the similar trends during the CV experiment (**Figure 5-3**), 2) the calculation and comparison of the affinity between probes and their targets via corresponding  $K_D$  values and 3) the

perfect frequency match that we had in the case of the VEGF<sub>165</sub> biomarker (**Figure 5-4**), we concluded that the conjugation of aptamer probes, be it for MUC1 or VEGF<sub>165</sub> had little or no effect on the spatial dynamics of the strands.

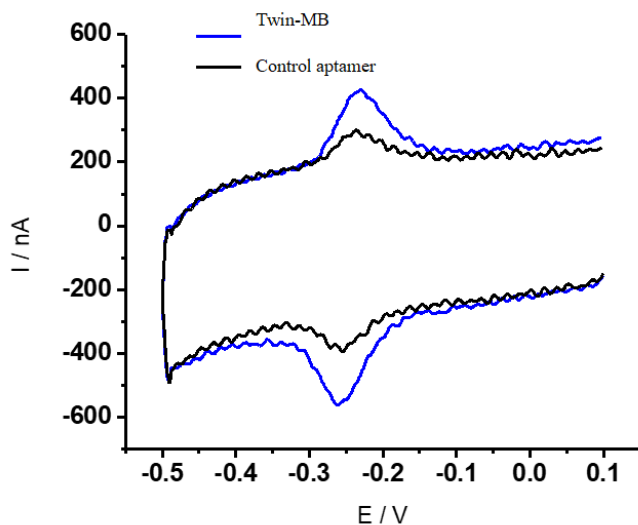


**Figure 5-3.** CVs of the control E-AB and Twin-MB sensors with a C-6 mercaptohexanol agent.

It should be noted that these methods, CV and  $K_D$  values, are widely-used in many research works<sup>10-12</sup>. however, due to the indirect nature of these experiments, one can always hold on to some degree of incertinty<sup>13</sup>. Alternatively, to unequivocally address the phenomenon, we could have instead utilized the circular dichroism spectroscopy method (CD spectroscopy) which, in turn, could reveal any minute changes in the natural folding-unfolding states of the DNA strand. And therefore, could provide an absolute answer.

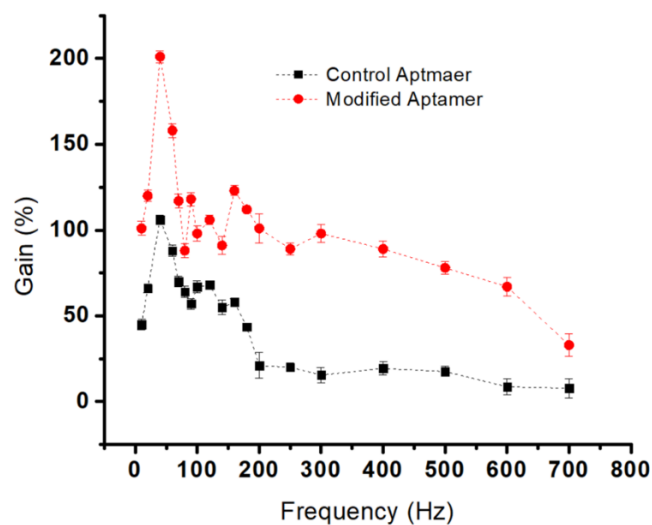


**Figure 5-4.** Plot of the SWV Frequency range (Hz) vs signal gain for the Control aptamer and the modified aptamer. The best results coincide at 40 Hz.

In the case of the MUC1 biomarker, the signal gain increased from switching from the conventional to modified E-AB sensors (**Figure 5-5**). The thicker passivation layer used for backfilling the surface, may have caused a bigger cleavage in folded and unfolded aptamer structures. According to many previous reports, thicker passivation layers generally tend to hamper the electron transfer efficiency by putting a higher barrier amongst the tag and the electrode<sup>14-17</sup>. This phenomena is observed in **Figure 5-5 A**, where the utilization of C<sub>9</sub>-OH profoundly suppressed the gain, and where the highest gain is with C<sub>6</sub>-OH (**Figure 5-5. A**). At the opposite in **Figure 5-5. B**, C<sub>9</sub>-OH improved the signal gain. These findings suggest that the higher length of lysine linker at the distal terminus of the probe aptamer creates a higher degree of proximity to the surface, and thus can somehow compensate the higher barrier effect.

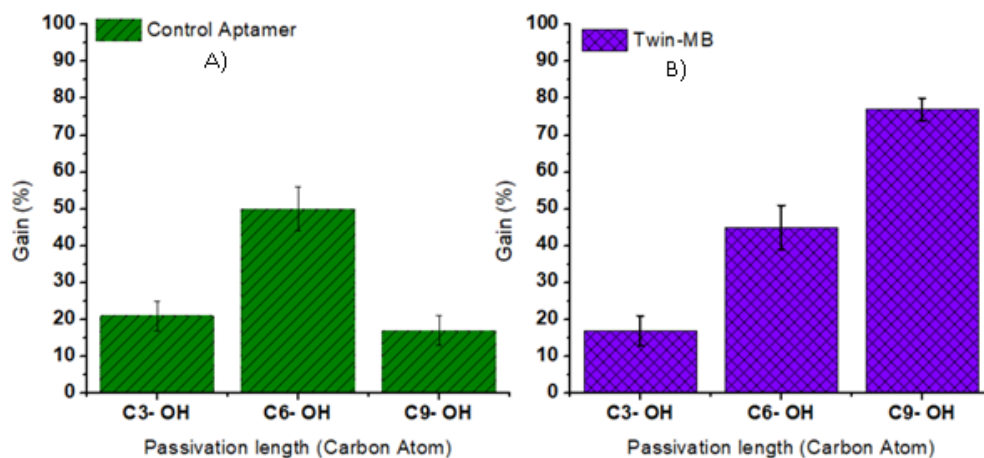


**Figure 5-5.** demonstrates the gain variations relative to systematic changes in SAMs layer thickness from C-3 to C-9. A) Control E-AB sensor, and B) E-AB sensor built upon Twin-MB.

In the case of VEGF<sub>165</sub>, similar effect associated with the lysine linker was observed (**Figure 5-6**), where progressive gain enhancements were observed for both control and modified E-AB sensors.

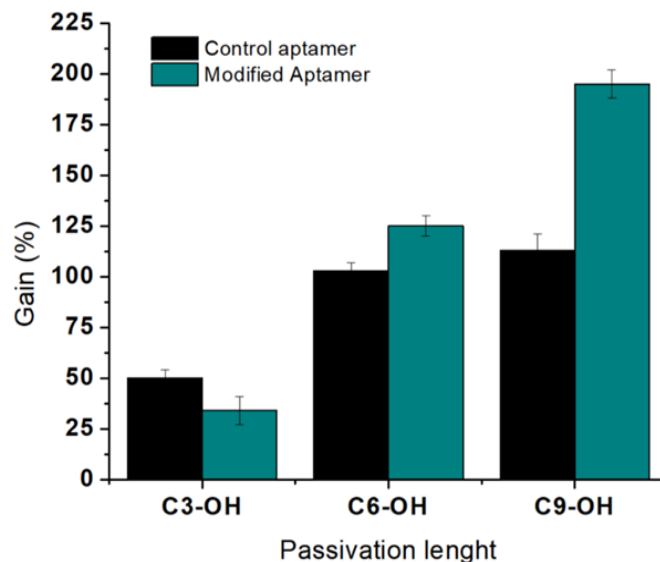


**Figure 5-6.** Gain measurement function of the passivation layer, i.e. C-3 to C-9. SWV was carried out with the VEGF<sub>165</sub> target.

This line of reasoning, though may sound reasonable, may need further consideration. For instance, by further extension in the length of backfilling agents from C<sub>9</sub>-OH to C<sub>11</sub>-OH or even higher, we could have gained better insight into the authentic effect of lysine linker. To consider this, we can, at least hypothetically, think of three possibilities..

**A)** only for Twin-MB, assuming that such an extension would result in further gain enhancement. Then it would give us reassurance about the positive effect of the lysine linker and our argument could have been unambiguously confirmed.

**B)** this time, let's suppose that such length extension in control, and Twin-MB, would result in a gain reduction, let's say by 50% and 30%, respectively. still, the relative gain reductions between control and Twin-MB, comparatively, could bear some implications regarding the lysine effect.

**C)** In the worst-case scenario, we would have ended up in a situation where we had proportional reductions, that is, both reductions in control and Twin-MB were equivalent to e.g., 60%. this

would serve as the most inconclusive situation where the most likely interpretation would be, multiple variables are involved.

Keeping these in mind, the maximum length studied in this work was C<sub>9</sub>-OH, in order to be able to find a common ground for future experiments while adhering to the objectives of the current research. Eventually, to elaborate on the higher gain, one can argue that the effect of linker lysine combined with the bigger cleavage in folded and unfolded structures, in a synergy effect, has resulted in a higher gain for Twin-MB. The use of backfilling agents has been the subject of much research so far<sup>15,18</sup>. For example, C11 agent resulted in a significant long storage ability of the sensor for up to one month. In chapters 2, and 3 we did observe that the utilization of longer backfilling agents for passivation of gold surface had a greater stability after being stored in the fridge compared to the control one with a short agent. However, compared to the literature, our data show a weaker effect. We hypothesize that in our case the short incubation time i.e., 2 h was the reason for shorter stability<sup>19</sup>. Indeed, it is believed that longer incubation time will lead to more homogenous and organized monolayer.

Throughout chapters 2 and 3, to enhance the signal-to-noise, we adopted multiple redox-tagged aptamers in the fabrication of E-AB sensors and showed that such a strategy could easily result in producing a twice higher signal-to-noise than the conventional methods with single redox-tagged aptamers. One of the biggest advantages of our technique compared to the conventional methods such as surface roughening or enzymatic activity, is the proportionality of signal enhancement. This proportionality can create much higher capacity in maintaining the signal-to-noise in miniaturized applications where micro- or ultramicroelectrodes are used but the signal enhancement capacity is limited to the number of redox molecules. Meaning that, due to the steric

hindrance restrictions, adding more molecules is challenging which potentially shrinks the expandability.

In chapter 4, we examined the effect of gold surface dimensionality on the analytical performance of the E-AB sensor in the detection of MUC1 in human serum samples. Our data showed a significant surface area enhancement with the highest pertaining to 3D morphology and the lowest to 2D one. According to research works available in the literature<sup>20-22</sup>, and based on the authors' conclusions, the utilization of nanoparticles on electrode surface has a meaningful effect on the surface area enhancement to which many of the biosensor's improvements have been addressed. Accordingly, we were expected to observe the highest sensitivity with the highest surface area, the E-AB sensor featuring 3D morphology, but our results suggested otherwise. Indeed, the highest sensitivity was obtained for the 1D Au based E-AB sensor. Potential explanation is the effect of surface orientation/organization on the efficiency of hybridization in the aptamer-target complex formation which was confirmed with the kinetics of hybridization. As shown in **Figure 5-7**, the well-ordered surface organization of the 1D morphology suggested a faster interaction in the corresponding hybridization kinetics.

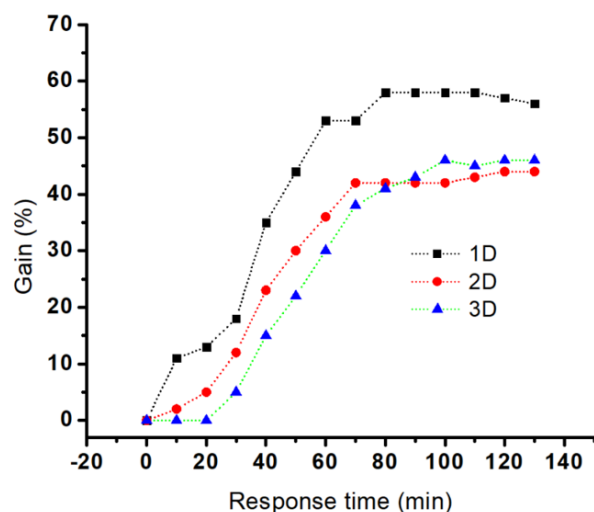


**Figure 5-7.** representation of the typical response time (signal suppression) of the various E-AB sensors featuring 1D, 2D, and 3D gold substrate with a saturated concentration of MUC1 in 50% diluted human serum. Data points have been collected from a single measurement.

The gain enhancement for 1D morphology aptasensor suggested that the well-ordered surface organization is less compact and provide a better spatial environment to assist aptamer-target hybridization. For example, Kim and his colleagues have demonstrated how secondary structures in oligonucleotide monolayer, affected by the surface property, can change the DNA-target hybridization efficiency<sup>23</sup>. This works reflects how oligonucleotide's surface orientation can change the course of target hybridization.

Many pioneering works have been done on the investigation of the effect of DNA probe length on the performance of the E-AB sensor, particularly on the signaling behavior and their hybridization efficiency<sup>24,25</sup>. They suggested that signaling efficiency in an E-AB sensor relies on the hybridization-link changes in probe flexibility, which will alter the efficiency with which the terminal redox tag collides the electrode. They concluded that the latter effect suggests the length

of the probe aptamer will affect the E-AB signaling. According to this, in the course of our argument to elaborate the final gain enhancement, we did not include the length difference that exists between MUC1 and VEGF<sub>165</sub> probe aptamers (24 and 30 meters, respectively). Consequently, studying a series of probe aptamers of varying lengths with C<sub>9</sub>-OH backfilled surface would help us elucidate the lysine linker effect and its relationship with the probe aptamer's length.

Alternatively, to further understand the role of the linker's length in gain enhancement, a survey with a series of linkers with varying lengths and their corresponding effects in signaling behavior of the E-AB sensor in both signal-off and signal-on types of sensors should be considered. To this end, introduction of asparagine, and glutamine amino acids with 4- and 5-carbon chains, respectively could be envisaged.

## References

- (1) Thévenot, D. R.; Toth, K.; Durst, R. A.; Wilson, G. S. Electrochemical Biosensors: Recommended Definitions and Classification. *Biosens. Bioelectron.* **2001**, *16* (1–2), 121–131. [https://doi.org/10.1016/S0956-5663\(01\)00115-4](https://doi.org/10.1016/S0956-5663(01)00115-4).
- (2) Li, P.; Lee, G. H.; Kim, S. Y.; Kwon, S. Y.; Kim, H. R.; Park, S. From Diagnosis to Treatment: Recent Advances in Patient-Friendly Biosensors and Implantable Devices. *ACS Nano* **2021**, *15* (2), 1960–2004. <https://doi.org/10.1021/ACS.NANO.0C06688>.
- (3) Vaddiraju, S.; Tomazos, I.; Burgess, D. J.; Jain, F. C.; Papadimitrakopoulos, F. Emerging Synergy between Nanotechnology and Implantable Biosensors: A Review. *Biosens. Bioelectron.* **2010**, *25* (7), 1553–1565. <https://doi.org/10.1016/J.BIOS.2009.12.001>.
- (4) Arroyo-Currás, N.; Dauphin-Ducharme, P.; Scida, K.; Chávez, J. L. From the Beaker to the Body: Translational Challenges for Electrochemical, Aptamer-Based Sensors. *Anal. Methods* **2020**, *12* (10), 1288–1310. <https://doi.org/10.1039/D0AY00026D>.
- (5) Arroyo-Currás, N.; Scida, K.; Ploense, K. L.; Kippin, T. E.; Plaxco, K. W. High Surface Area Electrodes Generated via Electrochemical Roughening Improve the Signaling of Electrochemical Aptamer-Based Biosensors. *Anal. Chem.* **2017**, *89* (22), 12185–12191. [https://doi.org/10.1021/ACS.ANALCHEM.7B02830/SUPPL\\_FILE/AC7B02830\\_SI\\_001.PDF](https://doi.org/10.1021/ACS.ANALCHEM.7B02830/SUPPL_FILE/AC7B02830_SI_001.PDF).
- (6) Ferguson, B. S.; Hoggarth, D. A.; Maliniak, D.; Ploense, K.; White, R. J.; Woodward, N.; Hsieh, K.; Bonham, A. J.; Eisenstein, M.; Kippin, T. E.; Plaxco, K. W.; Soh, H. T. Real-Time, Aptamer-Based Tracking of Circulating Therapeutic Agents in Living Animals. *Sci. Transl. Med.* **2013**, *5* (213). [https://doi.org/10.1126/SCITRANSLMED.3007095/SUPPL\\_FILE/5-213RA165\\_SM.PDF](https://doi.org/10.1126/SCITRANSLMED.3007095/SUPPL_FILE/5-213RA165_SM.PDF).
- (7) Dunn, M. R.; Jimenez, R. M.; Chaput, J. C. Analysis of Aptamer Discovery and Technology. *Nat. Rev. Chem.* **2017**, *1* (10), 1–16. <https://doi.org/10.1038/s41570-017-0076>.
- (8) Soleymani, L.; Li, F. Mechanistic Challenges and Advantages of Biosensor Miniaturization into the Nanoscale. *ACS Sensors* **2017**, *2* (4), 458–467. [https://doi.org/10.1021/ACSSENSORS.7B00069/ASSET/IMAGES/MEDIUM/SE-2017-00069T\\_0004.GIF](https://doi.org/10.1021/ACSSENSORS.7B00069/ASSET/IMAGES/MEDIUM/SE-2017-00069T_0004.GIF).
- (9) Li, S. K.; Chen, A. Y.; Chai, Y. Q.; Yuan, R.; Zhuo, Y. Electrochemiluminescence Aptasensor Based on Cascading Amplification of Nicking Endonuclease-Assisted Target Recycling and Rolling Circle Amplifications for Mucin 1 Detection. *Electrochim. Acta* **2016**, *212*, 767–774. <https://doi.org/10.1016/J.ELECTACTA.2016.07.074>.
- (10) Pheaney, C. G.; Barton, J. K. DNA Electrochemistry with Tethered Methylene Blue. *Langmuir* **2012**, *28* (17), 7063–7070. [https://doi.org/10.1021/LA300566X/ASSET/IMAGES/MEDIUM/LA-2012-00566X\\_0009.GIF](https://doi.org/10.1021/LA300566X/ASSET/IMAGES/MEDIUM/LA-2012-00566X_0009.GIF).
- (11) Drummond, T. G.; Hill, M. G.; Barton, J. K. Electron Transfer Rates in DNA Films as a Function of Tether Length. *J. Am. Chem. Soc.* **2004**, *126* (46), 15010–15011. [https://doi.org/10.1021/JA044910I/SUPPL\\_FILE/JA044910ISI20041001\\_041557.PDF](https://doi.org/10.1021/JA044910I/SUPPL_FILE/JA044910ISI20041001_041557.PDF).
- (12) White, R. J.; Phares, N.; Lubin, A. A.; Xiao, Y.; Plaxco, K. W. Optimization of Electrochemical Aptamer-Based Sensors via Optimization of Probe Packing Density and Surface Chemistry. *Langmuir* **2008**, *24* (18), 10513–10518. <https://doi.org/10.1021/la800801v>.
- (13) Kypr, J.; Kejnovská, I.; Renčiuk, D.; Vorlíčková, M. Circular Dichroism and Conformational Polymorphism of DNA. *Nucleic Acids Res.* **2009**, *37* (6), 1713–1725. <https://doi.org/10.1093/NAR/GKP026>.
- (14) Lai, R. Y.; Seferos, D. S.; Heeger, A. J.; Bazan, G. C.; Plaxco, K. W. Comparison of the Signaling and Stability of Electrochemical DNA Sensors Fabricated from 6- or 11-Carbon Self-Assembled Monolayers. *Langmuir* **2006**, *22* (25), 10796–10800. [https://doi.org/10.1021/LA0611817/SUPPL\\_FILE/LA0611817SI20060613\\_051605.PDF](https://doi.org/10.1021/LA0611817/SUPPL_FILE/LA0611817SI20060613_051605.PDF).

- (15) Stuart, D. A.; Yonzon, C. R.; Zhang, X.; Lyandres, O.; Shah, N. C.; Glucksberg, M. R.; Walsh, J. T.; Van Duyne, R. P. Glucose Sensing Using Near-Infrared Surface-Enhanced Raman Spectroscopy: Gold Surfaces, 10-Day Stability, and Improved Accuracy. *Anal. Chem.* **2005**, *77* (13), 4013–4019. <https://doi.org/10.1021/AC0501238>.
- (16) Smalley, J. F.; Feldberg, S. W.; Chidsey, C. E. D.; Linford, M. R.; Newton, M. D.; Liu, Y. P. Kinetics of Electron Transfer through Ferrocene-Terminated Alkanethiol Monolayers on Gold. *J. Phys. Chem.* **1995**, *99* (35), 13141–13149. [https://doi.org/10.1021/J100035A016/ASSET/J100035A016.FP.PNG\\_V03](https://doi.org/10.1021/J100035A016/ASSET/J100035A016.FP.PNG_V03).
- (17) Miller, C.; Cuendet, P.; Grätzel, M. Adsorbed  $\omega$ -Hydroxy Thiol Monolayers on Gold Electrodes: Evidence for Electron Tunneling to Redox Species in Solution. *J. Phys. Chem.* **1991**, *95* (2), 877–886. [https://doi.org/10.1021/J100155A072/ASSET/J100155A072.FP.PNG\\_V03](https://doi.org/10.1021/J100155A072/ASSET/J100155A072.FP.PNG_V03).
- (18) Flynn, N. T.; Tran, T. N. T.; Cima, M. J.; Langer, R. Long-Term Stability of Self-Assembled Monolayers in Biological Media. *Langmuir* **2003**, *19* (26), 10909–10915. <https://doi.org/10.1021/LA035331E>.
- (19) Steel, A. B.; Levicky, R. L.; Herne, T. M.; Tarlov, M. J. Immobilization of Nucleic Acids at Solid Surfaces: Effect of Oligonucleotide Length on Layer Assembly. *Biophys. J.* **2000**, *79* (2), 975–981. [https://doi.org/10.1016/S0006-3495\(00\)76351-X](https://doi.org/10.1016/S0006-3495(00)76351-X).
- (20) Roushani, M.; Valipour, A. Using Electrochemical Oxidation of Rutin in Modeling a Novel and Sensitive Immunosensor Based on Pt Nanoparticle and Graphene–Ionic Liquid–Chitosan Nanocomposite to Detect Human Chorionic Gonadotropin. *Sensors Actuators B Chem.* **2016**, *222*, 1103–1111. <https://doi.org/10.1016/J.SNB.2015.08.031>.
- (21) Wang, X.; Liao, X.; Mei, L.; Zhang, M.; Chen, S.; Qiao, X.; Hong, C. An Immunosensor Using Functionalized Cu<sub>2</sub>O/Pt NPs as the Signal Probe for Rapid and Highly Sensitive CEA Detection with Colorimetry and Electrochemistry Dual Modes. *Sensors Actuators, B Chem.* **2021**, *341*. <https://doi.org/10.1016/J.SNB.2021.130032>.
- (22) Liu, J.; Wagan, S.; Dávila Morris, M.; Taylor, J.; White, R. J. Achieving Reproducible Performance of Electrochemical, Folding Aptamer-Based Sensors on Microelectrodes: Challenges and Prospects. *Anal. Chem.* **2014**, *86* (22), 11417–11424. [https://doi.org/10.1021/AC503407E/SUPPL\\_FILE/AC503407E\\_SI\\_001.PDF](https://doi.org/10.1021/AC503407E/SUPPL_FILE/AC503407E_SI_001.PDF).
- (23) Zheng, S.; Choi, J. H.; Lee, S. M.; Hwang, K. S.; Kim, S. K.; Kim, T. S. Analysis of DNA Hybridization Regarding the Conformation of Molecular Layer with Piezoelectric Microcantilevers. *Lab Chip* **2010**, *11* (1), 63–69. <https://doi.org/10.1039/C0LC00122H>.
- (24) Lubin, A. A.; Hunt, B. V. S.; White, R. J.; Plaxco, K. W. Effects of Probe Length, Probe Geometry, and Redox-Tag Placement on the Performance of the Electrochemical E-DNA Sensor. *Anal. Chem.* **2009**, *81* (6), 2150–2158. [https://doi.org/10.1021/AC802317K/SUPPL\\_FILE/AC802317K\\_SI\\_001.PDF](https://doi.org/10.1021/AC802317K/SUPPL_FILE/AC802317K_SI_001.PDF).
- (25) Peterson, A. W.; Heaton, R. J.; Georgiadis, R. M. The Effect of Surface Probe Density on DNA Hybridization. *Nucleic Acids Res.* **2001**, *29* (24), 5163–5168. <https://doi.org/10.1093/NAR/29.24.5163>.

## Conclusion and summary

E-AB sensors have thus far enabled highly sensitive measurement of physiologically and clinically important molecular targets. E-AB sensors owe this success to the nucleic acid aptamers as the recognition elements. Although this can be considered an unprecedented way in the realm of biosensors, where detection is achieved by relying on the target-induced changes in electron transfer efficiency between the redox-tagged aptamer and the surface of the electrode, we are still far away from the ideal translation of this platform to be realistically used in clinics. This is, at least partially, dependent on further innovations in interfacial chemistry.

Motivated by this, we have proposed a novel, yet simple molecular design for the engineering of the interfacial layer that can partially unblock some sensor bottlenecks, particularly in the signaling behavior. To accomplish this, unlike the commercially available single redox-tagged probe aptamers, we employed a MUC1 probe aptamer tethered to two spatially resolved redox tags (methylene blue) via the inclusion of a lysine linker. Furthermore, to create a bigger ratio between folded and unfolded states at equilibrium, we have concomitantly probed the effect of various thicknesses of the thiolated SAMs that are commonly used for surface passivation. We found that these fabrication parameters have a positive combined effect leading to a significant improvement in the signaling efficiency of the E-AB sensor, probably due to the assembly of molecular redox tags that evidently increased the signal-to-noise capacity.

The interfacial manipulation was tested for the detection of two important biomarkers, MUC1 and VEGF<sub>165</sub> which are clinically known as biomarkers in breast cancer. According to our findings, the resultant E-AB sensors significantly outperformed their conventional counterparts in both areas of sensitivity and stability. The adaptability of the strategy with both signaling behaviors, i.e.,

signal-on and signal-off was confirmed. Moreover, since the interfacial manipulation doesn't require any additional steps during the signal acquisition, it can fully support a reagentless, and sensitive E-AB sensing platform without compromising its performance and, due to the higher capacity of its electronic source, it is readily amenable to miniaturization and to be used in implantable E-AB sensors.

The nano-dimensionality of the interfacial layer and its probable effect on the sensor's performance applied for the detection of MUC1 biomarker in human serum samples was studied. Among 1D, 2D, and 3D surface morphologies, the E-AB sensor featuring the 1D morphology proved to be the most sensitive one, suggesting that the aptamer's organization could be influenced by morphological-induced conditions and not only by the enhanced surface area.

According to the bulk of research presented in this thesis, these biomarkers qualify to be used in the metastasis stage of breast cancer, at least to some extent, especially toward tumor size or survival rate of the patients. Thus, their routine monitoring will be meaningful.

Current research demonstrates a proof-of-concept reagentless sensing platform that enables quick, and sensitive serum-based biomarker detection with no need for sample preparation. meaning that, if envisioned as a point-of-care device, it can provide a higher degree of accessibility and ease in the detection of desired biomarkers and therefore greatly contributes to a more rapid clinical decision.

The limitation of our strategy lies in the conjugation of the higher number of redox tag molecules. This makes the S/N enhancement (gain amplification) potentially restricted as follows: a linker that can accommodate more than two redox-tag molecules is hardly found. Next, even when accessibility is not an issue, further conjugations of the molecules become progressively more problematic as the steric hindrance element will present itself to compromise the efficiency of the

desired reactions, and thus making the higher conjugations less productive. To overcome the first problem, we need to specifically design and synthesize a linker with abundant of reactive functionalities and devise a way to sequentially protect them via protecting groups to be able to control the reaction progress. The second issue is unlikely solvable as it lies with the intrinsic of organic reactions. Many arguments in the discussion across the whole thesis are subject to change or temper since other elements such as the length of the probe aptamers, length of the linkers, etc....., are, at least theoretically, thought to be impactful on the sensor performance. Therefore, these explorations should be carried out in future to gain deeper insights into interfacial layer manipulations and the corresponding impacts.

## Reference list:

### Chapter 1: References:

- W. H. Organization, WHO Report on Cancer: Setting Priorities, Investing Wisely and Providing Care for All. 2020.
- 2 Surveys and statistical programs - Canadian Cancer Registry (CCR), <https://www23.statcan.gc.ca/imdb/p2SV.pl?Function=getSurvey&SDDS=3207&lang=en&db=imdb&adm=8&dis=2>, (accessed 6 August 2022).
  - 3 Cancer Research UK, <https://www.cancerresearchuk.org/>, (accessed 6 August 2022).
  - 4 E. L. Bird-Lieberman and R. C. Fitzgerald, *Br. J. Cancer*, 2009, **101**, 1–6.
  - 5 S. Abati, C. Bramati, S. Bondi, A. Lissoni and M. Trimarchi, *Int. J. Environ. Res. Public Heal.* 2020, Vol. 17, Page 9160, 2020, **17**, 9160.
  - 6 T. Baykul, H. H. Yilmaz, Ü. Aydin, M. A. Aydin, M. Ç. Aksoy and D. Yildirim, *J. Int. Med. Res.*, 2010, **38**, 737–749.
  - 7 S. Lam and H. Shibuya, *Clin. Chest Med.*, 1999, **20**, 53–61.
  - 8 J. Austoker, *BMJ*, 1994, **308**, 1682–1686.
  - 9 A. M. Lutz, J. K. Willmann, C. W. Drescher, P. Ray, F. V. Cochran, N. Urban and S. S. Gambhir, *Radiology*, 2011, **259**, 329–345.
  - 10 C. Coleman, *Semin. Oncol. Nurs.*, 2017, **33**, 141–155.
  - 11 W. Hamilton, F. M. Walter, G. Rubin and R. D. Neal, *Nat. Rev. Clin. Oncol.*, 2016, **13**, 740–749.
  - 12 S. S. Raab and D. M. Grzybicki, *CA. Cancer J. Clin.*, 2010, **60**, 139–165.
  - 13 M. P. Coleman, D. Forman, H. Bryant, J. Butler, B. Rachet, C. Maringe, U. Nur, E. Tracey, M. Coory, J. Hatcher, C. E. McGahan, D. Turner, L. Marrett, M. L. Gjerstorff, T. B. Johannesen, J. Adolfsson, M. Lambe, G. Lawrence, D. Meechan, E. J. Morris, R. Middleton, J. Steward and M. A. Richards, *Lancet*, 2011, **377**, 127–138.
  - 14 B. Crew, *Nature*, 2020, **580**, S5–S7.
  - 15 J. Feng, B. Li, J. Ying, W. Pan, C. Liu, T. Luo, H. Lin and L. Zheng, *Small Struct.*, 2020, **1**, 2000063.
  - 16 D. Crosby, *Br. J. Cancer* 2021 1263, 2022, **126**, 313–315.
  - 17 A. K. Mattox, C. Bettegowda, S. Zhou, N. Papadopoulos, K. W. Kinzler and B. Vogelstein, *Sci. Transl. Med.*, , DOI:10.1126/SCITRANSLMED.AAY1984.
  - 18 G. Siravegna, S. Marsoni, S. Siena and A. Bardelli, *Nat. Rev. Clin. Oncol.* 2017 149, 2017, **14**, 531–548.
  - 19 J. Marrugo-Ramírez, M. Mir and J. Samitier, *Int. J. Mol. Sci.*, , DOI:10.3390/IJMS19102877.
  - 20 M. Bahassi, J. Mol Biomark Diagn and E. Mustapha Bahassi, *J Mol Biomark Diagn*, 2013, **4**, 157.
  - 21 M. L. Wroclawski, A. Serpa-Neto, F. L. A. Fonseca, O. Castro-Neves-Neto, A. S. F. L. Pompeo, M. T. Machado, A. C. L. Pompeo and A. Del Giglio, *Tumor Biol.* 2013 345, 2013, **34**, 2921–2927.
  - 22 H. Schwarzenbach, J. Stoehlmacher, K. Pantel and E. Goekkurt, *Ann. N. Y. Acad. Sci.*, 2008, **1137**, 190–196.
  - 23 Analysis of circulating tumor DNA in plasma at diagnosis and during follow-up of lung cancer patients -

- PubMed, <https://pubmed.ncbi.nlm.nih.gov/11406535/>, (accessed 6 August 2022).
- 24 T. Frisk, N. Sandström, L. Eng, W. Van Der Wijngaart, P. Månsson and G. Stemme, *pubs.rsc.org*, , DOI:10.1039/b800487k.
- 25 T. Sakata and Y. Miyahara, *ChemBioChem*, 2005, **6**, 703–710.
- 26 H. J. Park, S. K. Kim, K. Park, H. K. Lyu, C. S. Lee, S. J. Chung, W. S. Yun, M. Kim and B. H. Chung, *FEBS Lett.*, 2009, **583**, 157–162.
- 27 M. Gouzy, M. Keß, P. K.-B. and Bioelectronics and undefined 2009, *Elsevier*.
- 28 R. Rich, G. Papalia, P. Flynn, ... J. F.-A. and undefined 2009, *Elsevier*.
- 29 Y. Du, B. Li, H. Wei, Y. Wang and E. Wang, *Angew. Chem., Int. Ed.*, 1990, **346**, 5110–5117.
- 30 A. Bogomolova, E. Komarova, K. Reber, T. Gerasimov, O. Yavuz, S. Bhatt and M. Aldissi, *Anal. Chem.*, 2009, **81**, 3944–3949.
- 31 N. S. Que-Gewirth and B. A. Sullenger, *Gene Ther. 2007 144*, 2007, **14**, 283–291.
- 32 S. Song, L. Wang, J. Li, C. Fan and J. Zhao, *TrAC Trends Anal. Chem.*, 2008, **27**, 108–117.
- 33 C. M. Dollins, S. Nair and B. A. Sullenger, <https://home.liebertpub.com/hum>, 2008, **19**, 443–450.
- 34 R. Reid, B. Chatterjee, S. J. Das, S. Ghosh and T. K. Sharma, *Anal. Biochem.*, 2020, **593**, 113574.
- 35 K. Han, L. Chen, Z. Lin and G. Li, *Electrochem. commun.*, 2009, **11**, 157–160.
- 36 J. Liu and Y. Lu, *Angew. Chemie Int. Ed.*, 2006, **45**, 90–94.
- 37 W. Zhao, W. Chiuman, J. C. F. Lam, S. A. McManus, W. Chen, Y. Cui, R. Pelton, M. A. Brook and Y. Li, *J. Am. Chem. Soc.*, 2008, **130**, 3610–3618.
- 38 Y. Xiao, A. A. Lubin, A. J. Heeger and K. W. Plaxco, *Angew. Chemie*, 2005, **117**, 5592–5595.
- 39 J. Wang, W. Meng, X. Zheng, S. Liu and G. Li, *Biosens. Bioelectron.*, 2009, **24**, 1598–1602.
- 40 J. H. T. Luong, K. B. Male and J. D. Glennon, *Biotechnol. Adv.*, 2008, **26**, 492–500.
- 41 Y. Xiao, A. A. Lubin, A. J. Heeger and K. W. Plaxco, *Angew. Chemie Int. Ed.*, 2005, **44**, 5456–5459.
- 42 L. Bock, L. Griffin, J. Latham, E. Vermaas, J. T.- Nature and undefined 1992, *nature.com*.
- 43 A. Ellington, J. S.- nature and undefined 1990, *nature.com*, , DOI:10.1038/346818a0.
- 44 L. Gold, *J. Mol. Evol.*, 2015, **81**, 140–143.
- 45 J. Kohn, K. P. the N. A. of Sciences and undefined 2005, *Natl. Acad Sci*.
- 46 K. J. Oh, K. J. Cash and K. W. Plaxco, *Chem. - A Eur. J.*, 2009, **15**, 2244–2251.
- 47 A. A. Lubin and K. W. Plaxco, *Acc. Chem. Res.*, 2010, **43**, 496–505.
- 48 F. Ricci, A. Vallée-Bélisle, A. J. Simon, A. Porchetta and K. W. Plaxco, *Acc. Chem. Res.*, 2016, **49**, 1884–1892.
- 49 F. L. Kiechle, *Diabetes Technol. Ther.*, 2001, **3**, 647–650.
- 50 R. J. White, N. Phares, A. A. Lubin, Y. Xiao and K. W. Plaxco, *Langmuir*, 2008, **24**, 10513–10518.
- 51 L. M. Demers, C. A. Mirkin, R. C. Mucic, R. A. Reynolds, R. L. Letsinger, R. Elghanian and G. Viswanadham, *Anal. Chem.*, 2000, **72**, 5535–5541.

- 52 A. B. Steel, T. M. Herne and M. J. Tarlov, *Anal. Chem.*, 1998, **70**, 4670–4677.
- 53 P. V. Riccelli, F. Merante, K. T. Leung, S. Bortolin, R. L. Zastawny, R. Janeczko and A. S. Benight, *Nucleic Acids Res.*, 2001, **29**, 996–1004.
- 54 A. Meller, L. Nivon and D. Branton, *Phys. Rev. Lett.*, 2001, **86**, 3435–3438.
- 55 A. Reuter, W. U. Dittmer and F. C. Simmel, *Eur. Phys. J. E*, 2007, **22**, 33–40.
- 56 Q. Zhou, K. Son, Y. Liu and A. Revzin, *Annu. Rev. Biomed. Eng.*, 2015, **17**, 165–190.
- 57 Y. Liu, Z. Matharu, M. C. Howland, A. Revzin and A. L. Simonian, *Anal. Bioanal. Chem.*, 2012, **404**, 1181–1196.
- 58 A. L. Furst, M. G. Hill and J. K. Barton, *Langmuir*, 2015, **31**, 6554–6562.
- 59 A. Z. Bradley, M. G. Kociolek and R. P. Johnson, *J. Org. Chem.*, 2000, **65**, 7134–7138.
- 60 K. S. Sykes, L. F. L. Oliveira, G. Stan and R. J. White, *Langmuir*, 2019, **35**, 12962–12970.
- 61 L. Qi, H. Tian and H. Z. Yu, *Anal. Chem.*, 2018, **90**, 9174–9181.
- 62 L. R. Schoukroun-Barnes, F. C. Macazo, B. Gutierrez, J. Lottermoser, J. Liu and R. J. White, *Annu. Rev. Anal. Chem.*, 2016, **9**, 163–181.
- 63 Y. Xiao, T. Uzawa, R. J. White, D. DeMartini and K. W. Plaxco, *Electroanalysis*, 2009, **21**, 1267–1271.
- 64 D. E. Weisshaar, B. D. Lamp and M. D. Porter, *J. Am. Chem. Soc.*, 1992, **114**, 5860–5862.
- 65 H. Ron and I. Rubinstein, *J. Am. Chem. Soc.*, 1998, **120**, 13444–13452.
- 66 A. Peterson, R. H.-N. acids research and undefined 2001, *academic.oup.com*.
- 67 K. Leung, A. Gaxiola, H. Yu, D. B.-E. Acta and undefined 2018, *Elsevier*.
- 68 D. Jambrec, M. Gebala, F. La Mantia and W. Schuhmann, *Angew. Chemie Int. Ed.*, 2015, **54**, 15064–15068.
- 69 D. Jambrec, F. Conzuelo, A. Estrada-Vargas and W. Schuhmann, *ChemElectroChem*, 2016, **3**, 1484–1489.
- 70 R. Levicky, T. M. Herne, M. J. Tarlov and S. K. Satija, *J. Am. Chem. Soc.*, 1998, **120**, 9787–9792.
- 71 T. M. Herne and M. J. Tarlov, *J. Am. Chem. Soc.*, 1997, **119**, 8916–8920.
- 72 K. A. Peterlinz, R. M. Georgiadis, T. M. Herne and M. J. Tarlov, *J. Am. Chem. Soc.*, 1997, **119**, 3401–3402.
- 73 C. Y. Lee, P. Gong, G. M. Harbers, D. W. Grainger, D. G. Castner and L. J. Gamble, *Anal. Chem.*, 2006, **78**, 3316–3325.
- 74 F. Ricci, N. Zari, F. Caprio, S. Recine, A. Amine, D. Moscone, G. Palleschi and K. W. Plaxco, *Bioelectrochemistry*, 2009, **76**, 208–213.
- 75 E. Ostuni, R. G. Chapman, M. N. Liang, G. Meluleni, G. Pier, D. E. Ingber and G. M. Whitesides, *ACS Publ.*, 2001, **17**, 6336–6343.
- 76 R. E. Holmlin, X. Chen, R. G. Chapman, S. Takayama and G. M. Whitesides, *Langmuir*, 2001, **17**, 2841–2850.
- 77 H. Li, P. Dauphin-Ducharme, N. Arroyo-Currás, C. H. Tran, P. A. Vieira, S. Li, C. Shin, J. Somerson, T. E. Kippin and K. W. Plaxco, *Angew. Chemie Int. Ed.*, 2017, **56**, 7492–7495.
- 78 X. Xu, A. Makaraviciute, S. Kumar, C. Wen, M. Sjödin, E. Abdurakhmanov, U. H. Danielson, L. Nyholm and Z. Zhang, *Anal. Chem.*, , DOI:10.1021/acs.analchem.9b03946.

- 79 A. Steel, R. Levicky, T. Herne, M. T.-B. journal and undefined 2000, *Elsevier*.
- 80 D. Rekes, Y. Lyubchenko, L. S.-B. journal and undefined 1996, *Elsevier*.
- 81 C. A. Mirkin, R. L. Letsinger, R. C. Mucic and J. J. Storhoff, *Nature*, 1996, **382**, 607–609.
- 82 \* Bernard Tinland, Alain Pluen, and Jean Sturm and G. Weill, , DOI:10.1021/MA970381+.
- 83 D. Kang, F. Ricci, R. J. White and K. W. Plaxco, *Anal. Chem.*, 2016, **88**, 10452–10458.
- 84 D. Kang, X. Zuo, R. Yang, F. Xia, K. W. Plaxco and R. J. White, *Anal. Chem.*, 2009, **81**, 9109–9113.
- 85 H. Li, N. Arroyo-Currás, D. Kang, F. Ricci and K. W. Plaxco, *J. Am. Chem. Soc.*, 2016, **138**, 15809–15812.
- 86 E. González-Fernández, N. Avlonitis, A. F. Murray, A. R. Mount and M. Bradley, *Biosens. Bioelectron.*, 2016, **84**, 82–88.
- 87 R. Prins, A. R. Korswagen and A. G. T. G. Kortbeek, *J. Organomet. Chem.*, 1972, **39**, 335–344.
- 88 R. Prins, A. R. Korswagen and A. G. T. G. Kortbeek, *J. Organomet. Chem.*, 1972, **39**, 335–344.
- 89 E. E. Ferapontova and K. V. Gothelf, *Electroanalysis*, 2009, **21**, 1261–1266.
- 90 E. E. Ferapontova and K. V. Gothelf, *Electroanalysis*, 2009, **21**, 1261–1266.
- 91 P. Dauphin-Ducharme and K. W. Plaxco, *Anal. Chem.*, 2016, **88**, 11654–11662.
- 92 M. D. Mayer and R. Y. Lai, *Talanta*, 2018, **189**, 585–591.
- 93 S. D. Curtis, K. L. Ploense, M. Kurnik, G. Ortega, C. Parolo, T. E. Kippin, K. W. Plaxco and N. Arroyo-Currás, *Anal. Chem.*, 2019, **91**, 12321–12328.
- 94 P. Dauphin-Ducharme, N. Arroyo-Currás, R. Adhikari, J. Somerson, G. Ortega, D. E. Makarov and K. W. Plaxco, *J. Phys. Chem. C*, 2018, **122**, 21441–21448.
- 95 R. J. White and K. W. Plaxco, *Anal. Chem.*, 2010, **82**, 73–76.
- 96 L. A. Torre, F. Bray, R. L. Siegel, J. Ferlay, J. Lortet-Tieulent and A. Jemal, *CA. Cancer J. Clin.*, 2015, **65**, 87–108.
- 97 F. Cardoso, D. Spence, S. Mertz, D. Corneliusen-James, K. Sabelko, J. Gralow, M. J. Cardoso, F. Peccatori, D. Paonessa, A. Benares, N. Sakurai, M. Beishon, S. J. Barker and M. Mayer, *Breast*, 2018, **39**, 131–138.
- 98 H. K. Weir, T. D. Thompson, S. L. Stewart and M. C. White, *Prev. Chronic Dis.*, 2021, **18**, 1–8.
- 99 R. Etzioni, N. Urban, S. Ramsey, M. McIntosh, S. Schwartz, B. Reid, J. Radich, G. Anderson and L. Hartwell, *Nat. Rev. Cancer* 2003 34, 2003, **3**, 243–252.
- 100 A. Jemal, R. Siegel, E. Ward, Y. Hao, J. Xu, T. Murray and M. J. Thun, *CA. Cancer J. Clin.*, 2008, **58**, 71–96.
- 101 S. Y. Loke and A. S. G. Lee, *Eur. J. Cancer*, 2018, **92**, 54–68.
- 102 S. A. Eccles, E. O. Aboagye, S. Ali, A. S. Anderson, J. Armes, F. Berditchevski, J. P. Blaydes, K. Brennan, N. J. Brown, H. E. Bryant, N. J. Bundred, J. M. Burchell, A. M. Campbell, J. S. Carroll, R. B. Clarke, C. E. Coles, G. J. R. Cook, A. Cox, N. J. Curtin, L. V. Dekker, I. dos Santos Silva, S. W. Duffy, D. F. Easton, D. M. Eccles, D. R. Edwards, J. Edwards, D. G. Evans, D. F. Fenlon, J. M. Flanagan, C. Foster, W. M. Gallagher, M. Garcia-Closas, J. M. W. Gee, A. J. Gescher, V. Goh, A. M. Groves, A. J. Harvey, M. Harvie, B. T. Hennessy, S. Hiscox, I. Holen, S. J. Howell, A. Howell, G. Hubbard, N. Hulbert-Williams, M. S. Hunter, B. Jasani, L. J. Jones, T. J. Key, C. C. Kirwan, A. Kong, I. H. Kunkler, S. P. Langdon, M. O. Leach, D. J. Mann, J. F. Marshall, L. A. Martin, S. G. Martin, J. E. Macdougall, D. W. Miles, W. R. Miller, J. R. Morris, S. M. Moss, P. Mullan, R. Natrajan, J. P. B. O’Connor, R. O’Connor, C. Palmieri, P. D. P. Pharoah, E. A. Rakha,

- E. Reed, S. P. Robinson, E. Sahai, J. M. Saxton, P. Schmid, M. J. Smalley, V. Speirs, R. Stein, J. Stingl, C. H. Streuli, A. N. J. Tutt, G. Velikova, R. A. Walker, C. J. Watson, K. J. Williams, L. S. Young and A. M. Thompson, *Breast Cancer Res. 2013 155*, 2013, **15**, 1–37.
- 103 R. Simon, *JNCI J. Natl. Cancer Inst.*, 2015, **107**, 153.
- 104 V. Gajdosova, L. Lorencova, P. Kasak and J. Tkac, *Sensors (Switzerland)*, 2020, **20**, 1–37.
- 105 S. Mittal, H. Kaur, N. Gautam and A. K. Mantha, *Biosens. Bioelectron.*, 2017, **88**, 217–231.
- 106 S. Akbari Nakhjavani, B. Khalilzadeh, P. Samadi Pakchin, R. Saber, M. H. Ghahremani and Y. Omidi, *Biosens. Bioelectron.*, 2018, **122**, 8–15.
- 107 M. J. Duffy, *Ann. Clin. Biochem.*, 1999, **36**, 579–586.
- 108 M. J. Duffy, D. Evoy and E. W. McDermott, *Clin. Chim. Acta*, 2010, **411**, 1869–1874.
- 109 M. J. Duffy, *Clin. Chem.*, 2006, **52**, 345–351.
- 110 M. Brooks, *Methods Mol. Biol.*, 2009, **472**, 307–321.
- 111 M. Gion, R. Mione, A. E. Leon and R. Dittadi, *Clin. Chem.*, 1999, **45**, 630–637.
- 112 V. M. Asiago, L. Z. Alvarado, N. Shanaiah, G. A. N. Gowda, K. Owusu-Sarfo, R. A. Ballas and D. Raftery, *Cancer Res.*, 2010, **70**, 8309–8318.
- 113 C. Denkert, E. Bucher, M. Hilvo, R. Salek, M. Orešič, J. Griffin, S. Brockmöller, F. Klauschen, S. Loibl, D. K. Barupal, J. Budczies, K. Iljin, V. Nekljudova and O. Fiehn, *Genome Med.*, 2012, **4**, 1–9.
- 114 P. L. Bedard and F. Cardoso, *Nat. Rev. Clin. Oncol. 2011 85*, 2011, **8**, 272–279.
- 115 M. Kaufmann and L. Pusztai, *Cancer*, 2011, **117**, 1575–1582.
- 116 R. Roy, J. Chun and S. N. Powell, *Nat. Rev. Cancer 2012 121*, 2011, **12**, 68–78.
- 117 S. Bayraktar and S. Glück, *Breast Cancer Res. Treat.*, 2012, **135**, 355–366.
- 118 C. M. Sturgeon, M. J. Duffy, U. H. Stenman, H. Lilja, N. Brünner, D. W. Chan, R. Babaian, R. C. Bast, B. Dowell, F. J. Esteva, C. Haglund, N. Harbeck, D. F. Hayes, M. Holten-Andersen, G. G. Klee, R. Lamerz, L. H. Looijenga, R. Molina, H. J. Nielsen, H. Rittenhouse, A. Semjonow, I. M. Shih, P. Sibley, G. Sölétormos, C. Stephan, L. Sokoll, B. R. Hoffman and E. P. Diamandis, *Clin. Chem.*, 2008, **54**, e11–e79.
- 119 A. Ziegler, U. Zangemeister-Wittke and R. A. Stahel, *Cancer Treat. Rev.*, 2002, **28**, 255–271.
- 120 M. Murtaza, S. J. Dawson, K. Pogrebniak, O. M. Rueda, E. Provenzano, J. Grant, S. F. Chin, D. W. Y. Tsui, F. Marass, D. Gale, H. R. Ali, P. Shah, T. Contente-Cuomo, H. Farahani, K. Shumansky, Z. Kingsbury, S. Humphray, D. Bentley, S. P. Shah, M. Wallis, N. Rosenfeld and C. Caldas, *Nat. Commun. 2015 61*, 2015, **6**, 1–6.
- 121 E. Heitzer, P. Ulz and J. B. Geigl, *Clin. Chem.*, 2015, **61**, 112–123.
- 122 N. Eigeliene, J. Saarenheimo and A. Jekunen, *Oncology*, 2019, **96**, 115–124.
- 123 L. De Mattos-Arruda and C. Caldas, *Mol. Oncol.*, 2016, **10**, 464–474.
- 124 E. Crowley, F. Di Nicolantonio, F. Loupakis and A. Bardelli, *Nat. Rev. Clin. Oncol. 2013 108*, 2013, **10**, 472–484.
- 125 C. Bettgowda, M. Sausen, R. J. Leary, I. Kinde, Y. Wang, N. Agrawal, B. R. Bartlett, H. Wang, B. Lubber, R. M. Alani, E. S. Antonarakis, N. S. Azad, A. Bardelli, H. Brem, J. L. Cameron, C. C. Lee, L. A. Fecher, G. L. Gallia, P. Gibbs, D. Le, R. L. Giuntoli, M. Goggins, M. D. Hogarty, M. Holdhoff, S. M. Hong, Y. Jiao, H. H. Juhl, J. J. Kim, G. Siravegna, D. A. Laheru, C. Lauricella, M. Lim, E. J. Lipson, S. K. N. Marie, G. J. Netto,

- K. S. Oliner, A. Olivi, L. Olsson, G. J. Riggins, A. Sartore-Bianchi, K. Schmidt, I. M. Shih, S. M. Oba-Shinjo, S. Siena, D. Theodorescu, J. Tie, T. T. Harkins, S. Veronese, T. L. Wang, J. D. Weingart, C. L. Wolfgang, L. D. Wood, D. Xing, R. H. Hruban, J. Wu, P. J. Allen, C. M. Schmidt, M. A. Choti, V. E. Velculescu, K. W. Kinzler, B. Vogelstein, N. Papadopoulos and L. A. Diaz, *Sci. Transl. Med.*, , DOI:10.1126/SCITRANSLMED.3007094/SUPPL\_FILE/6-224RA24\_TABLES\_S1\_TO\_S8.ZIP.
- 126 K. Uzawa, T. Baba, F. Uchida, M. Yamatoji, A. Kasamatsu, Y. Sakamoto, K. Ogawara, M. Shiiba, H. Bukawa and H. Tanzawa, *Oncotarget*, 2012, **3**, 670–677.
- 127 V. Swarup and M. R. Rajeswari, *FEBS Lett.*, 2007, **581**, 795–799.
- 128 V. Swarup and M. R. Rajeswari, *FEBS Lett.*, 2007, **581**, 795–799.
- 129 B. Bystricky and M. Mego, *Neoplasma*, 2016, **63**, 18–29.
- 130 P. S. Mitchell, R. K. Parkin, E. M. Kroh, B. R. Fritz, S. K. Wyman, E. L. Pogosova-Agadjanyan, A. Peterson, J. Noteboom, K. C. O’Briant, A. Allen, D. W. Lin, N. Urban, C. W. Drescher, B. S. Knudsen, D. L. Stirewalt, R. Gentleman, R. L. Vessella, P. S. Nelson, D. B. Martin and M. Tewari, *Proc. Natl. Acad. Sci. U. S. A.*, 2008, **105**, 10513–10518.
- 131 H. Valadi, K. Ekström, A. Bossios, M. Sjöstrand, J. J. Lee and J. O. Lötvall, *Nat. Cell Biol.* 2007 96, 2007, **9**, 654–659.
- 132 T. Miyashita, H. Tajima, I. Makino, H. Nakagawara, H. Kitagawa, S. Fushida, J. W. Harmon and T. Ohta, *J. Surg. Res.*, 2015, **193**, 289–294.
- 133 F. André, E. Ciruelos, G. Rubovszky, M. Campone, S. Loibl, H. S. Rugo, H. Iwata, P. Conte, I. A. Mayer, B. Kaufman, T. Yamashita, Y.-S. Lu, K. Inoue, M. Takahashi, Z. Pápai, A.-S. Longin, D. Mills, C. Wilke, S. Hirawat and D. Juric, *N. Engl. J. Med.*, 2019, **380**, 1929–1940.
- 134 E. Fina, M. Callari, C. Reduzzi, F. D’Aiuto, G. Mariani, D. Generali, M. A. Pierotti, M. G. Daidone and V. Cappelletti, *Clin. Chem.*, 2015, **61**, 278–289.
- 135 G. Kallergi, S. Agelaki, M. A. Papadaki, D. Nasias, A. Matikas, D. Mavroudis and V. Georgoulas, *Breast Cancer Res.*, 2015, **17**, 1–11.
- 136 M. J. Duffy, S. Shering, F. Sherry, E. McDermott and N. O’Higgins, <https://doi.org/10.1177/172460080001500410>, 2018, **15**, 330–333.
- 137 M. Gerlinger, A. J. Rowan, S. Horswell, J. Larkin, D. Endesfelder, E. Gronroos, P. Martinez, N. Matthews, A. Stewart, P. Tarpey, I. Varela, B. Phillimore, S. Begum, N. Q. McDonald, A. Butler, D. Jones, K. Raine, C. Latimer, C. R. Santos, M. Nohadani, A. C. Eklund, B. Spencer-Dene, G. Clark, L. Pickering, G. Stamp, M. Gore, Z. Szallasi, J. Downward, P. A. Futreal and C. Swanton, *N. Engl. J. Med.*, 2012, **366**, 883–892.
- 138 H. Aoki, R. Ogura, Y. Tsukamoto, M. Okada, M. N. Sumeda, M. Isogawa, S. Yoshida and Y. Fujii, *Cent. Nerv. Syst. Cancers Version*, 2011, **2**, 19–21.
- 139 A. Ravelli, J. M. Reuben, F. Lanza, S. Anfossi, M. R. Cappelletti, L. Zanotti, A. Gobbi, C. Senti, P. Brambilla, M. Milani, D. Spada, P. Pedrazzoli, M. Martino, A. Bottini and D. Generali, *Tumor Biol.*, 2015, **36**, 6653–6665.
- 140 F. J, V. L and S. D, *Front. Biosci.*, 2001, **6**, d1207-1215.
- 141 L. K. Diaz, E. L. Wiley and M. Morrow, *Breast J.*, 2001, **7**, 40–45.
- 142 M. A. Hollingsworth and B. J. Swanson, *Nat. Rev. Cancer* 2004 41, 2004, **4**, 45–60.
- 143 Y. Masaki, M. Oka, Y. Ogura, T. Ueno, K. Nishihara, A. Tangoku, M. Takahashi, M. Yamamoto and T. Irimura, *Hepatology*, 1999, **46**, 2240–2245.
- 144 J. Wesseling, S. W. Van Der Valk and J. Hilken, <https://doi.org/10.1091/mbc.7.4.565>, 2017, **7**, 565–577.

- 145 M. Yamamoto, A. Bharti, Y. Li and D. Kufe, *J. Biol. Chem.*, 1997, **272**, 12492–12494.
- 146 S. Z. Yang, N. Kohno, A. Yokoyama, K. Kondo, H. Hamada and K. Hiwada, *Int. J. Oncol.*, 2001, **18**, 541–548.
- 147 Decreased MUC1 Expression Induces E-Cadherin-mediated Cell Adhesion of Breast Cancer Cell Lines1 | Cancer Research | American Association for Cancer Research, <https://aacrjournals.org/cancerres/article/58/9/2014/505124/Decreased-MUC1-Expression-Induces-E-Cadherin>, (accessed 1 January 2023).
- 148 Association of the DF3/MUC1 Breast Cancer Antigen with Grb2 and the Sos/Ras Exchange Protein1 | Cancer Research | American Association for Cancer Research, <https://aacrjournals.org/cancerres/article/55/18/4000/501392/Association-of-the-DF3-MUC1-Breast-Cancer-Antigen>, (accessed 1 January 2023).
- 149 J. A. Schroeder, M. C. Thompson, M. M. Gardner and S. J. Gendler, *J. Biol. Chem.*, 2001, **276**, 13057–13064.
- 150 J. J. Rahn, L. Dabbagh, M. Pasdar and J. C. Hugh, , DOI:10.1002/1097-0142.
- 151 S. J. Gendler, *J. Mammary Gland Biol. Neoplasia*, 2001, **6**, 339–353.
- 152 J. R. Gum, J. W. Hicks, N. W. Toribara, B. Siddiki and Y. S. Kim, *J. Biol. Chem.*, 1994, **269**, 2440–2446.
- 153 M. Osako, S. Yonezawa, B. Siddiki, J. Huang, J. J. L. Ho, Y. S. Kim and E. Sato, , DOI:10.1002/1097-0142.
- 154 Expression of MUC1 and MUC2 mucins in gastric carcinomas: its relationship with the prognosis of the patients. | Clinical Cancer Research | American Association for Cancer Research, <https://aacrjournals.org/clincancerres/article/4/11/2605/12649/Expression-of-MUC1-and-MUC2-mucins-in-gastric>, (accessed 1 January 2023).
- 155 Selection of tumor antigens as targets for immune attack using immunohistochemistry: protein antigens. | Clinical Cancer Research | American Association for Cancer Research, <https://aacrjournals.org/clincancerres/article/4/11/2669/12479/Selection-of-tumor-antigens-as-targets-for-immune>, (accessed 1 January 2023).
- 156 F. Clayton, *Hum. Pathol.*, 1986, **17**, 34–38.
- 157 M. D. Walsh, M. A. McGuckin, P. L. Devine, B. G. Hohn and R. G. Wright, *J. Clin. Pathol.*, 1993, **46**, 922–925.
- 158 C. De Bolós, M. Garrido and F. X. Real, *Gastroenterology*, 1995, **109**, 723–734.
- 159 Mucin Gene Expression in Normal, Preneoplastic, and Neoplastic Human Gastric Epithelium1 | Cancer Research | American Association for Cancer Research, <https://aacrjournals.org/cancerres/article/55/12/2681/501420/Mucin-Gene-Expression-in-Normal-Preneoplastic-and>, (accessed 1 January 2023).
- 160 M. B. Pereira, A. J. Dias, C. A. Reis and F. C. Schmitt, *J. Clin. Pathol.*, 2001, **54**, 210–213.
- 161 R. Q. Wang and D. C. Fang, *J. Clin. Pathol.*, 2003, **56**, 378–384.
- 162 K. L. Carraway, S. A. Price-Schiavi, M. Komatsu, S. Jepson, A. Perez and C. A. Carothers Carraway, *J. Mammary Gland Biol. Neoplasia*, 2001, **6**, 323–337.
- 163 K. L. Carraway, E. A. Rossi, M. Komatsu, S. A. Price-Schiavi, D. Huang, P. M. Guy, M. E. Carvajal, N. Fregien, C. A. Carothers Carraway and K. L. Carraway, *J. Biol. Chem.*, 1999, **274**, 5263–5266.
- 164 S. A. Price-Schiavi, S. Jepson, P. Li, M. Arango, P. S. Rudland, L. Yee and K. L. Carraway, *Int. J. Cancer*, 2002, **99**, 783–791.
- 165 P. L. Nguyen, G. A. Niehans, D. L. Cherwitz, Y. S. Kim and S. B. Ho, *Tumor Biol.*, 1996, **17**, 176–192.

- 166 J. S. Chu and K. J. Chang, *Cancer Lett.*, 1999, **142**, 121–127.
- 167 S. Nath and P. Mukherjee, *Trends Mol. Med.*, 2014, **20**, 332–342.
- 168 M. Bose and P. Mukherjee, *Trends Mol. Med.*, 2020, **26**, 324–336.
- 169 T. Gao, Q. Cen and H. Lei, *Biomed. Pharmacother.*, , DOI:10.1016/J.BIOPHA.2020.110888.
- 170 M. Marczynski, B. Winkeljann and O. Lieleg, *Biopolym. Biomed. Biotechnol. Appl.*, 2021, 181–208.
- 171 A. Kasprzak and A. Adamek, *Int. J. Mol. Sci. 2019, Vol. 20, Page 1288*, 2019, **20**, 1288.
- 172 C. L. Hattrup and S. J. Gendler, <https://doi.org/10.1146/annurev.physiol.70.113006.100659>, 2008, **70**, 431–457.
- 173 M. S. Syrkina, A. A. Maslakova, D. M. Potashnikova, V. P. Veiko, Y. S. Vassetzky and M. A. Rubtsov, *J. Cell. Biochem.*, 2017, **118**, 4002–4011.
- 174 R. Singh and D. Bandyopadhyay, <http://dx.doi.org/10.4161/cbt.6.4.4201>, 2007, **6**, 481–486.
- 175 D. M. Beckwith and M. Cudic, *Semin. Immunol.*, 2020, **47**, 101389.
- 176 W. Chen, Z. Zhang, S. Zhang, P. Zhu, J. K. S. Ko and K. K. L. Yung, *Int. J. Mol. Sci. 2021, Vol. 22, Page 6567*, 2021, **22**, 6567.
- 177 L. Sanislo, K. B. Vertakova, P. Kuliffay, J. Brtko, A. Galbava and S. Galbavy, *Endocr. Regul.*, 2011, **45**, 113–124.
- 178 D. Marrinucci, K. Bethel, A. Kolatkar, M. S. Luttgen, M. Malchiodi, F. Baehring, K. Voigt, D. Lazar, J. Nieva, L. Bazhenova, A. H. Ko, W. M. Korn, E. Schram, M. Coward, X. Yang, T. Metzner, R. Lamy, M. Honnatti, C. Yoshioka, J. Kunken, Y. Petrova, D. Sok, D. Nelson and P. Kuhn, *Phys. Biol.*, 2012, **9**, 016003.
- 179 M. Y. Sha, H. Xu, M. J. Natan and R. Cromer, *J. Am. Chem. Soc.*, 2008, **130**, 17214–17215.
- 180 A. De Albuquerque, S. Kaul, G. Breier, P. Krabisch and N. Fersis, *Breast Care*, 2012, **7**, 7–12.
- 181 J. F. Rovet, *Endocr. Dev.*, 2014, **26**, 26–43.
- 182 A. De Albuquerque, I. Kubisch, D. Ernst, G. Breier, G. Stamminger, N. Fersis, U. Stölzel, J. Boese-Landgraf, A. Eichler and S. Kaul, *Clin. Lab.*, 2012, **58**, 373–384.
- 183 B. Aktas, V. Müller, M. Tewes, J. Zeitz, S. Kasimir-Bauer, C. R. Loehberg, B. Rack, A. Schneeweiss and T. Fehm, *Gynecol. Oncol.*, 2011, **122**, 356–360.
- 184 L. Karthik, G. Kumar, T. Keswani, A. Bhattacharyya, S. Sarath Chandar and K. V. Bhaskara Rao, *PLoS One*, 2014, **9**, e90972.
- 185 J. C. Grutters, .
- 186 A. González-Sistal, J. I. Arias and Á. Ruibal, <https://doi.org/10.5301/JBM.2011.8591>, 2018, **27**, 47–52.
- 187 A. Fakhari, E. Gharepapagh, S. Dabiri, A. Fakhari, E. Gharepapagh, S. Dabiri and N. Gilani, *Med. J. Islam. Repub. Iran*, 2019, **33**, 142.
- 188 J. S. Lee, S. Park, J. M. Park, J. H. Cho, S. I. Kim and B. W. Park, *Ann. Oncol.*, 2013, **24**, 1225–1231.
- 189 M. Incoronato, P. Mirabelli, O. Catalano, M. Aiello, C. Parente, A. Soricelli and E. Nicolai, *BMC Cancer*, 2014, **14**, 1–6.
- 190 D. Al-Azawi, G. Kelly, E. Myers, E. W. McDermott, A. D. K. Hill, M. J. Duffy and N. O. Higgins, *BMC Cancer*, 2006, **6**, 1–7.
- 191 W. G. Chu and D. W. Ryu, *Ann. Surg. Treat. Res.*, 2015, **90**, 57–63.

- 192 A. Berruti, M. Tampellini, M. Torta, T. Buniva, G. Gorzegno and L. Dogliotti, *Eur. J. Cancer*, 1994, **30**, 2082–2084.
- 193 P. Bliss, R. C. F. Leonard, J. Fiskens and J. Roulsten, *Dis. Markers*, 1993, **11**, 45–48.
- 194 I. A. Darwish, T. A. Wani, N. Y. Khalil and D. A. Blake, *Talanta*, 2012, **97**, 499–504.
- 195 M. J. Duffy, C. Duggan, R. Keane, A. D. K. Hill, E. McDermott, J. Crown and N. O’Higgins, *Clin. Chem.*, 2004, **50**, 559–563.
- 196
- 197 F. G. Ebeling, P. Stieber, M. Untch, D. Nagel, G. E. Konecny, U. M. Schmitt, A. Fateh-Moghadam and D. Seidel, *Br. J. Cancer* 2002 868, 2002, **86**, 1217–1222.
- 198 N. Ferrara, H. P. Gerber and J. LeCouter, *Nat. Med.* 2003 96, 2003, **9**, 669–676.
- 199 K. A. Houck, N. Ferrara, J. Winer, G. Cachianes, B. Li and D. W. Leung, *Mol. Endocrinol.*, 1991, **5**, 1806–1814.
- 200 E. Tischer, R. Mitchell, T. Hartman, M. Silva, D. Gospodarowicz, J. C. Fiddes and J. A. Abraham, *J. Biol. Chem.*, 1991, **266**, 11947–11954.
- 201 D. W. Leung, G. Cachianes, W. J. Kuang, D. V. Goeddel and N. Ferrara, *Science (80-. )*, 1989, **246**, 1306–1309.
- 202 G. NEUFELD, T. COHEN, S. GENGRINOVITCH and Z. POLTORAK, *FASEB J.*, 1999, **13**, 9–22.
- 203 B. A. Keyt, L. T. Berleau, H. V. Nguyen, H. Chen, H. Heinsohn, R. Vandlen and N. Ferrara, *J. Biol. Chem.*, 1996, **271**, 7788–7795.
- 204 N. Ferrara, *J. Mol. Med.*, 1999, **77**, 527–543.
- 205 N. Ferrara, K. Mayo, J. Cidlowski, N. Kochupillai and G. Cutler, *Recent Prog. Horm. Res.*, 2000, **55**, 15–35; discussion 35.
- 206 M. J. Cross, J. Dixelius, T. Matsumoto and L. Claesson-Welsh, *Trends Biochem. Sci.*, 2003, **28**, 488–494.
- 207 I. J. Fidler and L. M. Ellis, *Cell*, 1994, **79**, 185–188.
- 208 D. Hanahan and R. A. Weinberg, *Cell*, 2000, **100**, 57–70.
- 209 V. Permeability, F. Endothelial, G. Factor, M. Hyperpermeability, A. Harold, F. Dvorak, L. F. Brown, M. Detmar and A. M. Dvorak, *Am. J. Pathol.*, 1995, **146**, 1029.
- 210 H. F. Dvorak, J. A. Nagy, D. Feng, L. F. Brown, A. M. Dvorak, H. Yoshiji, S. R. Harris and U. P. Thorgeirsson, *Curr. Top. Microbiol. Immunol.*, 1999, **237**, 98–132.
- 211 N. Reinmuth, A. A. Parikh, S. A. Ahmad, W. Liu, O. Stoeltzing, F. Fan, A. Takeda, M. Akagi and L. M. Ellis, *Microsc. Res. Tech.*, 2003, **60**, 199–207.
- 212 S. Rafii, D. Lyden, R. Benezra, K. Hattori and B. Heissig, *Nat. Rev. Cancer* 2002 211, 2002, **2**, 826–835.
- 213 F. Iovino, F. Ferraraccio, M. Orditura, G. Antoniol, F. Morgillo, T. Cascone, M. R. Diadema, G. Aurilio, G. Santabarbara, R. Ruggiero, C. Belli, E. Irlandese, M. Fasano, F. Ciardiello, E. Procaccini, F. Lo Schiavo, G. Catalano and F. De Vita, <http://dx.doi.org/10.1080/07357900701560612>, 2009, **26**, 250–255.
- 214 M. Banyś-Paluchowski, I. Witzel, S. Riethdorf, K. Pantel, B. Rack, W. Janni, P. A. Fasching, B. Aktas, S. Kasimir-Bauer, A. Hartkopf, E. F. Solomayer, T. Fehm and V. Müller, *Breast Cancer Res. Treat.*, 2018, **172**, 93–104.
- 215 M. Toi, T. Matsumoto and H. Bando, *Lancet Oncol.*, 2001, **2**, 667–673.

- 216 M. Toi, K. Inada, H. Suzuki and T. Tominaga, *Breast Cancer Res. Treat.*, 1995, **36**, 193–204.
- 217 F. De Paola, A. M. Granato, E. Scarpi, F. Monti, L. Medri, S. Bianchi, D. Amadori and A. Volpi, *Int. J. Cancer*, 2002, **98**, 228–233.
- 218 E. Zhong, E. Brogi, T. M. D’Alfonso, H. Wen, D. Frosina, N. K. Cheung, A. A. Jungbluth and D. S. Ross, *Appl. Immunohistochem. Mol. Morphol.*, , DOI:10.1097/PAI.0000000000000974.
- 219 K. Grankvist, M. Johansson and B. Tavelin, *Artic. J. Clin. Oncol.*, , DOI:10.1200/JCO.2000.18.7.1423.
- 220 G. Gasparini, M. Toi, R. Miceli, P. B. Vermeulen, R. Dittadi, E. Biganzoli, A. Morabito, M. Fanelli, C. Gatti, H. Suzuki, T. Tominaga, L. Y. Dirix and M. Gion, *Cancer J. Sci. Am.*, 1999, **5**, 101–111.
- 221 B. Linderholm, B. Lindh, B. Tavelin, K. Grankvist and R. Henriksson, *Int. J. Cancer (Pred. Oncol.)*, 2000, **89**, 51–62.
- 222 Serum Vascular Endothelial Growth Factor in Breast Cancer | Clinical Cancer Research | American Association for Cancer Research, <https://aacrjournals.org/clincancerres/article/7/11/3491/288564/Serum-Vascular-Endothelial-Growth-Factor-in-Breast>, (accessed 2 January 2023).
- 223 V. Permeability, F. Endothelial, G. Factor, M. Hyperpermeability, A. Harold, F. Dvorak, L. F. Brown, M. Detmar and A. M. Dvorak, *Am. J. Pathol.*, 1995, **146**, 1029.
- 224 R. Mead, M. Duku, P. Bhandari and I. A. Cree, *Br. J. Cancer 2011 1052*, 2011, **105**, 239–245.
- 225 E. Sunami, A. T. Vu, S. L. Nguyen, A. E. Giuliano and D. S. B. Hoon, *Ann. N. Y. Acad. Sci.*, 2008, **1137**, 171–174.
- 226 E. Sunami, A. T. Vu, S. L. Nguyen and D. S. B. Hoon, *Methods Mol. Biol.*, 2009, **507**, 349–356.
- 227 A. R. Thierry, F. Mouliere, S. El Messaoudi, C. Mollevi, E. Lopez-Crapez, F. Rolet, B. Gillet, C. Gongora, P. Dechelotte, B. Robert, M. Del Rio, P. J. Lamy, F. Bibeau, M. Nouaille, V. Lorient, A. S. Jarrousse, F. Molina, M. MATHONNET, D. Pezet and M. Ychou, *Nat. Med. 2014 204*, 2014, **20**, 430–435.
- 228 E. Zandberga, V. Kozirovskis, A. Abols, D. Andrejeva, G. Purkalne and A. Line, *Genes, Chromosom. Cancer*, 2013, **52**, 356–369.
- 229 P. Ulivi, G. Foschi, M. Mengozzi, E. Scarpi, R. Silvestrini, D. Amadori and W. Zoli, *Int. J. Mol. Sci. 2013, Vol. 14, Pages 10332-10342*, 2013, **14**, 10332–10342.
- 230 C. Sanfiorenzo, M. I. Ilie, A. Belaid, F. Barlési, J. Mouroux, C. H. Marquette, P. Brest and P. Hofman, *PLoS One*, 2013, **8**, e54596.
- 231 C. M. Hindson, J. R. Chevillet, H. A. Briggs, E. N. Gallichotte, I. K. Ruf, B. J. Hindson, R. L. Vessella and M. Tewari, *Nat. Methods 2013 1010*, 2013, **10**, 1003–1005.
- 232 R. Molina, S. Holdenrieder, J. M. Auge, A. Schalhorn, R. Hatz and P. Stieber, *Cancer Biomarkers*, 2010, **6**, 163–178.
- 233 C. Wittwer, S. Boeck, V. Heinemann, M. Haas, P. Stieber, D. Nagel and S. Holdenrieder, *Int. J. Cancer*, 2013, **133**, 2619–2630.
- 234 C. Alix-Panabieres and K. Pantel, *Clin. Chem.*, 2013, **59**, 110–118.
- 235 P. Gao, S. C. Jiao, L. Bai, H. Wang, F. F. Jing and J. L. Yang, *J. Int. Med. Res.*, 2013, **41**, 923–933.
- 236 K. Pantel and C. Alix-Panabieres, *Cancer Res.*, 2013, **73**, 6384–6388.
- 237 F. Bidard, D. Peeters, T. Fehm, F. N.-T. lancet oncology and undefined 2014, *Elsevier*.
- 238 S. Riethdorf, H. Fritsche, V. Müller, T. Rau, C. Schindlbeck, B. Rack, W. Janni, C. Coith, K. Beck, F. Jänicke, S. Jackson, T. Gornet, M. Cristofanilli and K. Pantel, *Clin. Cancer Res.*, 2007, **13**, 920–928.

- 239 B. Hong and Y. Zu, *Theranostics*, 2013, **3**, 377–394.
- 240 F. Ma, C. Ho, A. K. H. Cheng and H. Z. Yu, *Electrochim. Acta*, 2013, **110**, 139–145.
- 241 T. Li, Q. Fan, T. Liu, X. Zhu, J. Zhao and G. Li, *Biosens. Bioelectron.*, 2010, **25**, 2686–2689.
- 242 C. Liu, X. Liu, Y. Qin, C. Deng and J. Xiang, *RSC Adv.*, 2016, **6**, 58469–58476.
- 243 C. Ma, H. Liu, L. Zhang, H. Li, M. Yan, X. Song and J. Yu, *Biosens. Bioelectron.*, 2018, **99**, 8–13.
- 244 J. Zhao, X. He, B. Bo, X. Liu, Y. Yin and G. Li, *Biosens. Bioelectron.*, 2012, **34**, 249–252.
- 245 S. Zhao, W. Yang and R. Y. Lai, *Biosens. Bioelectron.*, 2011, **26**, 2442–2447.
- 246 J. Xiang, X. Pi, X. Chen, L. Xiang, M. Yang, H. Ren, X. Shen, N. Qi and C. Deng, *Biosens. Bioelectron.*, 2017, **96**, 268–274.
- 247 W. Wen, R. Hu, T. Bao, X. Zhang and S. Wang, *Biosens. Bioelectron.*, 2015, **71**, 13–17.
- 248 C. Lin, H. Zheng, Y. Huang, Z. Chen, F. Luo, J. Wang, L. Guo, B. Qiu, Z. Lin and H. Yang, *Biosens. Bioelectron.*, 2018, **117**, 474–479.

## Chapter 2: References:

- 1 D. J. Thornton, K. Rousseau and M. A. McGuckin, *Annu. Rev. Physiol.*, 2008, **70**, 459–486.
- 2 Increased invasiveness of MUC11 cDNA-transfected human gastric cancer MKN74 cells, <https://onlinelibrary.wiley.com/doi/epdf/10.1002/%28SICI%291097-0215%2819980504%2976%3A3%3C377%3A%3AAID-IJC15%3E3.0.CO%3B2-8>, (accessed 9 August 2022).
- 3 N. W. Toribara, A. M. Robertson, S. B. Ho, W. L. Kuo, E. Gum, J. W. Hicks, J. R. Gum, J. C. Byrd, B. Siddiki and Y. S. Kim, *J. Biol. Chem.*, 1993, **268**, 5879–5885.
- 4 A. Ohgami, T. Tsuda, T. Osaki, T. Mitsudomi, Y. Morimoto, T. Higashi and K. Yasumoto, *Ann. Thorac. Surg.*, 1999, **67**, 810–814.
- 5 D. F. Hayes, R. Mesa-Tejada, L. D. Papsidero, G. A. Croghan, A. H. Korzun, L. Norton, W. Wood, J. A. Strauchen, M. Grimes, R. B. Weiss, H. J. Ree, A. D. Thor, F. C. Koerner, M. A. Rice, M. Barcos and D. W. Kufe, <https://doi.org/10.1200/JCO.1991.9.7.1113>, 2016, **9**, 1113–1123.
- 6 C. H. M. J. Van Elssen, P. W. H. Frings, F. J. Bot, K. K. Van De Vijver, M. B. Huls, B. Meek, P. Hupperets, W. T. V. Germeraad and G. M. J. Bos, *Histopathology*, 2010, **57**, 597–606.
- 7 W. M. C. Mulder, M. J. Stukart, E. De Windt, J. Wagstaff, R. J. Scheper and E. Bloemena, *Cancer Immunol. Immunother.* 1996 426, 1996, **42**, 351–356.
- 8 R. Aoki, S. Tanaka, K. Haruma, M. Yoshihara, K. Sumii, G. Kajiyama, F. Shimamoto and N. Kohno, *Dis. Colon Rectum* 1998 4110, 1998, **41**, 1262–1272.
- 9 F. Marin, P. Corstjens, B. De Gaulejac, E. De Vrind-De Jong and P. Westbroek, *J. Biol. Chem.*, 2000, **275**, 20667–20675.
- 10 M. Retz, J. Lehmann, C. Röder, B. Plötz, J. Harder, J. Eggers, J. Pauluschke, H. Kalthoff and M. Stöckle, *Cancer Res.*
- 11 A. L. Beautrais, P. R. Joyce and R. T. Mulder, *J. Am. Acad. Child Adolesc. Psychiatry*, 1996, **35**, 1174–1182.
- 12 C. Alarcón, A. I. Zaromytidou, Q. Xi, S. Gao, J. Yu, S. Fujisawa, A. Barlas, A. N. Miller, K. Manova-Todorova, M. J. Macias, G. Sapkota, D. Pan and J. Massagué, *Cell*, 2009, **139**, 757–769.
- 13 V. P. Balachandran, M. J. Cavnar, S. Zeng, Z. M. Bamboat, L. M. Ocuin, H. Obaid, E. C. Sorenson, R. Popow, C. Ariyan, F. Rossi, P. Besmer, T. Guo, C. R. Antonescu, T. Taguchi, J. Yuan, J. D. Wolchok, J. P. Allison and R. P. Dematteo, *Nat. Med.* 2011 179, 2011, **17**, 1094–1100.
- 14 F. Demichelis, K. Fall, S. Perner, O. Andrés, F. Schmidt, S. R. Setlur, Y. Hoshida, J. M. Mosquera, Y. Pawitan, C. Lee, H. O. Adami, L. A. Mucci, P. W. Kantoff, S. O. Andersson, A. M. Chinnaiyan, J. E. Johansson and M. A. Rubin, *Oncogene* 2007 2631, 2007, **26**, 4596–4599.
- 15 C. F. Qu, Y. Li, Y. J. Song, S. M. A. Rizvi, C. Raja, D. Zhang, J. Samra, R. Smith, A. C. Perkins, C. Apostolidis and B. J. Allen, *Br. J. Cancer*, 2004, **91**, 2086–2093.
- 16 G. A. Dent, C. J. Civalier, M. E. Brecher and S. A. Bentley, *Am. J. Clin. Pathol.*, 1999, **111**, 741–747.
- 17 C. S. M. Ferreira, K. Papamichael, G. Guilbault, T. Schwarzacher, J. Garipey and S. Missailidis, *Anal. Bioanal. Chem.* 2007 3904, 2007, **390**, 1039–1050.
- 18 S. Von Mensdorff-Pouilly, M. M. Gourevitch, P. Kenemans, A. A. Verstraeten, G. J. Van Kamp, A. Kok, K. Van Uffelen, F. G. M. Snijdwint, M. A. Paul, S. Meijer and J. Hilgers, *Tumor Biol.*, 1998, **19**, 186–195.
- 19 B. Jezeršek, J. Červek, Z. Rudolf and S. Novaković, *Cancer Lett.*, 1996, **110**, 137–144.

- 20 C. A. Harrop, D. J. Thornton and M. A. McGuckin, *Methods Mol. Biol.*, 2012, **842**, 49–66.
- 21 B. J. Privett, J. H. Shin and M. H. Schoenfisch, *Anal. Chem.*, 2010, **82**, 4723–4741.
- 22 N. J. Ronkainen, H. B. Halsall and W. R. Heineman, *Chem. Soc. Rev.*, 2010, **39**, 1747–1763.
- 23 E. Bakker and E. Pretsch, *TrAC Trends Anal. Chem.*, 2008, **27**, 612–618.
- 24 J. Wang, *Chem. Rev.*, 2008, **108**, 814–825.
- 25 B. Derkus, *Biosens. Bioelectron.*, 2016, **79**, 901–913.
- 26 J. Yoon, H. Y. Cho, M. Shin, H. K. Choi, T. Lee and J. W. Choi, *J. Mater. Chem. B*, 2020, **8**, 7303–7318.
- 27 Y. Xiao, A. A. Lubin, B. R. Baker, K. W. Plaxco and A. J. Heeger, *Proc. Natl. Acad. Sci.*, 2006, **103**, 16677–16680.
- 28 Y. C. Lim, A. Z. Kouzani and W. Duan, *J. Biomed. Nanotechnol.*, 2010, **6**, 93–105.
- 29 A. A. Lubin and K. W. Plaxco, *Acc. Chem. Res.*, 2010, **43**, 496–505.
- 30 R. J. White, N. Phares, A. A. Lubin, Y. Xiao and K. W. Plaxco, *Langmuir*, 2008, **24**, 10513–10518.
- 31 C. E. Immoos, S. J. Lee and M. W. Grinstaff, *J. Am. Chem. Soc.*, 2004, **126**, 10814–10815.
- 32 Y. Xiao, X. Qu, K. W. Plaxco and A. J. Heeger, *J. Am. Chem. Soc.*, 2007, **129**, 11896–11897.
- 33 F. Ricci, R. Y. Lai, A. J. Heeger, K. W. Plaxco and J. J. Sumner, *Langmuir*, 2007, **23**, 6827–6834.
- 34 A. Peterson, R. H.-N. acids research and undefined 2001, *academic.oup.com*.
- 35 C. S. M. Ferreira, C. S. Matthews and S. Missailidis, *Tumor Biol.*, 2006, **27**, 289–301.
- 36 E. Laviron, *J. Electroanal. Chem. Interfacial Electrochem.*, 1979, **101**, 19–28.
- 37 Electrochemical Methods: Fundamentals and Applications - Allen J. Bard, Larry R. Faulkner, Henry S. White  
- Google Books,  
[https://books.google.ca/books?hl=en&lr=&id=4ShuEAAAQBAJ&oi=fnd&pg=PT44&ots=SIFyBQUxqD&sig=5llmS\\_iIGM4ahdGCfruTt4ex5bA&redir\\_esc=y#v=onepage&q&f=false](https://books.google.ca/books?hl=en&lr=&id=4ShuEAAAQBAJ&oi=fnd&pg=PT44&ots=SIFyBQUxqD&sig=5llmS_iIGM4ahdGCfruTt4ex5bA&redir_esc=y#v=onepage&q&f=false), (accessed 19 August 2022).
- 38 D. Li, S. Song and C. Fan, *Acc. Chem. Res.*, 2010, **43**, 631–641.
- 39 K. K. Leung, A. D. Gaxiola, H. Z. Yu and D. Bizzotto, *Electrochim. Acta*, 2018, **261**, 188–197.
- 40 T. M. Herne and M. J. Tarlov, *J. Am. Chem. Soc.*, 1997, **119**, 8916–8920.
- 41 C. Y. Lee, P. Gong, G. M. Harbers, D. W. Grainger, D. G. Castner and L. J. Gamble, *Anal. Chem.*, 2006, **78**, 3316–3325.
- 42 A. K. H. Cheng, H. Su, Y. A. Wang and H. Z. Yu, *Anal. Chem.*, 2009, **81**, 6130–6139.
- 43 M. Moreno, H. J. Bontkes, R. J. Scheper, P. Kenemans, R. H. M. Verheijen and S. von Mensdorff-Pouilly, *Cancer Lett.*, 2007, **257**, 47–55.
- 44 A. Rughetti, A. Fama, S. von Mensdorff-Pouilly, F. Taurino, H. Rahimi, M. Ribersani, F. Natalino, G. M. D’Elia, L. Bizzoni, R. Latagliata, M. Breccia, R. Foà, G. Alimena, G. Girelli, L. Frati, M. Nuti and A. Tafuri, *Blood*, 2008, **112**, 5237.
- 45 E. Gheybi, J. Amani, A. H. Salmanian, F. Mashayekhi and S. Khodi, *Tumor Biol.*, 2014, **35**, 11489–11497.
- 46 J. Zhao, X. He, B. Bo, X. Liu, Y. Yin and G. Li, *Biosens. Bioelectron.*, 2012, **34**, 249–252.
- 47 Y. He, Y. Lin, H. Tang and D. Pang, *Nanoscale*, 2012, **4**, 2054–2059.

- 48 Z. Wang, N. Xia, J. Shi, S. Li, Y. Zhao, H. Wang and L. Liu, <http://dx.doi.org/10.1080/00032719.2014.905953>, 2014, **47**, 2431–2442.
- 49 S. Shin, H. Y. Nam, E. J. Lee, W. Jung and S. S. Hah, *Bioorg. Med. Chem. Lett.*, 2012, **22**, 6081–6084.
- 50 C. S. M. Ferreira, K. Papamichael, G. Guilbault, T. Schwarzacher, J. Garipey and S. Missailidis, *Anal. Bioanal. Chem.* 2007 3904, 2007, **390**, 1039–1050.
- 51 W. Wei, D. F. Li, X. H. Pan and S. Q. Liu, *Analyst*, 2012, **137**, 2101–2106.
- 52 F. Ma, C. Ho, A. K. H. Cheng and H. Z. Yu, *Electrochim. Acta*, 2013, **110**, 139–145.

## Chapter 3: References:

- 1 L. Jing, C. Xie, Q. Li, M. Yang, S. Li, H. Li and F. Xia, *Anal. Chem.*, 2022, **94**, 269–296.
- 2 S. Herath, S. Razavi Bazaz, J. Monkman, M. Ebrahimi Warkiani, D. Richard, K. O’Byrne and A. Kulasinghe, *Expert Rev. Mol. Diagn.*, 2020, **20**, 1139–1147.
- 3 E. S. McDonald, A. S. Clark, J. Tchou, P. Zhang and G. M. Freedman, *J Nucl Med*, 2016, **57**, 9–16.
- 4 E. A. Krupinski and Y. Jiang, *Med. Phys.*, 2008, **35**, 645–659.
- 5 L. Hartwell, D. Mankoff, A. Paulovich, S. Ramsey and E. Swisher, *Nat. Biotechnol.*, 2006, **24**, 905–908.
- 6 M. Banys-Paluchowski, I. Witzel, S. Riethdorf, K. Pantel, B. Rack, W. Janni, P. A. Fasching, B. Aktas, S. Kasimir-Bauer, A. Hartkopf, E. F. Solomayer, T. Fehm and V. Müller, *Breast Cancer Res. Treat. 2018 1721*, 2018, **172**, 93–104.
- 7 S. Li, L. Wang, Y. Meng, Y. Chang, J. Xu, Q. Zhang, S. Li, L. Wang, Y. Meng, Y. Chang, J. Xu and Q. Zhang, *Oncotarget*, 2017, **8**, 41282–41293.
- 8 R. Roskoski, *Crit. Rev. Oncol. Hematol.*, 2007, **62**, 179–213.
- 9 M. Toi, H. Bando, T. Ogawa, M. Muta, C. Hornig and H. A. Weich, *Int. J. Cancer*, 2002, **98**, 14–18.
- 10 G. C. McKeeman, J. E. S. Ardill, C. M. Caldwell, A. J. Hunter and N. McClure, *Am. J. Obstet. Gynecol.*, 2004, **191**, 1240–1246.
- 11 S. R. Piersma, U. Fiedler, S. Span, A. Lingnau, T. V. Pham, S. Hoffmann, M. H. G. Kubbutat and C. R. Jiménez, *J. Proteome Res.*, 2010, **9**, 1913–1922.
- 12 A. A. Lubin and K. W. Plaxco, *Acc. Chem. Res.*, 2010, **43**, 496–505.
- 13 D. Li, S. Song and C. Fan, *Acc. Chem. Res.*, 2010, **43**, 631–641.
- 14 F. Ricci and K. W. Plaxco, *Microchim. Acta 2008 1633*, 2008, **163**, 149–155.
- 15 Y. Xiao, X. Qu, K. W. Plaxco and A. J. Heeger, *J. Am. Chem. Soc.*, 2007, **129**, 11896–11897.
- 16 C. E. Immoos, S. J. Lee and M. W. Grinstaff, *J. Am. Chem. Soc.*, 2004, **126**, 10814–10815.
- 17 Y. Xiao, A. A. Lubin, B. R. Baker, K. W. Plaxco and A. J. Heeger, *Proc. Natl. Acad. Sci.*, 2006, **103**, 16677–16680.
- 18 Y. Xiao, X. Qu, K. W. Plaxco and A. J. Heeger, *J. Am. Chem. Soc.*, 2007, **129**, 11896–11897.
- 19 Y. Xiao, A. A. Lubin, B. R. Baker, K. W. Plaxco and A. J. Heeger, *Proc. Natl. Acad. Sci. U. S. A.*, 2006, **103**, 16677–16680.
- 20 Y. Gao, L. K. Wolf and R. M. Georgiadis, *Nucleic Acids Res.*, 2006, **34**, 3370–3377.
- 21 N. Arroyo-Currás, K. Scida, K. L. Ploense, T. E. Kippin and K. W. Plaxco, *Anal. Chem.*, 2017, **89**, 12185–12191.
- 22 L. R. Schoukroun-Barnes, S. Wagan and R. J. White, *Anal. Chem.*, 2014, **86**, 1131–1137.
- 23 A. Hauke, L. S. S. Kumar, M. Y. Kim, J. Pegan, M. Khine, H. Li, K. W. Plaxco and J. Heikenfeld, *Biosens. Bioelectron.*, 2017, **94**, 438–442.
- 24 S. Zhao, W. Yang and R. Y. Lai, *Biosens. Bioelectron.*, 2011, **26**, 2442–2447.
- 25 J. Nick Taylor, Q. Darugar, K. Kourentzi, R. C. Willson and C. F. Landes, *Biochem. Biophys. Res. Commun.*, 2008, **373**, 213–218.

- 26 A. S. R. Potty, K. Kourentzi, H. Fang, G. W. Jackson, X. Zhang, G. B. Legge and R. C. Willson, *Biopolymers*, 2009, **91**, 145–156.
- 27 R. Levicky, T. M. Herne, M. J. Tarlov and S. K. Satija, *J. Am. Chem. Soc.*, 1998, **120**, 9787–9792.
- 28 X. Zhang and V. K. Yadavalli, *Biosens. Bioelectron.*, 2011, **26**, 3142–3147.
- 29 C. M. A. Brett, S. Kresak, T. Hianik and A. M. Oliveira Brett, *Electroanalysis*, 2003, **15**, 557–565.
- 30 F. Ma, C. Ho, A. K. H. Cheng and H. Z. Yu, *Electrochim. Acta*, 2013, **110**, 139–145.
- 31 Z. gang Yu, A. L. Sutlief and R. Y. Lai, *Sensors Actuators, B Chem.*, 2018, **258**, 722–729.
- 32 Serum Vascular Endothelial Growth Factor in Breast Cancer | Clinical Cancer Research | American Association for Cancer Research, <https://aacrjournals.org/clincancerres/article/7/11/3491/288564/Serum-Vascular-Endothelial-Growth-Factor-in-Breast>, (accessed 3 January 2023).
- 33 L. Feng, Z. Lyu, A. Offenhäusser and D. Mayer, *Eng. Life Sci.*, 2016, **16**, 550–559.
- 34 O. S. Kwon, S. J. Park, J. Y. Hong, A. R. Han, J. S. Lee, J. S. Lee, J. H. Oh and J. Jang, *ACS Nano*, 2012, **6**, 1486–1493.
- 35 H. Chen, Y. Hou, F. Qi, J. Zhang, K. Koh, Z. Shen and G. Li, *Biosens. Bioelectron.*, 2014, **61**, 83–87.
- 36 Y. Li, J. L. Hye and R. M. Corn, *Anal. Chem.*, 2007, **79**, 1082–1088.
- 37 R. Freeman, J. Girsh, A. Fang-Ju Jou, J. A. A. Ho, T. Hug, J. Dervedde and I. Willner, *Anal. Chem.*, 2012, **84**, 6192–6198.
- 38 M. A. Al-Ameen and G. Ghosh, *Biosens. Bioelectron.*, 2013, **49**, 105–110.
- 39 G. Il Kim, K. W. Kim, M. K. Oh and Y. M. Sung, *Biosens. Bioelectron.*, 2010, **25**, 1717–1722.
- 40 W. Li, Q. Zhang, H. Zhou, J. Chen, Y. Li, C. Zhang and C. Yu, *Anal. Chem.*, 2015, **87**, 8336–8341.
- 41 O. S. Kwon, S. J. Park and J. Jang, *Biomaterials*, 2010, **31**, 4740–4747.

## Chapter 4: References

- (1) Que-Gewirth, N. S.; Sullenger, B. A. Gene Therapy Progress and Prospects: RNA Aptamers. *Gene Ther.* **2007**, *14* (4), 283–291. <https://doi.org/10.1038/SJ.GT.3302900>.
- (2) Song, S.; Wang, L.; Li, J.; Fan, C.; Zhao, J. Aptamer-Based Biosensors. *TrAC Trends Anal. Chem.* **2008**, *27* (2), 108–117. <https://doi.org/10.1016/J.TRAC.2007.12.004>.
- (3) Dollins, C. M.; Nair, S.; Sullenger, B. A. Aptamers in Immunotherapy. <https://home.liebertpub.com/hum> **2008**, *19* (5), 443–450. <https://doi.org/10.1089/HUM.2008.045>.
- (4) Xiao, Y.; Lai, R. Y.; Plaxco, K. W. Preparation of Electrode-Immobilized, Redox-Modified Oligonucleotides for Electrochemical DNA and Aptamer-Based Sensing. *Nat. Protoc.* **2007**, *2* (11), 2875–2880. <https://doi.org/10.1038/nprot.2007.413>.
- (5) Sharafeldin, M.; Davis, J. J. Characterising the Biosensing Interface. *Anal. Chim. Acta* **2022**, *1216*, 339759. <https://doi.org/10.1016/J.ACA.2022.339759>.
- (6) Muñoz, J.; Montes, R.; Baeza, M. Trends in Electrochemical Impedance Spectroscopy Involving Nanocomposite Transducers: Characterization, Architecture Surface and Bio-Sensing. *TrAC Trends Anal. Chem.* **2017**, *97*, 201–215. <https://doi.org/10.1016/J.TRAC.2017.08.012>.
- (7) Bizzotto, D.; Burgess, I. J.; Doneux, T.; Sagara, T.; Yu, H. Z. Beyond Simple Cartoons: Challenges in Characterizing Electrochemical Biosensor Interfaces. *ACS Sensors* **2018**, *3* (1), 5–12. [https://doi.org/10.1021/ACSSENSORS.7B00840/ASSET/IMAGES/LARGE/SE-2017-00840G\\_0001.JPEG](https://doi.org/10.1021/ACSSENSORS.7B00840/ASSET/IMAGES/LARGE/SE-2017-00840G_0001.JPEG).
- (8) Gooding, J. J.; Darwish, N. The Rise of Self-Assembled Monolayers for Fabricating Electrochemical Biosensors—an Interfacial Perspective. *Chem. Rec.* **2012**, *12* (1), 92–105. <https://doi.org/10.1002/TCR.201100013>.
- (9) Xiao, Y.; Uzawa, T.; White, R. J.; DeMartini, D.; Plaxco, K. W. On the Signaling of Electrochemical Aptamer-Based Sensors: Collision- and Folding-Based Mechanisms. *Electroanalysis* **2009**, *21* (11), 1267–1271. <https://doi.org/10.1002/ELAN.200804564>.
- (10) Cholko, T.; Chang, C. E. A. Modeling Effects of Surface Properties and Probe Density for Nanoscale Biosensor Design: A Case Study of Dna Hybridization near Surfaces. *J. Phys. Chem. B* **2021**, *125* (7), 1746–1754. [https://doi.org/10.1021/ACS.JPCB.0C09723/SUPPL\\_FILE/JP0C09723\\_SI\\_001.PDF](https://doi.org/10.1021/ACS.JPCB.0C09723/SUPPL_FILE/JP0C09723_SI_001.PDF).
- (11) Lin, M.; Wang, J.; Zhou, G.; Wang, J.; Wu, N.; Lu, J.; Gao, J.; Chen, X.; Shi, J.; Zuo, X.; Fan, C. Programmable Engineering of a Biosensing Interface with Tetrahedral DNA Nanostructures for Ultrasensitive DNA Detection. *Angew. Chemie* **2015**, *127* (7), 2179–2183. <https://doi.org/10.1002/ANGE.201410720>.
- (12) Furst, A. L.; Hill, M. G.; Barton, J. K. DNA-Modified Electrodes Fabricated Using Copper-Free Click Chemistry for Enhanced Protein Detection. *Langmuir* **2013**, *29* (52), 16141–16149. [https://doi.org/10.1021/LA403262V/SUPPL\\_FILE/LA403262V\\_SI\\_001.PDF](https://doi.org/10.1021/LA403262V/SUPPL_FILE/LA403262V_SI_001.PDF).
- (13) Steel, A. B.; Levicky, R. L.; Herne, T. M.; Tarlov, M. J. Immobilization of Nucleic Acids at Solid Surfaces: Effect of Oligonucleotide Length on Layer Assembly. *Biophys. J.* **2000**, *79* (2), 975–981. [https://doi.org/10.1016/S0006-3495\(00\)76351-X](https://doi.org/10.1016/S0006-3495(00)76351-X).
- (14) Herne, T. M.; Tarlov, M. J. Characterization of DNA Probes Immobilized on Gold Surfaces. *J. Am. Chem. Soc.* **1997**, *119* (38), 8916–8920. <https://doi.org/10.1021/JA9719586>.
- (15) Ricci, F.; Lai, R. Y.; Heeger, A. J.; Plaxco, K. W.; Sumner, J. J. Effect of Molecular Crowding on the Response of an Electrochemical DNA Sensor. *Langmuir* **2007**, *23* (12), 6827–6834. <https://doi.org/10.1021/LA700328R/ASSET/IMAGES/MEDIUM/LA700328RN00001.GIF>.

- (16) Ricci, F.; Zari, N.; Caprio, F.; Recine, S.; Amine, A.; Moscone, D.; Palleschi, G.; Plaxco, K. W. Surface Chemistry Effects on the Performance of an Electrochemical Sensor. *Bioelectrochemistry* **2009**, *76* (0), 208–213. <https://doi.org/10.1016/J.BIOELECHEM.2009.03.007>.
- (17) Mayer, M. D.; Lai, R. Y. Effects of Redox Label Location on the Performance of an Electrochemical Aptamer-Based Tumor Necrosis Factor-Alpha Sensor. *Talanta* **2018**, *189*, 585–591. <https://doi.org/10.1016/J.TALANTA.2018.07.055>.
- (18) Lee, C. Y.; Gong, P.; Harbers, G. M.; Grainger, D. W.; Castner, D. G.; Gamble, L. J. Surface Coverage and Structure of Mixed DNA/Alkylthiol Monolayers on Gold: Characterization by XPS, NEXAFS, and Fluorescence Intensity Measurements. *Anal. Chem.* **2006**, *78* (10), 3316–3325. <https://doi.org/10.1021/AC052137J>.
- (19) Leung, K. K.; Gaxiola, A. D.; Yu, H. Z.; Bizzotto, D. Tailoring the DNA SAM Surface Density on Different Surface Crystallographic Features Using Potential Assisted Thiol Exchange. *Electrochim. Acta* **2018**, *261*, 188–197. <https://doi.org/10.1016/J.ELECTACTA.2017.12.114>.
- (20) Dimcheva, N. Nanostructures of Noble Metals as Functional Materials in Biosensors. *Curr. Opin. Electrochem.* **2020**, *19*, 35–41. <https://doi.org/10.1016/J.COEELEC.2019.09.008>.
- (21) Urmann, K.; Modrejewski, J.; Scheper, T.; Walter, J. G. Aptamer-Modified Nanomaterials: Principles and Applications. *BioNanoMaterials* **2017**, *18* (1–2). <https://doi.org/10.1515/BNM-2016-0012>.
- (22) Shariati, M.; Ghorbani, M.; Sasanpour, P.; Karimizefreh, A. An Ultrasensitive Label Free Human Papilloma Virus DNA Biosensor Using Gold Nanotubes Based on Nanoporous Polycarbonate in Electrical Alignment. *Anal. Chim. Acta* **2019**, *1048*, 31–41. <https://doi.org/10.1016/J.ACA.2018.09.062>.
- (23) Tulli, F.; Gulotta, F. A.; Martino, D. M.; Zanini, V. I. P.; Borsarelli, C. D. Ultrasensitive Amperometric Biosensing of Polyphenols Using Horseradish Peroxidase Immobilized in a Laponite/Au/DNA-Bioinspired Polycation Nanocomposite. *J. Electrochem. Soc.* **2018**, *165* (10), B452–B457. <https://doi.org/10.1149/2.1191810JES/PDF>.
- (24) Kumar, N.; Kumbhat, S. Unique Properties. *Essentials Nanosci. Nanotechnol.* **2016**, 326–360. <https://doi.org/10.1002/9781119096122.CH8>.
- (25) Navya, P. N.; Daima, H. K. Rational Engineering of Physicochemical Properties of Nanomaterials for Biomedical Applications with Nanotoxicological Perspectives. *Nano Conver.* **2016**, *3* (1). <https://doi.org/10.1186/S40580-016-0064-Z>.
- (26) Solanki, P. R.; Kaushik, A.; Agrawal, V. V.; Malhotra, B. D. Nanostructured Metal Oxide-Based Biosensors. *NPG Asia Mater.* **2011**, *3* (1), 17–24. <https://doi.org/10.1038/asiamat.2010.137>.
- (27) Zhou, Q.; Kim, T. Review of Microfluidic Approaches for Surface-Enhanced Raman Scattering. *Sensors Actuators B Chem.* **2016**, *227*, 504–514. <https://doi.org/10.1016/J.SNB.2015.12.069>.
- (28) Soleymani, L.; Fang, Z.; Sargent, E. H.; Kelley, S. O. Programming the Detection Limits of Biosensors through Controlled Nanostructuring. *Nat. Nanotechnol.* **2009**, *4* (12), 844–848. <https://doi.org/10.1038/NNANO.2009.276>.
- (29) Sheehan, P. E.; Whitman, L. J. Detection Limits for Nanoscale Biosensors. *Nano Lett.* **2005**, *5* (4), 803–807. <https://doi.org/10.1021/NL050298X>.
- (30) Hammami, I.; Alabdallah, N. M.; jomaa, A. Al; kamoun, M. Gold Nanoparticles: Synthesis Properties and Applications. *J. King Saud Univ. - Sci.* **2021**, *33* (7). <https://doi.org/10.1016/J.JKSUS.2021.101560>.
- (31) Yan, Z.; Taylor, M. G.; Mascareno, A.; Mpourmpakis, G. Size-, Shape-, and Composition-Dependent Model for Metal Nanoparticle Stability Prediction. *Nano Lett.* **2018**, *18* (4), 2696–2704. [https://doi.org/10.1021/ACS.NANOLETT.8B00670/SUPPL\\_FILE/NL8B00670\\_SI\\_001.PDF](https://doi.org/10.1021/ACS.NANOLETT.8B00670/SUPPL_FILE/NL8B00670_SI_001.PDF).
- (32) Taylor, M. G.; Austin, N.; Gounaris, C. E.; Mpourmpakis, G. Catalyst Design Based on Morphology- and

- Environment-Dependent Adsorption on Metal Nanoparticles. *ACS Catal.* **2015**, *5* (11), 6296–6301. [https://doi.org/10.1021/ACSCATAL.5B01696/SUPPL\\_FILE/CS5B01696\\_SI\\_001.PDF](https://doi.org/10.1021/ACSCATAL.5B01696/SUPPL_FILE/CS5B01696_SI_001.PDF).
- (33) Bratlie, K. M.; Lee, H.; Komvopoulos, K.; Yang, P.; Somorjai, G. A. Platinum Nanoparticle Shape Effects on Benzene Hydrogenation Selectivity. *Nano Lett.* **2007**, *7* (10), 3097–3101. [https://doi.org/10.1021/NL0716000/SUPPL\\_FILE/NL0716000SI20070914\\_111617.PDF](https://doi.org/10.1021/NL0716000/SUPPL_FILE/NL0716000SI20070914_111617.PDF).
- (34) Arenz, M.; Landman, U.; Heiz, U. CO Combustion on Supported Gold Clusters. *ChemPhysChem* **2006**, *7* (9), 1871–1879. <https://doi.org/10.1002/CPHC.200600029>.
- (35) Huang, X. J.; O'Mahony, A. M.; Compton, R. G. Microelectrode Arrays for Electrochemistry: Approaches to Fabrication. *Small* **2009**, *5* (7), 776–788. <https://doi.org/10.1002/SMLL.200801593>.
- (36) Walcarius, A.; Minter, S. D.; Wang, J.; Lin, Y.; Merkoçi, A. Nanomaterials for Bio-Functionalized Electrodes: Recent Trends. *J. Mater. Chem. B* **2013**, *1* (38), 4878–4908. <https://doi.org/10.1039/C3TB20881H>.
- (37) Shi, L.; Chu, Z.; Dong, X.; Jin, W.; Dempsey, E. A Highly Oriented Hybrid Microarray Modified Electrode Fabricated by a Template-Free Method for Ultrasensitive Electrochemical DNA Recognition. *Nanoscale* **2013**, *5* (21), 10219–10225. <https://doi.org/10.1039/C3NR03097K>.
- (38) Downs, A. M.; Gerson, J.; Hossain, M. N.; Ploense, K.; Pham, M.; Kraatz, H. B.; Kippin, T.; Plaxco, K. W. Nanoporous Gold for the Miniaturization of in Vivo Electrochemical Aptamer-Based Sensors. *ACS Sensors* **2021**, *6* (6), 2299–2306. [https://doi.org/10.1021/ACSSENSORS.1C00354/SUPPL\\_FILE/SE1C00354\\_SI\\_001.PDF](https://doi.org/10.1021/ACSSENSORS.1C00354/SUPPL_FILE/SE1C00354_SI_001.PDF).
- (39) Arroyo-Currás, N.; Scida, K.; Ploense, K. L.; Kippin, T. E.; Plaxco, K. W. High Surface Area Electrodes Generated via Electrochemical Roughening Improve the Signaling of Electrochemical Aptamer-Based Biosensors. *Anal. Chem.* **2017**, *89* (22), 12185–12191. [https://doi.org/10.1021/ACS.ANALCHEM.7B02830/SUPPL\\_FILE/AC7B02830\\_SI\\_001.PDF](https://doi.org/10.1021/ACS.ANALCHEM.7B02830/SUPPL_FILE/AC7B02830_SI_001.PDF).
- (40) Bin, X.; Sargent, E. H.; Kelley, S. O. Nanostructuring of Sensors Determines the Efficiency of Biomolecular Capture. *Anal. Chem.* **2010**, *82* (14), 5928–5931. [https://doi.org/10.1021/AC101164N/SUPPL\\_FILE/AC101164N\\_SI\\_001.PDF](https://doi.org/10.1021/AC101164N/SUPPL_FILE/AC101164N_SI_001.PDF).
- (41) Ranjbar, S.; Shahrokhian, S.; Nurmohammadi, F. Nanoporous Gold as a Suitable Substrate for Preparation of a New Sensitive Electrochemical Aptasensor for Detection of Salmonella Typhimurium. *Sensors Actuators B Chem.* **2018**, *255*, 1536–1544. <https://doi.org/10.1016/J.SNB.2017.08.160>.
- (42) Ferreira, C. S. M.; Matthews, C. S.; Missailidis, S. DNA Aptamers That Bind to MUC1 Tumour Marker: Design and Characterization of MUC1-Binding Single-Stranded DNA Aptamers. *Tumor Biol.* **2006**, *27* (6), 289–301. <https://doi.org/10.1159/000096085>.
- (43) Plowman, B.; Ippolito, S. J.; Bansal, V.; Sabri, Y. M.; O'Mullane, A. P.; Bhargava, S. K. Gold Nanospikes Formed through a Simple Electrochemical Route with High Electrocatalytic and Surface Enhanced Raman Scattering Activity. *Chem. Commun.* **2009**, No. 33, 5039–5041. <https://doi.org/10.1039/B910830K>.
- (44) Hill, H. D.; Millstone, J. E.; Banholzer, M. J.; Mirkin, C. A. The Role Radius of Curvature Plays in Thiolated Oligonucleotide Loading on Gold Nanoparticles. *ACS Nano* **2009**, *3* (2), 418–424. [https://doi.org/10.1021/NN800726E/ASSET/IMAGES/MEDIUM/NN-2008-00726E\\_0010.GIF](https://doi.org/10.1021/NN800726E/ASSET/IMAGES/MEDIUM/NN-2008-00726E_0010.GIF).
- (45) Mahshid, S. S.; Camiré, S.; Ricci, F.; Vallée-Bélisle, A. A Highly Selective Electrochemical DNA-Based Sensor That Employs Steric Hindrance Effects to Detect Proteins Directly in Whole Blood. *J. Am. Chem. Soc.* **2015**, *137* (50), 15596–15599. [https://doi.org/10.1021/JACS.5B04942/SUPPL\\_FILE/JA5B04942\\_SI\\_001.PDF](https://doi.org/10.1021/JACS.5B04942/SUPPL_FILE/JA5B04942_SI_001.PDF).

## Chapter 5: References:

- (1) Thévenot, D. R.; Toth, K.; Durst, R. A.; Wilson, G. S. Electrochemical Biosensors: Recommended Definitions and Classification. *Biosens. Bioelectron.* **2001**, *16* (1–2), 121–131. [https://doi.org/10.1016/S0956-5663\(01\)00115-4](https://doi.org/10.1016/S0956-5663(01)00115-4).
- (2) Li, P.; Lee, G. H.; Kim, S. Y.; Kwon, S. Y.; Kim, H. R.; Park, S. From Diagnosis to Treatment: Recent Advances in Patient-Friendly Biosensors and Implantable Devices. *ACS Nano* **2021**, *15* (2), 1960–2004. <https://doi.org/10.1021/ACS.NANO.0C06688>.
- (3) Vaddiraju, S.; Tomazos, I.; Burgess, D. J.; Jain, F. C.; Papadimitrakopoulos, F. Emerging Synergy between Nanotechnology and Implantable Biosensors: A Review. *Biosens. Bioelectron.* **2010**, *25* (7), 1553–1565. <https://doi.org/10.1016/J.BIOS.2009.12.001>.
- (4) Arroyo-Currás, N.; Dauphin-Ducharme, P.; Scida, K.; Chávez, J. L. From the Beaker to the Body: Translational Challenges for Electrochemical, Aptamer-Based Sensors. *Anal. Methods* **2020**, *12* (10), 1288–1310. <https://doi.org/10.1039/D0AY00026D>.
- (5) Arroyo-Currás, N.; Scida, K.; Ploense, K. L.; Kippin, T. E.; Plaxco, K. W. High Surface Area Electrodes Generated via Electrochemical Roughening Improve the Signaling of Electrochemical Aptamer-Based Biosensors. *Anal. Chem.* **2017**, *89* (22), 12185–12191. [https://doi.org/10.1021/ACS.ANALCHEM.7B02830/SUPPL\\_FILE/AC7B02830\\_SI\\_001.PDF](https://doi.org/10.1021/ACS.ANALCHEM.7B02830/SUPPL_FILE/AC7B02830_SI_001.PDF).
- (6) Ferguson, B. S.; Hoggarth, D. A.; Maliniak, D.; Ploense, K.; White, R. J.; Woodward, N.; Hsieh, K.; Bonham, A. J.; Eisenstein, M.; Kippin, T. E.; Plaxco, K. W.; Soh, H. T. Real-Time, Aptamer-Based Tracking of Circulating Therapeutic Agents in Living Animals. *Sci. Transl. Med.* **2013**, *5* (213). [https://doi.org/10.1126/SCITRANSLMED.3007095/SUPPL\\_FILE/5-213RA165\\_SM.PDF](https://doi.org/10.1126/SCITRANSLMED.3007095/SUPPL_FILE/5-213RA165_SM.PDF).
- (7) Dunn, M. R.; Jimenez, R. M.; Chaput, J. C. Analysis of Aptamer Discovery and Technology. *Nat. Rev. Chem.* **2017**, *1* (10), 1–16. <https://doi.org/10.1038/s41570-017-0076>.
- (8) Soleymani, L.; Li, F. Mechanistic Challenges and Advantages of Biosensor Miniaturization into the Nanoscale. *ACS Sensors* **2017**, *2* (4), 458–467. [https://doi.org/10.1021/ACSSENSORS.7B00069/ASSET/IMAGES/MEDIUM/SE-2017-00069T\\_0004.GIF](https://doi.org/10.1021/ACSSENSORS.7B00069/ASSET/IMAGES/MEDIUM/SE-2017-00069T_0004.GIF).
- (9) Li, S. K.; Chen, A. Y.; Chai, Y. Q.; Yuan, R.; Zhuo, Y. Electrochemiluminescence Aptasensor Based on Cascading Amplification of Nicking Endonuclease-Assisted Target Recycling and Rolling Circle Amplifications for Mucin 1 Detection. *Electrochim. Acta* **2016**, *212*, 767–774. <https://doi.org/10.1016/J.ELECTACTA.2016.07.074>.
- (10) Pheaney, C. G.; Barton, J. K. DNA Electrochemistry with Tethered Methylene Blue. *Langmuir* **2012**, *28* (17), 7063–7070. [https://doi.org/10.1021/LA300566X/ASSET/IMAGES/MEDIUM/LA-2012-00566X\\_0009.GIF](https://doi.org/10.1021/LA300566X/ASSET/IMAGES/MEDIUM/LA-2012-00566X_0009.GIF).
- (11) Drummond, T. G.; Hill, M. G.; Barton, J. K. Electron Transfer Rates in DNA Films as a Function of Tether Length. *J. Am. Chem. Soc.* **2004**, *126* (46), 15010–15011. [https://doi.org/10.1021/JA044910I/SUPPL\\_FILE/JA044910ISI20041001\\_041557.PDF](https://doi.org/10.1021/JA044910I/SUPPL_FILE/JA044910ISI20041001_041557.PDF).
- (12) White, R. J.; Phares, N.; Lubin, A. A.; Xiao, Y.; Plaxco, K. W. Optimization of Electrochemical Aptamer-Based Sensors via Optimization of Probe Packing Density and Surface Chemistry. *Langmuir* **2008**, *24* (18), 10513–10518. <https://doi.org/10.1021/la800801v>.
- (13) Kypr, J.; Kejnovská, I.; Renčíuk, D.; Vorlíčková, M. Circular Dichroism and Conformational Polymorphism of DNA. *Nucleic Acids Res.* **2009**, *37* (6), 1713–1725. <https://doi.org/10.1093/NAR/GKP026>.
- (14) Lai, R. Y.; Seferos, D. S.; Heeger, A. J.; Bazan, G. C.; Plaxco, K. W. Comparison of the Signaling and Stability of Electrochemical DNA Sensors Fabricated from 6- or 11-Carbon Self-Assembled Monolayers. *Langmuir* **2006**, *22* (25), 10796–10800. [https://doi.org/10.1021/LA0611817/SUPPL\\_FILE/LA0611817SI20060613\\_051605.PDF](https://doi.org/10.1021/LA0611817/SUPPL_FILE/LA0611817SI20060613_051605.PDF).

- (15) Stuart, D. A.; Yonzon, C. R.; Zhang, X.; Lyandres, O.; Shah, N. C.; Glucksberg, M. R.; Walsh, J. T.; Van Duyne, R. P. Glucose Sensing Using Near-Infrared Surface-Enhanced Raman Spectroscopy: Gold Surfaces, 10-Day Stability, and Improved Accuracy. *Anal. Chem.* **2005**, *77* (13), 4013–4019. <https://doi.org/10.1021/AC0501238>.
- (16) Smalley, J. F.; Feldberg, S. W.; Chidsey, C. E. D.; Linford, M. R.; Newton, M. D.; Liu, Y. P. Kinetics of Electron Transfer through Ferrocene-Terminated Alkanethiol Monolayers on Gold. *J. Phys. Chem.* **1995**, *99* (35), 13141–13149. [https://doi.org/10.1021/J100035A016/ASSET/J100035A016.FP.PNG\\_V03](https://doi.org/10.1021/J100035A016/ASSET/J100035A016.FP.PNG_V03).
- (17) Miller, C.; Cuendet, P.; Grätzel, M. Adsorbed  $\omega$ -Hydroxy Thiol Monolayers on Gold Electrodes: Evidence for Electron Tunneling to Redox Species in Solution. *J. Phys. Chem.* **1991**, *95* (2), 877–886. [https://doi.org/10.1021/J100155A072/ASSET/J100155A072.FP.PNG\\_V03](https://doi.org/10.1021/J100155A072/ASSET/J100155A072.FP.PNG_V03).
- (18) Flynn, N. T.; Tran, T. N. T.; Cima, M. J.; Langer, R. Long-Term Stability of Self-Assembled Monolayers in Biological Media. *Langmuir* **2003**, *19* (26), 10909–10915. <https://doi.org/10.1021/LA035331E>.
- (19) Steel, A. B.; Levicky, R. L.; Herne, T. M.; Tarlov, M. J. Immobilization of Nucleic Acids at Solid Surfaces: Effect of Oligonucleotide Length on Layer Assembly. *Biophys. J.* **2000**, *79* (2), 975–981. [https://doi.org/10.1016/S0006-3495\(00\)76351-X](https://doi.org/10.1016/S0006-3495(00)76351-X).
- (20) Roushani, M.; Valipour, A. Using Electrochemical Oxidation of Rutin in Modeling a Novel and Sensitive Immunosensor Based on Pt Nanoparticle and Graphene–Ionic Liquid–Chitosan Nanocomposite to Detect Human Chorionic Gonadotropin. *Sensors Actuators B Chem.* **2016**, *222*, 1103–1111. <https://doi.org/10.1016/J.SNB.2015.08.031>.
- (21) Wang, X.; Liao, X.; Mei, L.; Zhang, M.; Chen, S.; Qiao, X.; Hong, C. An Immunosensor Using Functionalized Cu<sub>2</sub>O/Pt NPs as the Signal Probe for Rapid and Highly Sensitive CEA Detection with Colorimetry and Electrochemistry Dual Modes. *Sensors Actuators, B Chem.* **2021**, *341*. <https://doi.org/10.1016/J.SNB.2021.130032>.
- (22) Liu, J.; Wagan, S.; Dávila Morris, M.; Taylor, J.; White, R. J. Achieving Reproducible Performance of Electrochemical, Folding Aptamer-Based Sensors on Microelectrodes: Challenges and Prospects. *Anal. Chem.* **2014**, *86* (22), 11417–11424. [https://doi.org/10.1021/AC503407E/SUPPL\\_FILE/AC503407E\\_SI\\_001.PDF](https://doi.org/10.1021/AC503407E/SUPPL_FILE/AC503407E_SI_001.PDF).
- (23) Zheng, S.; Choi, J. H.; Lee, S. M.; Hwang, K. S.; Kim, S. K.; Kim, T. S. Analysis of DNA Hybridization Regarding the Conformation of Molecular Layer with Piezoelectric Microcantilevers. *Lab Chip* **2010**, *11* (1), 63–69. <https://doi.org/10.1039/C0LC00122H>.
- (24) Lubin, A. A.; Hunt, B. V. S.; White, R. J.; Plaxco, K. W. Effects of Probe Length, Probe Geometry, and Redox-Tag Placement on the Performance of the Electrochemical E-DNA Sensor. *Anal. Chem.* **2009**, *81* (6), 2150–2158. [https://doi.org/10.1021/AC802317K/SUPPL\\_FILE/AC802317K\\_SI\\_001.PDF](https://doi.org/10.1021/AC802317K/SUPPL_FILE/AC802317K_SI_001.PDF).
- (25) Peterson, A. W.; Heaton, R. J.; Georgiadis, R. M. The Effect of Surface Probe Density on DNA Hybridization. *Nucleic Acids Res.* **2001**, *29* (24), 5163–5168. <https://doi.org/10.1093/NAR/29.24.5163>.

